

VOLUME 75 DECEMBER 9, 1971 NUMBER 25

JPCHAx

THE JOURNAL OF

PHYSICAL

CHEMISTRY

PUBLISHED BIWEEKLY BY THE AMERICAN CHEMICAL SOCIETY

Reprints from Chemical & Engineering News

On orders of \$10 or less please remit check or money order

Keeping broadly informed challenges every person today. If you missed these features from recent issues of C&EN, you can still get copies by filling in the coupon below.

Population

A 2-part feature
David M. Kiefer, C&EN
Oct. 7 & 14, 1968 **75¢**

Mr. Kiefer finds that population is growing unchecked in much of the world, and that U.S. population will expand 50% in the next 30 years or so. Social as well as technological innovation is needed to thwart this advance. **10148**

Computers in Chemical Education

Dr. Frederick D. Tabbutt
Reed College
Portland, Oregon
January 19, 1970 **50¢**

A number of experiments with computers in education have been undertaken in the past few years. Some of the approaches to computer-assisted education now show promise as useful adjuncts as surrogate teachers. **11970**

Arthritis

A 3-part feature
Howard J. Sanders, C&EN
July 22, 29, & Aug. 12, 1968 **75¢**

Causes of arthritis are still a mystery, although more and more evidence points to infection as a possible trigger. Mr. Sanders discusses and examines the possible causes and the past, present, and future of treatment. **07228**

Industrial Research Careers

Howard Reiss
University of California
Los Angeles
June 29, 1970 **50¢**

A major concern of those beginning careers in science is, of course, where to carry out their careers—in a university, private industry, a foundation or wherever. An industrial research career can be a rewarding one, both professionally and financially. **62970**

Public Policy and the Environment

February 9, 1970 **50¢**
Speaking at the 158th ACS National Meeting, Lee DuBridge, Herbert Doan, and Barry Commoner urged cooperation among government, industry, and university in tackling environmental improvement. **02970**

Pollution Control Instrumentation

Michael Heylin, C&EN
February 15, 1971 **50¢**

Efforts to control air and water resources intelligently depends on the ability to detect and to monitor pollutants. The challenge to produce better instrumentation for this purpose is now receiving intense attention from industry and government researchers. **21571**

Allergy

Howard J. Sanders, C&EN
May 11, 1970 **50¢**

Although hay fever, bronchial asthma, and other allergies will not be conquered, they will be better understood and better treated. The expanding study of these diseases in fundamental scientific terms, using the latest research techniques, allergic disorders will yield more and more of their secrets that only a few years ago seemed almost unfathomable. **51170**

Food Additives

Howard J. Sanders, C&EN
October 10, 1966 **75¢**

Makers of food additives are keeping their eyes on the spectacular growth of new foods and the shifting moods of regulation-minded Washington. An array of chemicals enhances the wholesomeness, attractiveness, convenience, and nutritional value of American foods. **10176**

Technology Assessment

David M. Kiefer, C&EN
October 5, 1970 **50¢**

Technology assessment is an attempt—still halting and uncertain—to establish an early-warning system to control, direct, and, if necessary, restrain technological development so as to maximize the public good while minimizing the public risks. **10570**

Chemistry and the Atmosphere

Howard J. Sanders, C&EN
March 28, 1966 **75¢**

The earth's atmosphere is a vast, churning mixture of gases and trace quantities of liquids and solids. Held to the earth by the pull of gravity, it is the transparent envelope without which life on earth would cease to exist. **32866**

Career Opportunities The New Priorities

March 8, 1971 **50¢**

C&EN's annual career guide for chemists and chemical engineers. In the search for new priorities, new opportunities are emerging. Here C&EN looks at three such areas—food, shelter, and health. **03871**

Chaos in Science Teaching

Dr. Conrad E. Ronneberg
Professor Emeritus, Denison University
June 1, 1970 **50¢**

To many people familiar with the situation in teaching introductory science courses, both in high school and college, the situation is utter chaos. To place attempts to improve science teaching in proper perspective requires a brief review of the progress of science teaching since World II. **06170**

Artificial Organs

A 2-part feature
Howard J. Sanders, C&EN
April 5 and 12, 1971 **75¢**

The implanting of a total artificial heart in a human has been the most dramatic single advance to date in the field of artificial organs. In recent years, however, many other artificial organs have also been developed, and scientists foresee a vast increase in the number of body parts that, in the years ahead, will be replaceable by mechanical devices. **04571**

Scientific Societies and Public Affairs

K. M. Reese, C&EN
May 3, 1971 **50¢**

Scientific and engineering societies for many years have fostered research, published papers, and sponsored meetings without great regard for the world beyond their particular disciplines. Only in the past decade or so have the learned societies edged into the realm of public affairs. **05371**

1 to 49 copies—single copy price 50 to 299 copies—20% discount

Prices for larger quantities available on request

<input type="checkbox"/>	<input type="checkbox"/>	<input type="checkbox"/>	
10148	11970	07228	
<input type="checkbox"/>	<input type="checkbox"/>	<input type="checkbox"/>	
62970	02970	51170	
<input type="checkbox"/>	<input type="checkbox"/>	<input type="checkbox"/>	<input type="checkbox"/>
21571	10176	10570	32866
<input type="checkbox"/>	<input type="checkbox"/>	<input type="checkbox"/>	<input type="checkbox"/>
03871	06170	04571	05371

TO: REPRINT DEPARTMENT

ACS Publications
1155 Sixteenth St., N.W.
Washington, D.C. 20036

FROM:

Name _____
Street _____
City _____
State _____ Zip Code _____
Amount enclosed \$ _____

THE JOURNAL OF PHYSICAL CHEMISTRY

BRYCE CRAWFORD, Jr., *Editor*

STEPHEN PRAGER, *Associate Editor*

ROBERT W. CARR, Jr., FREDERIC A. VAN-CATLEDGE, *Assistant Editors*

EDITORIAL BOARD: A. O. ALLEN (1970-1974), R. BERSOHN (1967-1971), J. R. BOLTON (1971-1975), S. BRUNAUER (1967-1971), M. FIXMAN (1970-1974), H. S. FRANK (1970-1974), J. R. HUIZENGA (1969-1973), M. KASHA (1967-1971), W. J. KAUZMANN (1969-1973), W. R. KRIGBAUM (1969-1973), R. A. MARCUS (1968-1972), W. J. MOORE (1969-1973), J. A. POPLÉ (1971-1975), B. S. RABINOVITCH (1971-1975), H. REISS (1970-1974), S. A. RICE (1969-1975), R. E. RICHARDS (1967-1971), F. S. ROWLAND (1968-1972), R. L. SCOTT (1968-1972), R. SEIFERT (1968-1972)

CHARLES R. BERTSCH, *Manager, Editorial Production*

AMERICAN CHEMICAL SOCIETY, 1155 Sixteenth St., N.W., Washington, D. C. 20036

FREDERICK T. WALL, *Executive Director*

Books and Journals Division

JOHN K. CRUM, *Director (Acting)*

JOSEPH H. KUNEY, *Head, Business Operations Department*

RUTH REYNARD, *Assistant to the Director*

©Copyright, 1971, by the American Chemical Society. Published biweekly by the American Chemical Society at 20th and Northampton Sts., Easton, Pa. 18042. Second-class postage paid at Washington, D. C., and at additional mailing offices.

All manuscripts should be sent to *The Journal of Physical Chemistry*, Department of Chemistry, University of Minnesota, Minneapolis, Minn. 55455.

Additions and Corrections are published once yearly in the final issue. See Volume 74, Number 26 for the proper form.

Extensive or unusual alterations in an article after it has been set in type are made at the author's expense, and it is understood that by requesting such alterations the author agrees to defray the cost thereof.

The American Chemical Society and the Editor of *The Journal of Physical Chemistry* assume no responsibility for the statements and opinions advanced by contributors.

Correspondence regarding accepted copy, proofs, and reprints should be directed to Editorial Production Office, American Chemical Society, 20th and Northampton Sts., Easton, Pa. 18042. Manager: CHARLES R. BERTSCH. Assistant Editor: EDWARD A. BORGER. Editorial Assistant: WILLIAM T. BOYD. Advertising Office: Century Communications Corporation, 142 East Avenue, Norwalk, Conn. 06851.

Business and Subscription Information

Remittances and orders for subscriptions and for single copies,

notices of changes of address and new professional connections, and claims for missing numbers should be sent to the Subscription Service Department, American Chemical Society, 1155 Sixteenth St., N.W., Washington, D. C. 20036. Allow 4 weeks for changes of address. Please include an old address label with the notification.

Claims for missing numbers will not be allowed (1) if received more than sixty days from date of issue, (2) if loss was due to failure of notice of change of address to be received before the date specified in the preceding paragraph, or (3) if the reason for the claim is "missing from files."

Subscription rates (1971): members of the American Chemical Society, \$20.00 for 1 year; to nonmembers, \$40.00 for 1 year. Those interested in becoming members should write to the Admissions Department, American Chemical Society, 1155 Sixteenth St., N.W., Washington, D. C. 20036. Postage to Canada and countries in the Pan-American Union, \$4.00; all other countries, \$5.00. Single copies for current year: \$2.00. Rates for back issues from Volume 56 to date are available from the Special Issues Sales Department, 1155 Sixteenth St., N.W., Washington, D. C. 20036.

This publication and the other ACS periodical publications are now available on microfilm. For information write to: MICROFILM, Special Issues Sales Department, 1155 Sixteenth St., N.W., Washington, D. C. 20036.

1972 Preview: Selected Physical Chemistry

WATER AND AQUEOUS SOLUTIONS Structure, Thermodynamics, and Transport Processes

Edited by R. A. Horne, *JBF Scientific Corporation, Burlington, Massachusetts*

Here is a collection of papers on the structure and properties of liquid water and aqueous solution and on related systems, such as ice and fused salts. The topics range from the surface and transport properties of ice, through the structure, thermodynamics and transport properties of water and aqueous solutions, to the state of water in living cells and tissues.

1971 832 pages 172 illus. \$37.50

SYMMETRY, ORBITALS, AND SPECTRA (S. O. S.)

By Milton Orchin and H. H. Jaffé,
both with the *University of Cincinnati*

This volume lifts the common core material from traditional advanced courses and welds it into a unified approach essential to a firm understanding of modern chemical theory. It exposes the reader to essential, basic knowledge concerning quantum mechanics, molecular orbital theory, ultraviolet and infrared absorption spectroscopy, selection rules, group theory, photochemistry, and the many varied applications of symmetry considerations. Problems are given at the end of each chapter and detailed answers are offered in a separate supplement.

1971 396 pages 28 illus. \$16.50

ATOMIC AND MOLECULAR RADIATION PHYSICS

By L. G. Christophorou, *Oak Ridge National Laboratory and University of Tennessee*

A volume in Wiley Monographs in Chemical Physics, edited by John B. Birks and Sean P. McGlynn

Atomic and Molecular Radiation Physics presents a coherent picture of many seemingly different areas of research in atomic and molecular photophysics. The author focuses on matter rather than on radiation and is mainly concerned with the interaction of radiation with single atoms and single molecules.

1971 672 pages illus. \$29.00

SURFACE AND COLLOID SCIENCE Volumes 1, 2, 3, and 4

Edited by Egon Matijevic,
Clarkson College of Technology

from a review of Volumes One and Two—

"... these volumes comprise a good beginning for the fulfillment of the editors' aim of providing a comprehensive treatise on surface and colloid science."

—*Science*

Volume 1: 1969 260 pages \$14.95

Volume 2: 1969 298 pages \$14.95

from a review of Volume Three—

"... well correlated and comprehensive information on various special topics of contemporary interest."—*Journal of the American Chemical Society*

Volume 3: 1971 296 pages 89 illus. \$16.95

Just published—

the latest addition to the series—

VOLUME FOUR, CONTENTS AND CONTRIBUTORS:

Computer Simulation of Colloidal Systems—*Avrom I. Medalia*. Physical Adsorption: The Interaction of Gases with Solids—*R. A. Pierotti and H. E. Thomas*. Convection Diffusion in Laminar and Turbulent Hyperfiltration (Reverse Osmosis) Systems—*William N. Gill, Lewis J. Derzansky, and Mahendra R. Doshi*. Bimolecular Lipid Membranes—*H. Ti Tien*. Author Index. Subject Index.

Volume 4: 1971 445 pages 81 illus. \$24.95

*Frederick Eirich was consulting editor for Volumes 1 and 2.

PHOTOCHEMISTRY AND SPECTROSCOPY

By J. P. Simons, *University of Birmingham*

Since photochemistry is a hybrid interdisciplinary subject, the details of the primary photochemical process can be explained only if the language and concepts of both spectroscopy and chemistry are understood. This is the *first* book to explore some of the common territory between these two fields.

1971 343 pages \$16.50

PRINCIPLES OF ACTIVATION ANALYSIS

By Paul Kruger, *Stanford University*

This text provides a comprehensive description of the principles on which the methods of activation analysis are founded, including the essentials of basic nuclear science, nuclear reactions, radioisotope production, radiochemical separations, and radiation measurement. These principles are then synthesized to examine the practices, limitations, and applications of activation analysis. Specific examples are drawn from the biological, physical, and engineering sciences.

1971 522 pages 174 illus. \$25.00

Titles For Your Professional Library

PHOTOCHROMISM

Edited by Glenn H. Brown, *Kent State University*
Volume III in the series, *Techniques of Chemistry*,
edited by Arnold Weissberger

In this book, thirteen contributing authors classify the various photochromic processes on the basis of their mechanisms. Discussion covers not only theoretical and experimental aspects of photochromism, but also such applications as photochromic glasses, data displays, photochromic microimages, decorations, temperature indicators, and Q-switches. In addition, an entire chapter is devoted to photochromism in living systems, with emphasis on photosynthesis and vision.

1971 853 pages 193 illus. \$47.50

REACTIONS OF MOLECULES AT ELECTRODES

By N. S. Hush, *University of Bristol*

Reactions of Molecules at Electrodes reveals current electrochemical trends in analyzing reaction mechanisms. A particularly significant development is the combination of different techniques (especially spectroscopy) with electrical measurements in order to study reaction mechanisms more effectively. In addition, the book demonstrates the usefulness of electrochemical methods in preparative chemistry.

1971 498 pages \$24.50

ELECTRON PROBE MICROANALYSIS Second Edition

By L. S. Birks,

U.S. Naval Research Laboratory, Washington, D. C.
Volume 17 in *Chemical Analysis: a Series of Texts and Monographs on Analytical Chemistry and its Applications*, edited by P. J. Elving and I. M. Kolthoff

Rapid advances in the electron probe technique have created the need for a second edition of *Electron Probe Microanalysis*. This new, completely revised edition fully incorporates new equipment and techniques, yet continues to present the basic concepts and principles of electron probe microanalysis. It will be a valuable resource for all chemists, serving both as a reference and as an upper-level text.

1971 224 pages \$150 illus. \$14.95

PERSPECTIVES IN STRUCTURAL CHEMISTRY

Volumes I, II, III, and IV

Edited by J. D. Dunitz,
Laboratorium für Organische Chemie, Zurich and
J. A. Ibers, *Northwestern University*

"Our objective here is to create a forum for such constructive reviews in which the attempt is made to weave the results of individual structure determinations into some kind of cohesive pattern."

—from the series preface

from a review of the first volume—

"This first volume has shot far towards the goal and sets 'perspectives' in the wide field of structural chemistry. Chemists and crystallographers should be grateful to the editors and authors for undertaking this task."—*ACTA Crystallographica*

Volume I: 1967 199 pages illus. \$ 9.95

Volume II: 1968 178 pages illus. \$10.95

Volume III: 1970 259 pages illus. \$14.95

Volume IV: 1971 416 pages illus. \$24.95

FAST REACTIONS

By David N. Hague,
University of Kent at Canterbury

Here is an introduction to the study of the kinetics of fast chemical reactions—an exciting new area of scientific inquiry. The volume explores newly developed experimental techniques, the ideas behind these techniques, and the more significant patterns of reactivity revealed by the study of fast reactions.

1971 159 pages \$8.50

THEORY OF THE HYPERFINE STRUCTURE OF FREE ATOMS

By Lloyd Armstrong, Jr.,
The Johns Hopkins University

This is the first book to use modern physical techniques in the study of hyperfine atomic structure. Clearly stated approximations and a consistent set of techniques serve to bring together diverse subfields of hyperfine structure such as correlation effects, hyperfine anomalies, and the Zeeman effect. Thus, the book makes the entire field more readily accessible to student and active researcher alike.

1971 240 pages illus. \$14.95

MOLECULAR THERMODYNAMICS

An Introduction to Statistical Mechanics for Chemists

By John Knox, *University of Edinburgh*

This introduction to the concepts of statistical mechanics is divided into two major sections. Part 1, **Fundamentals**, includes an elementary account of the concepts of quantum and classical mechanics, a brief summary of classical thermodynamics, foundations of molecular thermodynamics, and formulae for thermodynamic properties in terms of the molecular partition function. Part 2, **Partition Functions and their Applications**, treats such topics as classical partition functions, thermodynamic functions for ideal assembly of localized and non-localized systems, and the Maxwell-Boltzmann distribution law.

1971 64 pages \$11.95

a new thermodynamics text that is both clear and comprehensive—

THERMODYNAMICS

Principles and Applications

By Frank C. Andrews,
University of California, Santa Cruz

Thermodynamics presents the underlying principles of thermodynamics with a thorough description of the physical and mathematical ideas on which they are based. These principles are then applied to the quantitative solution of a variety of specific problems that are basic to the disciplines of chemistry, biology, engineering, physics, and earth sciences.

1971 288 pages 80 illus. \$9.95

the product of the author's 21 years of research experience in the field—

PHOTOPHYSICS OF AROMATIC MOLECULES

By John B. Birks, *University of Manchester*

A volume in Wiley Monographs in Chemical Physics, edited by John B. Birks and Sean P. McGlynn

"A monumental work . . . It should prove to be an extraordinarily useful book to chemists, physicists and engineers interested in research on and applications of molecular luminescence."

—*Applied Optics*

1970 704 pages illus. \$29.00

Available from your bookstore or from Dept. 093—



THERMODYNAMICS OF CRYSTALS

By Duane C. Wallace, *CSIRO National Standards Laboratory, Australia*

This book presents the basic theory of the equilibrium thermodynamic properties of perfect crystals. Topics treated include thermodynamics of anisotropic crystals, anharmonic lattice dynamics, band structure theory of the crystal potential, electronic excitation and electron-phonon interactions, and procedures for calculating thermodynamic functions and comparing the calculations with experimental data.

1971 480 pages 57 illus. \$22.50

THE THEORY OF OPTICAL ACTIVITY

By Dennis J. Caldwell and Henry Eyring,
both of the *University of Utah*

A volume in the series, Interscience Monographs on Physical Chemistry, edited by I. Prigogine

Until now, no single source for all the necessary background material in the intricate development of optical activity theory has been available. With the publication of *The Theory of Optical Activity*, basic, background information is presented in a single, convenient volume. In addition, the book includes a discussion of the Faraday effect, a comprehensive outline of general approaches to investigating problems in this field, and a large number of diagrams and illustrations, which serve to clarify the text.

1971 244 pages 70 illus. \$14.95

ADVANCES IN ELECTROCHEMISTRY AND ELECTROCHEMICAL ENGINEERING

Volume 8

Edited by Charles W. Tobias,
University of California, Berkeley, and
Paul Delahay, *New York University*

CONTENTS AND CONTRIBUTORS: Solid Electrolyte Batteries—*Boone B. Owens*. Thermal Phenomena in Fuel Cells and Batteries—*Bernard S. Baker, Dimitri Gidaspow, and Darshanlal Wasan*. The Lead-Acid Cell—*Jeanne Burbank, Albert C. Simon, and Eugene Willihnganz*. Electrochemistry and Application of Propylene Carbonate—*Raymond Jasinski*. The Anodic Oxidation of Hydrocarbons and the Hydrocarbon Fuel Cell—*Elton J. Cairns*. Author Index. Subject Index. Cumulative Index, Volumes 1-8.

1971 406 pages 110 illus. \$24.95

WILEY-INTERSCIENCE

a division of JOHN WILEY & SONS, Inc.
605 Third Avenue, New York, N.Y. 10016
In Canada: 22 Worcester Road, Rexdale, Ontario

THE JOURNAL OF
PHYSICAL CHEMISTRY

Volume 75, Number 25 December 9, 1971

- The Reactions of Recoil Tritium Atoms with 1-Butene and *cis*-2-Butene. Average Energy of the Addition Reaction **Richard Kushner and F. S. Rowland** 3771
- Recoil Tritium Reactions with Cyclobutane-*d*₄. Excitation Energies Accompanying Substitution of Energetic Tritium for Deuterium **Akio Hosaka and F. S. Rowland** 3781
- On the Accuracy of Theories of the Primitive Model of Ionic Solutions **Robert W. Jones and Franz Mohling** 3790
- Ion-Molecule Reactions in Ethanol by Photoionization **M. E. Russell and W. A. Chupka** 3797
- The Photochemistry of Charge-Transfer Systems. II. Complexes of Pyromellitic Dianhydride with Polynuclear Aromatic Hydrocarbons **Yvan P. Pilette and Karl Weiss** 3805
- Nanosecond Pulse Radiolysis Studies of Aqueous Thymine Solutions **Leslie M. Theard, Frank C. Peterson, and L. S. Myers, Jr.** 3815
- On Physisorption of Water on Zinc Oxide Surface **Mahiko Nagao** 3822
- Metal-Ligand Bonding in Copper(II) Chelates—an Electron Paramagnetic Resonance Study **I. Adato, A. H. I. Ben-Bassat, and S. Sarel** 3828
- Nuclear Magnetic Relaxation in a Homologous Series of Nematic Liquid Crystals **C. R. Dybowski, B. A. Smith, and C. G. Wade** 3834
- Vibrational Spectra and Structure of Dimethylaminodichlorophosphine **J. R. Durig and J. M. Casper** 3837
- Equilibrium Constants for the Formation of Weak Complexes **Robert L. Scott** 3843
- Mechanism and Kinetics of Isotopic Exchange in Zeolites. I. Theory **L. M. Brown, H. S. Sherry, and F. J. Krambeck** 3846
- Mechanism and Kinetics of Isotopic Exchange in Zeolites. II. Experimental Data **L. M. Brown and H. S. Sherry** 3855
- Interaction Virial Coefficients in Hydrocarbon-Fluorocarbon Mixtures **E. M. Dantzer Siebert and C. M. Knobler** 3863
- Study of the Adsorption of Insoluble and Sparingly Soluble Vapors at the Gas-Liquid Interface of Water by Gas Chromatography **Barry L. Karger, Reynaldo C. Castells, Peter A. Sewell, and Arleigh Hartkopf** 3870
- Proton Magnetic Resonance Study of Ion-Pairing Effects on Arsenic-75 Quadrupole Relaxation in Tetraalkylarsonium Ions **David W. Larsen** 3880
- Continuous γ and Pulse Radiolysis of Aqueous Benzene Solutions: Some Reactions of the Hydroxycyclohexdienyl Radical **Anastasia Mantaka, D. G. Marketos, and Gabriel Stein** 3886

NOTES

- A Further Examination of the Additivity Rule **Jacob A. Marinsky** 3890
- No Evidence for the Dimerization of Nitromethane in Carbon Tetrachloride and Benzene Solutions **Glen Farmer and Hyunyoung Kim** 3892
- Conductometric Pulse Radiolysis Determination of Ionic Yields and Neutralization Kinetics in Liquid Ethanol **J. Rabani, M. Grätzel, and S. A. Chaudhri** 3893
- Laser Photolysis of Perylene Solutions **Chmouel R. Goldschmidt and Michael Ottolenghi** 3894
- Cationic Polymerization of Vinyl Monomers by Porous Glass **John G. Koelling and Kenneth E. Kolb** 3897

Photolysis of Gaseous 1,4-Dioxane at 1470 Å	Robert R. Hentz and C. F. Parrish	3899
On the Nuclear Magnetic Resonance Line Shape of Solid Heptane	K. van Putte and J. van den Enden	3901
Absolute Rate Constants for the Reaction of Atomic Oxygen with 1-Butene over the Temperature Range of 259–493°K	Robert E. Huie, John T. Herron, and Douglas D. Davis	3902

COMMUNICATIONS TO THE EDITOR

A Case for Solvated Electrons	M. C. R. Symons	3904
Solvated Electron in Any Case, but What Kind?	T. R. Tuttle, Jr., and Philip Graceffa	3905
Solubilization of Benzene in Aqueous Cetyltrimethylammonium Bromide Measured by Differential Spectroscopy	Selwyn J. Rehfeld	3905
Comment on "Solubilization of Benzene in Aqueous Cetyltrimethylammonium Bromide Measured by Differential Spectroscopy"	Janos H. Fendler and Larry K. Patterson	3907
Comment on a Recent Vibrational Analysis for the Molecules Gallium Oxide, Indium Oxide, and Thallium Oxide	A. J. Hinchcliffe and J. S. Ogden	3908

AUTHOR INDEX

Adato, I., 3828	Fendler, J. H., 3907	Kim, H., 3892	Ogden, J. S., 3908	Sherry, H. S., 3846, 3855
Ben-Bassat, A. H. I., 3828	Goldschmidt, C. R., 3894	Knobler, C. M., 3863	Ottolenghi, M., 3894	Siebert, E. M. D., 3863
Brown, L. M., 3846, 3855	Graceffa, P., 3905	Koelling, J. G., 3897	Parrish, C. F., 3899	Smith, B. A., 3834
Casper, J. M., 3837	Grätzel, M., 3893	Kolb, K. E., 3897	Patterson, L. K., 3907	Stein, G., 3886
Castells, R. C., 3870	Hartkopf, A., 3870	Krambeck, F. J., 3846	Peterson, F. C., 3815	Symons, M. C. R., 3904
Chaudhri, S. A., 3893	Hentz, R. R., 3899	Kushner, R., 3771	Pilette, Y. P., 3805	Theard, L. M., 3815
Chupka, W. A., 3797	Herron, J. T., 3902	Larsen, D. W., 3880	Rabani, J., 3893	Tuttle, T. R., Jr., 3905
Davis, D. D., 3902	Hinchcliffe, A. J., 3908	Mantaka, A., 3886	Rehfeld, S. J., 3905	van den Enden, Jr., 3901
Durig, J. R., 3837	Hosaka, A., 3781	Marinsky, J. A., 3890	Rowland, F. S., 3771, 3781	van Putte, K., 3901
Dybowski, C. R., 3834	Huie, R. E., 3902	Marketos, D. G., 3886	Russell, M. E., 3797	Wade, C. G., 3834
Farmer, G., 3892	Jones, R. W., 3790	Mohling, F., 3790	Sarel, S., 3828	Weiss, K., 3805
	Karger, B. L., 3870	Myers, L. S., Jr., 3815	Scott, R. L., 3843	
		Nagao, M., 3822	Sewell, P. A., 3870	

In papers with more than one author the name of the author to whom inquiries about the paper should be addressed is marked with an asterisk in the by-line.

THE JOURNAL OF PHYSICAL CHEMISTRY

Registered in U. S. Patent Office © Copyright, 1971, by the American Chemical Society

VOLUME 75, NUMBER 25 DECEMBER 9, 1971

The Reactions of Recoil Tritium Atoms with 1-Butene and *cis*-2-Butene.

Average Energy of the Addition Reaction¹

by Richard Kushner and F. S. Rowland*

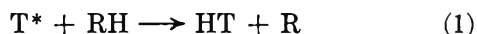
Department of Chemistry, University of California, Irvine, California 92664 (Received June 1, 1971)

Publication costs assisted by Division of Research, U. S. Atomic Energy Commission

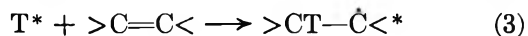
Consistent yields of propylene-*t* and CH₂=CHT are found from recoil tritium reactions with 1-butene in O₂-scavenged, H₂S-scavenged, and unscavenged experiments. A large yield of *n*-C₄H₉T in the H₂S system confirms that substantial yields of butyl-*t* radicals are collisionally stabilized prior to decomposition to the smaller olefinic products. Similar observations are made with *cis*-2-butene as the parent molecule. Pressure-dependent studies show a complementary relationship between the yields of the stabilization product (*n*-C₄H₉T) and the decomposition products (CH₂=CHT and CH₂TCH=CH₂ from 1-butene; CH₃CH=CHT from *cis*-2-butene). Pressure-dependent decomposition of the labeled parent molecules is also observed. From calculated rate constants for butyl-*t* radical decomposition, the median kinetic energy of tritium atoms undergoing addition to the olefinic positions is estimated as <0.5 eV, far below the median energies for energetic T-for-H or T-for-CH₃ substitution reactions. The relative yields of all tritiated products from T* reactions with butene (except the abstraction product, HT) are essentially independent of O₂/butene mole fraction over the range to >70% O₂.

Introduction

Basic studies of the reactions of energetic tritium with saturated hydrocarbons have demonstrated that most hot reactions are either abstraction or substitution processes, as in (1) and (2). With olefins, addition to



the double bond, as in (3), is also an important reac-



tion.^{2,3} Decomposition of the excited species formed in (2) or (3) accounts for almost all of the other radioactive products found in hydrocarbon systems. Several studies of the qualitative and quantitative yields of reactions with particular olefins have been carried out, establishing the mechanistic details for each system.⁴⁻¹³ A pressure dependence of the yield of the products from

decomposition of the radicals from (3) has been demonstrated.^{12,13}

(1) This research formed part of the material submitted in partial fulfillment of the requirements for the Ph.D. degree by R. Kushner. This research was supported by AEC Contract No. AT-(04-3)-34, Agreement No. 126. Fellowship support for R. K. from NASA is gratefully acknowledged.

(2) F. Schmidt-Bleek and F. S. Rowland, *Angew. Chem., Int. Ed. Engl.*, **3**, 769 (1964).

(3) R. Wolfgang, *Progr. React. Kinet.*, **3**, 97 (1965).

(4) D. S. Urch and R. Wolfgang, *J. Amer. Chem. Soc.*, **81**, 2025 (1959).

(5) D. Urch and R. Wolfgang, *ibid.*, **83**, 2982 (1961).

(6) E. K. C. Lee and F. S. Rowland, *J. Chem. Phys.*, **36**, 554 (1962).

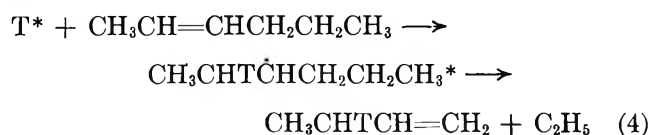
(7) E. K. C. Lee and F. S. Rowland, *J. Inorg. Nucl. Chem.*, **25**, 133 (1963).

(8) B. G. Dzantiev and A. P. Schvedchikov, "Chemical Effects of Nuclear Transformations," Vol. 1, IAEA, Vienna, 1965, p 87.

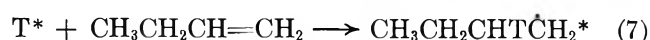
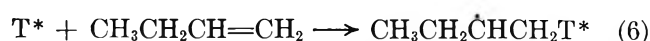
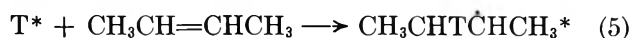
(9) J. K. Lee, B. Musgrave, and F. S. Rowland, *J. Amer. Chem. Soc.*, **82**, 3545 (1960).

(10) A. H. Rosenberg and R. Wolfgang, *J. Chem. Phys.*, **41**, 2159 (1964).

Of particular interest was the early recognition that the excited radicals from (3) were sufficiently excited to undergo decomposition by multiple pathways—indicative of excitation energies much higher than those known for the corresponding thermal radicals.^{4,5} These experiments also showed appreciable reaction at both unsaturated carbon positions in asymmetric olefins—a result that is in sharp contrast to observations in thermal systems and thereby demonstrates the presence of “hot” addition reactions.⁵ The excitation energies from such reactions were, at least in a small fraction of the additions, sufficiently high that some excited alkyl radicals—such as the *sec*-hexyl-*t* radical of (4)—decomposed even when formed in the collisional deexcitation conditions of the liquid phase.^{6,7} Reaction in the liquid phase implies decomposition rate constants for the reacting radicals of $\sim 10^{12} \text{ sec}^{-1}$.



In our present experiments, we have made a more detailed, quantitative study of the reactions of energetic tritium atoms with *cis*-2-butene and 1-butene. With the former, only the one addition reaction (eq 5) can occur, while the use of 1-butene as the substrate involves possible addition reactions at either end of the double bond, as shown in (6) and (7).^{12,13} The quantitative interpretation of such experiments is greatly facilitated by the extensive collection of data, especially by Rabinovitch and his collaborators, on the decomposition rates of excited alkyl radicals in chemical activation experiments.¹⁴⁻²¹



Experimental Section

Sample Preparation. Energetic tritium atoms were produced by the nuclear reaction ${}^3\text{He}(n,p)\text{T}$.^{2,3} Techniques of sample preparation have been described in substantial detail earlier^{2,3,22,23} and do not differ in any significant factors for the present experiments.²⁴

Chemicals. Both *cis*-2-butene and 1-butene were Phillips Research grade chemicals, while O_2 and H_2S were obtained from Matheson Co. The purification of ${}^3\text{He}$ has been described previously.^{2,3}

Experiments involving absolute yield measurements of tritiated products were carried out by simultaneous irradiation in the constant neutron flux of the rotating specimen rack of a TRIGA reactor—either that of the University of California at Berkeley or of General Atomics in San Diego. Other irradiations were conducted with the TRIGA reactor of the Northrup Laboratories in Hawthorne, Calif.

Sample Analysis. The irradiated samples were analyzed by the usual technique of radiogas chromatography.²⁵ The separations involved chiefly hydrocarbon products and did not cause any special problems. Separation of HT, CH_3T , $\text{C}_2\text{H}_3\text{T}$, and $\text{C}_2\text{H}_5\text{T}$ was carried out with a 74-ft column of propylene carbonate on alumina. Most samples were analyzed on a 50-ft dimethyl sulfolane (DMS) column; samples containing H_2S as a scavenger, or no scavenger at all, had both *trans*-2-butene-*t* and isopentane-*t* as products, a difficult separation on DMS, and were analyzed with a 50-ft silicone oil column. Column operating conditions and retention times are all given in detail elsewhere.²⁴

The separation of $\text{CH}_2\text{TCH}=\text{CD}_2$ from $\text{CD}_2\text{TCH}=\text{CH}_2$ in $\text{CH}_3\text{CH}_2\text{CH}=\text{CD}_2$ enabled us to distinguish propylene-*t* arising from an energetic T-for- CH_3 reaction from that formed by decomposition of excited $\text{CH}_3\text{CH}_2\text{CHCD}_2\text{T}^*$.^{13,26} This separation was carried out with a 340-ft column of silver nitrate-ethylene glycol, recycled once to give an effective column length of 680 ft.

The tritium radioactivity was normally measured with 85-ml silver-walled gas flow proportional counters. Observed radioactivity yields for HT were corrected for the 7- μsec “dead” time of the proportional counter; these corrections were negligible for all other peaks, as well as for HT count rates less than 50,000 counts/min.

Experiments with H_2S as a Scavenger. The most serious defect in previous experiments insofar as the evaluation of the fractional decomposition of excited butyl-*t* radicals formed by hot T-atom addition reactions are concerned has been the lack of data as to the yield of radicals which were stabilized *without* decomposition. In O_2 -scavenged systems, these radicals react with O_2 and the subsequent chemistry is not simple; it is certain,

(11) E. K. C. Lee and F. S. Rowland, *J. Amer. Chem. Soc.*, **84**, 3085 (1962).

(12) R. Kushner and F. S. Rowland, *ibid.*, **91**, 1539 (1969).

(13) E. K. C. Lee and F. S. Rowland, *J. Phys. Chem.*, **74**, 439 (1970).

(14) B. S. Rabinovitch and R. W. Diesen, *J. Chem. Phys.*, **30**, 735 (1959).

(15) R. E. Harrington, B. S. Rabinovitch, and R. W. Diesen, *ibid.*, **32**, 1245 (1960).

(16) R. E. Harrington, B. S. Rabinovitch, and M. R. Hoare, *ibid.*, **33**, 744 (1961).

(17) B. S. Rabinovitch, R. F. Kubin, and R. E. Harrington, *ibid.*, **38**, 405 (1963).

(18) G. H. Kohlmaier and B. S. Rabinovitch, *ibid.*, **38**, 1692 (1963).

(19) G. H. Kohlmaier and B. S. Rabinovitch, *ibid.*, **38**, 1709 (1963).

(20) D. W. Placzek, B. S. Rabinovitch, and F. J. Dorer, *ibid.*, **44**, 279 (1966).

(21) G. Z. Whitten and B. S. Rabinovitch, *ibid.*, **38**, 2466 (1963).

(22) J. W. Root, Ph.D. Thesis, University of Kansas, 1964.

(23) E. Tachikawa, Ph.D. Thesis, University of California, Irvine, Calif., 1967.

(24) R. Kushner, Ph.D. Thesis, University of California, Irvine, Calif., 1969.

(25) J. K. Lee, E. K. C. Lee, B. Musgrave, Y.-N. Tang, J. W. Root, and F. S. Rowland, *Anal. Chem.*, **30**, 903 (1962).

(26) E. K. C. Lee and F. S. Rowland, *ibid.*, **36**, 2181 (1964).

however, that the analytical procedures used previously did *not* measure quantitatively any product characteristic of stabilized butyl-*t* radicals. These labeled radicals, however, can be converted to a measurable stable product through H abstraction from H₂S, as in (8) for *sec*-



butyl-*t* radicals.¹² This procedure is very effective and is without complication in the 1-butene system. A number of additives,²⁷ including H₂S,²⁸ facilitate during irradiation a rapid *cis*-*trans* isomerization in mixtures with either *cis*- or *trans*-2-butene, with the result that significant individual yields of these two products cannot be determined. The *trans*-2-butene-*t*/*cis*-2-butene-*t* ratio is ~ 2.5 at 24° for both radioactivity and mass peaks, in rough agreement with the values found for iodine-catalyzed thermal systems at 125.7°. No catalyzed isomerization to 1-butene or isobutene was observed.

Absolute Yields. The absolute percentage yields of various products can best be measured by comparison with the total tritium yield in a suitable monitor system exposed simultaneously to the identical neutron flux. The ideal characteristic of such a monitor system is that 100% of the tritium react with its components to form volatile products readily measurable by the same counting system used for the experimental samples. We intended to use unscavenged *n*-C₄H₁₀ as the substrate in our monitor samples, as has been done previously. However, after the usual corrections for ³He content and recoil loss,²⁹ we found that the total activity observed with H₂S-scavenged butenes was slightly but significantly greater than that found in our *n*-butane monitor samples. This difference varied from 2% or less above 1 atm pressure to $\sim 8\%$ in the 50 Torr range. Accordingly, we have assigned the total observed volatile activity in the H₂S-butene samples as 100% and have normalized our O₂-scavenged samples to this new monitor. Probably the chief uncertainty involved in this procedure is that no allowance has been made for the possible existence of a small yield of HTS, for which we have no measurement. Variation in the choice of column conditions to permit the emergence of an H₂S peak would not help appreciably because of the rapid loss of the tritium content of H₂S by isotopic exchange with vessel walls and column materials.

We estimate that our assumed "100%" is actually $>95\%$. Our monitor samples were run forward through the HT and CH₃T peaks, and then the flow through the chromatographic column was reversed, and the remainder of the tritiated products was "back-flushed" through the proportional counter. The HT peak was approximately double the "back-flush" peak, while the CH₃T/HT ratio was about 0.04. Finally, none of our conclusions are strongly dependent upon these absolute quantitative yields but are affected rather

by the relative quantitative yields from one sample to another.

Results

Standards for Intercomparison of Results. In recoil tritium systems, comparisons involving changes in one or more parameters (*e.g.*, identity of the scavenger molecule, pressure during irradiation, etc.) always present the problem of the choice of a suitable standard. This is not a minor problem in these olefin studies, since as shown below, *all* of the major products show yield changes with one or more of the parameters varied in the experiments. Even the comparison of the absolute percentage yields is not free from reservations in principle (as well as experimental limitations), since the tritium atom fluxes—and therefore the absolute yields of each product—are dependent upon the composition of the individual samples. The chief variables in our experiments have been the identity of the scavenger, the total pressure in gas samples, and the ratio of scavenger to substrate.

H₂S as a Scavenger in Recoil Tritium Studies. As indicated above, many olefin studies have relied upon O₂ as a scavenger for the removal of thermal atoms and radicals and have therefore lacked positive measurements of the yields of collision-stabilized alkyl radicals. The most important radicals that can be identified in these butene systems by reaction with H₂S are CH₂T, *sec*-butyl-*t*, and *n*-butyl-*t*, as indicated in (8)–(10).



A comparison of the relative yields of products from 1-butene is shown in Table I for two different pressures and three scavenger situations: none, O₂, or H₂S. A similar comparison for reactions with *cis*-2-butene is given in Table II. These yields are expressed relative to arbitrary internal standards in order to display the major trends.

The chief differences among the three compositions at a given pressure are as follows: (a) radicals fail to react with other radicals because of prior abstraction of H from H₂S, most obviously with the formation of CH₃T and *n*-C₄H₉T; (b) normalization of H₂S results to the yields of propylene-*t* indicates relatively slight changes in any of the olefinic product yields plus an increase in HT attributable to abstraction from H₂S; (c) O₂ eliminates thermal radical reactions while having little or no effect on nonradical or excited radical reactions.

The yields of *trans*- and *cis*-2-butene-*t* from *cis*-2-bu-

(27) W. Ando, K. Sugimoto, and S. Oae, *Bull. Chem. Soc. Jap.*, **38**, 226 (1965).

(28) M. W. Schmidt and E. K. C. Lee, *J. Chem. Phys.*, **51**, 2024 (1969).

(29) Recoil loss corrections have been made in the standard manner described in J. W. Root and F. S. Rowland, *Radiochim. Acta*, **10**, 104 (1968).

Table I: Relative Yields of Tritiated Products from Recoil Tritium Reactions with 1-Butene for Various Scavenging Conditions

Sample compn	Pressure, Torr					
	50	50	50	720	760	760
1-Butene	50	50	50	720	760	760
H ₂ S	0	10	0	0	70	0
O ₂	0	0	8	0	0	30
³ He	15	15	15	10	10	10
Tritiated products	Rel yields (standards in parentheses)					
HT	(100)	128.8	(100)	(100)	113.4	(100)
CH ₃ T	6.4	19.3	4.2	7.0	15.1	4.2
CH ₂ =CHT	32.6	35.8	33.7	29.8	31.0	29.2
C ₂ H ₅ T	4.1	3.9	1.4	2.0	3.2	1.5
CH≡CT	1.7	1.8	~1.8	1.6	1.5	1.6
C ₃ H ₇ T	1.5	0.4	None	0.3	0.2	None
Propylene- <i>t</i>	44.8	(44.7)	44.6	33.2	(33.1)	33.1
<i>n</i> -C ₄ H ₉ T	13.4	75.9	None	15.8	89.3	None
1-Butene- <i>t</i>	59.8	58.4	54.5	76.0	69.8	70.9
CH ₂ =C=CHT	0.9	nd	1.3	0.8	0.7	0.7
<i>trans</i> -2-Butene- <i>t</i>	5.4	4.0	3.1	5.3	3.6	3.0
<i>cis</i> -2-Butene- <i>t</i>	3.2	1.5	2.3	3.1	1.5	2.6
<i>i</i> -C ₅ H ₁₁ T	2.7	None	None	2.9	None	None
<i>n</i> -C ₅ H ₁₁ T	2.2	None	None	1.7	?	None
C ₈ H ₁₇ T ^a	9.7	<1	None	12.2	<1	None

^a Combined peak of 3,4-dimethylhexane and 2-methylheptane.

Table II: Relative Yields of Tritiated Products from Recoil Tritium Reactions with *cis*-2-Butene for Various Scavenging Conditions

Sample compn	Pressure, Torr					
	43	50	50	400	760	760
<i>cis</i> -2-Butene	43	50	50	400	760	760
H ₂ S	0	10	0	0	70	0
O ₂	0	0	8	0	0	30
³ He	10	10	10	8	8	8
Tritiated products	Rel yields (standards in parentheses)					
HT	(100)	108.7	(100)	(100)	123.0	(100)
CH ₃ T	4.2	8.3	4.3	5.1	7.8	4.8
CH ₂ =CHT	2.3	3.5	3.9	2.3	3.2	2.2
C ₂ H ₅ T	1.1	1.0	0.2	0.7	0.8	0.1
CH≡CT	1.9	1.6	2.4	1.6	1.2	1.2
C ₃ H ₇ T	} 51.1	0.8	None	} 41.1	Trace	None
Propylene- <i>t</i>		(44.2)	44.2		(39.6)	39.6
<i>n</i> -C ₄ H ₉ T	4.3	64.3	None	15	81.9	None
1-Butene- <i>t</i>	10.2 ^a	5.0	4.8	10.3 ^a	5.8	5.2
CH ₂ =C=CHT	1.4 ^b	0.4	0.8	0.9 ^b	0.3	0.4
<i>trans</i> -2-Butene- <i>t</i>	7.7	40.3	7.4	8.9	51.7	6.0
<i>cis</i> -2-Butene- <i>t</i>	47.9	16.6	42.4	56.7	20.8	59.6
<i>i</i> -C ₅ H ₁₁ T	4.3	~0	None	5.6	None	None
<i>n</i> -C ₅ H ₁₁ T	None	None	None	None	None	None
C ₈ H ₁₇ T	3.5	≤0.3	None	9.2	None	None

^a Includes . ^b Includes .

tene illustrate the catalyzed *cis*-*trans* isomerization of 2-butene in the presence of H₂S and a radiation field.²⁸

Efficiency of H₂S as a Scavenger. In both the 1-butene and *cis*-2-butene systems, most H₂S-scavenged samples were run with 8-10% H₂S present. To ascertain the effect of varying the H₂S concentration, samples

were run with 1 atm of *cis*-2-butene and with H₂S concentrations varying by a factor of 10. Typical results are shown in Table III, expressed relative to the sum of the equilibrated 2-butene-*t* yields. The estimated accuracies of relative yields are indicated for one sample and are typical of the counting errors involved in these

Table III: Radioactive Products from Recoil Tritium Reactions with *cis*-2-Butene vs. H₂S Concentration (24°)

Sample compn	Pressure, Torr	
	758	773
<i>cis</i> -2-Butene	758	773
H ₂ S	70	6
³ He	10	10
Tritiated product	Rel yield [Σ (2-butene) = 100]	
HT	176.9 ± 1.0	154.4
CH ₃ T	11.4 ± 0.2	11.8
CH ₂ =CHT	4.4 ± 0.1	3.6
C ₂ H ₅ T	1.4 ± 0.1	1.3
CH≡CT	1.8 ± 0.1	1.7
C ₃ H ₇ T	0.4 ± 0.1	0.3
Propylene- <i>t</i>	57.4 ± 0.5	55.5
<i>n</i> -C ₄ H ₉ T	115.2 ± 0.8	121.5
1-Butene- <i>t</i>	7.9 ± 0.1	7.7
<i>trans</i> -2-Butene- <i>t</i>	71.9	71.7
<i>cis</i> -2-Butene- <i>t</i>	29.1	29.3
<i>i</i> -C ₅ H ₁₁ T	None	None
CH ₂ =C=CHT + methylacetylene- <i>t</i>	0.7 ± 0.1	1.0
C ₈ H ₁₇ T	None	Nd

experiments. The general reproducibility of results can be inferred from the scatter of points in Figures 1-4.

The agreement in yields of CH₃T and *n*-C₄H₉T shows that less than 1% H₂S is sufficient for scavenging of CH₃CHTCHCH₃ and CH₂T radicals and confirms that such scavenging should be complete for samples with 8-10% H₂S present. There is clearly a competition for low-energy tritium atoms between olefin and H₂S, with the latter forming HT and the former C₄H₉T and

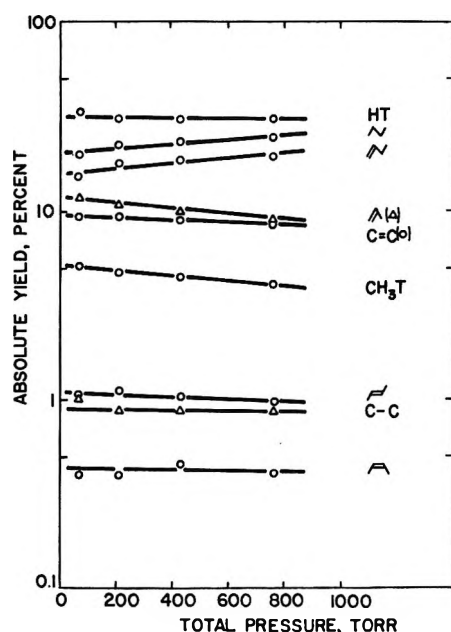


Figure 1. Pressure dependence of absolute yields for products of recoil tritium reactions with H₂S-scavenged 1-butene.

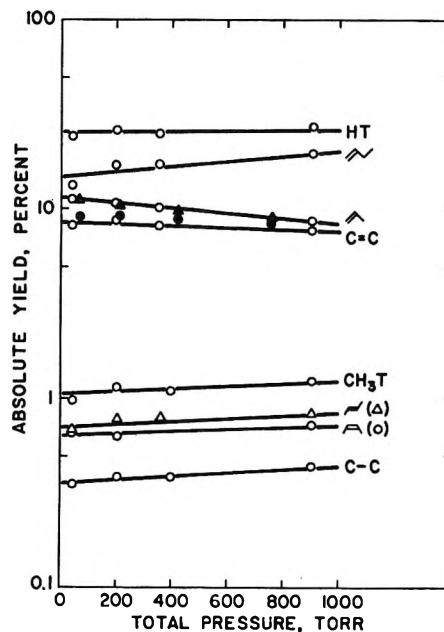


Figure 2. Pressure dependence of absolute yields for products of recoil tritium reactions with O₂-scavenged 1-butene: open symbols, O₂ scavenged; closed symbols, H₂S scavenged (from Figure 1).

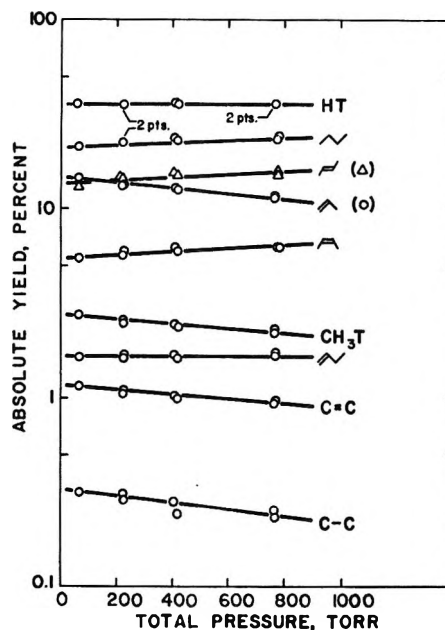


Figure 3. Pressure dependence of absolute yields for products of recoil tritium reactions with H₂S-scavenged *cis*-2-butene.

ultimately *n*-C₄H₉T. The abstraction of H from H₂S by low-energy (including thermal) tritium atoms occurs with good efficiency, consistent with the observations that such abstraction proceeds more easily with weaker bonds.^{2,3}

Unscavenged. Several unscavenged samples were run in the gas phase to determine the fate of the thermalized *sec*-butyl-*t* radicals in the absence of O₂ or H₂S in order to confirm that these scavengers were not seriously alter-

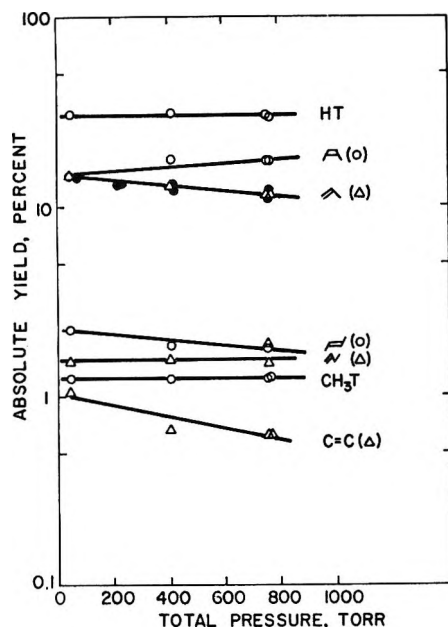


Figure 4. Pressure dependence of absolute yields for products of recoil tritium reactions with O_2 -scavenged *cis*-2-butene: open symbols, O_2 scavenged; closed symbols, H_2S scavenged (from Figure 3).

ing the hot processes in the system. Typical results were included in Tables I and II. A number of products were observed whose retention times characterized them as C_8 hydrocarbons; most of these were produced in small yields and were not identified. The only large peak in this retention time range was identified by calibration with authentic samples as a mixture of 3,4-dimethylhexane-*t* and/or 3-methylheptane-*t*—the combination products of two *sec*-butyl radicals and *sec*-butyl + *n*-butyl, respectively. The other prominent new product is *i*- $C_5H_{11}T$, again a *sec*-butyl radical combination product. *sec*-Butyl radicals formed by H-atom addition to the parent molecule should be an important reactive component from the concurrent radiolysis of the unlabeled materials during irradiation. These qualitative observations in the unscavenged systems are thus quite consistent with the scavenged results, and indicate that no important change in hot mechanisms occurs when O_2 or H_2S is included in the irradiated samples.

The total recovery of tritium as volatile products is only about 80% as large with the unscavenged butenes as with the H_2S -scavenged samples. The increase in *n*- C_4H_9T yield with the inclusion of H_2S is alone much larger than can be accounted for by decreases in other observable yields, including the C_8 peaks, implying that some butyl-*t* radicals are lost through some undefined polymerization reactions in the unscavenged systems. This observation is quite consistent with the earlier finding of significant amounts of activity on the walls of the sample bulb in unscavenged 1-butene samples.¹⁰

Comparison of "Absolute" Yields from Samples with Different Scavengers. The results of a series of runs with

varying total pressures and constant relative composition of butene to scavenger are shown graphically in Figures 1 and 2 for 1-butene and Figures 3 and 4 for *cis*-2-butene as substrate. Both H_2S and O_2 have been used as scavengers over this pressure range with each substrate molecule. As described above, the observed total tritium activities in the H_2S samples have been assigned the value of 100%, and the individual yields are expressed as percentages of this total activity. Since very little tritium activity is believed to have been lost to unobserved products, these percentages should be very close to the absolute yields—the percentage of tritium atoms found as a particular product relative to the total number of tritium atoms stopped in the gas phase.

The percentages in the O_2 -scavenged samples are calculated from the observed radioactivity, using the total activities observed in the H_2S -scavenged samples as a comparison basis, 100%. The sums of yields in O_2 -scavenged samples are always less than 100%, for the observed volatile activities in these samples do not include the oxygenated products resulting from addition of labeled radicals or thermalized T atoms to the scavenger O_2 molecules. The absolute yields of the radical-decomposition products from H_2S -scavenged systems are also shown on Figures 2 and 4 to indicate the close agreement between these two scavenger systems for these products.

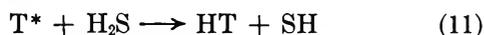
The two scavenger systems are shown to be in reasonable agreement with each other through several facets of these data: (a) the independence of HT yield *vs.* pressure, as found in other systems—and as expected for the abstraction reaction, for which no pressure-dependent decomposition reactions are anticipated; (b) the close agreement in yields and in dependence upon pressure for the major olefinic products; (c) the good agreement with earlier measurements of O_2 -scavenged 1-butene as substrate, as shown in Table IV.

Table IV: Absolute Yields from Recoil Tritium Reactions with 1-Butene

Tritiated product	Absolute yields, %	
	This work (extrapolated to 102 cm pressure)	Ref 10 (102 cm pressure)
HT	26.0	26.6
1-Butene- <i>t</i>	20.5	21.2
Propylene- <i>t</i>	8.4	8.6
$CH_2=CHT$	7.6	7.4
CH_3T	1.2	1.1
<i>trans</i> -2-Butene- <i>t</i>	0.84	1.3
<i>cis</i> -2-Butene- <i>t</i>	0.62	1.9
C_2H_6T	0.44	0.3

The higher HT yields in the presence of H_2S indicate that many additional T atoms react with H_2S by ab-

straction, as in (11), adding to the HT yield obtained by reaction with the butene substrate.



The yields of CH_3T , C_2H_5T , and $n-C_4H_9T$ are also increased by radical reaction with H_2S . In addition, small amounts of tritiated olefins seem also to have been formed by attack of vinylic radicals on H_2S . The approximate increase in these products—a direct measure of the stabilized radical yields in these systems—is given in Table V, from the data shown in Figures 1–4.

Table V: Stabilized Radical Yields Following T^* Reactions with 1-Butene and *cis*-2-Butene

Product	Incremental absolute yields, ^a %			
	1-Butene		<i>cis</i> -2-Butene	
	50 Torr	760 Torr	50 Torr	760 Torr
HT	5.0	5.0	6.0	6.0
$n-C_4H_9T$	20.2	24.8	21.3	23.6
CH_3T	4.0	2.9	1.5	1.0
C_2H_5T	0.5	0.4	0.3	0.3
C_3H_7T	0	0	0	0
C_4H_9T	0.8	0.7	0.2	0.3

^a Incremental absolute yields with H_2S as scavenger *vs.* yields with O_2 scavenger (read at 50 and 760 Torr from straight-line fits to the data illustrated in Figures 1–4).

The yield changes with pressure clearly show that the parent molecule yields decrease at lower pressures, consistent with the decomposition of the excited molecules (*e.g.*, $CH_2TCH_2CH=CH_2^*$, *cis*- $CH_2TCH=CHCH_3^*$, etc.) formed by direct T-for-H substitution. A previous measurement of the pressure dependence of 1-butene-*t* has indicated a decrease in stabilized yield by $12 \pm 3\%$ over the smaller pressure range from 685 to 68 Torr,¹³ in reasonable agreement with our observations.

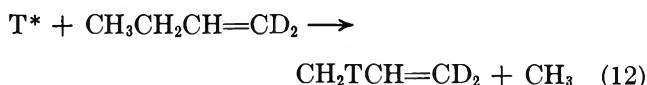
Similarly, the $n-C_4H_9T$ yield in the H_2S -scavenged systems also falls at lower pressure, as expected since a smaller fraction of $C_4H_9T^*$ radicals are collisionally stabilized at the lower molecular densities. The chief products of excited radical decompositions ($CH_3CH=CHT$ from $CH_3CHCHTCH_3^*$, $CH_2TCH=CH_2$ from $CH_3CH_2CHCH_2T^*$, $CH_2=CHT$ from $CH_3CH_2CHTCH_2^*$) all increase markedly at low pressures as more decomposition is able to occur. The larger effect for $CH_2TCH=CH_2$ than $CH_2=CHT$ from 1-butene indicates a greater sensitivity to pressure effects for *sec*-butyl-*t* parent radical of the former than for the *n*-butyl-*t* parent of the latter.

Another quantitative comparison can be made: if the sources of ethylene-*t* and propylene-*t* are the decompositions of butyl radicals and the latter are converted by H_2S to $n-C_4H_9T$, then the sum of $n-C_4H_9T + CH_2TCH=CH_2 + CH_2=CHT$ from 1-butene should be constant with pressure. The values for this sum at 760, 400, 150, and 50 Torr are 41.8, 41.4, 41.2, and

41.0%, respectively. This near constancy is additional evidence for the validity of the mechanism presented.

A similar comparison can be made for T^* reactions with *cis*-2-butene by summing the values for $n-C_4H_9T$ and $CH_3CH=CHT$. These sums, for the same pressures, are 35.0, 35.2, 35.7, and 36.0%, again showing a near constancy consistent with the suggested mechanism.

Other Hot Reactions Forming Olefinic Products. Propylene-*t* can also be formed by direct T-for- CH_3 substitution in 1-butene



as well as by the addition-decomposition mechanism. However, as illustrated in (12), the two mechanisms lead to isotopically distinguishable products with 1,1-dideuterio-1-butene: $CH_2TCH=CD_2$ from direct T-for- CH_3 and $CD_2TCH=CH_2$ from addition-decomposition. Gas chromatographic separation of the isotopic propylene-*t* molecules from $CH_3CH_2CH=CD_2$ has demonstrated that the T-for- CH_3 reaction is both small in yield (<5% under all of our gas phase conditions) and essentially pressure independent.^{13,24} Consequently, this small propylene-*t* contribution has a negligible effect on the conclusions drawn from variations in the pressure-dependent yield of propylene-*t* from $CH_3CH_2CH=CH_2$. By inference, we assume that direct T-for- CH_3 substitution with *cis*-2-butene with no *sec*-butyl radical intermediate is also negligible in yield compared to the addition-decomposition mechanism.

The yields of the "nonparent" C_4 olefins, *i.e.*, 1-butene-*t* and *trans*-2-butene-*t* from *cis*-2-butene, and the 2-butene-*t* molecules from 1-butene presumably result primarily from radical decomposition by the less exothermic pathway of H atom loss, as illustrated in (13)



for the *sec*-butyl-*t* radical from 1-butene. These pathways are of negligible importance for *sec*-butyl radicals formed by *thermal* addition of hydrogen atoms but are not so unfavored for the addition of hot hydrogen atoms. The yields from such reactions are unlikely to be either (a) more than a minor pathway for excited radical decomposition or (b) pressure-dependent reactions, and little information is generated about them by our experiments. The detailed assignment of the yields of nonparent olefinic products is complicated by the possibility of *cis*-*trans* isomerizations by highly excited parent molecules, *i.e.*, *cis*- $CH_2TCH=CHCH_3^* \rightarrow trans$ - $CH_2TCH=CHCH_3$. It is noteworthy that *skeletal* isomerization of such excited molecules can be essentially excluded, for isobutene-*t* is *not* a product of any of these reaction systems (yield <0.1%).

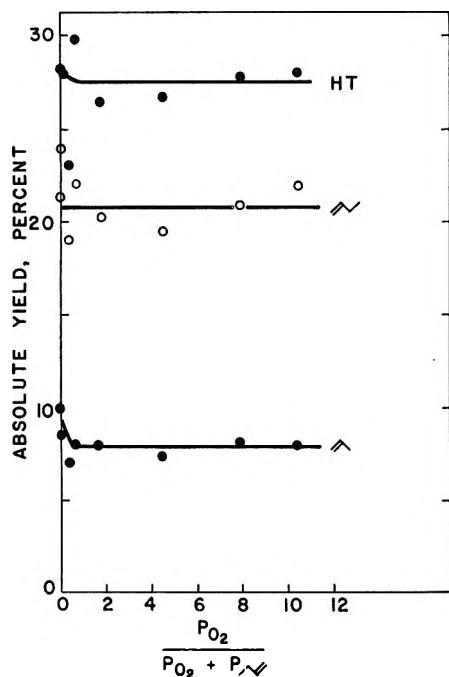


Figure 5. Effect of 0–10% O_2 scavenger on yields of recoil tritium reactions with 1-butene (from ref 10).

O₂ as Scavenger and as Major Component. The dependence of product yields on oxygen concentration for the unmoderated 1-butene system has been previously studied up to about 10 mol % O_2 , as shown in Figure 5. In contrast to the saturated hydrocarbon systems, the unsaturated system appears to require very small amounts of oxygen to obtain consistent yields of the various products. We have extended this study to more than 70 mol % O_2 concentration at 24°, as shown in Figure 6. Equivalent conditions for collisional stabilization of excited species have been sought by keeping constant at about 70 Torr the total "effective pressure," defined as $1.0(P_{1\text{-butene}}) + 0.2(P_{O_2}) + 0.1(P_{He})$. The constancy of $CH_2=CHT$ and propylene-*t* vs. O_2 concentration attests to the suitability of the choice of coefficients for this "effective pressure." The constant ratio of yields of $CH_2T-CH=CH_2$ to 1-butene-*t* also indicates no appreciable change in the distribution vs. energy of collisions by energetic tritium atoms, since the average energy for formation of these two products is probably quite different.

Molecular HT is the only major product with a significant decrease in yield vs. increasing O_2 concentration, while the yields of *trans*- and *cis*-2-butene-*t* rise very slightly. The former is presumably the result of competitive removal by O_2 of lower energy hot tritium atoms which otherwise would have abstracted hydrogen atoms to yield HT. This reduction in HT illustrates that the cross section for reaction with O_2 is not negligible in the "hot" energy range—or at least in that part of it in which HT is formed. It is also

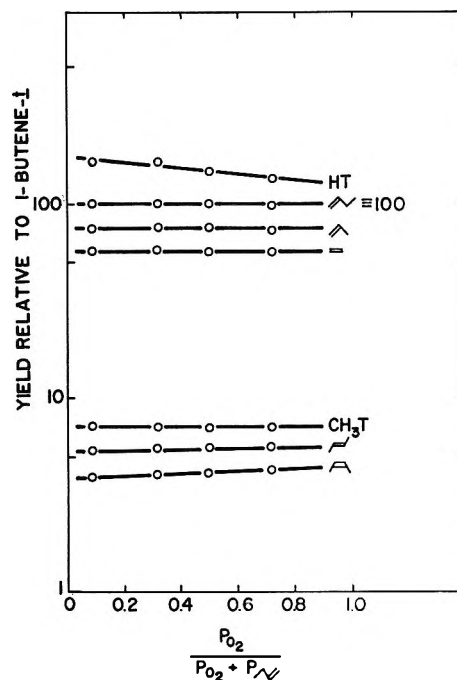


Figure 6. Effect of O_2 upon relative yields of recoil tritium reactions with 1-butene.

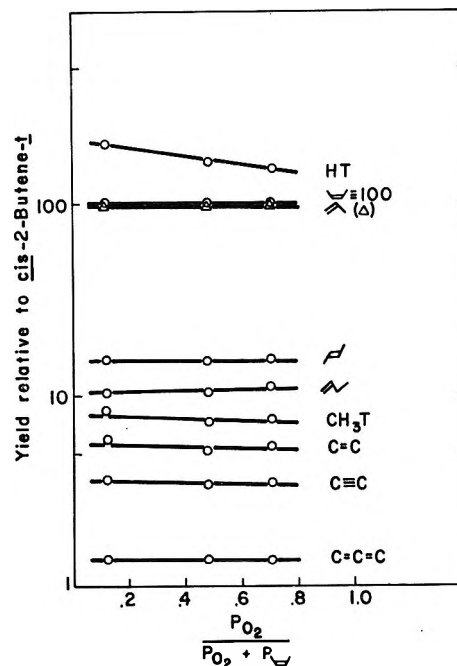


Figure 7. Effect of O_2 upon relative yields of recoil tritium reactions with *cis*-2-butene.

clear that O_2 concentrations up to 10% have a negligible effect on relative yields. Similar results were obtained with *cis*-2-butene, as shown in Figure 7.

These data are all expressed relative to the labeled parent olefin yield as 100. We are unable to assess the variations in *absolute* yields from these experiments because these calculated numbers are very sensitive to the recoil loss of tritium in pure O_2 —*i.e.*, to the stop-

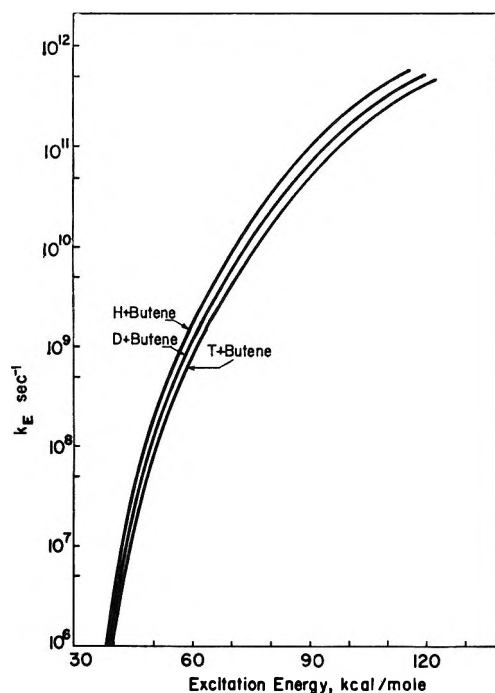
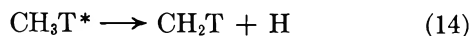


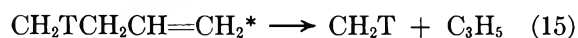
Figure 8. Estimated rate constants for decomposition of *sec*-butyl radicals after addition of isotopic hydrogen atoms.

ping power of O_2 for recoil tritium—a factor which has not yet been accurately measured by experiment.

Formation of CH_2T Radicals. The incremental yield of CH_3T when H_2S - and O_2 -scavenged experiments are compared indicates the presence of CH_2T radicals in the system. One possible source of CH_2T radicals is the decomposition of CH_3T^* formed in a primary substitution process as in (14).^{30,31} The rate



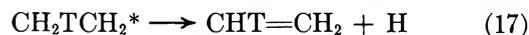
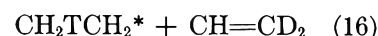
constants for the isotopic reaction of CH_4^* have been calculated and are shown to change from 10^8 to 10^{11} sec^{-1} for less than 10-kcal/mol increase in excitation energy. Consequently, pressure dependence of CH_3T yields should be very difficult to observe, and none is indicated for either of the O_2 -scavenged butenes (Tables I and II) over a 15-fold range in pressure.³² The increase in CH_3T yield with H_2S (Table V)—therefore, the yield of CH_2T —is 1.0 ± 0.1 at 760 Torr and 1.5 ± 0.1 at 50 Torr for *cis*-2-butene (Table V). The corresponding differences for 1-butene are 2.9 ± 0.1 and 4.0 ± 0.1 , respectively. The CH_2T yields from 1-butene are substantially larger than from *cis*-2-butene and are clearly pressure dependent, indicating contributions from an additional mechanism. This second source of CH_2T radicals is the decomposition of parent $CH_2TCH_2CH=CH_2^*$ molecules, as in (15), a well-established



reaction for photolytically excited 1-butene molecules.³³ While substitution of tritium into other positions in 1-butene should also be expected, there

does not appear to be a corresponding increase in propylene-*t* from the scavenging by H_2S of allyl-*t*. This apparent lack could arise from (a) inefficient scavenging of allyl radicals by the almost thermoneutral reaction with H_2S , (b) lesser substitution per C-H bond in olefinic positions, or (c) lesser average energy deposition following substitution in olefinic C-H positions. The present data do not permit a choice among these alternatives.

At least one alternate minor decomposition path is also indicated for excited 1-butene molecules by the observation of $CH_2=CHT$ from the reaction of T^* with $CH_3CH_2CH=CD_2$, probably as illustrated in (16) and (17).¹³ (Decomposition of $CH_3CHTCH=CD_2^*$



could also lead to the formation of $CH_2=CHT$ by the same reaction sequence, but substitution onto the other two carbon positions should lead to vinyl-*t* radicals and an incremental yield of $CH_2=CHT$ in H_2S -scavenged systems.)

Excitation Energy of Butyl-*t* Radicals. Extensive studies have been made of the decomposition of excited alkyl radicals formed by the addition of H or D atoms to butenes, and the rate constants for thermal addition have been calculated for many combinations of initial isotopic hydrogen, identity of the bath molecule, and temperature of the bath molecule.¹⁴⁻²¹ For example, the *sec*-butyl-*t* radicals formed by H addition to 2-butene at 25° are known to decompose competitively with collisional stabilization in the pressure range ~ 5 Torr. The observation in our experiments of appreciable pressure dependence of yields in the vicinity of 500 Torr implies immediately that the decomposition rate constants for some molecules in this system are about 100 times faster than in the typical thermal system and that this extra excitation energy is the result of excess kinetic energy on the tritium atom at the time of addition to the olefin.

Detailed calculations are available for the rate constants for decomposition of butyl radicals formed by H or D addition to *cis*-2-butene when excited to energies as high as 60 kcal/mol.¹⁴⁻¹⁷ We have extended these calculations to higher energies for H and D and have also calculated the corresponding curve for T atom addition, as shown in Figure 8.²⁴ From these rate constants, we have also calculated in Table VI the incremental change in per cent decomposition for

(30) D. Seewald and R. Wolfgang, *J. Chem. Phys.*, **47**, 143 (1967).

(31) Y.-N. Tang and F. S. Fowland, *J. Phys. Chem.*, **72**, 707 (1968).

(32) With CH_3T^* from $T^* + CH_4$, about 10% change is observed over a pressure range of a factor of 30 (see ref 30).

(33) See, for example, J. P. Chesick, *J. Chem. Phys.*, **45**, 3934 (1966).

excited $sec\text{-C}_4\text{H}_9\text{T}^*$ radicals between 50 and 760 Torr.²⁴ These data show that the largest increments in such decomposition occur for rate constants of $10^9\text{--}10^{10}\text{ sec}^{-1}$ or excitation energies of roughly 55–85 kcal/mol. Since about 43.5 kcal/mol is always available from the exothermicity of the addition reaction,³⁴ the corresponding tritium kinetic energies are only about 10–40 kcal/mol. Above a tritium kinetic energy of 2 eV (90 kcal/mol total excitation energy), most (>80%) excited radicals decompose even at 760 Torr and hence contribute substantially to the yield of propylene-*t* at all pressures but very little to any observed dependence of this yield upon pressure. Similarly, with a tritium kinetic energy of 0.4 eV (53-kcal/mol total excitation energy) more than 80% of the radicals are stabilized even at 50 Torr pressure. From the approximately 59% (64.3 *n*-C₄H₉T vs. 44.2 propylene-*t*) stabilization of the *sec*-butyl-*t* radicals at 50 Torr pressure, a monoenergetic distribution of radical energies would correspond to a tritium kinetic energy of only about 0.6 eV. However, when coupled with the 67% stabilization (81.9 vs. 39.6) at 760 Torr, the data indicate a broad distribution of excitation energies with a median tritium kinetic energy of <0.5 eV and not more than 20–25% with $\geq 2\text{ eV}$.

Table VI: Calculated Per Cent Decomposition of C₄H₉T Radicals from *cis*-2-Butene at 50 and 760 Torr

Excitation energy, kcal/mol	k_E , sec ⁻¹	% decompn		Incremental % decompn (50–760 Torr)
		50 Torr	760 Torr	
49.8	7.4×10^7	6.9	0.5	6.4
53.5	2.0×10^8	16.3	1.2	15.1
61	1.1×10^9	51.9	6.5	45.4
71	6.5×10^9	86.6	29.4	57.2
81	2.5×10^{10}	96.1	61.3	34.8
91	7.4×10^{10}	98.7	82.7	16.0
101	1.8×10^{11}	99.4	92.1	7.3

The rates of decomposition for butyl radicals formed in 1-butene are slightly different²⁴ because of the slight energy changes between 1-butene and *cis*-2-butene. Nevertheless, a very similar conclusion is reached: the median kinetic energy of the tritium atom at addition is <0.5 eV.

Energy Ranges of Various Hot Reactions. The smooth variations of yields with pressure in these experiments suggest a broad distribution of excitation energies, corresponding to a broad distribution of tritium kinetic energies at reaction. However, this distribution is very different from that found with the energetic substitution reactions for the <0.5-eV median energy of the addition reaction is far lower than the 5 eV estimated for T-for-H in cyclobutane³⁵ or 6–8 eV for T-for-CH₃ in 1,3-dimethylcyclobutane.³⁶ While

the energetic addition reaction can take place at higher energies too, the bulk of the addition reactions found in nuclear recoil tritium systems are relatively low-energy processes occurring after the tritium atom has dropped below the threshold of the substitution reactions. This, of course, does not mean that the double bond is less reactive than C–H bonds at higher energies—the yields of *decomposed* radicals at 760 Torr (signifying 1–2 eV or more kinetic energy of tritium) are comparable to the cumulative yields observed for substitution at *all* eight C–H bonds (see Tables I and II).

The competition (Table III) between H₂S and *cis*-2-butene for T atoms obviously involves low-energy tritium atoms, for an increase in H₂S diminishes the yield of the “low”-energy addition product, *n*-C₄H₉T, without reducing the yield of the “high”-energy addition product, CH₃CH=CHT. An appreciable fraction of the recoil tritium atoms thus survive down into an energy region where the remaining reactions open to them are the competing processes of addition to an olefin or abstraction to form HT. Again, the abstraction reaction can also be initiated at higher energies and our experiments offer little information about the reaction probabilities at energies in the electronvolt region. However, the data of Figures 6 and 7 show reaction with O₂ competing with abstraction (falling yield of HT) but not with “energetic” addition (no change in yields of CH₃CH=CHT from *cis*-butene-*t* or of CH₂=CHT or CH₂TCH=CH₂ from 1-butene).

The yields of propylene-*t* and CH₂=CHT correspond crudely to the sum of the highest energy addition reactions to the asymmetric 1-butene and indicate that directional preferences in addition to double bonds are not very strong in the several electronvolts range.⁵ However, in the lower parts of the hot region terminal addition becomes measurably more probable than non-terminal addition; finally, of course, terminal addition is very heavily favored in the thermal region.

We are, of course, unable to distinguish the addition of thermal tritium atoms from the hypothetical addition of monoenergetic 0.2-eV atoms, since the *sec*-butyl-*t* radicals from either system are completely stabilized at 50 Torr pressure and are either observed as *n*-C₄H₉T in an H₂S-scavenged system or not measured at all in an O₂ system. The effective lower limit of 50 Torr for these experiments has been a practical one involving the necessity for “stopping” 192-keV tritons in the gas phase in bulbs of 2-cm diameter. Further progress in this low-pressure region could be made after substantial alterations in the neutron irradiation facili-

(34) This estimate is based upon the 40.0- and 41.8-kcal/mol exothermicities estimated for H + *cis*-2-butene and D + *cis*-2-butene, respectively. See ref 17.

(35) E. K. C. Lee and F. S. Rowland, *J. Amer. Chem. Soc.*, **85**, 897 (1963).

(36) C. T. Ting and F. S. Rowland, *J. Phys. Chem.*, **74**, 445 (1970).

ties to accommodate much larger irradiation vessels. With these changes, a more precise evaluation could be made of median kinetic energies of tritium atoms to olefins. The basic qualitative conclusion would,

however, remain unchanged—these addition processes are for the most part quite low-energy processes occurring well below the energy region in which substitution processes are observed for saturated positions.

Recoil Tritium Reactions with Cyclobutane- d_8 . Excitation Energies

Accompanying Substitution of Energetic Tritium for Deuterium¹

by Akio Hosaka and F. S. Rowland*

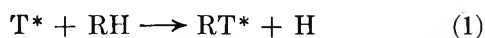
Department of Chemistry, University of California, Irvine, California 92664 (Received July 1, 1971)

Publication costs assisted by Division of Research, U. S. Atomic Energy Commission

The median residual excitation energy left on $c\text{-C}_4\text{D}_7\text{T}^*$ following the energetic substitution of T-for-D in $c\text{-C}_4\text{D}_8$ is essentially the same (± 0.2 eV) as for $c\text{-C}_4\text{H}_7\text{T}^*$ from T-for-H in $c\text{-C}_4\text{H}_8$ and is estimated to be 5 eV. The fraction of excited $c\text{-C}_4\text{D}_7\text{T}^*$ molecules which are collisionally stabilized is higher than for $c\text{-C}_4\text{H}_7\text{T}^*$ at the same pressure because of the fourfold faster decomposition of the protonated species for equal excitation energies. The per cent collisional stabilization is about 60 for $c\text{-C}_4\text{H}_7\text{T}^*$ and 67 for $c\text{-C}_4\text{D}_7\text{T}^*$ at 1 atm pressure. The per cent stabilization is about 83 in the liquid phase and 95 in the solid at -196° for both $c\text{-C}_4\text{H}_7\text{T}^*$ and $c\text{-C}_4\text{D}_7\text{T}^*$. The temperature effect on these decomposition reactions is $\leq 2\%$ over the range $24\text{--}125^\circ$.

Introduction

Energetic recoil tritium atoms can substitute for hydrogen atoms in all substrate molecules, as in (1), with



product yields which show both pressure and phase effects.²⁻⁵ The most important source of the yield changes found with variations in gas pressure arise from secondary decomposition of the excited RT^* molecules on a time scale competitive with collisional stabilization in this pressure range, *i.e.*, in most experiments, 0.1–5 atm—roughly 10^{-9} – 10^{-10} sec. Comparison of recoil tritium results with thermal pyrolysis studies of the same molecules has shown that the primary RT^* products are formed with a broad spread of excitation energies in the several electronvolts region,⁶⁻⁹ while a detailed study of cyclobutane showed that the median excitation energy in this system was approximately 5 eV.⁷ The T-for- CH_3 substitution reaction in 1,3-dimethylcyclobutane has shown an even higher (estimated 6–8 eV) median energy deposition following the replacement of this heavier group.¹⁰ Further, a series of similar experiments has established that high deposition energies are also commonly observed following the energetic reactions of both ^{18}F atoms¹¹⁻¹⁵ and ^{38}Cl or ^{39}Cl atoms,¹⁶ with excitation energies in some cases ≥ 10 eV.^{12,14,15}

We have now carried out studies with cyclobutane- d_8 to complement the earlier $c\text{-C}_4\text{H}_8$ experiments, thereby permitting evaluation of the isotope effects in these substitution reactions. The excited $c\text{-C}_4\text{D}_7\text{T}^*$ molecules formed by the initial substitution reactions can then undergo the competitive reactions of colli-

(1) This research has been supported by AEC Contract No. AT-(04-3)-34, Agreement No. 126.

(2) F. Schmidt-Bleek and F. S. Rowland, *Angew. Chem., Int. Ed. Engl.*, **3**, 769 (1964).

(3) R. Wolfgang, *Progr. React. Kinet.*, **3**, 97 (1965).

(4) R. Wolfgang, *Ann. Rev. Phys. Chem.*, **16**, 15 (1965).

(5) F. S. Rowland, "Molecular Beams and Reaction Kinetics," Academic Press, New York, N. Y., 1970, pp 108–138.

(6) B. Musgrave, J. K. Lee, and F. S. Rowland, *Can. J. Chem.*, **38**, 1760 (1960).

(7) E. K. C. Lee and F. S. Rowland, *J. Amer. Chem. Soc.*, **85**, 897 (1963).

(8) Y.-N. Tang and F. S. Rowland, *J. Phys. Chem.*, **72**, 707 (1968).

(9) C. T. Ting and F. S. Rowland, *ibid.*, **74**, 4080 (1970).

(10) C. T. Ting and F. S. Rowland, *ibid.*, **74**, 445 (1970).

(11) Y.-N. Tang and F. S. Rowland, *ibid.*, **74**, 4576 (1967).

(12) Y.-N. Tang, T. Smail, and F. S. Rowland, *J. Amer. Chem. Soc.*, **91**, 2130 (1969).

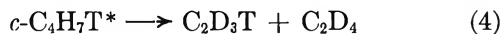
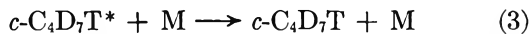
(13) C. McKnight and J. W. Root, *J. Phys. Chem.*, **73**, 4430 (1969).

(14) C. McKnight, N. J. Parks, and J. W. Root, *ibid.*, **74**, 217 (1970).

(15) K. A. Krohn, J. N. Parks, and J. W. Root, *J. Chem. Phys.*, in press.

(16) Y.-N. Tang, W. S. Smith, J. L. Williams, K. Lowery, and F. S. Rowland, *J. Phys. Chem.*, **75**, 440 (1971).

sional stabilization or decomposition to two molecules of ethylene, as summarized in eq 2-4. Evaluation of



the excitation energies of $c\text{-C}_4\text{D}_7\text{T}^*$ permits comparison of the residual energies left following substitution of T-for-D vs. T-for-H.

Experimental Section

Irradiations. The energetic recoil atoms were formed by standard thermal neutron irradiation procedures:²⁻⁵ (a) condensed phases, ${}^6\text{Li}(n,\alpha)\text{T}$ in capillaries containing LiF plus the substrate; (b) gas phase, ${}^3\text{He}(n,p)\text{T}$ on mixtures of ${}^3\text{He}$, substrate, and scavenger molecules in glass ampoules. The irradiations generally lasted for about 1 hr in a thermal neutron flux of $10^{11} \text{ n cm}^{-2} \text{ sec}^{-1}$. Most irradiations were carried out in the dry exposure room of the Hawthorne TRIGA reactor under conditions for which absolute yield determinations were not possible.

The 125° samples were irradiated in an oil bath kept at a temperature of $125 \pm 5^\circ$. The duplicates for this comparison were irradiated in an unheated oil bath at the same time, in order to keep neutron irradiation conditions as comparable as possible. The -196° samples were frozen and then irradiated while inside a large dewar of liquid nitrogen. The nitrogen level was depleted at an accelerated rate in the radiation field but visibly lasted to the end of the irradiation in some cases. No yield differences were observed for the others, and we believe that the sample temperatures remained at -196° for essentially the entire period of irradiation. Cyclobutane contained in capillaries with LiF remained visibly transparent when cooled to -78° with Dry Ice and is presumed to have been liquid during irradiation. (Literature values for the melting point vary from -50 to -90° .)

Chemicals. Cyclobutane (Merck Sharp and Dohme) contained less than 1% *n*-butane and was used without further purification. Cyclobutane- d_8 was supplied by Merck Sharp and Dohme and was stated to be 98% isotopically pure in deuterium. The most important impurities observed in $c\text{-C}_4\text{D}_8$ by gas chromatography were *n*-butane ($\sim 2\%$) and propane ($\sim 0.2\%$). The material was used with these hydrocarbon impurities present.

Sample Preparation. Samples were filled by the standard vacuum line procedures described earlier.²⁻⁵ While initial compositions of all samples were monitored by measurement of input gas pressures, the relative ratios of $c\text{-C}_4\text{H}_8$, $c\text{-C}_4\text{D}_8$, and CH_4 in mixtures with each other were determined by thermal conductivity measurements during the postirradiation analysis. The relative thermal conductivities used in this analysis

were determined as follows ($n\text{-C}_4\text{H}_{10} = 1.00$): $c\text{-C}_4\text{H}_8$, 0.936; $c\text{-C}_4\text{D}_8$, 0.867; CH_4 , 0.459.

Chromatographic Separation and Analysis. The various radioactive products were separated by gas chromatography and analyzed with an internal flow proportional counter in the standard manner.¹⁷ Most samples were analyzed with a 50-ft dimethyl sulfolane column or a 50-ft safrole column for the hydrocarbon peaks, while HT and/or DT was separated from methane-*t* with a second aliquot on a 50-ft PCA column (propylene carbonate on activated alumina).

Isotopic components were separately measured in samples containing both protonated and deuterated components by the following columns: (a) HT from DT, 8 ft of activated alumina preceded by a 12-ft buffer column of Chromosorb P; (b) $c\text{-C}_4\text{H}_7\text{T}$ from $c\text{-C}_4\text{D}_7\text{T}$, these peaks separate readily on the 50-ft safrole column; (c) $\text{CH}_2=\text{CHT}$ from $\text{CD}_2=\text{CDT}$, 200-ft column of AgNO_3 in ethylene glycol. No corrections have been made to the observed data for the estimated 16% $c\text{-C}_4\text{D}_7\text{H}$ in $c\text{-C}_4\text{D}_8$.

Results

Samples with Only One Hydrocarbon Present: $c\text{-C}_4\text{H}_8$ or $c\text{-C}_4\text{D}_8$. The distribution of radioactivity among the chief volatile products following recoil tritium reaction with $c\text{-C}_4\text{D}_8$ is shown in Table I, together with some concurrently measured samples of $c\text{-C}_4\text{H}_8$. In each case, the yields have been expressed relative to the sum of $c\text{-C}_4\text{D}_7\text{T} + \text{C}_2\text{D}_3\text{T}$ (or $c\text{-C}_4\text{H}_7\text{T} + \text{C}_2\text{H}_3\text{T}$) as 100. In the presence of O_2 scavenger in the gas phase, the only products with important yields are the abstraction product DT (or HT) and the complementary pair of cyclobutane-*t* plus ethylene-*t*. The addition of H_2S raises the yields of CH_3T and $\text{C}_2\text{H}_5\text{T}$, indicating the presence of moderate yields of CH_2T and $\text{C}_2\text{H}_4\text{T}$ radicals. The very small yield of $n\text{-C}_4\text{H}_9\text{T}$ indicates that a negligible yield of $n\text{-C}_4\text{H}_8\text{T}$ and $\text{sec-C}_4\text{H}_8\text{T}$ radicals can be found in the gas-phase samples. In the condensed phases—in the absence of a scavenger molecule—several products have increased yields, most notably that of *n*-butane-*t* in the solid phase. The much shorter time prior to stabilizing collisions substantially reduces the secondary decomposition of both $c\text{-C}_4\text{D}_7\text{T}^*$ and $c\text{-C}_4\text{H}_7\text{T}^*$ in the condensed phases, as shown by the diminished relative yields of $\text{C}_2\text{D}_3\text{T}$ and $\text{C}_2\text{H}_3\text{T}$.

The pressure and phase dependence of the yields of the three major products are summarized in Table II for $c\text{-C}_4\text{D}_8$ and $c\text{-C}_4\text{H}_8$ in concurrent experiments. The relative yield of cyclobutane-*t* for each of these experiments is displayed in Figure 1, together with the earlier $c\text{-C}_4\text{H}_8$ data of Lee and Rowland⁷ and some mixture experiments described below. The two sets of $c\text{-C}_4\text{H}_8$ data were measured in completely different laboratories,

(17) J. K. Lee, E. K. C. Lee, B. Musgrave, Y.-N. Tang, J. W. Root, and F. S. Rowland, *Anal. Chem.*, **34**, 741 (1962).

Table I: Observed Tritiated Products from Recoil Tritium Reactions with *c*-C₄H₈ and *c*-C₄D₈

Product ^b	Irradiation conditions ^a				Product ^b	Irradiation conditions ^a					
	<i>c</i> -C ₄ D ₈					<i>c</i> -C ₄ H ₈					
	266 gas	258 gas	Liquid	Solid ^c		277 gas	610 gas	259 gas	Liquid	Liquid	Solid ^c
	Other					Other					
	19 O ₂ 10 ³ He	19 O ₂ 10 ³ He	LiF	LiF		15 O ₂ 12 ³ He	66 H ₂ S 14 ³ He	15 O ₂ 12 ³ He	LiF	LiF	LiF
Temp., °C				Temp., °C							
24				24							
Rel yields ^d				Rel yields ^d							
<i>c</i> -C ₄ D ₇ T	61.8	61.7	83.7	95.2	<i>c</i> -C ₄ H ₇ T	52.9	57.0	52.6	82.0	83.1	94.6
C ₂ D ₃ T	38.2	38.3	16.3	4.8	C ₂ H ₃ T	47.1	43.0	47.4	18.0	16.9	5.4
DT	150	159	199	215	HT	154	259	186	213	207	241
CD ₃ T	0.6	0.2	4.4	5.0	CH ₂ T	0.1	16.0	0.4	6.5	4.7	4.5
C ₂ D ₅ T	0.2	0.1	9.5	8.3	C ₂ H ₅ T	0.1	15.1	0.3	10.8	11.0	8.3
C ₃ D ₇ T	0.3	0.4	1.9	1.9	C ₃ H ₇ T	0.6	0.4	0.4	1.6	2.2	1.9
<i>n</i> -C ₄ D ₉ T	1.7	1.8	13.0	54.1	<i>n</i> -C ₄ H ₉ T	0.4	1.0	0.2	11.2	13.0	46.6
CD≡CT	1.3	1.1	0.9	<0.5	CH≡CT	1.5	1.3	1.2	1.1	0.9	<0.5
C ₃ D ₅ T	0.7	0.6	2.2	1.0	C ₃ H ₅ T	1.0	1.0	1.2	1.6	1.8	0.4
1-C ₄ D ₇ T	1.5	1.4	8.8	10.4	1-C ₄ H ₇ T	1.5	2.3	1.7	7.0	11.1	11.6

^a Gas pressures in Torr. ^b Small yields (always <1.0) were also observed for *cis*-2-butene-*t*, *trans*-2-butene-*t*, and 1,3-butadiene-*t*. ^c Total radioactivity is considerably lower for solid samples because of lowered neutron flux inside the liquid nitrogen dewars. ^d Cyclobutane-*t* + ethylene-*t* = 100.

Table II: Relative Yields of Major Products from Recoil Tritium Reactions with *c*-C₄H₈ and *c*-C₄D₈

Phase	<i>c</i> -C ₄ H ₈ reactions			Phase	<i>c</i> -C ₄ D ₈ reactions		
	C ₄ H ₈ pressure, ^a Torr	Rel yields ^d			C ₄ D ₈ pressure, ^a Torr	Rel yields ^d	
		<i>c</i> -C ₄ H ₇ T	HT			<i>c</i> -C ₄ D ₇ T	DT
Gas, 24°	51	47.4 ± 0.6	172 ± 2	53	54.0 ± 0.7	146 ± 2	
	96 ^b	46.9 ± 0.3	276 ± 2	76	56.4 ± 0.7	151 ± 2	
	116	49.9 ± 0.5	160 ± 2	192	60.3 ± 0.5	151 ± 2	
	277	52.9 ± 0.3	155 ± 2	266	61.8 ± 0.5	150 ± 2	
	285	53.5 ± 0.3	157 ± 2	281	62.8 ± 1.3	146 ± 2	
	551	56.9 ± 0.4	164 ± 2	395	62.4 ± 0.5	145 ± 2	
	610 ^c	57.0 ± 0.3	259 ± 2	431	63.1 ± 0.5	144 ± 2	
Liquid, 24°	708	59.1 ± 0.4	165 ± 2	73 ^c	66.4 ± 0.6	150 ± 2	
		84.2 ± 0.7	198 ± 2		83.2 ± 0.6	200 ± 2	
		84.0 ± 0.6	207 ± 2		84.3 ± 0.7	205 ± 2	
		82.0 ± 0.6	213 ± 2		83.0 ± 0.7	197 ± 2	
Liquid, -78°		83.1 ± 1.0	207 ± 3		83.7 ± 0.8	199 ± 2	
Solid, -196°		94.4 ± 1.4	254 ± 4		95.0 ± 1.4	203 ± 3	
		94.7 ± 1.4	266 ± 4		94.5 ± 1.4	206 ± 3	
		92.5 ± 1.6	233 ± 4		95.7 ± 1.5	200 ± 3	
		94.6 ± 1.5	241 ± 4		95.2 ± 1.3	215 ± 3	

^a Gas samples also contained 10–14 Torr ³He and 13–24 Torr O₂, except as marked. ^b 15 Torr H₂S, no O₂. ^c 66 Torr H₂S, no O₂. ^d Cyclobutane-*t* + ethylene-*t* = 100.

albeit with the same basic techniques, and are in excellent agreement. The comparison of the data from the isotopic molecules shows clearly that the fractional stabilization of *c*-C₄D₇T* is greater than that for *c*-C₄H₇T* at all gas pressures, while being very nearly equivalent in the condensed-phase experiments.

Samples Containing Two Hydrocarbons in Competition. Since the spectrum of recoil tritium energies is controlled by collisions with the molecules of each system, the tritium atom spectra in *c*-C₄H₈ and *c*-C₄D₈ need not be the same. Indeed, measurements with methyl fluo-

ride^{18,19} and methane^{20,21} have shown that energy loss is about 20% greater for energetic tritium atoms in the protonated substrate than in the deuterated counterpart.

These variations in tritium fluxes have a direct influ-

(18) E. K. C. Lee and F. S. Rowland, *J. Amer. Chem. Soc.*, **85**, 2907 (1963).

(19) E. K. C. Lee, G. Miller, and F. S. Rowland, *ibid.*, **87**, 190 (1965).

(20) J. W. Root and F. S. Rowland, *J. Chem. Phys.*, **46**, 4299 (1967).

(21) J. W. Root and F. S. Rowland, *J. Phys. Chem.*, **74**, 451 (1970).

Table III: Yields of Major Products from Recoil Tritium Reactions in $c\text{-C}_4\text{H}_8$ - $c\text{-C}_4\text{D}_8$ Mixtures

Product	Gas pressure, Torr		
	481	326	105
$c\text{-C}_4\text{H}_8 + c\text{-C}_4\text{D}_8^a$	481	326	105
O_2	18	17	17
^3He	10	10	10
Obsd radioactivity counts above background			
$c\text{-C}_4\text{H}_7\text{T}$	21,640	8,690	16,710
$c\text{-C}_4\text{D}_7\text{T}$	15,440	6,280	12,040
$\text{CH}_2=\text{CHT}$	16,140	7,210	16,470
$\text{CD}_2=\text{CDT}$	8,770	3,800	9,280
HT	} 100,650	26,630	55,530
DT		15,440	30,660
Ratio			
$(c\text{-C}_4\text{H}_8)/(c\text{-C}_4\text{D}_8)^a$	1.11 ± 0.02	1.08 ± 0.02	1.15 ± 0.02
$[(c\text{-C}_4\text{H}_7\text{T} + \text{C}_2\text{H}_3\text{T})/(c\text{-C}_4\text{D}_7\text{T} + \text{C}_2\text{D}_3\text{T})]/[(c\text{-C}_4\text{H}_8)/(c\text{-C}_4\text{D}_8)]$	1.41 ± 0.07	1.47 ± 0.07	1.35 ± 0.08
$(c\text{-C}_4\text{H}_7\text{T})/(c\text{-C}_4\text{H}_7\text{T} + \text{C}_2\text{H}_3\text{T})$	0.573	0.547	0.504
$(c\text{-C}_4\text{D}_7\text{T})/(c\text{-C}_4\text{D}_7\text{T} + \text{C}_2\text{D}_3\text{T})$	0.683	0.623	0.565
$[(\text{HT})/(\text{DT})]/[(c\text{-C}_4\text{H}_8)/(c\text{-C}_4\text{D}_8)]$...	1.61^b	1.57^b

^a The relative composition of $c\text{-C}_4\text{H}_8$ and $c\text{-C}_4\text{D}_8$ was measured by thermal conductivity of observed mass peaks. ^b Uncorrected for $c\text{-C}_4\text{D}_7\text{H}$ impurity.

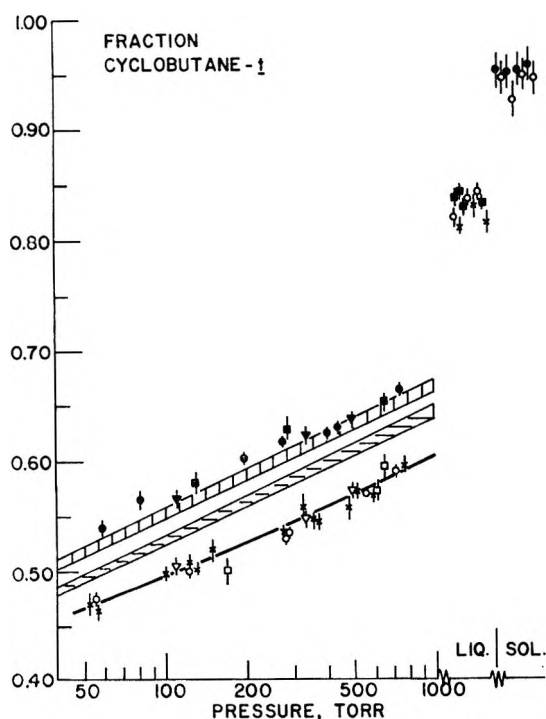


Figure 1. Fractional stabilization of excited cyclobutane- t molecules following energetic tritium atom substitutions: \circ , $c\text{-C}_4\text{H}_7\text{T}^*$ from $c\text{-C}_4\text{H}_8$; \bullet , $c\text{-C}_4\text{D}_7\text{T}^*$ from $c\text{-C}_4\text{D}_8$; \times , $c\text{-C}_4\text{H}_7\text{T}^*$ from $c\text{-C}_4\text{H}_8$; \square , $c\text{-C}_4\text{H}_7\text{T}^*$ from $c\text{-C}_4\text{H}_8\text{-CH}_4$ mixtures; \blacksquare , $c\text{-C}_4\text{D}_7\text{T}^*$ from $c\text{-C}_4\text{D}_8\text{-CH}_4$ mixtures; ∇ , $c\text{-C}_4\text{H}_7\text{T}^*$, and \blacktriangledown , $c\text{-C}_4\text{D}_7\text{T}^*$, both from $c\text{-C}_4\text{H}_8\text{-}c\text{-C}_4\text{D}_8$ mixtures; vertical crosshatching, predicted values for $c\text{-C}_4\text{D}_7\text{T}^*$ with same distribution of excitation energies as $c\text{-C}_4\text{H}_7\text{T}^*$; horizontal crosshatching, predicted values for $c\text{-C}_4\text{D}_7\text{T}^*$ with distribution of excitation energies of $c\text{-C}_4\text{H}_7\text{T}^*$ increased by 0.2 eV.

ence upon the *total* observed yields of substitution + decomposition products but need not have any effect at all on the fractional stabilization of excited molecules, which is dependent on the *fraction* of molecules formed with each energy and not at all on the total yield. Nevertheless, we have made several measurements of the major product yields in samples simultaneously containing both $c\text{-C}_4\text{H}_8$ and $c\text{-C}_4\text{D}_8$. In such mixtures, both molecules are exposed to the same recoil tritium atom flux and the fractional stabilizations have thus been measured for equivalent conditions. The results from three such mixture experiments are given in Table III.

The total substitution into $c\text{-C}_4\text{H}_8$ is 1.41 ± 0.04 times larger per molecule than into $c\text{-C}_4\text{D}_8$ under these competitive conditions, although the greater fractional decomposition of the protonated molecules reduces the observed $c\text{-C}_4\text{H}_7\text{T}/c\text{-C}_4\text{D}_7\text{T}$ ratio somewhat below this value in the gas phase. In the same systems, abstraction to form HT from $c\text{-C}_4\text{H}_8$ is 1.59 ± 0.04 times more probable than that to form DT from $c\text{-C}_4\text{D}_8$. The individual fractional stabilizations of $c\text{-C}_4\text{H}_7\text{T}^*$ and $c\text{-C}_4\text{D}_7\text{T}^*$ are both quite consistent with the values found for these molecules separately at the same total pressure, as shown in Figure 1.

Competitive experiments have also been conducted in mixtures with CH_4 for both $c\text{-C}_4\text{H}_8$ and $c\text{-C}_4\text{D}_8$ over the range of pressures shown in Table IV. A minor correction [0.5% \times sum of cyclobutane- t and ethylene- t for both $c\text{-C}_4\text{H}_8$ and $c\text{-C}_4\text{D}_8$] has been applied to the observed methane- t yields for the formation of methane- t by direct reaction of tritium atoms with cyclobutane. The specific activity ratios for total substitution into $c\text{-}$

Table IV: Relative Yields from Recoil Tritium Reactions in *c*-C₄H₈-CH₄ and *c*-C₄D₈-CH₄ Mixtures

	Gas pressure, Torr				Gas pressure, Torr		
	<i>c</i> -C ₄ H ₈	544	497		110	<i>c</i> -C ₄ D ₈	551
CH ₄	200	192	51	CH ₄	198	75	39
O ₂	21	25	30	O ₂	20	20	20
³ He	9	11	13	³ He	10	10	10
Obsd radioactivity, counts				Obsd radioactivity, counts			
<i>c</i> -C ₄ H ₇ T	56,440	46,980	70,480	<i>c</i> -C ₄ D ₇ T	57,780	39,980	36,080
C ₂ H ₅ T	38,290	35,130	70,590	C ₂ D ₅ T	30,790	23,940	25,740
CH ₃ T	16,450	15,540	28,900	CH ₃ T	22,090	13,530	15,330
CH ₃ T, cor	15,980	15,130	28,200	CH ₃ T, cor	21,640	13,210	15,020
HT	173,700	146,700	291,200	DT	144,000	110,500	101,100
Ratios				Ratios			
$I = \frac{(c\text{-C}_4\text{H}_7\text{T} + \text{C}_2\text{H}_5\text{T})}{(\text{CH}_3\text{T})}$	5.92	5.43	5.00	$I = \frac{(c\text{-C}_4\text{D}_7\text{T} + \text{C}_2\text{D}_5\text{T})}{(\text{CH}_3\text{T})}$	4.09	4.84	4.12
$I = \frac{(c\text{-C}_4\text{H}_8)^a}{(\text{CH}_4)}$	2.21	2.10	2.32	$I = \frac{(c\text{-C}_4\text{D}_8)^a}{(\text{CH}_4)}$	1.47	1.49	1.53

^a Mass ratio from filling pressures.

Table V: Temperature Dependence of Major Product Yields in Recoil Tritium Reactions with *c*-C₄H₈ and *c*-C₄D₈

	Sample compn, Torr						
	<i>c</i> -C ₄ H ₈	277	250	259	0	0	0
<i>c</i> -C ₄ D ₈	0	0	0	266	281	258	265
O ₂	15	16	15	19	18	19	18
³ He	12	12	12	10	10	10	10
Irradiation temp, °C							
	24	125	125	24	24	125	125
Rel product yields (cyclobutane- <i>t</i> + ethylene- <i>t</i> = 100)							
Cyclobutane- <i>t</i>	0.53	0.53	0.53	0.62	0.63	0.62	0.60
HT (or DT)	1.54	1.73	1.86	1.50	1.46	1.51	1.59

C₄H₈ and *c*-C₄D₈ vs. CH₄ are 2.20 ± 0.10 and 1.49 ± 0.04 , respectively. Cross comparison of these two ratios gives a value of 1.48 ± 0.07 for the primary reaction yields with *c*-C₄H₈ vs. *c*-C₄D₈, in good agreement with the 1.41 ± 0.05 obtained in the direct competition between the two cyclobutanes. Again, the observed fractional stabilizations of *c*-C₄H₇T* and *c*-C₄D₇T* are consistent with those found in other experiments at the same total pressure.

Several gas samples of each cyclobutane were also run under comparable conditions at both 24 and 125°, as shown in Table V. The statistical counting errors (1σ) are approximately ± 0.01 for the cyclobutane-*t* and ± 0.02 for HT (or DT).

Discussion

Possible Isotope Effects in Recoil Tritium Reactions. Several different kinds of high-energy isotope effects

have been identified and discussed in recoil tritium atom systems:²⁻⁵ (a) reactivity, varying probability of bond formation per collision of the tritium atom with a substrate molecule; (b) moderator, varying rates of energy loss in the nonreactive collisions of the tritium atom with the substrate molecules; (c) average energy, shifting maxima of probabilities for reaction with isotopic substitution in the substrate molecule. The reactivity isotope effects have been further divided into primary replacement isotope effects involving the substitution of tritium atoms for isotopic atoms and secondary isotope effects involving the influence of isotopic substitution at positions other than that of the atom being replaced by the energetic tritium atom. The reactivity and moderator isotope effects are of relatively lesser interest in this study, for they chiefly affect the total yield of labeled products and not the distribution of them between the stabilization and decomposition products of (3) and (4). Estimates of the average-energy isotope effect in CH₃F vs. CD₃F showed that it was small in that comparison and probably negligible in its effect in the present situation. This conclusion is substantiated by the agreement among fractional stabilizations found in pure cyclobutane systems and for the same molecule in mixtures with methane or with the isotopic cyclobutane.

One additional high-energy isotope effect and one isotope effect measurable in chemical activation systems are of importance in this study, with the former the primary focus of the experiment. The high-energy isotope effect involves the comparison of average or median energy depositions accompanying energetic T-for-H vs. T-for-D substitution reactions. These energy depositions are in turn related to the distribution of initial ki-

netic energies of the tritium atoms just prior to successful substitution, being essentially the difference in kinetic energies of the incoming tritium atom and the outgoing H or D atom. The other isotopic difference strongly affecting these experiments is the known effect of progressive deuterium substitution upon the rates of decomposition of excited molecules. Evaluation of the isotope effect in average energy deposition first requires correction of the observed data for this isotope effect upon decomposition rates.

Isotopic Variation in Decomposition Rates for Equal Excitation Energies. One method of making full correction for isotopic variation in rates of decomposition would involve the utilization of detailed RRKM calculations for $c\text{-C}_4\text{H}_7\text{T}$ and $c\text{-C}_4\text{D}_7\text{T}$ over the entire postulated range of excitation energies, coupled with particular postulated distributions of excited molecules *vs.* energy. In the absence of any precise knowledge of the real characteristics of such distributions, we have not made such a full-correction calculation but have instead chosen to make an empirical correction based on chemical activation experiments providing similar molecules with lifetimes of the same approximate 10^{-9} – 10^{-10} sec as those which are sensitive to the pressure changes in our gas-phase recoil experiments.

A detailed study has been reported for the isotope effects found in the competitive pyrolysis of $c\text{-C}_4\text{H}_8$ *vs.* $c\text{-C}_4\text{D}_8$, as summarized in the high-pressure equation $k_{\text{H}}/k_{\text{D}} = 0.75 \exp(900/RT)$ and the values of $k_{\text{H}}/k_{\text{D}}$ (all at 449°) of 1.41 ± 0.02 at 100 Torr pressure, 1.0 at about 0.08 Torr, and 0.83 at 0.005 Torr.²² These thermal studies, however, are themselves a mixture of isotope effects: the relative probabilities of activation to a certain energy by collision, the relative probabilities of deactivation—and the average energy losses—in a subsequent collision, and the rates of decomposition for a given excitation energy. The progressively decreasing $k_{\text{H}}/k_{\text{D}}$ values as the pressure is lowered reflect the slow shift from an (activation + deactivation + decomposition) composite isotope effect at high pressure to (activation + decomposition) at very low pressures. A separate measurement of the isotope effect in the decomposition step alone cannot readily be extricated from such thermal experiments.

A much more direct measurement of the isotope effects in decomposition rates can be obtained from chemical activation experiments, *e.g.*, the relative rates of loss of HCl from $\text{CH}_3\text{-CH}_2\text{Cl}$ *vs.* $\text{CH}_3\text{-CD}_2\text{Cl}$.^{23,24} No such experiments have been reported for cyclobutanes, but several experiments with hydrocarbons and halocarbons indicate $k_{\text{H}}/k_{\text{D}}$ effects of 1.2–1.3 per H/D difference in the isotopic molecules, or $(1.2\text{--}1.3)^7$ for $c\text{-C}_4\text{H}_7\text{T}$ *vs.* $c\text{-C}_4\text{D}_7\text{T}$. This crude estimate suggests that excited $c\text{-C}_4\text{H}_7\text{T}^*$ will decompose 3.6–6 times as rapidly as $c\text{-C}_4\text{D}_7\text{T}^*$ for equal excitation energies. This estimate has been confirmed by a chemical activation experiment involving the insertion of CHT (from $\text{CHT}=\text{CO}$ photol-

ysis) into $c\text{-C}_4\text{H}_8$ and $c\text{-C}_4\text{D}_8$. The experimental observations indicated that these nearly monoenergetic $c\text{-C}_4\text{H}_7\text{CH}_2\text{T}^*$ molecules decomposed approximately 3.7 times as rapidly as $c\text{-C}_4\text{D}_7\text{CHDT}^*$ molecules.²⁵ In similar experiments with methylcyclopropane and methylcyclopropane- d_3 , Simons and Rabinovitch measured $(k_{\text{H}}/k_{\text{D}})_{\text{structural}} = 4.2$ and $(k_{\text{H}}/k_{\text{D}})_{\text{geometrical}} = 4.5$.²⁶ The appropriate ratio of isotope rate constants is thus probably in the 3.7–4.5 range for 8 H/D differences, and should be about the $7/8$ power of these values for the 7 H/D differences between $c\text{-C}_4\text{H}_7\text{T}^*$ and $c\text{-C}_4\text{D}_7\text{T}^*$. We have accordingly estimated this isotopic rate ratio to be 3.4 ± 0.3 .

Median Excitation Energies for Cyclobutane-t Products. The observed $c\text{-C}_4\text{H}_7\text{T}^*$ data can be converted into a prediction for the "expected" results for $c\text{-C}_4\text{D}_7\text{T}^*$ data simply by shifting the fractional stabilization curve to a pressure lowered by a factor of 3.4 ± 0.3 , as shown by the vertical crosshatching on Figure 1. The agreement between the $c\text{-C}_4\text{D}_7\text{T}^*$ data and this prediction is quite good and has the following significance: within the available accuracy of corrections for differences in the secondary decomposition rates, the distributions of excitation energies for $c\text{-C}_4\text{H}_7\text{T}^*$ from T-for-H in $c\text{-C}_4\text{H}_8$ and for $c\text{-C}_4\text{D}_7\text{T}^*$ from T-for-D in $c\text{-C}_4\text{D}_8$ have essentially identical median values.

One hypothetical distribution which fits the $c\text{-C}_4\text{H}_7\text{T}$ data is shown in Figure 2.²⁷ An indication of the sensitivity of the predictions from such distributions can be obtained by shifting the entire distribution of Figure 2 upward by 0.2 eV, again correcting by the factor of 3.4 ± 0.3 in pressure for the slower decomposition of excited deuterated molecules. This prediction is shown by the horizontal crosshatching on Figure 1 and is obviously in poor agreement with the experimental results for $\text{T}^* + c\text{-C}_4\text{D}_8$. Actually, a slightly better fit²⁸ to the $c\text{-C}_4\text{D}_7\text{T}^*$ data than the vertical crosshatching can be obtained by shifting the $c\text{-C}_4\text{D}_7\text{T}^*$ spectrum down in energy by about 0.1 eV from that used for $c\text{-C}_4\text{H}_7\text{T}^*$. This difference is

(22) R. W. Carr, Jr., and W. D. Walters, *J. Amer. Chem. Soc.*, **88**, 884 (1966).

(23) D. Setser and B. S. Rabinovitch, *Advan. Photochem.*, **3**, 1 (1964).

(24) K. Dees and D. Setser, *J. Chem. Phys.*, **49**, 1193 (1968).

(25) At equal pressures, the measured rate constants are in the ratio $k_{\text{H}}/k_{\text{D}} = 3.66$ for $c\text{-C}_4\text{H}_8$ *vs.* $c\text{-C}_4\text{D}_8$. Correction for the greater frequency of collision in the lighter $c\text{-C}_4\text{H}_8$ leads to an estimated factor of 3.88 for equal collision densities. Our comparisons, however, are made for equal pressures and not equal collision densities, and 3.66 is the more appropriate figure: R. L. Russell and F. S. Rowland, unpublished results.

(26) J. W. Simons and B. S. Rabinovitch, *J. Phys. Chem.*, **68**, 1322 (1964).

(27) The distribution originally shown in ref 7 was based on an early RRK calculation of $k(E)$ *vs.* E . An RRKM fit to the data of ref 7 was calculated in the Ph.D. thesis of E. K. C. Lee, University of Kansas, 1963, and is illustrated in ref 3 and 5. Figure 2 has been modified to include no low-energy product molecules, consistent with the CH_2TNC^* experiments of ref 9.

(28) Only the lower pressure $c\text{-C}_4\text{D}_7\text{T}^*$ points are really tested by this fit, for the higher pressure $c\text{-C}_4\text{D}_7\text{T}$ yields correspond to those of $c\text{-C}_4\text{H}_7\text{T}^*$ at pressures above our measurement range.

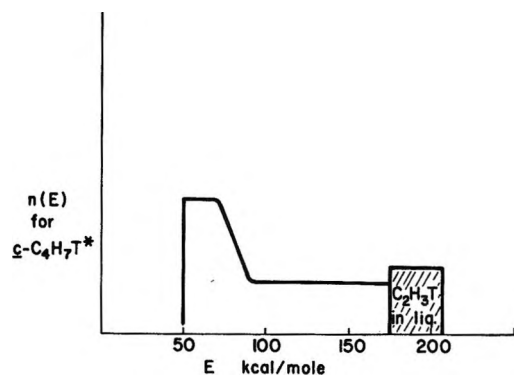


Figure 2. Hypothetical distribution of excited cyclobutane-*t* molecules *vs.* excitation energy. Crosshatched area indicates cyclobutane-*t* molecules which are excited enough to decompose to ethylene-*t* even in the liquid phase.

within the accuracy of our knowledge of the ratio of secondary decompositions $k_H/k_D = 3.4 \pm 0.3$.

The whole procedure for inferring excitation energy distributions from such hot-atom studies depends upon the not thoroughly justified assumption that the rates of decomposition of excited $c\text{-C}_4\text{H}_7\text{T}^*$ molecules are the same for equal excitation energies whether initially excited by thermolysis, by chemical activation, or by recoil substitution.²⁹ Nevertheless, even though the inference of 5 eV as the median excitation energy of $c\text{-C}_4\text{H}_7\text{T}^*$ in the recoil system is certainly open to quantitative questioning, the present experiments indicate that the median excitation energy for $c\text{-C}_4\text{D}_7\text{T}^*$ from T-for-D substitution is the same within about ± 0.2 eV as that for $c\text{-C}_4\text{H}_7\text{T}^*$ from T-for-H substitution—whatever value is accepted for the latter. This is simply equivalent to stating that, after the H/D correction for differences in decomposition rates is made directly from the chemical activation experiments, the results are then identical—without reference to the RRKM theory or any other theoretical model for converting variation of yields *vs.* pressure through $k(E)$ *vs.* E into a distribution of excitation energies.

Kinetic Energies of Displaced H or D atoms. Neither experimental measurements nor reliable theoretical estimates of the translational energies of the replaced atoms are yet available for such high-energy substitution reactions. An early experimental measurement showing no preference for substitution into CD_4 *vs.* CH_4 demonstrated that high kinetic energies for the displaced atoms—as in essentially two-body atom-atom collisions—should not be expected, *e.g.*, as in a “billiard ball” model for which the replacement of more nearly equal mass D should be sharply favored over H.³⁰ More accurate experiments have subsequently measured separately the various reactive and moderator effects present in RH *vs.* RD experiments and have shown that H replacement actually proceeds in higher yield than D.^{31–35} The ratio of 1.41 ± 0.05 in total

yield measurement found in the present experiments is in good agreement with earlier results.

Trajectory calculations for the three-particle substitution reaction $\text{T} + \text{RH} \rightarrow \text{RT} + \text{H}$, in which R is a structureless point of mass 15, have indicated substantial kinetic energies (as much as 50% or more of the initial kinetic energy) for the displaced H atoms when the reactions have been initiated by tritium atoms with 4-eV kinetic energy or higher.³⁶ However, a subsequent six-particle trajectory calculation for $\text{T}^* + \text{CH}_4$ has failed to substantiate some of the general conclusions of the three-particle calculations, while itself not satisfactorily accounting for some important facets of the known experimental data on the substitution reactions.³⁷ Significant conclusions from trajectory studies concerning the translational energies of replaced atoms require resolution of these present conflicts and difficulties.

An indirect measurement of any isotopic difference between E_H and E_D can be obtained from our experiments, for they indicate that the median excitation energies are the same for $c\text{-C}_4\text{H}_8$ and $c\text{-C}_4\text{D}_8$, *i.e.*, that the *difference* in kinetic energies of tritium and the replaced H or D atom are essentially identical. If this observation that $(E_{\text{T}^*} - E_H)_{\text{C}_4\text{H}_8} \cong (E_{\text{T}^*} - E_D)_{\text{C}_4\text{D}_8}$ is coupled with the observation that $(E_{\text{T}^*})_{\text{CH}_3\text{F}} \cong (E_{\text{T}^*})_{\text{CD}_3\text{F}}$ for the corresponding T-for-H and T-for-D reactions,^{18,19} the conclusion is reached that $E_H \cong E_D$ for H and D atoms replaced in isotopic molecules by energetic tritium atoms. While the estimate that $(E_{\text{T}^*} - E_H)_{\text{C}_4\text{H}_8} \cong (E_{\text{T}^*} - E_D)_{\text{C}_4\text{D}_8}$ is probably accurate to about ± 0.1 eV, no quantitative evaluation has yet been made for $(E_{\text{T}^*})_{\text{CH}_3\text{F}}$ *vs.* $(E_{\text{T}^*})_{\text{CD}_3\text{F}}$ in the methyl fluoride systems, depending as the experiment does on the absence of a shift in $[(\text{CH}_2\text{TF})/(\text{CD}_2\text{TF})]/[(\text{CH}_3\text{F})/(\text{CD}_3\text{F})]$ ratios with increasing moderator (and measured in each case indirectly against a third component, cyclobutane). Nevertheless, the postulated equivalence in translational energies of replaced H and D atoms suggests a further hypothesis—that the lack of difference between them arises naturally from the low, perhaps not much above thermal, energies of the displaced atoms emerging from these substitution reactions.

A simple hard-sphere calculation of energy trans-

(29) See, for example, the discussions of “non-RRKM” molecules and nonequilibrium decompositions: ref 5; J. N. Rynbrandt and B. S. Rabinovitch, *J. Chem. Phys.*, **54**, 2275 (1971).

(30) R. J. Cross and R. Wolfgang, *ibid.*, **35**, 2000 (1961).

(31) E. K. C. Lee, J. W. Root, and F. S. Rowland, “Chemical Effects of Nuclear Transformations,” Vol. 1, International Atomic Energy Agency, Vienna, 1965, p 55.

(32) T. Smail and F. S. Rowland, *J. Phys. Chem.*, **74**, 456 (1970).

(33) T. Smail and F. S. Rowland, *ibid.*, **74**, 1859 (1970).

(34) C. C. Chou and F. S. Rowland, *ibid.*, **75**, 1283 (1971).

(35) E. K. C. Lee and F. S. Rowland, *ibid.*, **74**, 439 (1970).

(36) P. J. Kuntz, E. M. Nemeth, J. C. Polanyi, and W. H. Wong, *J. Chem. Phys.*, **52**, 4654 (1970).

(37) D. L. Bunker and M. Pattengill, *ibid.*, **53**, 3041 (1970).

mitted to free monatomic atoms of mass 1 vs. 2 by an 8-eV tritium atom shows that the energy transferred to mass 2 is always higher at each collision angle by a factor of 1.28, with absolute energy differences ranging up to 1.68 eV and averaging 0.84 eV. Inasmuch as the actual substitution collisions would include chiefly the more "head-on" collisions, one can conclude that the median energy left after substitution simply does not reflect in any substantial manner the initial impulse that might be transmitted in a pseudo two-body T-H or T-D collision.

Decomposition in the Condensed Phases. Comparison of relative yields for recoil tritium experiments in gas- and liquid-phase experiments has shown that the most important parameter affecting observed yields is simply the increased collision density and the accompanying more rapid collisional deexcitation of excited molecules in the liquid phase.⁵ As shown in Table II, the ethylene-*t* yield is reduced in the liquid phase to $17 \pm 1\%$ for both *c*-C₄H₈ and *c*-C₄D₈. While other mechanisms can be postulated for the formation of ethylene-*t*,³⁸ e.g., $T^* + c\text{-C}_4\text{H}_8 \rightarrow \text{CH}_2\text{TCH}_2\text{CH}_2\text{CH}_2^* \rightarrow \text{CH}_2\text{TCH}_2^* \rightarrow \text{CHT}=\text{CH}_2$, the observation that the ethylene-*t* yields drop to 5% in the solid phase indicate that most of the liquid-phase ethylene-*t* arises from the expected pathway of secondary decomposition of cyclobutane-*t*. The diminution in ethylene-*t* yields between gas- and liquid-phase measurements is thus a direct measure of the fraction of excited cyclobutane-*t* molecules possessing lifetimes toward decomposition between about 10^{-10} and 10^{-12} sec. The corresponding energies lie roughly in the 6–8-eV range of excitation energies.

The significance of the absence of an isotopic difference in fractional stabilization is difficult to assess. The rate constants, $k(E)$, in the 10^{12} -sec⁻¹ range for an RRKM calculation with a C₄H₈ molecule must be extrapolated without experimental confirmation or test from the measured rate constants of chemical activation experiments in the 10^9 – 10^{10} -sec⁻¹ range. When coupled with the problems of nonequilibrium flow of energy in molecules at such excitation energies,³⁹ we have chosen not to attempt interpretations through such calculations. The isotopic rates of decomposition should have a smaller $k_{\text{H}}/k_{\text{D}}$ ratio than that appropriate for the 10^9 – 10^{10} -sec range, while the effect of isotopic substitution on nonequilibrium effects in decomposition is essentially an unexplored field.

Although we have no direct proof of the brief intermediacy of *c*-C₄H₇T* and *c*-C₄D₇T* in the solid-phase experiments, we believe that both the C₂H₃T and C₂-D₃T observed at -196° were chiefly formed by the same secondary decomposition processes found in the gas and liquid phases. The reported absence of tritium-labeled olefins in recoil tritium reactions with solid *n*-hexane has led to the suggestion that secondary decomposition processes are absent in the solid phase, thereby permitting much more straightforward mea-

surement of primary yields in such recoil tritium reaction systems.^{40,41} The nonzero yield of ethylene-*t* in these experiments is *not* consistent with this general postulate, although the 5% error in absolute yields incurred by neglect of ethylene-*t* would be much less important than in corresponding gas- or liquid-phase experiments. Too, preliminary solid-phase experiments with *n*-butane and *n*-pentane, involving relatively low total neutron dose, also show C₂ and C₃ tritiated olefinic products in yields comparable to the corresponding alkane-*t* molecules.⁴² Probably, the low yield of ethylene-*t* from solid cyclobutane reflects the relatively lower residual energy from T-for-H or T-for-D substitution reactions than for T-for-CH₃ and other heavy-group replacement reactions.

The crystalline cyclobutane lattice is clearly much more efficient (5% vs. 17%) than the liquid phase in preventing secondary decomposition of excited cyclobutane-*t* to ethylene-*t*. Probably this is just the result of much more efficient intermolecular energy transfer in the crystalline material. However, relatively few comparisons have yet been made of the reactions of recoil tritium atoms with saturated organic compounds in solid-phase systems,^{43,44} and it has not been established whether there are other important differences between crystalline and fluid surroundings for hot tritium reactions. For example, changes in the tritium atom energy loss spectra might occur with the switch in basic energy sinks from essentially bimolecular or termolecular collisions in the fluids to lattice collisions in the solid phase.

Isotope Effect in Substitution. Several measurements have established that the substitution of T-for-H is regularly favored over that of T-for-D by 25% or more in total yield.^{31–33} These experiments with cyclobutane provide an accurate additional measurement, especially since its decomposition product, ethylene, is a stable molecule which can be routinely measured without difficulty. The overall primary yield H/D isotope effect of 1.41 ± 0.05 is a composite effect involving both the primary replacement isotope effect of actual substitution for H vs. D and the secondary influence of the other H or D atom on the same carbon atom. Recent measurements of the primary replacement effect for re-

(38) The formation of small amounts of CHT=CH₂ from CH₃-CH₂CH=CD₂ has shown that the predominant mechanism (leading to CHT=CD₂) is not the exclusive ethylene-*t* forming reaction with 1-butene. See ref 35.

(39) See, for example, J. N. Rynbrandt and B. S. Rabinovitch, *J. Chem. Phys.*, **54**, 2275 (1971).

(40) E. N. Avdonina, D. S. Urch, and G. K. Winter, *Radiochim. Acta*, **12**, 215 (1969).

(41) E. N. Avdonina, *Khim. Vys. Energ.*, **4**, 291 (1970); *High Energy Chem. (USSR)*, **4**, 253 (1970).

(42) F. Steinkruger, E. Metz, and F. S. Rowland, unpublished results.

(43) W. J. Hoff and F. S. Rowland, *J. Amer. Chem. Soc.*, **79**, 4867 (1957).

(44) M. Menzinger and R. Wolfgang, *J. Phys. Chem.*, **72**, 1789 (1968).

coil tritium reactions with isobutane³² and fluoroform³³ show factors of 1.25 ± 0.05 and 1.35 ± 0.05 , respectively, for this effect alone, while the trend of secondary effects is also to favor substitution at $-\text{CH}_2-$ rather than $-\text{CD}_2-$.

Isotope Effect in Abstraction. Other comparisons have been made of the relative yields for abstraction of H and D from isotopic molecules and have uniformly shown higher yields from protonated positions. The magnitude of this isotope effect increases from 1.32 ± 0.01 with CH_2D_2 to about 1.65 ± 0.06 for the H/D effect at the tertiary position of isobutane [$(\text{CH}_3)_3\text{C}-\text{H}$ vs. $(\text{CH}_3)_3\text{C}-\text{D}$]. An intermolecular isotope effect of 1.53 ± 0.04 is calculated for the abstraction reaction with the cyclobutanes from the experimental data of Table III.⁴⁵ This value is quite consistent with the trend in bond dissociation energies of the protonated species: CH_3-H , 104 ± 1 kcal/mol; $c\text{-C}_4\text{H}_7-\text{H}$, 95 ± 3 kcal/mol; $(\text{CH}_3)_3\text{C}-\text{H}$, 91 ± 1 kcal/mol.⁴⁶ Both the trends toward higher yield and larger H/D isotope effect with abstraction from weaker C-H bonds are consistent with the low-energy cutoff model for abstraction reactions, in which the bulk of the abstraction reactions occur at energies in the range below that at which most substitution reactions occur.⁴⁷⁻⁴⁹

Temperature Dependence of Substitution Yields. The 5-10-eV excitation energies of the $c\text{-C}_4\text{H}_7\text{T}^*$ and $c\text{-C}_4\text{D}_7\text{T}^*$ molecules must be furnished chiefly from the translational kinetic energy of the tritium atom, and the influence of any initial energy of the substrate molecules is a much less important factor, sufficiently less that temperature effects have been of relatively small concern in the investigations of recoil tritium chemistry. As part of a general reassessment of temperature effects in recoil tritium reactions^{50,51} the duplicate cyclobutane samples of Table V were irradiated at 24 and 125°. The data show that the fractional stabilization of both $c\text{-C}_4\text{H}_7\text{T}^*$ and $c\text{-C}_4\text{D}_7\text{T}^*$ is essentially unaffected by the change in temperature. If the hot substitution reaction is postulated to occur by a path essentially independent of the thermal excitation of the substrate molecule, then one might still expect secondary effects attributable to the increased internal energy of the substrate at the higher temperature. Since the heat content of cyclobutane at constant volume is approximately 2 kcal/mol higher at 125° than at 24°, an estimate of the expected effect upon the substitution reaction can be simply made by displacing the entire spectrum of Figure 2 upward by 2 kcal/mol. The predicted effect of such a shift is approximately 1% more decomposition over the gas pressure range used in Figure 1, *e.g.*, from 53 to 52% stabilization for a given collision frequency at 24 and 125°. Further complications are involved because the 34% increase in temperature is accompanied by a 16% increase in collision frequency for a fixed density, together with the uncertain effects of temperature upon the average energy loss per collision—and thus upon the stabilizing

properties of the gases. In any event, the overall predicted shift is at the marginal limits of our experimental error in measurement of the fractional stabilization of cyclobutane molecules. Both the prediction and the measurement indicate no temperature effect on these substitution reactions larger than the experimental error in present measurements. By implication the initial assumption that the *hot* primary substitution reaction is essentially independent of the excitation of the substrate molecule is also confirmed. A measurable temperature effect on yields has been observed for the addition reaction of energetic tritium to 1-butene and to *cis*-2-butene over the same temperature range, but the average initial tritium energy for the addition reaction is only 0.4 eV or less.⁵⁰

A temperature effect is observed on the abstraction of H from $c\text{-C}_4\text{H}_8$, together with a much lesser effect on the removal of D from $c\text{-C}_4\text{D}_8$. Similar observations have been made with other alkanes⁵¹ (except methane) and are consistent with the bond dissociation energies of the bonds involved: more temperature effect is observed for weaker C-H bonds. However, the abstraction reaction is much more sensitive to the details of the scavenging reactions in each experimental system,²⁻⁵ and the experiments of Table V are too meager for any detailed consideration of the temperature effects on the abstraction reactions.

Radical-Forming Reactions. The formal counterpart with the cyclanes of the T-for-R reaction regularly observed with alkanes (*e.g.*, $\text{T}^* + \text{C}_3\text{H}_8 \rightarrow \text{C}_2\text{H}_5\text{T} + \text{CH}_3$) is the ring-opening reaction (eq 5).⁵² The re-



placement of CH_3 by an energetic tritium atom in an alkane usually leaves a product molecule excited to 6-8 eV or more.¹⁰ Such an excitation energy for the $n\text{-C}_4\text{H}_8\text{T}^*$ radical of (5) is far more energy than necessary for secondary decomposition reactions, and H_2S scavenging of the $c\text{-C}_4\text{H}_8$ system (Table I) showed only a negligible increase in the yield of the $n\text{-C}_4\text{H}_8\text{T}$ product expected if appreciable quantities of $n\text{-C}_4\text{H}_8\text{T}$ radicals were stabilized prior to decomposition. The marked

(45) Assuming that only 98% of the hydrogen atoms in $c\text{-C}_4\text{D}_8$ are actually D, about 2% of the nominally D—but actually H in $\text{C}_4\text{D}_7\text{H}$ molecules—are contributing to HT and not DT, for a 4% correction factor.

(46) J. A. Kerr, *Chem. Rev.*, **66**, 465 (1966).

(47) J. W. Root, W. Breckenridge, and F. S. Rowland, *J. Chem. Phys.*, **43**, 3694 (1965).

(48) E. Tachikawa and F. S. Rowland, *J. Amer. Chem. Soc.*, **90**, 4767 (1968).

(49) E. Tachikawa and F. S. Rowland, *ibid.*, **91**, 559 (1969).

(50) R. Kushner and F. S. Rowland, *ibid.*, **91**, 1539 (1969).

(51) R. Kushner, A. Hosaka, and F. S. Rowland, Abstracts, 158th National Meeting of the American Chemical Society, Atlantic City, N. J., Sept 1969.

(52) A detailed study of the ring-opening reaction was carried out with the *cis*- and *trans*-1,2-dimethylcyclopropanes as the substrate molecules: Y.-N. Tang and F. S. Rowland, *J. Phys. Chem.*, **69**, 4297 (1965).

increases in CH_3T and $\text{C}_2\text{H}_5\text{T}$ with H_2S probably reflect the formation of CH_2T and $\text{C}_2\text{H}_4\text{T}$ through the decomposition of $n\text{-C}_4\text{H}_8\text{T}^*$ by loss of C_3H_6 and C_2H_4 , respectively. On the other hand, the large yields of n -butane- t in solid-phase experiments probably indicate the stabilization (and then immobilization in the solid lat-

tice) of some $n\text{-C}_4\text{H}_8\text{T}$ radicals; since H atoms can still diffuse in solid lattices at -196° , combination of $n\text{-C}_4\text{H}_8\text{T}$ with H is more highly favored in the solid than in liquid experiments for which the radicals themselves are quite mobile and can recombine with one another instead of with H atoms.

On the Accuracy of Theories of the Primitive Model of Ionic Solutions^{1a}

by Robert W. Jones^{1b}

Department of Physics, University of South Dakota, Vermillion, South Dakota 57069, and Physics Division, Oak Ridge National Laboratory, Oak Ridge, Tennessee 37830

and Franz Mohling

Department of Physics and Astrophysics, University of Colorado, Boulder, Colorado 80302 (Received January 26, 1971)

Publication costs assisted by the U. S. Atomic Energy Commission under contract with Union Carbide Corporation and the University of Colorado

The accuracy of theories of the primitive model of ionic solutions is discussed. An alternative solution from grand canonical ensemble theory, which is an expansion in terms of the fugacity rather than the density, is given and is shown to be rapidly convergent up to moderate concentrations (1.0 M). The results are compared with earlier theories based on density expansions, such as the Debye-Hückel limiting law, and with experimental activity coefficient data.

I. Introduction

Since the original work of Debye and Hückel,² the statistical theory of the primitive model of ionic solutions has been developed to considerable maturity.³ [In the primitive model the ionic solution is represented by charged hard spheres in an ideal dielectric fluid.] By application of classical statistical mechanics, Mayer⁴ extracted the Debye-Hückel limiting law as a low-density, high-temperature limit of the full theory. This amounts essentially to keeping only the lowest order term (beyond the perfect gas term) in an infinite series in terms of powers (and logarithms) of the density. Subsequent workers⁵ have derived the next higher order term in the density. Thus estimates of the practical rate of convergence of the theory are possible. Put another way, one can determine the concentration range for which the Debye-Hückel limiting law is an accurate solution to the primitive model of point ions. Other terms in the Mayer theory give corrections to the Debye-Hückel limiting law due to finite ion sizes. Poirier⁶ has evaluated these terms for various electrolytes in aqueous solution by fitting an ion-size parameter (the sum of the hard-sphere radii) to the experimental data. The viewpoint of the present paper is that finite-size corrections should be based

on a more accurate theory of the primitive model of point ions than the Debye-Hückel limiting law.

Of course, the primitive model may not correspond very well to real ionic solutions at moderate concentrations (say, 1 M). But, to find which additional features of real solutions should be included in a model description, one must at least be sure of having an accurate solution to the primitive model. Friedman and Rasaiah⁷ have addressed themselves to this point and have found accurate solutions to the primi-

(1) (a) Research supported in part by grants from the National Science Foundation and in part by the U. S. Atomic Energy Commission under contract with Union Carbide Corp. (b) Correspondence should be addressed to Department of Physics, The University of Arizona, Tucson, Ariz. 85721. Consultant with ORNL Physics Division, summer 1970. On leave from University of South Dakota, 1971-1972.

(2) P. Debye and E. Hückel, *Phys. Z.*, **24**, 185, 305 (1923).

(3) H. L. Friedman, "Ionic Solution Theory," Interscience, New York, N. Y., 1962.

(4) J. E. Mayer, *J. Chem. Phys.*, **18**, 1426 (1950).

(5) (a) R. Abe, *Progr. Theor. Phys.*, **22**, 213 (1959); E. Meeron, *Phys. Fluids*, **1**, 139 (1958); H. L. Friedman, *Mol. Phys.*, **2**, 23 (1959); (b) H. E. DeWitt, *J. Math. Phys.*, **7**, 616 (1966).

(6) J. C. Poirier, *J. Chem. Phys.*, **21**, 965, 972 (1953).

(7) (a) H. L. Friedman and J. C. Rasaiah, *ibid.*, **48**, 2742 (1968); **50**, 3965 (1969); (b) J. C. Rasaiah, *ibid.*, **52**, 704 (1970).

tive model of charged hard spheres by an integral equation method.

The purpose of the present paper is to point out an alternative approach to the question of an accurate solution to the primitive model at moderate concentrations. The approach is grand canonical ensemble statistical mechanics, the result of which is an infinite series in the fugacity rather than the density. It is shown that the first term beyond the perfect gas term (*i.e.*, the term corresponding to the Debye-Hückel limiting law in the density expansion) is an accurate solution to the primitive model for *point* ions. This is seen by an evaluation of the next most important term which is found to amount to about a 7% correction to the mean activity coefficient of a 1 *M* aqueous solution of 1-1 electrolyte at room temperature.

Section II of this paper is an outline of some of the main developments in the theory of the primitive model of ionic solutions. Special emphasis is placed on the character of these solutions as density expansions. In section III, the fugacity expansion from grand canonical ensemble statistical mechanics is presented, and comparison with experiment is discussed.

II. The Standard Results

The original statistical theory of ionic solutions is that of Debye and Hückel² in which a Poisson-Boltzmann equation is solved for the charge distribution about a given ion in the solution. All the thermodynamic functions are then calculated from the resulting electrostatic interactions. For example, the limiting law result for the Helmholtz free energy F of the ions is

$$F - F_0 = -kTV\kappa^3/12\pi \quad (2.1)$$

where F_0 is the free energy of a perfect gas, V is the volume of the system, k is Boltzmann's constant, T is the temperature in °K, and κ is the inverse Debye length defined by

$$\kappa^2 = \frac{4\pi e^2}{\epsilon kT} \sum_{\alpha} n_{\alpha} Z_{\alpha}^2 \quad (2.2)$$

Here, $n_{\alpha} = N_{\alpha}/V$ is the number density of ions of type α , ϵ is the dielectric constant of the solvent, and Z_{α} is the charge of an α -type ion in units of e . The quantity e is the electronic charge in electrostatic units.

It is convenient to introduce a parameter Λ_{α} which is a measure of the average electrical potential energy between the ions of type α relative to their thermal energy. Specifically

$$\Lambda_{\alpha} = Z_{\alpha}^2 e^2 \kappa / \epsilon kT$$

In terms of Λ_{α} , eq 2.1 can be written

$$F - F_0 = -kTV \sum_{\alpha} n_{\alpha} \Lambda_{\alpha} / 3 \quad (2.3)$$

The Debye-Hückel limiting law, eq 2.1, is applicable to very dilute solutions where the electrical interactions are small compared with kT . The limitation is due mainly to the approximations made in the Debye-Hückel theory and is borne out by the poor agreement with experiment for all but very dilute solutions (see Figure 1). But, putting agreement with experiment aside temporarily, we would like to know how accurately eq 2.1 solves the model problem at hand, *i.e.*, the primitive model of point ions. One way to answer this question is to study the problem from a more rigorous standpoint where corrections to the Debye-Hückel limiting law can be evaluated.

Mayer and subsequent workers have applied classical statistical mechanics to ionic solutions. By summing a certain class of diagrams, Mayer⁴ derived the Debye-Hückel result in the low-density, high-temperature limit. Later, Abe^{5a} derived the next higher order term in the low-density limit for the case of an electron gas in a uniform, neutralizing background. His result is

$$F - F_0 = -NkT \left[\frac{\Lambda}{3} + \frac{\Lambda^2}{12} \times \left(\ln 3 + 2c - \frac{11}{6} + \ln \Lambda \right) + O(\Lambda^3) \right] \quad (2.4)$$

where c is Euler's constant = 0.577... Note that Λ is proportional to the square root of the ion density; thus eq 2.4 is a series in the density. Abe goes on to make plausible that the general series for $F - F_0$ retains the features of eq 2.4, *i.e.*, that it is a double infinite series in Λ and $\ln \Lambda$.

DeWitt^{5b} has shown that for a two-component plasma, a result similar to eq 2.4 holds, *i.e.*, a series in quantities Λ (and $\ln \Lambda$) defined for the ions involved.

We are now in a position to investigate the question of convergence of this theory. Since $F - F_0$ is a series in Λ and $\ln \Lambda$, the accuracy of the Debye-Hückel limiting law depends on Λ being very small. Unfortunately, Λ is small only for very dilute solutions. For a 0.2 *M* concentration of 1-1 electrolyte in water at room temperature, $\Lambda \approx 1$. Thus, the series (2.4) cannot be trusted to give accurate numerical values for concentrations above about 0.2 *M*.

One way of comparing eq 2.1 or 2.4 with experiment is through the measured activity coefficients γ_{α} defined by

$$\ln \gamma_{\alpha} = \frac{1}{kT} (\mu_{\alpha} - \mu_{\alpha}^{\circ}) \quad (2.5)$$

where μ_{α} is the chemical potential of α -type ions and μ_{α}° is the chemical potential of a perfect gas of α -type ions. The difference is derived from the free energy by means of the relation

$$(\mu_{\alpha} - \mu_{\alpha}^{\circ}) = \left[\frac{\partial (F - F_0)}{\partial N_{\alpha}} \right]_{V,T} \quad (2.6)$$

From eq 2.1, 2.2, 2.5, and 2.6, then, we can write

$$\ln \gamma_{\alpha} = \sqrt{\pi} \left(\frac{e^2}{\epsilon k T} \right)^{3/2} Z_{\alpha}^2 \left(\sum_{\beta} n_{\beta} Z_{\beta}^2 \right)^{1/2} = -^{1/2} \Lambda_{\alpha} \quad (2.7)$$

as another form of the Debye-Hückel limiting law.

For 1-1 electrolytes, the quantity measured is

$$\gamma_{\pm} = (\gamma_{+} \gamma_{-})^{1/2}$$

where the two values of α , + and -, designate the positive and negative ions, respectively. From eq 2.7 one finds the Debye-Hückel limiting law for γ_{\pm} to be

$$\ln \gamma_{\pm} = -^{1/2} \Lambda \quad (2.8)$$

where $\Lambda_{+} = \Lambda_{-} = \Lambda$.

Applying eq 2.5 and 2.6 to Abe's (single component) electron-gas result (eq 2.4) gives

$$\ln \gamma = - \left[\frac{\Lambda}{2} + \frac{\Lambda^2}{6} \times \left(\ln 3 + 2c - \frac{19}{12} + \ln \Lambda \right) + O(\Lambda^3) \right] \quad (2.9)$$

Again, the accuracy of the solutions 2.8 and 2.9 to the primitive model of point ions depends on the parameter Λ being small. The corresponding restriction on the concentration of 1-1 electrolytes as discussed above, is to a range below about 0.2 M where $\Lambda \approx 1$.

The unsuitability of the density-expansion solution to the primitive model for moderate concentrations (0.1 to 1.0 M) is well known. Friedman and Rasaiyah^{7a} pointed out that, while the primitive model may not correspond very well to real ion solutions at moderate concentrations, it is nevertheless important to have an accurate solution of this model problem. Only then can one judge which features of real ionic solutions should be incorporated in a model description which is an improvement on the primitive model. Thus, Friedman and Rasaiyah⁷ have applied an integral equation method to ionic solutions. They find their solutions to the primitive model to be accurate up to 1.0 M . In the next section we present an alternative solution to the point-ion model problem which is both accurate for moderate concentrations (1.0 M) and whose leading term is just as simple in form as the Debye-Hückel limiting law.

III. Grand Canonical Ensemble Results

If the thermodynamics of ionic solutions are calculated using the statistical mechanics of the grand canonical ensemble, the result is a series for the grand potential f in terms of the fugacity. [We are using the notation $fV = PV/kT = \ln Z_G$ where Z_G is the grand partition function.] The fugacity of ions of type α is defined in terms of the chemical potential μ_{α} of ions of type α as

$$\partial_{\alpha} = e^{\mu_{\alpha}/kT} \quad (3.1)$$

The thermodynamics are obtained from the grand potential by taking various partial derivatives. For example, the density of α -type ions is

$$n_{\alpha} = \partial_{\alpha} \left(\frac{\partial f}{\partial \partial_{\alpha}} \right)_{T,V} \quad (3.2)$$

We consider the following three terms in the grand potential, in increasing order in the fugacity

$$f = f_0 + f_{DH} + f_A + (\text{terms of higher order in } \partial) \quad (3.3)$$

The term f_0 is the perfect gas term; the other terms are, respectively, those which lead in the zero-density limit to the Debye-Hückel limiting law and to the Abe term in the classical electron gas result (eq 2.4).

We first note that

$$f_0 = \sum_{\alpha} (2s_{\alpha} + 1) \frac{\partial_{\alpha}^3}{\lambda_{\alpha}^3} \quad (3.4)$$

where s_{α} is the spin of α -type ions, λ_{α} is the thermal wavelength of α -type ions defined by

$$\lambda_{\alpha} = \frac{h^2}{2\pi m_{\alpha} k T} \quad (3.5)$$

h is Planck's constant and m_{α} is the mass of α -type ions. If we define $\partial_{\alpha}^{(0)}$ as the fugacity of a perfect gas of α -type ions, then from eq 3.2 and 3.4

$$n_{\alpha} = (2s_{\alpha} + 1) \frac{\partial_{\alpha}^{(0)3}}{\lambda_{\alpha}^3} \quad (3.6)$$

Vedenov and Larkin⁸ have calculated the next higher order term f_{DH} . Including factors $(2s_{\alpha} + 1)$ which arise from a quantum-mechanical calculation, the result is

$$f_{DH} = ^{2/3} \sqrt{\pi} \left(\frac{e^2}{\epsilon k T} \right)^{3/2} \times \left(\sum_{\alpha} (2s_{\alpha} + 1) \frac{\partial_{\alpha}^3 Z_{\alpha}^2}{\lambda_{\alpha}^3} \right)^{1/2} = \frac{\kappa'^3}{12\pi} \quad (3.7)$$

where

$$\kappa' = \left[\frac{4\pi e^2}{\epsilon k T} \sum_{\alpha} (2s_{\alpha} + 1) \frac{\partial_{\alpha}^3 Z_{\alpha}^2}{\lambda_{\alpha}^3} \right]^{1/2} \quad (3.8)$$

is the inverse Debye length with n_{α} replaced by $(2s_{\alpha} + 1) \partial_{\alpha} / \lambda_{\alpha}^3$. Of course, s_{α} , the spin of an α -type ion, is zero in the present classical context. We include the factor $(2s_{\alpha} + 1)$ here for completeness since it is required in the definition of κ' in quantum-statistical mechanics. Inclusion of f_0 and f_{DH} in f , and the application of eq 3.2, gives

(8) A. A. Vedenov and A. I. Larkin, *Sov. Phys.-JETP*, 9, 866 (1959).

$$n_{\alpha} = (2s_{\alpha} + 1) \frac{\partial_{\alpha}}{\lambda_{\alpha}^3} \left[1 + \sqrt{\pi} \left(\frac{e^2}{\epsilon k T} \right)^{3/2} Z_{\alpha}^2 \times \right. \\ \left. \left(\sum_{\beta} (2s_{\beta} + 1) \frac{\partial_{\beta}}{\lambda_{\beta}^3} Z_{\beta}^2 \right)^{1/2} \right] + 0(\partial^2) = \\ (2s_{\alpha} + 1) \frac{\partial_{\alpha}}{\lambda_{\alpha}^3} \left[1 + \frac{\Lambda_{\alpha}'}{2} \right] + 0(\partial^2) \quad (3.9)$$

where

$$\Lambda_{\alpha}' = \frac{e^2 Z_{\alpha}^2 \kappa'}{\epsilon k T} \quad (3.10)$$

is the same as Λ_{α} with κ replaced by κ' .

Now, we give some discussion of this result. It can be used to provide an expression for the activity coefficients γ_{α} . From definitions 2.5 and 3.1, and noting that the chemical potential of μ_{α}° of a perfect (spinless) gas is $kT \ln n_{\alpha} \lambda_{\alpha}^3$, we can write

$$\gamma_{\alpha} = \partial_{\alpha} / n_{\alpha} \lambda_{\alpha}^3 \quad (3.11)$$

Thus, from eq 3.9, setting $s_{\alpha} = 0$

$$\gamma_{\alpha} = [1 + \Lambda_{\alpha}'/2]^{-1} + 0(\partial) \quad (3.12)$$

In the zero-density limit where $\Lambda_{\alpha}' \rightarrow \Lambda_{\alpha} \ll 1$, eq 3.11 reduces to eq 2.7. Thus, $f = f_0 + f_{DH}$ does indeed give rise to the Debye-Hückel limiting law in the zero-density limit.

However, eq 3.12 as it stands provides an *alternative* to the Debye-Hückel limiting law for *moderate* concentrations. The activity coefficient γ_{\pm} for an aqueous solution of 1-1 electrolyte at room temperature obtained by use of eq 3.12 is graphed *vs.* concentration in Figure 1. It is the GCE curve labeled DH. See Appendix B for the details of obtaining this curve from eq 3.12.

To estimate the accuracy of eq 3.12 as a solution to the primitive model of point ions, we estimate the size of some of the higher order terms. Grandy^{9,10} has given an exhaustive quantum-statistical evaluation of all the terms in the grand potential through fifth order in the electronic charge. These $O(e^6)$ terms include f_{DH} as well as $O(\partial^2)$ and higher corrections. We have estimated the $O(\partial^2)$ terms to contribute about 0.35% relative to the $O(\partial^{3/2})$ term to γ_{\pm} for a 1 M aqueous solution of NaCl at room temperature (see Appendix A for the details). Thus, $f_0 + f_{DH}$ is an accurate approximation to f considering only contribution of order e^6 and lower.

More recently, Grandy¹¹ has made an extensive and careful analysis of those $O(e^6)$ terms in the quantum-statistical grand potential which might give, in the classical limit, Abe's $\Lambda^2 \ln \Lambda$ term of eq 2.4. He has concluded that although $O(e^6)$ logarithmic terms do indeed occur in the free energy, these are very difficult to identify unambiguously. In the classical limit, however, he obtains a term in the grand potential f

corresponding to Abe's result (2.4), and which for a multicomponent system is¹²

$$f_A = \frac{\pi}{3} \left(\frac{e^2}{\epsilon k T} \right)^3 \sum_{\alpha} (2s_{\alpha} + 1)^2 Z_{\alpha}^6 \frac{\partial_{\alpha}^2}{\lambda_{\alpha}^6} \ln \Lambda_{\alpha}' \quad (3.13)$$

The effect on the activity coefficients γ_{α} of including f_A with the grand potential is obtained by adding $\partial_{\alpha}(\partial f_A / \partial \partial_{\alpha})$ to eq 3.9, and applying eq 3.11. The result for a 1-1 electrolyte is

$$\gamma_{\alpha} = \left[1 + \frac{\Lambda_{\alpha}'}{2} + \frac{\Lambda_{\alpha}'^2}{12} \left(\ln \Lambda_{\alpha}' + \frac{1}{4} \right) \right]^{-1} + 0(\partial) \quad (3.14)$$

The mean activity coefficient γ_{\pm} obtained from eq 3.14 for an aqueous solution at room temperature is graphed in Figure 1. It is the GCE curve labeled DH + A. (See Appendix B for the details of how this graph is obtained.) Including the "Abe" term (3.13) with the grand potential amounts at 1 M to a 7% correction to γ_{\pm} . This is to be compared with an Abe correction of approximately 40% in the density expansion of γ_{\pm} .

IV. Conclusions

Investigation of the fugacity series for the grand potential of a gas of ions has shown it to have a rapid practical rate of convergence for the problem of the primitive model of a 1-1 electrolyte of point ions in water. In particular, the first term beyond the perfect gas term (which corresponds to the Debye-Hückel limiting law in a density expansion) is an accurate solution to this model problem; the next most important term (which corresponds to the Abe term in a density expansion) amounts to about a 7% correction to γ_{\pm} for a 1 M aqueous solution of 1-1 electrolyte at room temperature. In the conventional density expansion, the Abe term is about a 40% correction. Thus, use of the fugacity series enhances convergence.

We agree with Friedman and Rasaiah^{7a} that an accurate theory of the primitive model must precede future model developments. We propose the fugacity series from grand canonical ensemble statistical mechanics as an alternative to the integral-equation method of Friedman and Rasaiah.⁷ The advantage is one of formal simplicity: the first term beyond the perfect gas term is just as simple as the Debye-Hückel limiting law.

Friedman³ has objected to the use of the fugacity series as a solution to physical problems because the independent variables are the fugacities rather than

(9) W. T. Grandy and F. Mohling, *Ann. Phys.*, **34**, 424 (1965).

(10) W. T. Grandy, *Ann. Acad. Bras. Ciências (Brazil)*, **39**, 65 (1967).

(11) W. T. Grandy, *Il Nuovo Cimento*, **64B**, 73 (1970).

(12) W. T. Grandy, private communication.

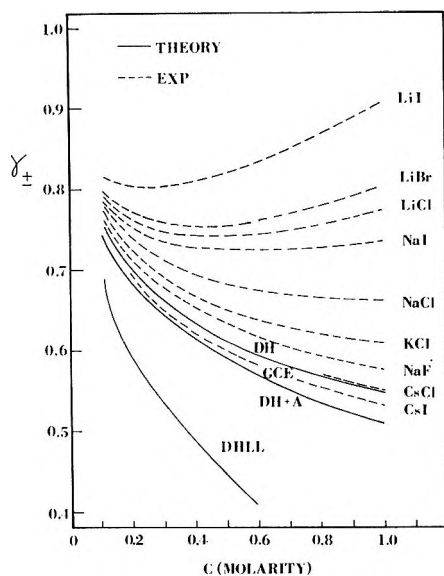


Figure 1. Mean activity coefficient vs. concentration in molarity of aqueous solutions of 1-1 electrolytes at 25°. The DHLL (Debye-Hückel limiting law) curve is from eq 2.7. The GCE (grand canonical ensemble) curves are from eq 3.12 and 3.14. The details of calculating the GCE curves from eq 3.12 and 3.14 are given in Appendix B. The dashed curves are experimental data; they have not been corrected to McMillan-Mayer standard states because the correction is not significant on the scale of Figure 1.

the densities, the more "natural" independent variables. However, we find no practical disadvantage with the fugacities appearing as independent variables and the densities as dependent variables, as in eq 3.9. One need not formally invert such an expression to compare it with experiment or other theories, but may merely graph it directly as explained in Appendix B.

The fugacity series is also objected to as a solution to physical problems on the grounds that it is slowly converging;³ however, we find that the practical rate of convergence for the problem at hand is rapid, more so than the corresponding density series.

Finally, the grand-canonical-ensemble (GCE) result agrees better with the experimental activity coefficient data than does the Debye-Hückel limiting law. To reiterate, each of these results is an infinite series terminated at the same order in the independent variable, fugacity on the one hand, density on the other. In the past, the discrepancy between the Debye-Hückel result and experiment was thought to be accounted for largely by the effect of the finite size of the ions. Further, it was generally found that the bare crystallographic sizes were insufficient to account for the discrepancy, so a particular amount of solvation to enhance the ions sizes was implied. Since the more accurate GCE result is closer to experiment, the relevance of a solvation effect in 1-1 electrolytes, as introduced in earlier treatments, needs to be re-examined.

In fact, the experimental curves seem to approach the GCE DH + A curve as an approximate lower bound. This behavior is certainly at odds with the expectation that the deviations of the experimental activity coefficients from the activity coefficient of a hypothetical point-ion electrolyte should be related to the finite size of the ions, at least from the standpoint of the primitive model. Just the opposite seems to be the case: CsI is the alkali halide with the largest distance of closest ionic approach, but it agrees most closely with the GCE point-ion result. This behavior is, however, not necessarily at odds with quantitative studies of the finite-size dependence of the primitive model results, since such studies show no simple correlation between the distance of closest ionic approach in the theory and the crystallographic ionic sizes.^{7b}

It is apparent that one must look beyond simple finite-size effects for an explanation of the deviations of the experimental activity coefficients from each other and from the point-ion case. Rasaiah^{7b} has explored the possibility of extending the primitive model by including other short-range effects besides a simple hard-core repulsion. Another possibility is to exploit more thoroughly the primitive model by working out the correction to the GCE curve due to a hard-core repulsion. This means applying, in the form of a fugacity series, the quantum-statistical mechanics of a multicomponent gas of charged, hard spheres.

Acknowledgments. The authors would like to thank Dr. W. T. Grandy for making available his most recent results and for helpful communications regarding the application of his results to the present work. Thanks is also due to members of the ORNL Chemistry Division, especially Drs. S. Lindenbaum and F. Vaslow, for helpful conversations.

Appendix A

In this Appendix, we quote the $O(\beta^2)$ terms in the grand potential as calculated by Grandy.^{9,10} In Appendix B of ref 10, Grandy has summarized the results through fifth order in the electronic charge e and given a more complete evaluation of the numerical constants involved. Dropping terms proportional to $\eta_\alpha = kT/m_\alpha c^2$, which is small for nonrelativistic temperatures, the result for the grand potential f through $O(e^5)$ is¹³

$$f = \sum_{\alpha} (2s_{\alpha} + 1) \beta_{\alpha} \lambda_{\alpha}^{-3} (A_{\alpha} + \epsilon_{\alpha} \beta_{\alpha} B_{\alpha}) + O(\beta)^{5/2} \quad (\text{A.1})$$

where

(13) In ref 10, Grandy has partially inverted the fugacity expansion for f by replacing $(2s_{\alpha} + 1) \beta_{\alpha} / \lambda_{\alpha}^3$ with n_{α} in the definitions of A_{α} and B_{α} . The result we quote is modified from Grandy's by keeping $(2s_{\alpha} + 1) \beta_{\alpha} / \lambda_{\alpha}^3$ everywhere. This modification is accomplished by our definitions of Λ_{α}' , γ_{α}' , Γ' , and M_{α}' .

$$\epsilon_\alpha = \begin{cases} +1 & \text{for Bosons} \\ -1 & \text{for Fermions} \end{cases}$$

$s_\alpha = \text{spin of } \alpha\text{-type particle}$

$$\begin{aligned} \Lambda_\alpha' &\approx 2 & \lambda_\alpha &\approx 0.18 \text{ \AA} \\ \gamma_\alpha' &\approx 0.06 & \bar{\partial}_\alpha &\approx 3.5 \times 10^{-6} \\ \Gamma_\alpha &\approx 40 \\ M_\alpha' &\approx \Gamma' \approx 3 \times 10^{-4} \end{aligned}$$

$$A_\alpha = 1 + a_1\Lambda_\alpha' + a_2\Lambda_\alpha'\gamma_\alpha' + a_3\Lambda_\alpha'\gamma_\alpha'^2 + a_4\Gamma_\alpha M_\alpha' + a_5\Lambda_\alpha'\Gamma'$$

$$B_\alpha = 2^{-3/2} + b_1\Lambda_\alpha' + b_2\Lambda_\alpha'\gamma_\alpha' + b_3\Lambda_\alpha'\gamma_\alpha'^2 + b_4\Gamma_\alpha + b_5\Gamma_\alpha^2 + b_6\Lambda_\alpha\Gamma_\alpha + b_7\Gamma_\alpha M_\alpha' + b_8\Lambda_\alpha'\Gamma'$$

and

$$\begin{aligned} \Lambda_\alpha' &= \frac{e^2 Z_\alpha^2 \kappa'}{\epsilon k T} \\ \gamma_\alpha' &= \lambda_\alpha \kappa' \\ \Gamma_\alpha &= \frac{e^2 Z_\alpha^2}{\epsilon k T \lambda_\alpha} \\ \Gamma' &= \sum_\alpha \Gamma_\alpha (2s_\alpha + 1) \bar{\partial}_\alpha \\ M_\alpha' &= \frac{e^2 \lambda_\alpha}{\epsilon k T} \sum_\beta (2s_\beta + 1) \frac{\bar{\partial}_\beta}{\lambda_\beta^3} Z_\beta^2 \lambda_{\alpha\beta} \\ \lambda_{\alpha\beta} &= [\lambda_\alpha^2 + \lambda_\beta^2]^{1/2} \end{aligned}$$

The numerical coefficients are¹⁴

$$\begin{aligned} a_1 &= 1/3 & b_3 &\cong -0.0342 \\ a_2 &= 0 & b_4 &= -1/2 \\ a_3 &= 13/(1512\pi) & b_5 &= \pi\sqrt{2}(5 + 2 \ln 2)/16 \\ a_4 &= -\pi/8 & b_6 &= -1/30 \\ a_5 &= -107/504 & b_7 &= -2\pi\sqrt{2}/32 \\ b_1 &= \sqrt{2}/6 & b_8 &= -107\sqrt{2}/1008 \\ b_2 &\cong -0.1992 \end{aligned}$$

The leading term in eq A.1, $\sum_\alpha (2s_\alpha + 1) \bar{\partial}_\alpha \lambda_\alpha^3$, is the free-particle term. The next term, $a_1 \Lambda_\alpha$ in A_α , is the Debye-Hückel term. All the other terms are $O(\bar{\partial}^2)$ and higher order corrections. For the case we have chosen to examine, NaCl dissolved in water at room temperature, we can easily make a rough estimate of the terms in eq A.1 by taking $m_+ \cong m_- \cong 30$ amu and $\bar{\partial}_\alpha \cong n_\alpha \lambda_\alpha^3 / (2s_\alpha + 1)$, the free particle value. (m_+ and m_- are the two values of m_α , the mass of an α -type ion; $+$ and $-$ denote Na^+ and Cl^- , respectively.) Substituting $T = 298^\circ\text{K}$, $\epsilon = 78.5$, $Z_+ = -Z_- = 1$, $s_+ = s_- = 0$, $\epsilon_+ = \epsilon_- = 1$ (Na^+ and Cl^- are Bosons with zero spin), we find for a concentration of 1.0 M the following approximate values of the parameters appearing in eq A.1

Then, for 1.0 M , we find that the Debye-Hückel term is approximately 50% of the free particle term and the largest $O(\bar{\partial}^2)$ terms ($a_4 \Gamma_\alpha M_\alpha$ and $b_5 \Gamma_\alpha^2$) are approximately 1% of the free-particle term. The other $O(\bar{\partial}^2)$ corrections are at least a factor of 10 smaller yet.

To evaluate the effect of these $O(\bar{\partial}^2)$ corrections on the value of γ_\pm , we now develop an explicit expression for γ_\pm . First, including only the largest $O(\bar{\partial}^2)$ terms in f , as found above, we have from eq A.1

$$f \cong \sum_\alpha (2s_\alpha + 1) \frac{\bar{\partial}_\alpha}{\lambda_\alpha^3} [1 + a_1 \Lambda_\alpha' + a_4 \Gamma_\alpha M_\alpha' + b_5 \epsilon_\alpha \Gamma_\alpha^2 \bar{\partial}_\alpha] + O(\bar{\partial}^{5/2})$$

Then, making use of $n_\alpha = \bar{\partial}_\alpha (\partial f / \partial \bar{\partial}_\alpha)$, we find

$$n_\alpha = (2s_\alpha + 1) \frac{\bar{\partial}_\alpha}{\lambda_\alpha^3} \left[1 + \frac{\Lambda_\alpha'}{2} + g_\alpha \right] + O(\bar{\partial}^{5/2}) \quad (\text{A.2})$$

where

$$g_\alpha = 2a_4 \Gamma_\alpha M_\alpha' + 2b_5 \epsilon_\alpha \Gamma_\alpha^2 \bar{\partial}_\alpha$$

In eq A.2, the first two terms in the square bracket are just the result which we have quoted earlier as eq 3.9. g_α contains the largest $O(\bar{\partial}^2)$ corrections to eq 3.9. We now formally invert eq A.2 to obtain $\bar{\partial}_\alpha$ as a function of the n_α 's. To do this, we first define $\bar{\partial}_\alpha^{(1)}$ and a corresponding $\Lambda_\alpha'^{(1)}$ such that

$$n_\alpha = (2s_\alpha + 1) \frac{\bar{\partial}_\alpha^{(1)}}{\lambda_\alpha^3} \left[1 + \frac{\Lambda_\alpha'^{(1)}}{2} \right]$$

Then, we define the α -independent parameter η as

$$\eta \equiv \frac{\Lambda_\alpha'^{(1)}}{2Z_\alpha^2} = \sqrt{\pi} \left(\frac{e^2}{\epsilon k T} \right)^{3/2} \left(\sum_\alpha (2s_\alpha + 1) \frac{\bar{\partial}_\alpha^{(1)}}{\lambda_\alpha^3} Z_\alpha^2 \right)^{1/2}$$

Now, we combine these two definitions into

$$\bar{\partial}_\alpha^{(1)} = \frac{n_\alpha \lambda_\alpha^3}{(2s_\alpha + 1)} \frac{1}{1 + Z_\alpha^2 \eta} \quad (\text{A.3})$$

and

$$\eta = \sqrt{\pi} \left(\frac{e^2}{\epsilon k T} \right)^{3/2} \left(\sum_\alpha \frac{n_\alpha Z_\alpha^2}{1 + Z_\alpha^2 \eta} \right)^{1/2} \quad (\text{A.4})$$

Equation A.3 is an approximation to the inversion of eq A.2 obtained by neglecting g_α . The quantity η is a function of the densities n_α through the transcendental eq A.4. Note that eq A.3 and A.4 are exactly equivalent.

(14) Many of these coefficients appeared incorrectly in ref 10. The values given here are revised according to an errata sheet prepared by Grandy.

lent to eq 3.9, and, although slightly more complicated, can equally well be used to obtain the γ_{\pm} vs. c plot of Figure 1. But, our purpose in obtaining the inverted form, eq A.3 and A.4, is to use them for getting an explicit expression for the $O(\beta^2)$ corrections. Since the effect of g_{α} in eq A.2 is expected to be small ($\sim 1\%$), we expect β_{α} to be accurately approximated by $\beta_{\alpha}^{(2)}$ defined by

$$\beta_{\alpha}^{(2)} \equiv \frac{n_{\alpha}\lambda_{\alpha}^3}{(2s_{\alpha} + 1)} \frac{1}{1 + Z_{\alpha}^2\eta + g_{\alpha}^{(1)}} \cong \beta_{\alpha}^{(1)} \left[1 - \frac{g_{\alpha}^{(1)}}{1 + Z_{\alpha}^2\eta} \right] \quad (\text{A.5})$$

where

$$g_{\alpha}^{(1)} = g_{\alpha} \beta_{\alpha} = \beta_{\alpha}^{(1)}$$

Now, we specialize eq A.4 and A.5 to the case of NaCl dissolved in water at room temperature. For NaCl, α takes on two values, say + and -, corresponding to Na^+ and Cl^- , respectively. Since in this case, $n_+ = n_-$ and $Z_+ = -Z_- = 1$, then $\beta_+/\lambda_+^3 = \beta_-/\lambda_-^3$. For this estimate we make the simplifying assumption $m_+ = m_- = 30$ amu. Then, $\lambda_+ = \lambda_-$ and

$$g_{\alpha}^{(1)} \cong 2(2^{1/2}a_4 + b_5)\Gamma_{\alpha}^2 \frac{n_{\alpha}\lambda_{\alpha}^3}{1 + \eta}$$

Furthermore, since now $\beta_+/\lambda_+^3 = \beta_-/\lambda_-^3$ and $n_+ = n_-$, we may conclude from eq 3.7 that $\gamma_+ = \gamma_- = \gamma_{\pm}$ and therefore

$$\gamma_{\pm} \cong \frac{\beta_{\alpha}^{(2)}}{n_{\alpha}\lambda_{\alpha}^3} = \frac{1}{1 + \eta} \left[1 - 2(2^{1/2}a_4 + b_5)\Gamma_{\alpha}^2 \frac{n_{\alpha}\lambda_{\alpha}^3}{(1 + \eta)^2} \right]$$

Upon substituting $T = 298^\circ\text{K}$ and $\epsilon = 78.5$, we find $\lambda_+ = \lambda_- \cong 0.18$ Å, $\Gamma_+ = \Gamma_- \cong 38$, and

$$\gamma_{\pm} \cong \frac{1}{1 + \eta} \left[1 - \frac{0.012c}{(1 + \eta)^2} \right] \quad (\text{A.6})$$

where c is the concentration of NaCl in molarity. Substituting the above data into eq A.4 gives

$$\eta^3 + \eta^2 - 1.375c = 0 \quad (\text{A.7})$$

At $c = 1.0$ M, for example, $\eta = 0.860$, and the second term in eq A.6 is approximately 0.0035. Thus, we have shown that the $O(\beta^2)$ corrections to eq 3.8 amount to approximately a 0.35% correction to γ_{\pm} at 1.0 M. They can thus be ignored and eq 3.11 gives γ_{\pm} very accurately at least as far as contributions of order e^5 and lower are concerned.

Appendix B

In this Appendix, we show how the γ_{\pm} vs. c curves of Figure 1 were obtained. For a 1-1 electrolyte, α takes the two values, say + and -, corresponding to the positive and negative ions, respectively. Since for this case $n_+ = n_-$ and $Z_+ = -Z_-$, then $\beta_+/\lambda_+^3 = \beta_-/\lambda_-^3$ and $\gamma_+ = \gamma_- = \gamma_{\pm}$. If we express n_{α} and $\beta_{\alpha}/\lambda_{\alpha}^3$ in molarity units

$$c = \frac{10^3}{N_0} n_{\alpha} = \frac{10^3}{N_0} n_{\alpha} \text{ moles/liter}$$

and

$$w = \frac{10^3}{N_0} \frac{\beta_{\alpha}}{\lambda_{\alpha}^3} = \frac{10^3}{N_0} \frac{\beta_{\alpha}}{\lambda_{\alpha}^3} \text{ moles/liter}$$

where N_0 is Avogadro's number. Substituting $T = 298.16^\circ\text{K}$ and $\epsilon = 78.54$, eq 3.9 becomes

$$c = w + 1.172w^{3/2} \text{ moles/liter} \quad (\text{B.1})$$

and eq 3.11 becomes

$$\gamma_{\pm} = \frac{w}{c} = [1 + 1.172w^{1/2}]^{-1} \quad (\text{B.2})$$

Thus, we obtain the GCE γ_{\pm} vs. c plot labeled DH by substituting a series of w values into eq B.1, calculating corresponding c values, and plotting γ_{\pm} ($=w/c$) vs. c from eq B.2 for this series of values.

When the Abe term 3.13 is included, the method is the same, and eq B.1 becomes

$$c = w + 1.172w^{3/2} + 0.460w^2(\ln 2.344w^{1/2} + 1/4) \quad (\text{B.3})$$

The GCE graph in Figure 1 of $\gamma_{\pm} = w/c$ vs. c for eq B.3 is labeled DH + A.

Ion-Molecule Reactions in Ethanol by Photoionization¹

by M. E. Russell*² and W. A. Chupka

Argonne National Laboratory, Argonne, Illinois (Received March 25, 1971)

Publication costs assisted by the Argonne National Laboratory

The high-pressure mass spectrum of ethanol has been examined by use of photoionization. The photon energy was adjusted so that the $C_2H_5OH^+$ ion was virtually the only primary ion. The reactions $C_2H_5OH^+ + C_2H_5OH \rightarrow C_2H_5OH_2^+ + C_2H_5O$ (or C_2H_5OH), $C_2H_5OH_2^+ + C_2H_5OH \rightarrow (C_2H_5OH)_2H^+$, $(C_2H_5OH)_2H^+ + C_2H_5OH \rightarrow (C_2H_5OH)_3H^+$, $(C_2H_5OH)_3H^+ + C_2H_5OH \rightarrow (C_2H_5OH)_4H^+$ were examined as a function of source pressure. Under the temporal conditions of these experiments, the product ions of the first two reactions were found to require little or no collisional stabilization; the latter two, however, required at least one and probably two collisions for stabilization. Cross-section equations were developed which permitted determination of the number of steps required for collisional stabilization. Ionization efficiency curves were obtained (from threshold to 12.87 eV) for the parent ion and the mono-, di-, and trisolvated protons. The varying shapes of these curves as a function of photon energy were interpreted in terms of the precursor ions m 46, m 45, and m 31 of the solvated proton and their differing internal energy content. A number of other ion-molecule reactions occurring in this system were noted as well as metastable transitions and collision-induced processes. A few runs were also made at a photon energy (13.27 eV) at which m 31 and m 45 are significant primary ions in addition to the parent ion.

Introduction

Ion-molecule reactions in ethanol have been examined by several workers.³ At higher pressures a large number of ions are formed from secondary and higher order reactions, and the task of sorting out the reactants for a given reaction is rendered more difficult by the number of possible primary ions that may be the reactants. The use of the appearance-potential method, for example, in determining the reactant ion(s) producing $C_2H_5OH_2^+$ in the ethanol system led Ryan, *et al.*,⁴ to erroneous conclusions; they later modified their conclusions on the basis of data from a tandem mass spectrometer.³ Potapov and Sorokin^{3b} in their photoionization study of methanol and ethanol did find evidence for reaction of fragment ions with ethanol to produce $C_2H_5OH_2^+$. They deduced this from the dependence of the cross section on photon energy.

The use of reactant ions produced by photon impact rather than electron impact offers a number of advantages in studying ion-molecule reactions.^{3b,5,6} In the present study, a particular advantage is the ability to examine reactions in which the parent ion is virtually the only primary ion present. The narrow energy band of the photons used and the relatively large ion intensity near the threshold of the parent ion make this feasible.

Experimental Section

The ethanol used was absolute pure ethanol, reagent quality, obtained from U. S. Industrial Chemicals. It was used without further purification other than outgassing. To ascertain the purity of the ethanol, samples were chromatographed in a 15% SE-30 column and a 20% Hallcomid M-18-OL column. In each case

only a single peak was detected. It was estimated, from standard samples, that the concentrations of water and benzene were less than 0.02%.

The mass spectrometer used for this study has been described earlier.^{7,8} The ionization chamber and collision chamber were identical with those used by Chupka, *et al.*⁶ A repeller field of 0.22 V/cm was used in the ionization chamber, and the effects of contact potentials and other electric fields were estimated to be negligible as indicated by the dependence of ion intensity on repeller voltage. The collision chamber served no useful purpose in the present experiment but could not easily be removed; no gas was introduced into it. Mass spectra were obtained by magnetically scanning at constant photon energy, a typical scan running from m 44 to m 190. Ions were detected by an electron multiplier, amplified by a vibrating-reed electrometer, and recorded on a strip-chart recorder. The intensities were read from the chart without correcting for changes in the electron-multiplier sensitivity as a function of mass or type of ion since the cor-

(1) Work performed under the auspices of the U. S. Atomic Energy Commission.

(2) Correspondence should be addressed to: Department of Chemistry, Northern Illinois University, DeKalb, Ill. 60115.

(3) (a) For references to earlier literature see L. W. Sieck, F. P. Abramson, and J. H. Futrell, *J. Chem. Phys.*, **45**, 2859 (1966); (b) V. K. Potapov and V. V. Sorokin, *Dokl. Akad. Nauk SSSR*, **192**, 590 (1970).

(4) K. R. Ryan, L. W. Sieck, and J. H. Futrell, *J. Chem. Phys.*, **41**, 111 (1964).

(5) I. Koyano, I. Omura, and I. Tanaka, *ibid.*, **44**, 3850 (1966).

(6) W. A. Chupka, K. M. Refaey, and M. E. Russell, *ibid.*, **48**, 1518 (1968).

(7) J. Berkowitz and W. A. Chupka, *ibid.*, **45**, 1287 (1966).

(8) W. A. Chupka and J. Berkowitz, *ibid.*, **47**, 2921 (1967).

Table I: Major Sequence of Condensation Reactions in the High-Pressure Mass Spectrum of C_2H_5OH at a Photon Energy at 10.68 eV

Reaction no.	Mass no. of product ion	Formula of product ion	Ionic reaction	Relative cross section	
				Hard sphere σ	Szabo's model q^a
1	46	$C_2H_5OH^+$	$h\nu + C_2H_5OH \rightarrow C_2H_5OH^+ + e$
2	47	$C_2H_5OH_2^+$	$C_2H_5OH^+ + C_2H_5OH \rightarrow C_2H_5OH_2^+ + C_2H_5O$	1	1
3	93	$(C_2H_5OH)_2H^+$	$C_2H_5OH_2^+ + C_2H_5OH \rightarrow (C_2H_5OH)_2H^+$	0.5	0.4
4	139	$(C_2H_5OH)_3H^+$	$(C_2H_5OH)_2H^+ + C_2H_5OH \rightarrow (C_2H_5OH)_3H^+$	0.6	0.5
5	185	$(C_2H_5OH)_4H^+$	$(C_2H_5OH)_3H^+ + C_2H_5OH \rightarrow (C_2H_5OH)_4H^+$	0.6	0.4

^a I. Szabo, *Int. J. Mass Spectrom. Ion Phys.*, **3**, 103 (1969).

reaction is small and has no significant effect on the results of this study.^{9,10} The light was detected using a nickel photocathode, and experimentally determined photoelectron corrections were used. Ionization efficiency curves were computed from the recorded ion and light intensities. The hydrogen many-line spectrum was used as the source of ionizing radiation; the slit width of the monochromator was 300 μ , which corresponds to an energy spread of about 0.03 eV in this wavelength region.

A photon energy of 10.68 eV (1161 \AA) was used to study the reactions of the parent ion. This energy is sufficiently above the appearance potential of the parent ion (10.47 eV) to give good ion intensities but is sufficiently below the appearance potential of the first fragment ion (10.78 eV for m 45) to give a negligible contribution from this primary ion.

The pressure in the ionization chamber was not measured directly in this work. The pressures reported here are those measured by an ionization gauge (in units of 10^{-5} Torr) which was adjacent to the ionization chamber. Based on later measurements we estimate that the pressure in the chamber was about 300 times higher than the measured value and was linear over the range of the experiments to within $\pm 20\%$. Thus the arbitrary units referred to in the figures and text have the approximate value of 3×10^{-3} Torr.

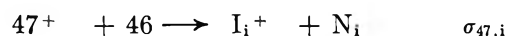
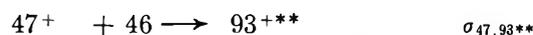
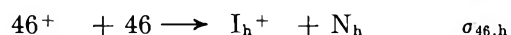
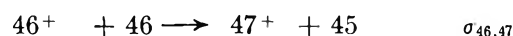
To ascertain background contributions to the mass spectra caused by stray photoelectrons and scattered light, a mass spectrum was obtained at a photon energy of 10.29 eV and at a pressure virtually the same as the highest used in this study. The total ion current at this energy was 0.6% of that at 10.68 eV. Furthermore, more than 80% of the ions at 10.29 eV were m 47 and m 93. These are the most intense ions at 10.68 eV and this pressure.

Since the mass resolution of the instrument in these experiments was approximately one part in 150, the molecular formula of the observed ions could not be established by using mass defects. The molecular formulas were established, where possible, by measuring the intensities of the $m + 1$ and $m + 2$ isotopic

masses and comparing the values with those given by Beynon.¹¹

Development of Cross-Section Equations

In this study the condensation sequence of ion-molecule reactions starting with $C_2H_5OH_2^+$ was examined in some detail, and relative reaction cross sections for those reactions were determined. Nearly all the products of the reaction of ethanol parent ion with ethanol can be accounted for by the reaction sequence shown in Table I.¹² Except for the photoionization act (reaction 1) and the formation of the monosolvated proton $C_2H_5OH_2^+$ (reaction 2), the reactions involve the simple addition of further ethanol molecules to the ion. Reaction 2 is an ordinary exothermic ion-molecule reaction with two products and hence is expected to be second order. For the succeeding reactions, one normally expects collisional stabilization of the reaction product (or previous removal of excess energy from the reactant by collision) to be necessary and thus the reaction to be third order. However, our results are not consistent with this in the case of the first condensation step (reaction 3) and so we will develop the cross-section equations for a sequence of reactions somewhat different from the expected set. The mass number of the most abundant isotopic species will be used to represent the ion (*i.e.*, 46⁺ represents $C_2H_5OH^+$, 47⁺ represents $C_2H_5OH_2^+$, 93⁺ represents $(C_2H_5OH)_2H^+$, etc.). The relevant reactions and their cross sections are

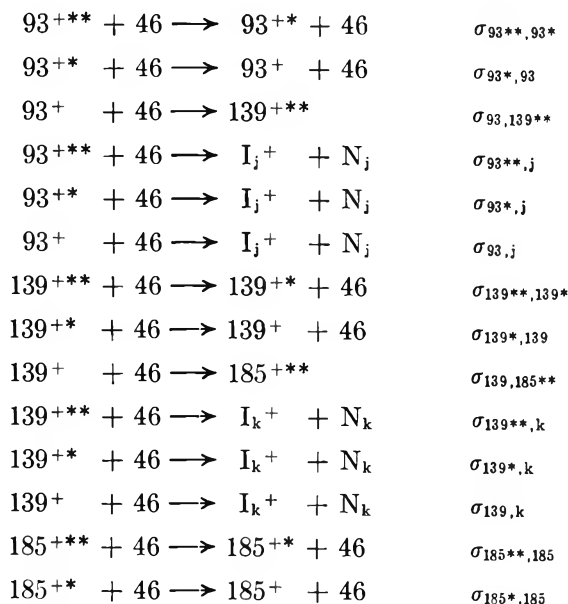


(9) M. G. Inghram and R. J. Hayden, "Mass Spectroscopy," Nuclear Science Series, Report No. 14, National Research Council, Washington, D. C., 1954, p 43.

(10) H. E. Stanton, W. A. Chupka, and M. G. Inghram, *Rev. Sci. Instrum.*, **27**, 109 (1956).

(11) J. H. Beynon, "Mass Spectrometry and its Application to Organic Chemistry," Elsevier, Amsterdam, 1960, Appendix 1.

(12) I. Szabo, *Int. J. Mass Spectrom. Ion Phys.*, **3**, 103 (1969).



where I_h^+ is an ionic product (other than 47^+) from the reaction of 46^+ with 46, I_i^+ is an ionic product (other than the condensation product 93^{***}) produced by the reaction of 47^+ with 46, etc. N_h is the neutral species produced together with I_h^+ . 93^{***} and 93^{*+} are m 93 ions with excess internal energy (*i.e.*, although 93^{***} and 93^{*+} may be stable ions themselves, they undergo two collisions and one collision, respectively, with ethanol molecules before enough energy has been removed so that condensation can take place); 139^{***} , etc., are excess energy ions also. The equations subsequently developed here may readily be altered to fit any number of collisional deactivation steps.

This sequence of reactions gives differential equations which are formally the same as the equations used to describe the quantities of nuclides present in consecutive radioactive decay.¹³ The first of the solutions of these equations is¹⁴

$$I_{46} = I_{46}^{\circ} e^{-\sigma_{46}^{\tau} Nd} \quad (1)$$

where I_{46} is the intensity of the $C_2H_5OH^+$ ion at the exit slit of the source chamber, I_{46}° is the intensity of the $C_2H_5OH^+$ ion at the photon beam in the source chamber, σ_{46}^{τ} is the total reaction cross section for $C_2H_5OH^+$ (*i.e.*, $\sigma_{46}^{\tau} \equiv \sigma_{46, 47} + \sum_b \sigma_{46, b}$), N is the concentration of neutral molecules in the source chamber, and d is the distance from the photon beam to the exit slit in the source chamber. Other solutions are

$$I_{47} = I_{46}^{\circ} \sigma_{46, 47} \left\{ \frac{e^{-\sigma_{46}^{\tau} Nd}}{\sigma_{47}^{\tau} - \sigma_{46}^{\tau}} + \frac{e^{-\sigma_{47}^{\tau} Nd}}{\sigma_{46}^{\tau} - \sigma_{47}^{\tau}} \right\} \quad (2)$$

$$I_{93^{***}} = I_{46}^{\circ} \sigma_{46, 47} \sigma_{47, 93^{***}} \left\{ \frac{e^{-\sigma_{46}^{\tau} Nd}}{(\sigma_{47}^{\tau} - \sigma_{46}^{\tau})(\sigma_{93^{***}}^{\tau} - \sigma_{46}^{\tau})} + \frac{e^{-\alpha_{47}^{\tau} Nd}}{(\sigma_{46}^{\tau} - \sigma_{47}^{\tau})(\sigma_{93^{***}}^{\tau} - \sigma_{47}^{\tau})} + \frac{e^{-\sigma_{93^{***}}^{\tau} Nd}}{(\sigma_{46}^{\tau} - \sigma_{93^{***}}^{\tau})(\sigma_{47}^{\tau} - \sigma_{93^{***}}^{\tau})} \right\} \quad (3)$$

etc. If one takes the ratios I_{47}/I_{46} , $\Sigma I_{93}/I_{47}$ ($\Sigma I_{93} \equiv I_{93^{***}} + I_{93^*} + I_{93}$), etc., given by eq 1, 2, 3... and expands the exponential terms, he obtains the approximations¹⁴ which are similar to those developed by Derwish, *et al.*, in ref 14c.

$$\frac{I_{47}}{I_{46}} = \sigma_{46, 47} Nd [1 + C_1 Nd + \dots] \quad (4)$$

$$\frac{\Sigma I_{93}}{I_{47}} = \sigma_{47, 93^{***}} \frac{Nd}{2} [1 + C_2 Nd + \dots] \quad (5)$$

$$\frac{\Sigma I_{139}}{\Sigma I_{93}} = \sigma_{93^{***}, 93^*} \sigma_{93^*, 93} \sigma_{93^+, 139^{***}} \times \frac{(Nd)^3}{5 \cdot 4 \cdot 3} [1 + C_3 Nd + \dots] \quad (6)$$

$$\frac{\Sigma I_{185}}{\Sigma I_{139}} = \sigma_{139^{***}, 139^*} \sigma_{139^*, 139} \sigma_{139^+, 185^{***}} \times \frac{(Nd)^3}{8 \cdot 7 \cdot 6} [1 + C_4 Nd + \dots] \quad (7)$$

where C_1 , C_2 , C_3 , and C_4 are constants [*e.g.*, $C_1 = (\sigma_{46}^{\tau} - \sigma_{47}^{\tau})/2$]. One would predict that the intensity ratios given by eq 4 and 5 would approach linearity at low pressures, whereas the ratios given by eq 6 and 7 would be cubic at low pressure. It should be noted that the exponent of Nd in the term outside the brackets of eq 4-7 can be altered by changing the number of deactivation steps in the reaction sequence.

Experimental Results

Condensation Sequence of Reactions. Figure 1 is a plot of the relative intensity of the parent ion, the m 47 ion, and subsequent condensation products as a function of pressure. The shape of the curves is similar to those reported by Sieck, *et al.*,^{3a} except that they

(13) See, for example, E. Rutherford, J. Chadwick, and C. D. Ellis, "Radiations from Radioactive Substances," Cambridge University Press, New York, N. Y., 1930, p 12.

(14) Cross-section equations for somewhat similar situations in ion-molecule reactions have been developed by (a) S. Wexler and N. Jesse, *J. Amer. Chem. Soc.*, **84**, 3425 (1962); (b) G. A. W. Derwish, A. Galli, A. Giardini-Guidoni, and G. G. Volpi, *J. Chem. Phys.*, **39**, 1599 (1963), and (c) G. A. W. Derwish, A. Galli, A. Giardini-Guidoni, and G. G. Volpi, *J. Amer. Chem. Soc.*, **87**, 1159 (1965). It should be borne in mind in the cross-section equations of the above references as well as those developed here that σ is assumed to be independent of the location of the ion and hence of its energy (*i.e.*, a hard-sphere approximation is used) and that the path length d is the same for all ions. Such assumptions mean that the cross sections obtained have only semiquantitative meaning. The resulting error will be lessened by the low repeller field used in this study (the field of 0.22 V/cm over the 0.5 cm from the region of ionization to the exit hole would, in the absence of any collisions, give an ion a maximum energy of 0.11 eV), but the uncertainty in the cross section will still be rather large. An additional assumption is a Lindemann-type mechanism in which the cross section for a given step is independent of the internal energy of the reactants. Hence one obtains a cross section that is averaged over the internal energy as well as kinetic energy. Equations in terms of rate constants have been derived by (d) F. W. Lampe, J. L. Franklin, and F. H. Field in "Progress in Reaction Kinetics," Vol. 1, G. Porter, Ed., Pergamon Press, Elmsford, N. Y., 1961, Chapter 3. Inclusion of a variable collision complex lifetime and the translational energy dependence of the cross section has been treated by (e) G. G. Meisels and H. F. Tibbals, *J. Phys. Chem.*, **72**, 3746 (1968).

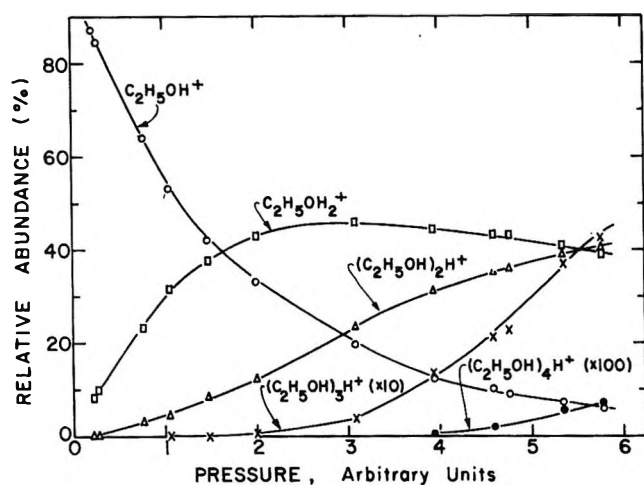


Figure 1. Variation of the relative abundance with pressure for the condensation sequence of reactions. The relative abundance of $(\text{C}_2\text{H}_5\text{OH})_3\text{H}^+$ has been multiplied by 10 and the relative abundance of $(\text{C}_2\text{H}_5\text{OH})_4\text{H}^+$ has been multiplied by 100. The photon energy is 10.68 eV.

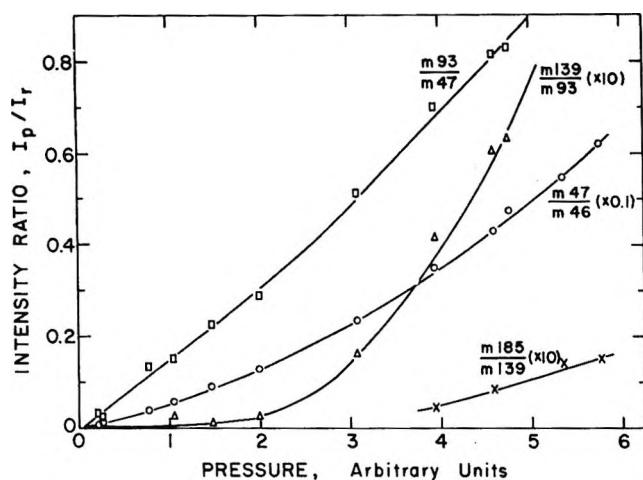


Figure 2. Pressure dependence of the ratio I_p/I_r of product-ion to reactant-ion intensity for the condensation sequence of reactions. I_{47^+}/I_{46^+} has been multiplied by 0.1; I_{139^+}/I_{93^+} and I_{185^+}/I_{139^+} have been multiplied by 10. The photon energy is 10.68 eV.

did not report the m 185 ion. It seems plausible to expect even higher molecular weight aggregates similar to those reported by Kebarle and coworkers¹⁵ for the ammonia and water systems. In Figure 2, the experimental intensity ratios I_{47^+}/I_{46^+} , I_{93^+}/I_{47^+} , etc., are plotted *vs.* pressure. The ratios I_{47^+}/I_{46^+} and I_{93^+}/I_{47^+} are virtually linear in pressure, as eq 4 and 5 predict. The deviation from linearity at higher pressures is, according to eq 4 and 5, caused by nonlinear terms becoming appreciable. The ratio I_{139^+}/I_{93^+} and probably I_{185^+}/I_{139^+} is not linear in pressure, however.

The exponent of the pressure can be obtained by plotting the intensity ratio *vs.* the pressure on logarithmic coordinates, the slope of this curve being the exponent of the pressure. This procedure will be valid at low pressures, at which higher order terms in eq

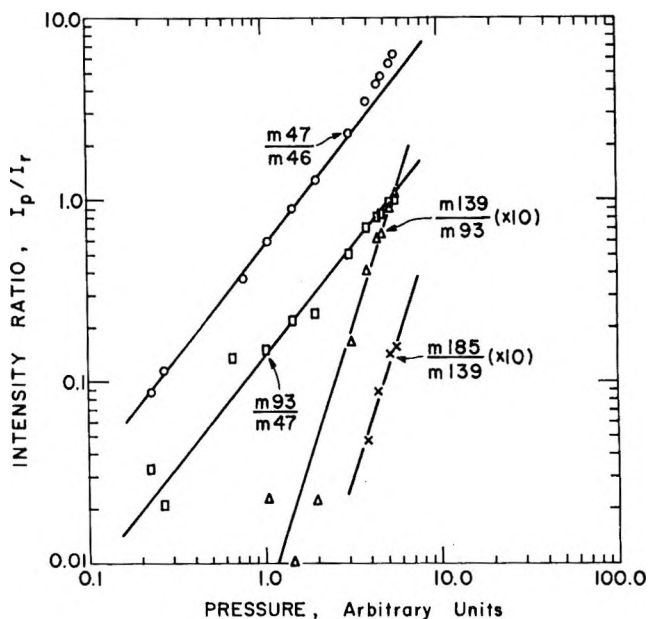


Figure 3. Pressure dependence of the ratio I_p/I_r of product-ion to reactant-ion intensity for the condensation sequence of reactions. I_{139^+}/I_{93^+} and I_{185^+}/I_{139^+} have been multiplied by 10. The photon energy is 10.68 eV.

4-7 (or ones similar to these if they do not predict the correct value of the exponent of pressure) are negligible. In Figure 3 the intensity ratios have been plotted *vs.* pressure. The slopes for I_{47^+}/I_{46^+} and I_{93^+}/I_{47^+} are each about 1.2. For I_{139^+}/I_{93^+} and I_{185^+}/I_{139^+} the slopes are about 3 for each, but more points for the latter ratio could alter this appreciably.

The relative cross sections for the ionic reactions are given in Table I. The hard-sphere relative cross sections (σ) were calculated from the experimental data using eq 4-7. Relative cross sections (q) were also calculated using the approach developed by Szabo¹² in which he assumes a v^{-1} velocity dependence of the cross sections. The equations which were used to calculate the relative cross sections (q) are

$$\frac{I_{47}}{I_{46}} = q_{46,47} N d (\Lambda_{46}/\Lambda_{47}) \quad (8)$$

$$\frac{\Sigma I_{93}}{I_{47}} = q_{47,93} N d (\Lambda_{93}/\Lambda_{47}) \quad (9)$$

$$\frac{\Sigma I_{139}}{\Sigma I_{93}} = q_{93^{**},93} q_{93^*,93} q_{139,139} (N d)^3 (\Lambda_{139^{**}}/\Lambda_{93^{**}}) \quad (10)$$

$$\frac{\Sigma I_{185}}{\Sigma I_{139}} = q_{139^{**},139} q_{139^*,139} q_{139,185} (N d)^3 (\Lambda_{185^{**}}/\Lambda_{139^{**}}) \quad (11)$$

where the Λ 's are defined by eq 10.4 in ref 12; values of Λ beyond Λ_{93^*} (Λ_4 in ref 12) were calculated by evaluating the multiple integrals numerically with a computer.

(15) (a) A. M. Hogg and P. Kebarle, *J. Chem. Phys.*, **43**, 449 (1965); (b) P. Kebarle, R. N. Haynes, and J. G. Collins, *J. Amer. Chem. Soc.*, **89**, 5753 (1967); (c) P. Kebarle, S. K. Searles, A. Zolla, J. Scarborough, and M. Arshadi, *ibid.*, **89**, 6393 (1967).

The cross sections calculated from the hard-sphere model and those calculated from Szabo's approach do not differ appreciably, probably because a low repeller field was used (0.22 V/cm) and because the cross sections are normalized to the cross section for reaction no. 2 (formation of m 47) in Table I.

Metastable Ions and Collision-Induced Dissociations. Several metastable transitions were observed in this study. These, as well as collision-induced dissociations, are found in Table II. The tabulated collision-induced dissociations took place in the collision chamber in which the ambient pressure was very much higher than in the differentially pumped analyzer section of the instrument. The ion collision energy was 450 eV (lab). It should be noted that several of the metastable transitions that would appear likely were not observed because they were coincident or nearly coincident with other masses (*e.g.*, the metastable transition $139^+ \rightarrow 121^+ + 18$ should occur at an apparent mass of 105.2, but a peak at m 105 obscured this transition).

Table II: Metastable Transitions and Collision-Induced Dissociations in the High-Pressure Mass Spectrum of C_2H_5OH at a Photon Energy of 10.68 eV

Process	Apparent mass m^*	
	Calcd	Obsd
Metastable Transitions		
$93^+ \rightarrow 47^+ + 46$	23.78	23.9
$93^+ \rightarrow 75^+ + 18$	60.56	60.5
$139^+ \rightarrow 93^+ + 46$	62.29	62.2
Collision-Induced Dissociations ^a		
$75^+ + (46) \rightarrow 29^+ + 46 + (46)$	26.9	26.9
$47^+ + (46) \rightarrow 29^+ + 18 + (46)$	27.8	27.9
$77^+ + (46) \rightarrow 31^+ + 46 + (46)$	28.9	28.9
$93^+ + (46) \rightarrow 47^+ + 46 + (46)$	44.6	44.5
$93^+ + (46) \rightarrow 75^+ + 18 + (46)$	73.4	73.5
$139^+ + (46) \rightarrow 93^+ + 46 + (46)$	89.5	89.7
$139^+ + (46) \rightarrow 121^+ + 18 + (46)$	119.2	119

^a The collision-induced dissociations were observed at only one collision energy; the reactions above are considered reasonable ones. Further work would have to be done to establish the reactants and products more firmly.

Ionization Efficiency Curves. The ionization efficiency curves¹⁶ (normalized at 10.68 eV) for $C_2H_5OH^+$, $C_2H_5OH_2^+$, $(C_2H_5OH)_2H^+$, and $(C_2H_5OH)_3H^+$, but not $(C_2H_5OH)_4H^+$ which was not examined, are plotted in Figure 4. It is evident that the appearance potential of each product ion is the same as $C_2H_5OH^+$. The shapes of these curves, however, are different and some further information can be obtained from these differences. As the photon energy increases, other primary ions are formed from ethanol and these may produce some secondary ions which are the same as those formed by

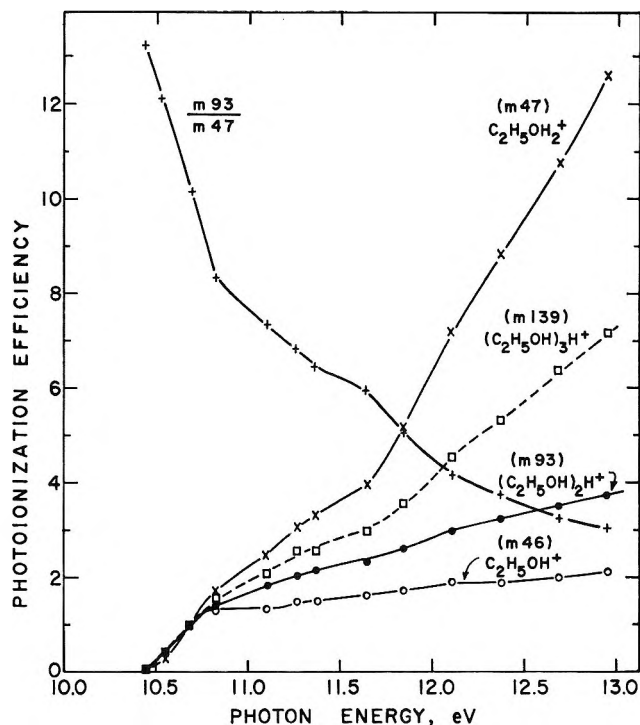


Figure 4. Ionization efficiency curves for the condensation sequence of reactions. Each ion has been normalized at 10.68 eV. The pressure is 1.9 (arbitrary units) for m 46, m 47, and m 93, and is 4.6 (arbitrary units) for m 139. The probable error in the ordinate is *ca.* $\pm 5\%$. Also plotted is the normalized ratio (multiplied by 10) of the m 93 ion intensity to that of m 47.

the parent ion. For example, the important primary ions in the range of photon energies used in this study are $C_2H_5OH^+$, $C_2H_4OH^+$, and CH_2OH^+ . If one examines the ionization efficiency curve for $C_2H_5OH_2^+$, three distinct portions can be seen—the first from 10.4 to 10.7 eV, the second from 10.7 to 11.6 eV, and the third from 11.6 to 12.9 eV. Examination of the ionization efficiency curves that Refaey and Chupka¹⁶ obtained for $C_2H_5OH^+$, $C_2H_4OH^+$, and CH_2OH^+ indicates that one may interpret the first portion of the $C_2H_5OH_2^+$ curve as the result of reaction of C_2H_5OH with $C_2H_5OH^+$ only, in the second portion $C_2H_4OH^+$ also becomes a reactant, and in the third portion CH_2OH^+ becomes the third reactant ion producing $C_2H_5OH_2^+$.

The curve for total ionization, whose derivative is given in ref 16, is similar to the one shown for m 47. This implies that the cross sections for the reaction of the ions m 46, m 45, and m 31 with ethanol to form m 47 are approximately the same. This is not unexpected since all these reactions are exothermic and the Gioumouis–Stevenson¹⁷ theoretical cross sections are nearly the same for all (experimental cross sections,

(16) K. M. Refaey and W. A. Chupka, *J. Chem. Phys.*, **48**, 5205 (1968).

(17) G. Gioumouis and D. P. Stevenson, *ibid.*, **29**, 294 (1958).

obtained under somewhat different conditions, are given in Table III of ref 3a. These are approximately equal, bearing out the above implication). However, it is immediately obvious that the cross section for the condensation reaction of m 47 differs very greatly, depending on its mode of formation which in turn determines its average internal energy content. This behavior, as well as the behavior of m 139, will be examined in the Discussion.

Other Ionic Species. In addition to those ions noted earlier, a large number of other ions were observed in this study. The pressure dependences of these ions (excluding those whose relative intensity was never greater than 0.1% and those ions below m 45) are plotted in Figures 5 and 6. Some preliminary data on ion intensities at selected photon energies show that all the ions in Figures 5 and 6 have appearance potentials within 0.1 V of the appearance potential of ethanol. This indicates that the ions arise from ethanol, but it does not exclude the possibility of a neutral impurity reacting with an ion originating from ethanol.

Ions of mass less than 44 were not examined as a function of pressure at a photon energy of 10.68 eV, so virtually nothing can be deduced concerning their nature or origin. They are probably created by stray photoelectrons, scattered light of shorter wavelengths, or by some ion-molecule reaction. At the one pressure ($p = 5.4$, arbitrary units) at which these were scanned, the three largest ions (mass 19, mass 29, and mass 31) had relative intensities of 0.4, 0.2, and 0.2% respectively. Therefore, they are not of major importance.

Studies at a Photon Energy of 13.27 eV. Mass spectra at several pressures were obtained at a photon energy of 13.27 eV. At this energy reactions of the fragment ions m 45 and m 31 will be significant, as will those of the parent ion; other fragments such as m 28 and m 29 are still rather small at this energy. The data for

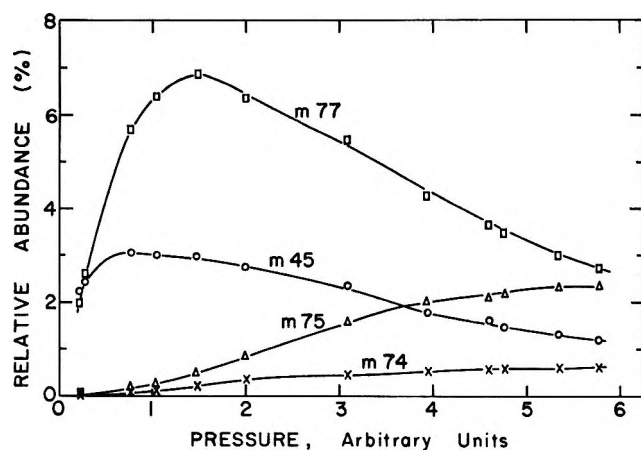


Figure 5. Pressure dependence of the relative abundance of ions above m 44 in the high-pressure spectrum of ethanol. Ions plotted in Figure 1 are omitted. The photon energy is 10.68 eV.

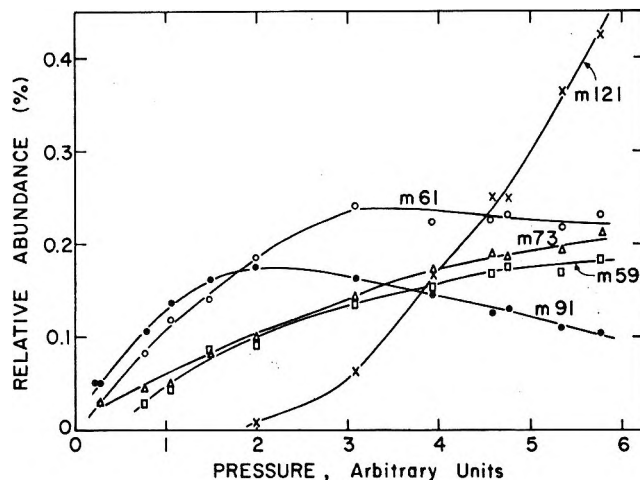


Figure 6. Pressure dependence of the relative abundance of ions above m 44 in the high-pressure spectrum of ethanol. Ions plotted in Figure 1 are omitted. The photon energy is 10.68 eV.

ions whose relative intensity is greater than 0.1% are given in Table III. No peak at a mass number greater than that of the parent was observed at this energy unless it was also observed at the photon energy (10.68 eV) that gives parent ion as virtually the only primary ion. It has already been noted that m 31 and m 45 form m 47. The results of Table III indicate that this is their major pathway for reaction.

Table III: Pressure Dependence of Ions in the Mass Spectrum of Ethanol at a Photon Energy of 13.27 eV^a

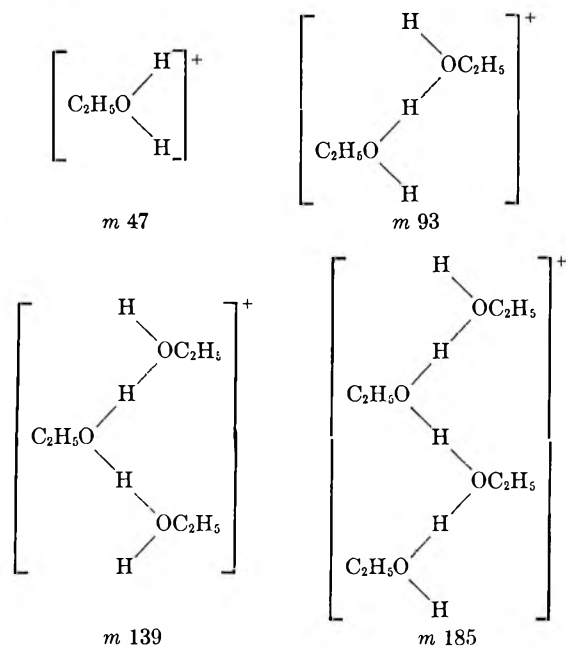
Mass no. of ion	Relative abundance %		
	Pressure, arbitrary units		
	0.36	0.97	5.6
18	0.02	0.04	0.006
19	1.1	2.3	1.8
28	0.3	0.4	0.008
29	0.7	1.0	0.9
30	1.7	1.3	0.2
31	42.0	32.4	4.9
44	0.2	0.1	0.04
45	26.1	18.7	3.2
46	14.3	11.1	0.9
47	12.9	30.9	54.2
59	~0	0.04	0.1
74	0.03	0.02	0.1
75	~0	0.2	3.7
77	0.5	0.7	0.4
93	0.09	0.7	25.5
121	NS ^b	~0	0.7
139	NS	~0	3.5
185	NS	NS	0.05

^a Ions whose relative intensity was never greater than 0.1% are not listed except for mass 18 and mass 185. ^b NS means not scanned.

Discussion

Gas phase, solvated protons have been observed earlier, *e.g.*, by Henis¹⁸ in a methanol system, by Beckey¹⁹

in a water system and in methanol, by Munson²⁰ in methanol and other hydrogen-bonding molecules, and by Futrell and coworkers^{3a} in the system examined here. One would expect, by analogy with aqueous protons, that the structure of the solvated species in the ethanol system would be



Further solvation could presumably take place at either end of the chain. This type of structure is similar to the polymeric chains formed by alcohols in the solid and liquid states²¹ but has, of course, an additional proton.

The pressure dependences for the solvation reactions are of some interest. Reaction 3 in Table I is second order according to our data; *i.e.*, collisional stabilization is apparently not necessary to obtain a measurable intensity of *m* 93. This is not too surprising in retrospect since the complexity of the product ion favors a longer lifetime for the reverse dissociation. Second-order behavior requires only that this lifetime be greater than the mean time for a deactivating collision or greater than the ion residence plus transit time in the mass spectrometer. That some of these collision complexes (or nondeactivated product ions) have a lifetime of the order of ion residence plus transit time (*ca.* 10^{-5} sec) is demonstrated by the observation of the reverse dissociation process as a metastable transition ($93^+ \rightarrow 47^+ + 46$). The observed second-order behavior for reaction 3, then, indicates that *most* collision complexes have lifetimes of this order or longer. It should be noted that this same result need not necessarily ensue in a similar experiment performed by electron impact for the following reasons. In the present experiment, the *m* 47 ion that begins the condensation sequence is formed almost entirely from $\text{C}_2\text{H}_5\text{OH}^+$ ions prepared by 10.68 eV photons which are only *ca.* 0.2 eV above the ionization threshold. In electron impact, the *m* 47 ion is created by many different reactions and may have

considerably more internal energy. Another significant effect is that of temperature. Electron-impact ionization chambers are usually at *ca.* 250° while ours was at 25°. The ethanol molecule at 250° has *ca.* 0.2 eV more average thermal (mostly vibrational) energy than at 25°. Thus, collision complexes of reaction 3 in the electron-impact case have average internal energies which are a large fraction of an electron volt greater than those produced by photoionization. Such energies can have great effects on lifetimes. Henis¹⁸ in an icr study of methanol found that the *m* 65 ion (presumed to be the protonated dimer of methanol) had a lifetime of *ca.* 2×10^{-6} sec. From this we can conclude that the protonated dimer of ethanol examined in this study would have a lifetime of at least 2×10^{-6} sec and very likely has an appreciably greater lifetime than this.

In contrast to *m* 93, *m* 139 and (probably) *m* 185 do require collisional stabilization. The data here indicate that about two collisions are necessary to carry away the excess energy. Whether the excess energy is taken from the reactant ion (as we have assumed because of the resulting mathematical convenience) or from the product ion or both cannot be determined from our data. The contrasting results on the *m* 93 and the *m* 139 ions suggest that the bond formed when a 47 ion condenses with an ethanol molecule is stronger than the bond formed by the subsequent condensation reaction (or reactions). It is of interest to compare the present results on ethanol with those of Henis¹⁸ on the ion-molecule reactions in methanol. He found that the formation of the protonated monomer did not require collisional stabilization whereas the protonated dimer did require one or more collisions for stabilization. The reason the protonated dimer (*m* 93) of ethanol does not require collisional stabilization but does for the methanol system he studied could be due to the fact that Henis used 70-eV electrons and to the effect of the increased number of degrees of freedom in the protonated dimer of ethanol.

The ionization efficiency curves (Figure 4) for the condensation sequence of reactions reveal the effect of internal energy and collisional stabilization on these reactions. The curve for *m* 93 shows that, at this pressure, the *m* 47 ions that react to form *m* 93 are those that have been formed principally from *m* 46 and *m* 45. The absence of a change in slope at the appearance potential of *m* 31 shows that this ion is not very effective in creating *m* 47 ions that will subsequently form *m* 93 ions.

The effect of internal energy can be seen by calculating ΔH for the reactions that form *m* 47. These reac-

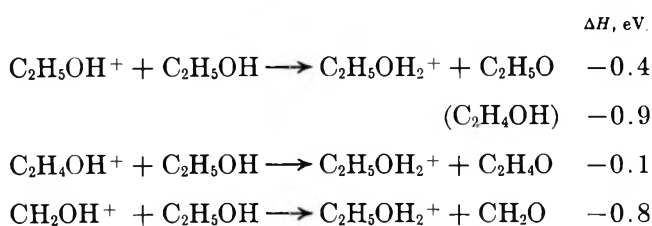
(18) J. M. S. Henis, *J. Amer. Chem. Soc.*, **90**, 844 (1968).

(19) H. D. Beckey in "Advances in Mass Spectrometry," Vol. 2, R. M. Elliot, Ed., Pergamon Press, Elmsford, N. Y., 1963, p 1.

(20) M. S. B. Munson, *J. Amer. Chem. Soc.*, **87**, 5313 (1965).

(21) L. Pauling, "The Nature of the Chemical Bond," Cornell University Press, Ithaca, N. Y., 1960, p 473.

tions and the associated values for ΔH obtained from Table IV²²⁻²⁶ are



In the case of reaction of alcohol with the parent ion the neutral product appears to be predominantly $\text{C}_2\text{H}_5\text{O}$. Potapov and Sorokin^{2b} found it to be preferred over $\text{C}_2\text{H}_4\text{OH}$ by a factor of *ca.* 3. We will use the value

Table IV: Values of $\Delta H_{f(g)}$ at 298°K

Species	$\Delta H_{f(g)}, \text{ eV}$	Reference
$\text{C}_2\text{H}_5\text{OH}^+$	7.85	16
$\text{C}_2\text{H}_4\text{OH}^+$	6.13	16
CH_2OH^+	7.38	16
$\text{C}_2\text{H}_5\text{OH}_2^+$	5.31	22
$\text{C}_2\text{H}_5\text{OH}$	-2.44	23
$\text{C}_2\text{H}_5\text{O}$	-0.26	24
$\text{C}_2\text{H}_4\text{O}$	-1.72	25
CH_2O	-1.20	25
$\text{C}_2\text{H}_4\text{OH}$	-0.78	26

-0.4 eV for ΔH in the subsequent discussion. These values of ΔH show that a m 47 formed from CH_2OH^+ will have greater energy (primarily internal²⁷) than one formed from $\text{C}_2\text{H}_5\text{OH}^+$ or $\text{C}_2\text{H}_4\text{OH}^+$. It should be noted that the difference between the internal energies may be greater than the difference between the enthalpy changes. The reason is that if partitioning of energy between the product species occurs statistically (as would be expected if a long-lived intermediate were formed), then this partitioning would give m 47 in the third reaction above a greater share of the energy liberated than in the second reaction; this in turn will be slightly greater than in the first reaction.

The absence of any break in the curve for m 93 at *ca.* 11.7 eV (Figure 4) can be taken as evidence that the reaction cross section for the formation of this ion from a m 47 created by CH_2OH^+ is quite small. Comparison between the m 93 curve and the m 47 curve in the region in which $\text{C}_2\text{H}_5\text{OH}^+$ and $\text{C}_2\text{H}_4\text{OH}^+$ are the reactant ions apparently reveals that the reaction cross section for the formation of m 93 with $\text{C}_2\text{H}_4\text{OH}^+$ as a precursor is less than the reaction cross section for formation from $\text{C}_2\text{H}_5\text{OH}^+$. The values of ΔH for the two reactions ap-

pear at first sight to run counter to this, the more exothermic reaction being the one in which the parent ion is the precursor. The partitioning of energy in these two cases is virtually the same. However, the values of ΔH given are those at the threshold of each process. As the photon energy is increased above the threshold, the average internal energy of the reactant ion increases (until a new fragment ion is formed). In general we may expect that the internal energy of the m 47 ion will increase with increasing photon energy. The effect of this increase in internal energy of m 47 on its subsequent reaction to form m 93 can be seen by plotting the ratio of m 93/ m 47 ion intensities as a function of photon energy. This plot, also shown in Figure 4, exhibits a strong decrease of reaction probability with internal energy.

On the basis of the above discussion, the ionization efficiency curve for m 139 would be expected to rise less rapidly than the m 93 curve and to show no break at *ca.* 11.7 eV. However, it can be seen from Figure 4 that the opposite is true; it rises more rapidly with photon energy than m 93 and has a definite change in slope at *ca.* 11.7 eV. The latter shows that m 31 is a precursor ion for m 139. This seemingly anomalous behavior can be rationalized by noting that the curve for m 139 was obtained at about 2.5 times the pressure used for m 93. At this higher pressure, considerably more m 47 ions formed from CH_2OH^+ will be deactivated enough to permit subsequent condensations with ethanol molecules. From this we can surmise that the m 93 and m 139 curves will be strongly pressure dependent, resembling the m 46 and m 45 curves at low pressure and the m 47 curve at higher pressure.

From the above discussion it is evident that intermolecular energy transfer and internal energy of the reactant ions will have appreciable effects on the condensation reactions in ethanol. The rather weak bonds formed are most likely the cause of this sensitivity.

(22) M. S. B. Munson, private communication, gave the proton affinity of $\text{C}_2\text{H}_5\text{OH}$ as 187 ± 2 kcal from which this value was calculated.

(23) "Selected Values of Properties of Chemical Compounds," Manufacturing Chemists Association Research Project, Chemical Thermodynamics Properties Center, Agricultural and Mechanical College of Texas, College Station, Texas, June 30, 1964.

(24) G. Baker, J. H. Littlefair, R. Shaw, and J. C. J. Thynne, *J. Chem. Soc.*, 6970 (1965).

(25) R. R. Bernecker and F. A. Long, *J. Phys. Chem.*, **65**, 1565 (1961).

(26) J. A. Kerr, *Chem. Rev.*, **66**, 464 (1966).

(27) (a) The experiments of J. L. Franklin and M. A. Haney, *J. Phys. Chem.*, **73**, 2857 (1969), show that for the systems they studied most of the excess energy released in ion-molecule reactions appears as internal energy of the products rather than as kinetic energy. This behavior is predicted by a statistical theory: (b) C. E. Klots, *J. Chem. Phys.*, **41**, 117 (1964).

The Photochemistry of Charge-Transfer Systems. II. Complexes of Pyromellitic Dianhydride with Polynuclear Aromatic Hydrocarbons¹

by Yvan P. Pilette and Karl Weiss*

Photochemistry and Spectroscopy Laboratory, Department of Chemistry, Northeastern University, Boston, Massachusetts 02115 (Received February 16, 1971)

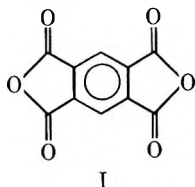
Publication costs borne completely by The Journal of Physical Chemistry

The pyromellitic dianhydride (PMDA) complexes of triphenylene, anthracene, and pyrene show charge-transfer absorption in the 400–500-nm region. Flash excitation in these bands gives rise to the same transient absorption between 500 and 700 nm which has been identified as due to the anion radical of PMDA and an ion pair consisting of this anion radical and the cation radical of the donor by spectral comparison with the species generated from the reaction of PMDA with alkali metals and by esr measurements. The photochemical changes appear to be completely reversible. The transient decay was studied in detail with the PMDA-triphenylene complex. It is rapid in dichloromethane and in acetonitrile (lifetime ~ 500 μsec) and slow in tetrahydrofuran and in acetone (half-lives ~ 10 and 1000 sec, respectively). The decay kinetics are interpreted in terms of the ion-pair equilibrium $D^+A^- \rightleftharpoons D^+ + A^-$ and the relaxation of the ion pair $D^+A^- \rightarrow DA$ (or $D + A$). The results indicate that the ion pair predominates in dichloromethane, tetrahydrofuran, and acetone, whereas in acetonitrile the ions are favored. In acetone, the transient decay is strictly first order, but the rate constants vary with the composition of the solution. Emission measurements at room temperature in solution and in a polymethyl methacrylate matrix and at 77°K in an ether-isopentane glass revealed fluorescence from the complex and phosphorescence which closely resembles that from the donor (triphenylene). The triplet state of the complex may be involved in the ionization process despite the finding that, at room temperature, the ion yield is unaffected by oxygen.

Introduction

In the first paper we described the photochemical behavior of several iodine-amine complexes in solution.² Irradiation in the visible iodine bands leads to homolytic scission of the iodine molecule and the reversible generation of amine- and solvent-complexed iodine atoms. This fragmentation of the acceptor can be considered unique for the halogens and structurally related compounds and is not likely to occur with organic acceptors. The photolysis of an iodine-amine complex in the charge-transfer absorption region takes an entirely different course and results in its irreversible destruction.

As part of a continuing investigation of the photochemistry of charge-transfer complexes, we have turned our attention to complexes involving organic acceptors, with particular emphasis on the consequences of irradiation in the charge-transfer band. In this paper we report on the photochemical behavior of the complexes of pyromellitic dianhydride (PMDA, I) with several polynuclear hydrocarbons in solutions. PMDA is a moderately strong acceptor with an electron affinity of 0.85 eV,³ and several of its complexes have been described.^{4–7} The absorption of PMDA is well below



400 nm, and the charge-transfer bands, which are well separated from the component absorption bands, appear in the 400–500-nm region. Thus the region above 500 nm is accessible for the observation of transient absorption.

Weller and coworkers³ have reported that the quenching of the fluorescence of certain aromatic hydrocarbons by typical electron donors gives rise to emission from a molecular complex which is stable only in the excited state. In highly polar solvents they obtained evidence of the formation of radical ions. We have previously suggested that excitation, in the charge-transfer band, of complexes which are stable in the ground state may give rise to radical ions by complete electron transfer.² This has indeed been found to be the case with the PMDA complexes of triphenylene, anthracene, pyrene, and naphthalene in several solvents.

(1) Presented at the Symposium on Photochemistry and Radiation Chemistry, U. S. Army Natick Laboratories, Natick, Mass., April 22–24, 1968.

(2) A. M. Halpern and K. Weiss, *J. Phys. Chem.*, **72**, 3863 (1968).

(3) G. Briegleb, *Angew. Chem. (Int. Ed.)*, **3**, 617 (1964).

(4) Y. Nakayama, Y. Ickikawa, and T. Matsuo, *Bull. Chem. Soc. Jap.*, **38**, 1674 (1965).

(5) T. Matsuo, *ibid.*, **38**, 2110 (1965).

(6) I. Ilmet and L. Kopp, *J. Phys. Chem.*, **70**, 3371 (1966).

(7) I. Ilmet and P. M. Rashba, *ibid.*, **71**, 1140 (1967).

(8) H. Knibbe, K. Röllig, F. P. Schäfer, and A. Weller, *J. Chem. Phys.*, **47**, 1184 (1967); H. Beens, H. Knibbe, and A. Weller, *ibid.*, **47**, 1183 (1967), and references cited therein.

Experimental Section

Materials. The solvents employed were all Fisher Certified (ACS or 99 mol % pure) reagents. Purities were checked by glpc (F & M Model 720 gas chromatograph). Methylene chloride was refluxed over phosphorus pentoxide and distilled from this drying agent. Tetrahydrofuran was treated with calcium hydride, degassed by the freeze-pump-thaw method, and trap-to-trap distilled several times over sodium-potassium alloy. The solvent was stored over the alloy on a high-vacuum line and was distilled into sample cells as needed. Acetone and acetonitrile were used without further purification. Methyl methacrylate (Eastman Organic Chemicals) was repeatedly shaken with 5% sodium hydroxide solution to remove the inhibitor and distilled under reduced pressure (30 mm) under nitrogen.

Pyromellitic dianhydride (Aldrich Chemical Co.) was sublimed at atmospheric pressure to give material of mp 282.5–283.0° (lit.⁹ mp 284°). Triphenylene (Aldrich Chemical Co.) was recrystallized three times from absolute ethanol and sublimed under vacuum. Thin layer chromatography (silica, benzene eluent) revealed no impurity. Pyrene (Eastman Organic Chemicals) was sublimed under vacuum to afford material of mp 150–151° (lit.¹⁰ mp 150.4°). Anthracene, blue-violet fluorescence grade, and naphthalene, recrystallized (alcohol) grade (Eastman Organic Chemicals), could be used without further purification.

Spectral Measurements. Visible and ultraviolet spectra were measured with a Beckman DK-1 spectrophotometer equipped with a constant-temperature cell holder. This instrument, fitted with its fluorescence attachment (Beckman No. 21850) and an external monochromatic excitation source, was also used for room temperature emission measurements. For low-temperature emission measurements an Aminco-Keirs spectrophosphorimeter was employed. Electron spin resonance measurements were performed with a Varian V-4500 spectrometer (100-kc field modulation, 6-in. magnet). In photochemical experiments, the samples (in 3-mm diameter tubes or a flat 1-mm quartz cell) were irradiated directly in the Varian V-4531A multipurpose cavity with the aid of an Osram HBO 500-W mercury lamp fitted with appropriate lenses and filters.

Continuous Photolysis Experiments. The monochromatic irradiation apparatus for this purpose is described in detail elsewhere.¹¹ In this study it was used with a GE BH-6 mercury lamp. Higher intensity constant irradiation experiments were performed with other mercury lamps (Phillips HPK 125-W and Osram HBO 500-W) used with and without appropriate filters.

Flash Photolysis Experiments. The essential features of the flash apparatus have been previously described.² The arrangement used in this study incorporates a photomultiplier (EMI 9558 AQ) detection

circuit without cathode follower. Signal collapse is prevented by employing very short coaxial leads to the oscilloscope. The flash tubes, which were designed by Dr. E. Wall, feature an expansion chamber behind each electrode which connects with the quartz discharge chamber by means of holes in the end cap. The Pyrex expansion chambers are permanently cemented to the end caps with epoxy cement, but the quartz tubes are held by commercial Swagelok fittings¹² with Teflon ferrules. These fittings provide a vacuum-tight seal and permit defective quartz jackets to be easily replaced and the electrodes to be cleaned and reconditioned.

Liquid samples, which were outgassed by the freeze-pump-thaw method, were flashed in cylindrical, jacketed Pyrex or quartz cells with 3-, 6-, and 12-cm path lengths. The rapid circulation of filter solution (aqueous, containing copper sulfate (0.4 M), ferric alum (0.02 M), and sulfuric acid (0.05 M)) from a thermostated bath through the jacket served not only to keep the temperature constant but also to confine light absorption to the charge-transfer region. The circulation system consists of a polyethylene circulating pump with steel shaft (Gorman-Rupp Industries) and a glass coil and 500-ml reservoir immersed in a 5-gal water bath. Temperature control to $\pm 0.1^\circ$ is achieved by counterbalancing a "Portatemp" heating unit (Precision Scientific Co.) with a portable bath cooler (Neslab Instruments, Durham, N. H.).

For low-temperature flash experiments (to -80°), the method described by Ottolenghi, Bar-Eli, and Linschitz¹³ was used. The flash light was limited to the charge-transfer absorption by covering the un-silvered Dewar vessel with a Roscolene No. 863 medium blue filter (Rosco Laboratories, Harrison, N. Y.).

Solid methyl methacrylate polymer containing charge-transfer complex was prepared by polymerizing a solution of the monomer at 30–40° with azobisisobutyronitrile (0.02%). The crude rod was machined into a 2-cm diameter, 6-cm long cylinder with optical faces.

The photographic records of the oscilloscope traces were processed as previously described,² and the transient absorption is recorded in terms of ΔD_λ , the time-dependent change in optical density at wavelength λ . For slow decay rates, the photomultiplier signal was recorded with a strip chart recorder. In acetone solution, it was possible to monitor the decay with the Beckman spectrophotometer.

(9) J. C. A. Boeyens and F. H. Herbstein, *J. Phys. Chem.*, **69**, 2153 (1965).

(10) N. A. Lange, Ed., "Handbook of Chemistry," 10th ed, McGraw-Hill, New York, N. Y., 1961, pp 688, 689.

(11) H. P. Wolf, J. J. Bohning, P. A. Schnieper, and K. Weiss, *Photochem. Photobiol.*, **6**, 321 (1967).

(12) Crawford Fitting Co., Cleveland, Ohio.

(13) M. Ottolenghi, K. Bar-Eli, and H. Linschitz, *J. Chem. Phys.*, **43**, 206 (1965). We are grateful to Dr. Linschitz for providing us with details of the cell design.

Table I: Thermodynamic and Spectral Properties of PMDA Complexes

Complex	Solvent	K_{298} , l./mol ^a	$-\Delta H$, kcal/mol ^b	λ_{\max} , nm	$\epsilon_{\lambda_{\max}}$
PMDA-triphenylene	Methylene chloride	5.8 ± 0.2	2.9 ± 0.2	415	1379 ± 24
	Tetrahydrofuran	18.3 ± 0.5	~ 0	385 ^c	300 ± 60
	Acetone	24 ± 8	0.50 ± 0.06	385 ^c	348 ± 90
	Acetonitrile	14.5 ± 0.4	2.7 ± 0.2	390 ^c	420 ± 80
PMDA-triphenylene	Methyl methacrylate	390 ^c	...
PMDA-pyrene	Methylene chloride	8.3 ± 0.3	3.8 ± 0.3	505	1048 ± 25
PMDA-anthracene	Methylene chloride	515	...
PMDA-naphthalene	Methylene chloride	405	...

^a Measured with PMDA and donor concentrations in the ranges $2-5 \times 10^{-3}$ and $5-50 \times 10^{-3} M$, respectively. ^b In the temperature range 5–40°. ^c Shoulder.

Anion Radical of PMDA.¹⁴ A solution of this radical and its ion pair with an alkali metal ion can be prepared by allowing a degassed solution of PMDA to contact a sodium mirror or sodium-potassium alloy. The reaction with sodium is incomplete since the metal rapidly becomes coated with a purple, insoluble substance. The reaction with the alloy is cleaner but requires elaborate manipulations to accomplish substantial conversion of the anhydride. The apparatus used for this purpose incorporated a reaction tube into which sodium-potassium alloy is distilled, two tubes for PMDA solution and solvent, fritted filters for the removal of unreacted alloy and a solid purple side product which inevitably formed, and cells for esr and optical measurements.

Results

a. Ground-State Properties of the Complexes. Knowledge of ground-state properties was deemed pertinent, and consequently equilibrium constants and extinction coefficients were measured by the Benesi-Hildebrand procedure.¹⁵ This involves the assumption that 1:1 complexes are formed, but the linearity of plots is no guaranty of this stoichiometry.¹⁶ The Job¹⁷ variational method, applied to the PMDA-pyrene system in dichloromethane at the charge-transfer maximum (505 nm) showed a maximum at 0.5 mole fraction.¹⁸ The phase diagram of the PMDA-triphenylene system shows the existence of a solid 1:1 compound; there are eutectics at 0.30 and 0.91 mole fraction of triphenylene. The results of the spectral and Benesi-Hildebrand measurements are summarized in Table I for the complexes and solvents used in the photochemical work. We see that the enthalpy of formation values in the oxygen-containing solvents tetrahydrofuran and acetone are abnormally low. This implies a positive entropy for association, which is possibly due to complex formation with the solvent. For present purposes, we use these numbers merely to evaluate the composition of solutions under various conditions.

b. Properties of the Anion Radical of PMDA. The PMDA anion radical (ion pair) spectrum obtained from

a $1.6 \times 10^{-4} M$ solution of PMDA in tetrahydrofuran and sodium-potassium alloy is shown in Figure 1. Based on the assumption, which appears to be borne out by the spectrum, that this species has almost no absorption at 325 nm where $\epsilon = 2.78 \times 10^3$ for PMDA, and neglecting the side product, the lower limit of $\sim 10^4$ is obtained for the extinction coefficient of the anion radical at 665 nm. Anion radical solutions prepared with the alloy under conditions which left little unreacted PMDA are quite stable and retain their blue color for 3–4 days. On the other hand, tetrahydrofuran solutions prepared by reaction with a sodium mirror which contain much unreacted anhydride decay in 3–4 hr by a first-order process. By irradiation of the decayed solution with an unfiltered mercury lamp, the anion radical could be repeatedly regenerated, but each successive decay furnished additional amounts of a photostable product which has a spectrum similar to that of the ground-state PMDA-triphenylene complex. The slower decay of the more stable solutions prepared from the alloy leads directly to the same product and, in this case, the anion radical cannot be photoregenerated.

c. Emission from the Complex. Excitation of the triphenylene-PMDA complex in dichloromethane solution at room temperature gives rise to a broad emission band with a maximum at 500 nm. The excitation and emission spectra in this solvent are almost identical with those for this complex in the solid polymethyl methacrylate matrix at room temperature, which are shown in Figure 2.

The behavior of the triphenylene-PMDA complex is different in a 1:1 ether-isopentane glass at 77°K. With excitation in the charge-transfer band at 420 nm, phosphorescence closely resembling that of triphenylene

(14) The species produced by the reaction of an alkali metal with PMDA in tetrahydrofuran is, for convenience, designated as the anion radical although, in this solvent, ion-pair formation is extensive.

(15) H. A. Benesi and J. H. Hildebrand, *J. Amer. Chem. Soc.*, **71**, 2703 (1949).

(16) G. D. Johnson and R. E. Bowen, *ibid.*, **87**, 1655 (1965).

(17) P. Job, *Ann. Chim. Phys.*, [10] **9**, 113 (1928).

(18) A 2:1 complex of PMDA and pyrene has been reported to be formed under extreme conditions; cf. ref 6.

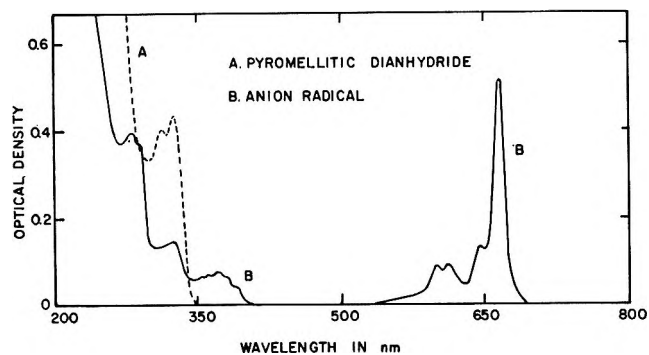


Figure 1. Spectrum of the PMDA anion radical in tetrahydrofuran: A, $1.6 \times 10^{-4} M$ PMDA; B, PMDA anion radical. Since part of the PMDA is converted into an insoluble product (see text), the actual anion radical concentration is not known.

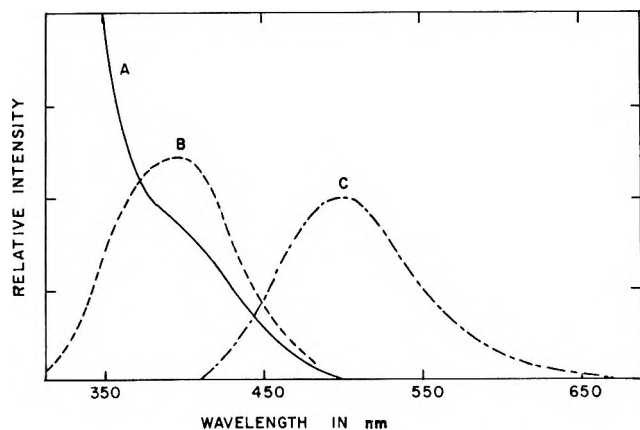


Figure 2. Emission and excitation spectra of the triphenylene-PMDA complex in polymethyl methacrylate at room temperature: A, ground-state absorption; B, excitation spectrum; C, emission spectrum.

is observed. This is shown in Figure 3 which, for comparison, includes the total emission spectrum of triphenylene with excitation at 280 nm. Excitation of the separated components at 420 nm produces no emission.

d. Electron Spin Resonance Spectra. The anion radical (ion pair) prepared from PMDA and sodium-potassium alloy in tetrahydrofuran shows the three-line electron spin resonance spectrum with intensities approximately in the ratio 1:2:1 which is expected on the basis of two equivalent protons in structure I. The splitting constant is $a_H = 0.78$ G. No splitting due to the alkali metal was evident.

Without irradiation, a solution of the PMDA-triphenylene complex in tetrahydrofuran solution shows no electron spin resonance signal. Irradiation in the charge-transfer band gives rise to a weak three-line signal which is not as well resolved as the signal from the chemically prepared anion radical of PMDA. The splitting constant ($a_H = 0.75$ G) is, however, the same as for the latter. An entirely analogous electron spin resonance spectrum with $a_H = 0.79$ G was produced by

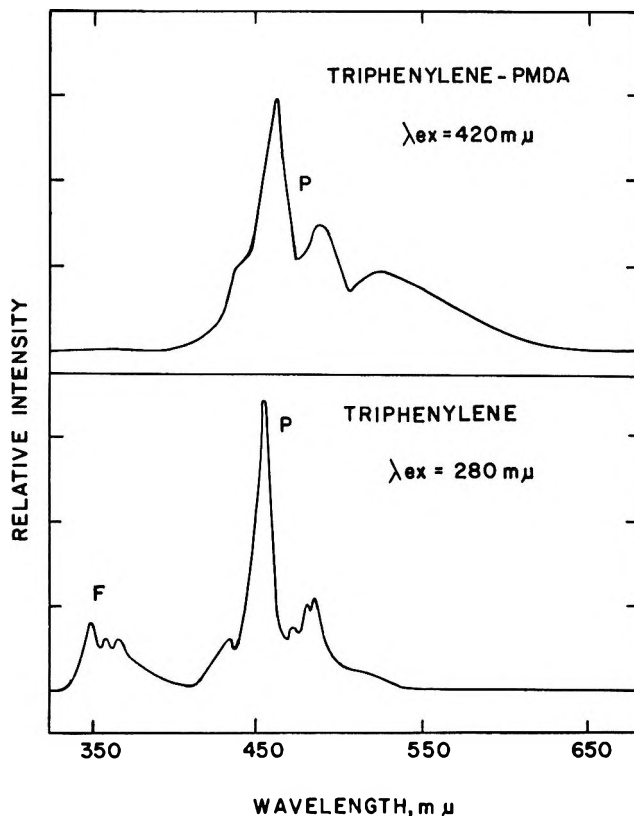


Figure 3. Emission spectra of triphenylene and its PMDA complex in an ether-isopentane glass at 77°K: F, fluorescence; P, phosphorescence.

irradiation of the naphthalene-PMDA complex in tetrahydrofuran solution. Variation of the donor: acceptor ratio from 100:1 to 1:100 failed to produce absorption which could be unequivocally assigned to the cation radicals of the aromatic hydrocarbons.

e. Continuous Irradiation of the Complexes. Photolysis of the PMDA-triphenylene complex in degassed dichloromethane solution with a Pyrex-filtered 125-W mercury lamp for 20 hr caused some chemical change which is reflected in an increase in absorption in the charge-transfer region. Under the same conditions, triphenylene alone, which has been reported to be photostable,¹⁹ yielded a colored product which was not further examined. Pyrex-filtered mercury lamp irradiation also caused some decomposition of the pyrene-containing complex and produced the hydrocarbon dimer from the PMDA-anthracene complex in tetrahydrofuran.

By contrast, the complex solutions were found to be stable to continuous monochromatic photolysis in the charge-transfer region. The apparatus used for this purpose provided *ca.* 4×10^{15} photons/cm² sec at 435 nm.¹¹ No detectable changes resulted from the photolysis, under these conditions, of the PMDA-triphenylene

(19) W. G. Herkstroeter, A. A. Lamola, and G. S. Hammond, *J. Amer. Chem. Soc.*, **86**, 4537 (1964).

complex in methylene chloride for 25 hr and in tetrahydrofuran solution for 50 hr.

f. Transient Spectra. The transient absorption generated by flash photolysis of the PMDA-triphenylene complex in dichloromethane solution at 15° is shown in Figure 4. The donor-to-acceptor ratio for this solution is 1:1. The spectral distribution of the transient absorption is the same in degassed and undegassed solution, and with a donor-to-acceptor ratio of 25:1. The transient spectral features of the PMDA complexes are summarized in Table II. In all cases the spectra are almost identical with each other and with the spectrum of the anion radical. However, the lifetime of the transient varies dramatically with the solvent. For the complex in dichloromethane and acetonitrile solutions, the lifetimes are in the microsecond range. For the PMDA-triphenylene complex in tetrahydrofuran solution, the lifetime is of the order of seconds and in acetone it is of the order of minutes. An important feature to be noted is that, in every case, the shape of transient spectrum is invariant with respect to time.

Table II: Spectral Features of Transient

Complex	Solvent	λ_{\max} , nm	
Anion radical	Tetrahydrofuran	597, 610	640, 665 ^a
Triphenylene-PMDA	Tetrahydrofuran	597, 612	643, 663
	Acetone	600, 610	640, 665
	Acetonitrile	605	645, ^b 665
	Dichloromethane	610	645, ^b 670
Pyrene-PMDA	Dichloromethane	605	665
Anthracene-PMDA	Dichloromethane	610	645, ^b 670
Triphenylene-PMDA	Methyl methacrylate polymer ^c	600	653

^a $\epsilon_{665} \geq 10^4$, prepared from sodium or sodium-potassium alloy in PMDA. ^b Shoulder. ^c Solid.

The only different spectrum is observed in solid methacrylate polymer, where the broad, low wavelength band at 600 nm is more intense than the band at 653 nm. Moreover, in this matrix the transient has a lifetime comparable to that of the flash.

The maximum initial optical density of the transient depends, in all cases, only on the ground-state optical density in the charge-transfer region and on the flash energy. Within experimental error, the presence of oxygen has no effect on the maximum transient density although the decay rate becomes more rapid. This is particularly marked in acetone and tetrahydrofuran solutions, where the lifetimes are reduced to the microsecond range by oxygen.

g. Decay Kinetics. The decay kinetics of the transient generated from the PMDA-triphenylene complex were measured in several solvents as a function of donor-to-acceptor ratio, wavelength, temperature, and the pressure of oxygen. The transient spectra in all the

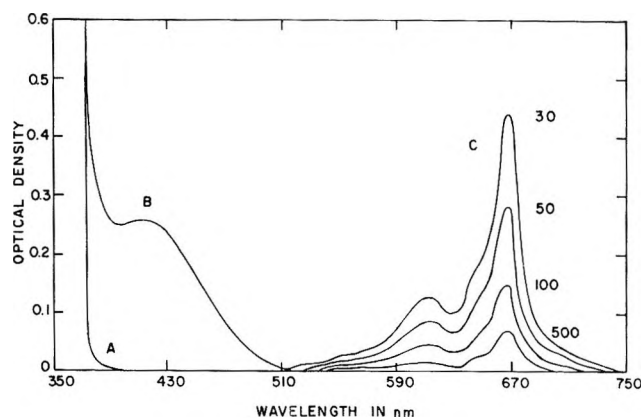


Figure 4. Transient spectrum of the triphenylene-PMDA complex in outgassed methylene chloride solution at 15°; the concentration of each component is $5 \times 10^{-2} M$: A, triphenylene; B, ground-state complex; C, transient. The numbers represent the time in microseconds after flash excitation.

solvents examined (dichloromethane, acetonitrile, tetrahydrofuran, acetone) indicate that the absorption is due to a single species or to several species with almost identical spectral features. There is every indication that the transient behavior is entirely reversible in undegassed solution when flash excitation is confined to the charge-transfer band. Kinetic laws were examined in terms of the time-dependent behavior of the transient change in optical density which, since there is no overlap with the ground-state complex absorption, is given by $\Delta D = \sum_i \epsilon_i c_i l$, where ϵ_i and c_i are the extinction coefficient and molar concentration, respectively, of the transient species, and l is the path length in centimeters.

1. *Dichloromethane.* The decay kinetics in this solvent are complex and follow no simple law over the entire time domain. Traces from a large number of experiments indicated that the decay can be analyzed in terms of an initial ($t < 100 \mu\text{sec}$) first-order process followed by a final ($t > 200 \mu\text{sec}$) second-order process. Rate constants at several wavelengths are summarized in Table III. The first-order rate constant is seen to be the same when donor-to-acceptor ratio is 1:1 and 25:1.

2. *Acetonitrile.* In degassed acetonitrile solution, the transient lifetime is of the same order of magnitude as in dichloromethane. Below 0°, the decay is strictly second order; k/ϵ values at 660 nm are $1.3 \times 10^5 \text{ cm sec}^{-1}$ at 0° and $1.8 \times 10^3 \text{ cm sec}^{-1}$ at -44°.

Above 0°, decay is more complex and a long-lived component appears. Even at 15°, the final decay is quite slow, and a trace made several seconds after the flash remains above the original base line. It was also noted that, at this temperature, a small amount of this long-lived absorption can be generated by the monitoring light of the flash apparatus and that it disappears in the presence of 1 mm of oxygen pressure. We believe that this long-lived species arises from a relatively slow,

Table III: Rate Constants for the Decay of Transients from the PMDA-Triphenylene Complex in Dichloromethane at 15°^a

Wavelength nm	Initial decay ($t < 100 \mu\text{sec}$) $k \times 10^{-4} \text{ sec}^{-1}$ ^b	Final decay ($t > 200 \mu\text{sec}$) $k/\epsilon \times 10^{-6} \text{ cm sec}^{-1}$
611	1.8 (2)	2.6 ± 0.1
617	1.5 (1)	2.8
644	1.6 (2)	2.5 ± 0.1
670	2.1 (7), 2.0 (2) ^c	0.8 ± 0.2
693	2.1 (1)	35.0
Av 1.9 ± 0.3		

^a 1:1 donor-to-acceptor ratio with concentrations of $5 \times 10^{-3} M$ each unless otherwise indicated. ^b Average value for the number of runs quoted in brackets. ^c 25:1 donor-to-acceptor ratio with concentrations of 2.5×10^{-2} and $1 \times 10^{-3} M$, respectively.

activated reaction involving the solvent which is entirely suppressed at lower temperatures.

3. *Tetrahydrofuran*. In this solvent there is an initial, very rapid decay which is followed by a much slower first-order process. This is illustrated by the traces in Figure 5. The initial decay is second order, and a plot of $1/(\Delta D - \Delta D_e)$ against time (ΔD_e is the op-

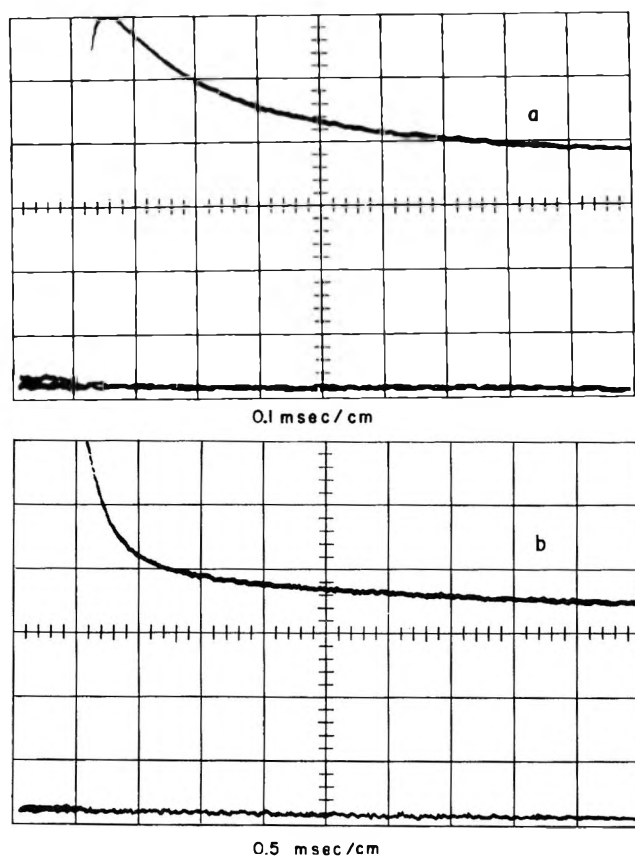


Figure 5. Oscilloscope traces for transient decay in tetrahydrofuran solution at 25° with PMDA and triphenylene concentrations each $5 \times 10^{-3} M$. The vertical scale is 0.5 V/cm, and the unattenuated intensity corresponds to 3 V.

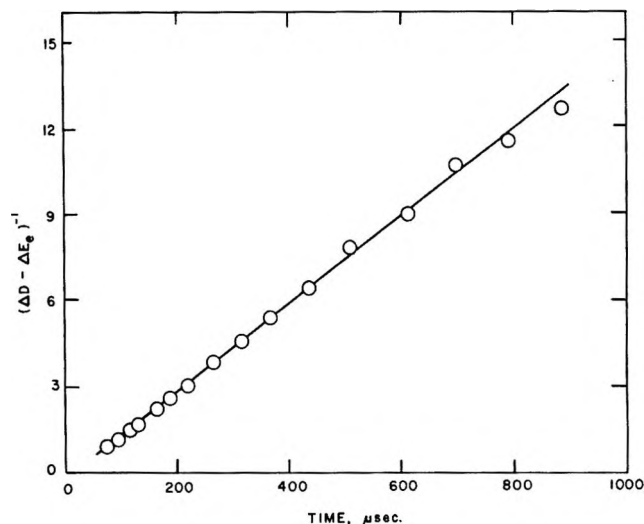


Figure 6. Initial transient decay in tetrahydrofuran solution at 25°. The concentrations of PMDA and triphenylene are each $5 \times 10^{-3} M$.

tical density at 2000 μsec , when the rapid process is essentially complete) is linear and provides k/ϵ (663 nm) = $9.0 \times 10^4 \text{ cm sec}^{-1}$ at 25° (cf. Figure 6). The slow decay has a rate constant of $(5.4 \pm 0.4) \times 10^{-2} \text{ sec}^{-1}$ (663 nm), corresponding to a half-life of 12.8 sec.

4. *Acetone*. In acetone, the decay occurs over a period of ca. 5000 sec, as compared with ca. 300 sec in tetrahydrofuran. We have, unfortunately, no experimental data in the microsecond range for this solvent. The slow process is strictly first order over several half-lives. Measurements were made at three donor-to-acceptor ratios and three temperatures, and the results are summarized in Table IV. These data provide activation energies which vary with the composition of the solution. The values are 11.4, 1.4, and 13.8 kcal/mol, respectively, for the donor-to-acceptor ratios of 26.5:1, 1.6:1, and 1:125. Thus the high activation energies are associated with solutions in which either the donor or the acceptor is in large excess, and there is little temperature dependence when the concentrations are comparable. This behavior may be taken as indicative of the involvement of one or more equilibria in the decay processes. In this connection, it may be noted that the concentration of the components in these solutions does not change substantially with temperature since the apparent enthalpy of association for the complex is small (Table I).

5. *Effect of Oxygen*. The transient decay in undegassed dichloromethane solution of the PMDA-triphenylene complex (1:1) is more rapid than in degassed solution. The decay is first order for over three half-lives with $k = (3.1 \pm 0.1) \times 10^4 \text{ sec}^{-1}$ at 15°. The marked effect of oxygen on the decay rates in tetrahydrofuran and acetone has already been noted. In undegassed solutions of the PMDA-triphenylene complex, the apparent transient half-lives are about 150 and 100

Table IV: Rate Constants for the Decay of the Transient from the PMDA-Triphenylene Complex in Acetone

Wavelength, nm	Donor-to-acceptor ratio								
	26.5:1 ^a			1.6:1 ^b			1:125 ^c		
	Temp, °C			Temp, °C			Temp, °C		
	29	38	50	25.5	38	50	15	28.5	38
	$k \times 10^4 \text{ sec}^{-1}$			$k \times 10^4 \text{ sec}^{-1}$			$k \times 10^4 \text{ sec}^{-1}$		
665	3.4	5.9	12.3	3.4	3.3	4.0	2.4	6.8	15.7
642	3.4	6.1	12.0	3.5	3.6	4.1	3.0	7.8	18.1
610	3.4	6.2	11.0	3.4	3.6	4.1	3.3	7.7	18.8
600	3.2	6.1	10.7	3.3	3.5	4.2	3.4	8.3	19.8
Av	3.4 ± 0.1	6.1 ± 0.1	11.5 ± 1.3	3.4 ± 0.1	3.5 ± 0.1	4.1 ± 0.1	3.0 ± 0.3	7.7 ± 0.5	18.1 ± 1.2

^a [Triphenylene] = $4.53 \times 10^{-2} M$, [PMDA] = $1.73 \times 10^{-3} M$. ^b [Triphenylene] = $1.68 \times 10^{-2} M$, [PMDA] = $1.03 \times 10^{-2} M$. ^c [Triphenylene] = $1.03 \times 10^{-3} M$, [PMDA] = $1.28 \times 10^{-1} M$.

μsec , respectively. In these solvents and in acetonitrile, the decay in the presence of oxygen is complex and appears to follow a combination of first- and second-order rate laws. Evidence for the participation of a second-order process in tetrahydrofuran solution is that the apparent initial first-order rate constants increase with increasing flash energy.

Discussion

The spectral results (Table II), electron spin resonance measurements, and sensitivity to oxygen establish a close similarity between the transient generated by photolysis of the PMDA-polynuclear hydrocarbons in solution and the anion radical of PMDA and/or ion pair (A^-Na^+)²⁰ prepared by the reaction of alkali metals with PMDA in tetrahydrofuran. In this solvent, ion association is expected to be important.²¹ Consequently, we identify the photochemical transient as the anion radical of the acceptor or the ion pair consisting of this anion radical and the cation radical of aromatic hydrocarbon donor. At any instant during the decay, one or the other or both of these species are present. The transient spectra are identical with respect to relative intensity at different wavelengths at all times during the decay. We conclude from this that the ion and the ion pair have the same spectral contour, although there is evidence (*vide infra*) that their extinction coefficients are different.²² The flash excitation produced no spectral features which can be ascribed to the cation radical D^+ . The spectrum of this cation radical has been reported.²³ Its absorption, which is in the same region as that of the anion radical of PMDA, shows maxima at 398, 573, 645, and 690 nm. The extinction coefficient at 690 nm can be estimated as ~ 5000 from the spectrum of the triphenylene anion radical on the basis that the spectra of the cation and anion radicals of alternant hydrocarbons are very similar. If the value of this extinction coefficient is approximately correct, spectral evidence of the cation radical should be present in the transient absorption. We can only surmise that the extinction coefficient of the PMDA anion radical has been substantially underestimated, possibly due to ne-

glect of the side product in the reaction of PMDA with alkali metal (*vide supra*). The apparent absence of electron spin resonance absorption due to the triphenylene cation radical can be rationalized on the basis that only a very small concentration of this species is generated by irradiation and that the width of the spectrum (>20 G) is such that it could easily be submerged in the noise.

It is of interest to note that flash excitation of the PMDA-mesitylene complex also produces no spectral evidence of the donor cation radical.²⁴ By contrast, the photolysis of pyrene-*p*-dicyanobenzene and pyrene-tetracyanoethylene solutions in acetonitrile generates transient absorption due to the pyrene cation radical.²⁵

The emission observed from dichloromethane solutions of the PMDA-triphenylene complex and from this complex dispersed in methyl methacrylate polymer is clearly fluorescence from the charge-transfer complex. This is evident not only from the excitation spectrum, but also from the approximate mirror image relationship to the charge-transfer band (Figure 2). The 0-0 band appears to be at *ca.* 440 nm. The phosphorescence spectrum of the complex at 77°K closely resembles that of triphenylene (Figure 3). The slight differences lie in the blurring of structure in the individual bands, which may be due to the weaker emission from the complex than from the hydrocarbon, and in the enhancement of a small band near 525 nm. The 0-0 band at *ca.* 430 nm (reported¹⁹ 429 nm) is unshifted in the complex.

(20) For convenience, radical ions are formulated simply as charged species. Thus A^- represents $PMDA^{\cdot -}$.

(21) C. Carvajal, K. J. Tölla, J. Smid, and M. Szwarc, *J. Amer. Chem. Soc.*, **87**, 5548 (1965).

(22) This interpretation is supported by the recent report that a series of amine picrate ion pairs have very similar spectra in acetonitrile. The maxima, which fall within an 8-nm range, are displaced *ca.* 25 nm to shorter wavelengths from the maximum for the picrate ion. Cf. M. K. Chantooni, Jr., and J. M. Kolthoff, *ibid.*, **90**, 3005 (1968).

(23) P. Bennema, G. J. Hoijtink, J. H. Lupinski, L. J. Oosterhoff, P. Selier, and J. D. W. van Voorst, *Mol. Phys.*, **2**, 431 (1959).

(24) R. Potashnik, C. R. Goldschmidt, and M. Ottolenghi, *J. Phys. Chem.*, **73**, 3170 (1969); R. Potashnik and M. Ottolenghi, *Chem. Phys. Lett.*, **6**, 525 (1970).

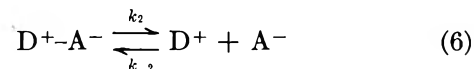
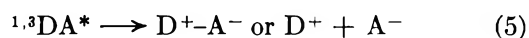
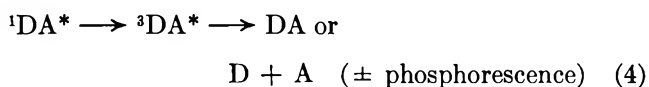
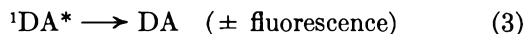
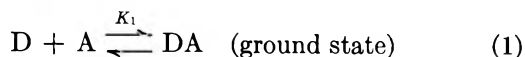
(25) K. H. Grellmann, A. Watkins, and A. Weller, *J. Luminescence*, **1**, 2, 678 (1970).

The phosphorescence of PMDA is broad with a maximum near 450 nm; its 0-0 band can be estimated to lie near 410 nm.²⁶ According to these spectra, the energies are in the order: triplet excited state of PMDA > singlet excited state of complex \simeq triplet excited state of triphenylene. The triplet excited state of the complex can be considered as a locally excited triplet state of the donor within the complex, which may be stabilized by the charge-transfer interaction, and which may or may not be dissociative.²⁷

In the solution flash experiments with the PMDA-triphenylene complex, no evidence was found for triplet-triplet absorption due to the complex or to the donor. Porter and Windsor have reported this absorption for triphenylene to have λ_{\max} 428 nm,²⁸ and this has been confirmed by our own flash experiments.

The question now arises whether the radical ions arise from the excited singlet or triplet state of the complex. For the PMDA-mesitylene system it has been shown by simultaneous phosphorescence decay and transient absorption growth measurements at low temperature that the triplet state of the complex ionizes.²⁴ The rate constant for this process is $\sim 800 \text{ sec}^{-1}$ at 117°K, and oxygen suppresses ionization. By contrast, we find for the PMDA-triphenylene complex that the initial amount of transient absorption produced in the 500-700-nm region is independent of the oxygen pressure. The ion yield is not changed by even one atmosphere pressure of pure oxygen. Under these conditions the solubility of oxygen is $\sim 10^{-2} M$ at room temperature and, with the assumption that the quenching rate is diffusion controlled, the effective lifetime of the complex triplet state would have to be comparable to that expected for the singlet excited state ($< 10^{-8} \text{ sec}$ at room temperature) for the ionization to be uninfluenced by oxygen. A triplet lifetime of this magnitude is not inconceivable, so that an unequivocal distinction between singlet and triplet ionization paths is not possible on the basis of the oxygen experiments alone. Although the general appearance of the phosphorescence spectra of the PMDA-mesitylene and PMDA-triphenylene complexes is quite different, the 0-0 bands appear to be close,²⁶ and differences in the behavior of these complexes may ultimately be due to differences in the energies of the corresponding donor ions or their ion pairs.

The experimental results for the PMDA-triphenylene system support the following general scheme, in which the acceptor and donor are designated as A and D, respectively, the corresponding ions as A^- and D^+ , the complex and the ion pair as DA and D^+A^- , respectively, and the singlet and triplet excited states of the complex as $^1DA^*$ and $^3DA^*$, respectively. The be-



havior in various solvents will be interpreted in terms of this scheme. Whether the excited states $^1,^3DA^*$ produce the ion pair or the separated ions is governed by the properties of the solvent.²⁹ The detailed structure of the ion pair is of obvious interest, in particular whether it is of the contact or solvent-shared type. This can be expected to depend in a rather specific way on the nature of the solvent and the ions involved.^{21,30,31} Possibly, the solvent-shared ion pair predominates in the oxygen-containing solvents (acetone and tetrahydrofuran), whereas the non-oxygen-containing solvents (dichloromethane and acetonitrile) favor the contact ion pair. In any case, the kinetic results show vastly different behavior in the oxygen-containing solvents, in which the transient decay is quite slow.

Since $\Delta D = \epsilon_A[A^-] + \epsilon_{D+A}[D^+A^-]$, and $[A^-] = [D^+]$ in the absence of other ionic species, the equation $-d\Delta D/dt = [D^+A^-][k_3\epsilon_{D+A} - k_2(\epsilon_A - \epsilon_{D+A})] + [A^-]^2k_{-2}(\epsilon_A - \epsilon_{D+A})$ (8)

rigorously describes the time-dependent behavior according to eq 6 and 7. This equation will now be used to delineate the decay in the different solvents examined.

a. Methylene Chloride. The behavior in this solvent may be rationalized if we assume that excitation produces the ion pair only, *i.e.*, $^1DA^* \rightarrow D^+A^-$. Since

(26) S. Iwata, J. Tanaka, and S. Nagakura, *J. Chem. Phys.*, **47**, 2203 (1967).

(27) According to the classification proposed in ref 26, the PMDA-triphenylene system may be viewed as a limiting case of case I(b) for which the energies of the locally excited triplet state of the complex, the triplet charge-transfer state, and the singlet charge-transfer state are approximately equal.

(28) G. Porter and M. W. Windsor, *Proc. Roy. Soc., Ser. A*, **245**, 238 (1958)

(29) One of the referees has pointed out that if the ion-ion pair system obtained immediately after the flash were to be only slightly displaced from equilibrium, equilibration would occur within times $\tau_{\text{equil}} = (2k_{-2}[A^-] + k_2)^{-1}$; *cf.*, M. Eigen, *Z. Phys. Chem. (Frankfurt am Main)*, **1**, 176 (1954). Consideration of the electrostatic forces involved then leads to an estimate of τ_{equil} which is substantially shorter than the flash duration of *ca.* 30 μsec , and interconversion between the ions and ion pair could not be observed under these circumstances. With flash excitation, however, a highly perturbed system is produced which is far removed from equilibrium, and the interconversion would be measurable.

(30) C. A. Kraus, *J. Phys. Chem.*, **60**, 129 (1956).

(31) It may be noted that some complexes involving strong donors and acceptors dissociate into radical ions in the dark. *Cf.* K. M. C. Davis and M. C. R. Symons, *J. Chem. Soc.*, 2079 (1965), and references cited therein.

the traces show a rapid initial decay followed by a final, slower process, we interpret this to indicate that, initially, there is a very fast decay of D^+A^- such that $k_3 \gg k_2$. From the results obtained in tetrahydrofuran (*vide infra*) we infer that $\epsilon_{A^-} \simeq 4\epsilon_{D^+A^-}$; this relationship between the extinction coefficients is assumed to hold for dichloromethane as well. Consequently, $k_2(\epsilon_{A^-} - \epsilon_{D^+A^-}) \ll k_3\epsilon_{D^+A^-}$, and the k_2 term can be dropped in eq 8. Also, in the initial stages ($<150 \mu\text{sec}$), D^+A^- is the predominant species so that the last term in eq 8 can be neglected as well and $\Delta D \simeq \epsilon_{D^+A^-}[D^+A^-]$. With these approximations, eq 8 reduces to $-d\Delta D/dt = k_3\Delta D$, and the first-order rate constants listed in Table III may be identified with k_3 .

Since k_3 is large, the ion-pair concentration rapidly becomes small, and after a few hundred microseconds, the rate of disappearance of D^+A^- becomes equal to its rate of formation from D^+ and A^- . The ion pair then assumes the role of an unstable intermediate and application of the condition $d[D^+A^-]/dt = 0$ yields the steady-state concentration $[D^+A^-] = k_{-2}/(k_2 + k_3)[A^-]^2$. From the magnitude of the dielectric constant for dichloromethane (8.9 at 25° ³²), we expect $K_{\text{diss}} = k_2/k_{-2} < 1$ ³⁰. Nonetheless, at the low total concentrations involved there are essentially only ions present in the final decay stages, so that $\Delta D \simeq \epsilon_{A^-}[A^-]$ and, with $k_2 \ll k_3$, eq 8 becomes $-d\Delta D/dt = (k_{-2}/\epsilon_{A^-}) \cdot (\Delta D)^2$. The constant k_{-2}/ϵ_{A^-} then represents k/ϵ given in Table III.

To obtain an estimate for k_{-2} , we utilize the extinction coefficient of $\sim 10^4$ at 665 nm for the absorbing species from the alkali metal-PMDA reaction. In the solvent used (tetrahydrofuran, dielectric constant 7.39 at 25° ²¹) one expects the ion pair A^-Na^+ to be favored. Consequently, we may identify 10^4 as the lower limit of $\epsilon_{A^-Na^+}$ at 665 nm. With the more tenuous assumption that the extinction is not substantially modified by exchanging Na^+ with D^+ , we may set $\epsilon_{A^-Na^+} \approx \epsilon_{D^+A^-}$. We have no means of estimating, in a meaningful manner, the effect of solvent on $\epsilon_{D^+A^-}$. We presume, however, since $\epsilon_{A^-} > \epsilon_{D^+A^-}$ in tetrahydrofuran, that this equality holds in the other solvents as well, and as a compromise, shall use the value of ϵ_{A^-} (665 nm) = 5×10^4 in all solvents.³³ For the wavelengths listed in Table III, this furnishes $k_{-2} = (4 \pm 0.5) \times 10^9$ l./mol sec in methylene chloride at 15° .

b. Acetonitrile. Acetonitrile has a higher dielectric constant than methylene chloride (36.7 at 25° ³²) and data for tetraalkylammonium salts indicate that in such solvents the ions would be favored.³⁰ As a point of departure we may assume that $K_{\text{diss}} > 1$ and that $k_2 > k_3$ as well. Under these conditions, ion-pair equilibrium would be established very rapidly. It is presumed to be complete during the lifetime of the flash ($\sim 30 \mu\text{sec}$) since no induction period or rapid initial decay is observed. According to this view, the concentration of D^+A^- at times greater than *ca.* 30 μsec is very small

and can be neglected. Therefore $\Delta D \simeq \epsilon_{A^-}[A^-]$, and eq 8 becomes $-d\Delta D/dt = [k_3(k_{-2}/k_2)]/\epsilon_{A^-}(\Delta D)$.² With this expression, $[k_3(k_{-2}/k_2)]/\epsilon_{A^-}$ may be equated with the k/ϵ values determined in this solvent. Using $\epsilon_{A^-} = 5 \times 10^4$ at the transient absorption maximum, the values for $k_3(k_{-2}/k_2)$ in units of l./mol sec are 6.5×10^9 (0°) and 9.0×10^9 (-44°).

With $k_3(k_{-2}/k_2) \sim 1 \times 10^9$ l./mol sec, $k_3 > 10^9 \text{sec}^{-1}$ is required if $k_{-2}/k_2 < 1$ as assumed above. Since we specified $k_2 > k_3$, this places the unrealistic requirement $k_2 \gg 10^9 \text{sec}^{-1}$ for the dissociation of D^+A^- . Fortunately, the data for some ammonium salts in solvents of reasonably high dielectric constant indicate that with $K_{\text{diss}} = k_2/k_{-2} \approx 10^{-2}$, the ion concentration is very much greater than the ion-pair concentration at the low total concentrations ($<10^{-4} M$) attained in our experiments. Even with $K_{\text{diss}} \approx 10^{-3}$ the ions predominate, and k_3 assumes the more reasonable value of $>10^6 \text{sec}^{-1}$. Hence, in order for the model to apply, we require $k_2 > k_3$ so that ion-pair equilibrium is maintained, and that K_{diss} is not extremely small.

c. Tetrahydrofuran. In this solvent (dielectric constant 7.39 at 25° ²¹), the transient optical density decays very rapidly at first (in the microsecond range) to approximately one-quarter of its original value. Despite the relatively low dielectric constant, we believe that with this solvent D^+ and A^- are initially produced from the complex excited state, but that these ions rapidly associate to the ion pair. In other words, the equilibrium of eq 6 is rapidly established and, with $K_{\text{diss}} \ll 1$, heavily favors the ion pair. This means that after equilibration absorption is almost entirely due to the ion pair and $\Delta D \simeq \epsilon_{D^+A^-}[D^+A^-]$.

In the initial fast decay, A^- is converted into D^+A^- without substantial loss of the latter *via* the reaction of eq 7. Thus, the initial concentration of the A^- ion ($[A^-]_0$) is essentially equal to the ion-pair concentration at the end of the rapid decay ($[D^+A^-]_e$), and the ratio of the maximum initial optical density in the plateau region of Figure 5b (ΔD_e) represents $\epsilon_{A^-}/\epsilon_{D^+A^-} \approx 4$. Further, since $[D^+A^-]_e \approx [A^-] + [D^+A^-]$ during the fast process, $\Delta D - \Delta D_e = (\epsilon_{A^-} - \epsilon_{D^+A^-})[A^-] \simeq 3\epsilon_{D^+A^-}[A^-]$. With $K_{\text{diss}} \ll 1$, the rate law $-d[A^-]/dt = k_{-2}[A^-]^2 - k_2[D^+A^-]$ becomes

$$-d(\Delta D - \Delta D_e)/dt = [k_{-2}/(3\epsilon_{D^+A^-})](\Delta D - \Delta D_e)^2 \quad (9)$$

The observed k/ϵ value then yields $k_{-2} = 2.7 \times 10^9$ l./mol sec at 25° .

If the ion pair is all that remains after equilibrium is established, the final slow decay is described by

(32) A. A. Maryott and E. R. Smith, *Nat. Bur. Stand. (U. S.) Circ.*, 514 (1951).

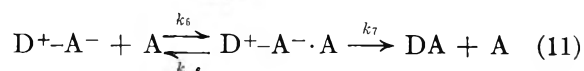
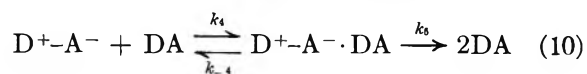
(33) Note that (see text) we believe the extinction coefficient for the ion pair A^-Na^+ has been substantially underestimated. In fact, if we assume the ion combination reaction to occur at the diffusion-controlled rate ($k_{-2} \approx 1 \times 10^{10}$ l./mol sec), we find ϵ_{A^-} (665 nm) $\approx 1 \times 10^5$.

$-\text{d}\Delta D/\text{d}t = k_3\Delta D$, which is the experimentally determined rate law.

d. Acetone. The dielectric constant of acetone is 20.7 at 25°,³² and one would expect the ions to be more favored in the equilibrium of eq 6 than they are in the case of tetrahydrofuran. Nonetheless, it appears from the results (first-order decay kinetics) that the ion-pair equilibrium is rapidly established and that, after equilibration, the ion pair is by far the predominant species present (*i.e.*, $\Delta D = \epsilon_{\text{D}^+\text{A}^-}[\text{D}^+\text{A}^-]$).

In this solvent the decay rate varies with the donor-to-acceptor ratio. To find out which of the components are participating in the decay processes, the compositions of the complex-containing solutions have been computed using values of the equilibrium constant K_1 which were calculated with the aid of the measured enthalpy of association of the complex. The results implicate the ground-state complex (DA) and acceptor (A) as responsible for the enhanced disappearance of the transient species. A calculation shows that with $\Delta D_{\text{max}} \simeq 2$, the maximum concentration of D^+A^- is *ca.* $5 \times 10^{-5} M$, so that the complex, donor, and acceptor concentrations are essentially those of the ground-state equilibrium and are not changed during the transient decay even if DA and/or A are involved in it.

Many schemes can be written which include reactions of the transient (D^+A^-) with the ground-state complex and the acceptor. A reasonable possibility involves the species $\text{D}^+\text{A}^- \cdot \text{DA}$ and $\text{D}^+\text{A}^- \cdot \text{A}$, which can be viewed as solvated ion pairs, in which part of the solvent is replaced by DA and A, respectively.



These equilibria will be maintained if $k_{-4} > k_5$ and k_{-6}

$> k_7$. Since the shape of the transient spectrum is independent of the solution composition, we assume that $\epsilon_{\text{D}^+\text{A}^-} \sim \epsilon_{\text{D}^+\text{A}^- \cdot \text{DA}} \approx \epsilon_{\text{D}^+\text{A}^- \cdot \text{A}}$. Then the rate law

$$-\text{d}\Delta D/\text{d}t = \left[\frac{k_3 + k_5 K_4 [\text{DA}] + k_7 K_6 [\text{A}]}{1 + K_4 [\text{DA}] + K_6 [\text{A}]} \right] \Delta D \quad (12)$$

can be derived, in which the bracketed term represents the rate constants listed in Table IV. This complex expression for k_{obsd} can account for the observed temperature behavior since the temperature dependence of the products $k_5 K_4$ and $k_7 K_6$ is determined by the relative magnitudes of the associated activation energies and enthalpies.

Finally, we note that the electron spin resonance spectrum of the organic donor-acceptor ion pair poses an interesting problem. No signals attributable to it were observed. This ion pair differs from that produced from an alkali metal in that it incorporates two unpaired electrons. Spin-spin interactions are bound to be strong, and if its behavior is similar to that of many triplet molecules, large zero field splitting can broaden the resonance beyond the detection limit. This question is worthy of detailed experimental study.

Acknowledgments. This research was supported by the Air Force Cambridge Research Laboratories, Office of Aerospace Research, under Contract No. F19628-67-C-0118. We are grateful to the staff of the Energetics Branch at AFCRL for use of their electron spin resonance spectrometer and spectrophosphorimeter. We also wish to thank Drs. J. L. Roebber and R. N. Wiener for many helpful discussions, Mr. E. Reid for his aid with the computation work, which was carried out at the M.I.T. Computation Center, and Mr. E. Kroch (participant in the NSF-sponsored Thayer Academy Summer Science Program, 1967) and Miss R. Levi for performing most of the association constant measurements.

Nanosecond Pulse Radiolysis Studies of Aqueous Thymine Solutions

by Leslie M. Theard, Frank C. Peterson,

Gulf Radiation Technology, A Division of Gulf Energy and Environmental Systems Inc., San Diego, California 92112

and L. S. Myers, Jr.*

Laboratory of Nuclear Medicine and Radiation Biology and Department of Radiology, University of California, Los Angeles, California 90024 (Received August 5, 1970)

Publication costs assisted by the Laboratory of Nuclear Medicine and Radiation Biology

Nanosecond pulse radiolysis of aqueous thymine solutions has been studied by producing optically detectable concentrations of transients with 10-nsec electron pulses from a Linac and employing an optical system with a signal rise time of 5 nsec. In deaerated $10^{-2} M$ thymine solutions containing 1 M ethanol at pH 6.0, thymine radical anion, T^- (λ_{\max} 325 nm), is present at the end of the pulse and its decay over the subsequent 10^{-6} sec is only slight. At pH 4.0, T^- decays exponentially with a half-life of *ca.* 10^{-7} sec, and upon decreasing the pH to 3.5 the decay half-life decreases in proportion to the increase of acid concentration, suggesting that T^- decays *via* $T^- + H_3O_{aq}^+ \rightarrow TH + H_2O$ with a reaction rate constant of $(6.4 \pm 0.3) \times 10^{10} M^{-1} sec^{-1}$. The slow decay of T^- at pH 6.0 suggests that for the reaction $T^- + H_2O \rightarrow TH + OH^-$, $k \leq 10^4 M^{-1} sec^{-1}$. An absorption signal presumed attributable to TH is present following decay of the T^- signal, with λ_{\max} also at 325 nm and an intensity about half that of T^- . Formation of the H-atom adduct of thymine, TH', produced *via* the reaction of $H + T \rightarrow TH'$ was observed to occur during the period 10^{-8} to 10^{-6} sec following the pulse for deaerated $10^{-2} M$ thymine at pH 0.65. The rate constant for TH' formation is $(6.8 \pm 0.2) \times 10^8 M^{-1} sec^{-1}$, and the absorption spectrum (λ_{\max} 400 nm) of TH' is different from that of TH. The data suggest that H-atom addition to thymine occurs at the 5,6 double bond while protonation of T^- occurs elsewhere. The submicrosecond decay of T^- and TOH resultant from their reactions with oxygen was observed; rate constants for the reactions are 4.3×10^9 and $1.9 \times 10^9 M^{-1} sec^{-1}$, respectively.

Introduction

Pulse radiolysis studies of aqueous solutions of pyrimidine-base components of nucleic acids¹⁻⁵ have shown that mechanistic aspects of the radiation chemistry of these biologically important systems can be detailed by the technique⁶ of time-resolved direct spectrophotometric detection of radiation-produced transient species. The present work concerns the use of a fast-response (5×10^{-9} sec rise time) pulse radiolysis apparatus to study aqueous solutions of the pyrimidine base thymine. The fast response of the apparatus permitted the study of certain reactions under conditions for which their lifetimes are less than a microsecond, thus minimizing interference from subsequent and/or competing reactions which occur on a microsecond or longer time scale. The reactions reported on are the protonation of thymine radical anion, the reaction of H atoms with thymine, and the reactions of thymine radical anion and thymine-OH adduct with oxygen.

It has been speculated that radical anions of thymine^{7,8} and other pyrimidines^{8,9} in aqueous solution protonate rapidly by reaction with water. The protonation reaction lifetime has been taken as less than 10^{-6} sec in the interpretation of pulse radiolysis experiments⁸ and as fast enough to compete with oxygenation of the radical anion in aerated solutions.⁷ In the present work, the study of the protonation reaction involved production of the anions by 10^{-8} -sec pulse

irradiation of deaerated solutions of $10^{-2} M$ thymine solutions containing 1 M ethanol. In this system hydrated electrons react with thymine in a few tens of nanoseconds, hydroxyl radicals are scavenged by ethanol during the pulse, and radiation-initiated radical-radical reactions occur with a half-life of tens of microseconds at the doses used in this work. It was expected, therefore, that if protonation of thymine radical anions occurs during the 10^{-8} to 10^{-6} -sec period following the pulse, the process might be observable as a rapid decay or buildup in intensity of light absorption at a wavelength at which the absorption spectra of the radical anion and the protonated radical anion differ significantly. The pH was varied in an effort to detect protonation of thymine radical anions by

(1) E. J. Hart, J. K. Thomas, and S. Gordon, *Radiat. Res., Suppl.*, **4**, 74 (1964).

(2) G. Scholes, P. Shaw, and R. L. Willson in "Pulse Radiolysis," M. Ebert, J. P. Keene, A. J. Swallow, and J. H. Baxendale, Ed., Academic Press, New York, N. Y., 1965, pp 151-164.

(3) L. S. Myers, Jr., M. L. Hollis, and L. M. Theard, *Advan. Chem. Ser.*, **No. 81**, 345 (1968).

(4) C. L. Greenstock, M. Ng, and J. W. Hunt, *ibid.*, **81**, 397 (1968).

(5) R. M. Danziger, E. Hayon, and M. E. Langmuir, *J. Phys. Chem.*, **72**, 3842 (1968).

(6) L. M. Dorfman and M. S. Matheson, *Progr. React. Kinet.*, **3**, 237 (1965).

(7) G. Scholes and R. L. Willson, *Trans. Faraday Soc.*, **63**, 2983 (1967).

(8) E. Hayon, *J. Chem. Phys.*, **51**, 4881 (1969).

(9) A. Kamal and W. M. Garrison, *Nature (London)*, **206**, 1315 (1965).

hydronium ions. It has been postulated^{4,7,8,10} that hydrated electrons do not destroy the 5,6 double bond upon reaction with thymine followed by protonation, while an opposing view^{9,11,12} has been that the protonated radical anion has a structure in which the 5,6 double bond has been destroyed and an H atom has been attached to the 5 or 6 carbon.

The reaction of H atoms with thymine was observed after a 10-nsec pulse irradiation of deaerated 10^{-2} M solutions of thymine at pH 0.65. In this system hydrated electrons react with H_3O^+ in less than 10^{-9} sec to produce H atoms. The H atoms react with thymine during the period 10^{-8} to 10^{-6} sec following the pulse, OH radicals react with thymine within a few tens of nanoseconds, and the radical products decay with half-lives of tens of microseconds. The kinetics of the H-atom addition reaction therefore can be studied without complication from simultaneous decay of the H adduct. The absorption spectra observed for this system are compared to the spectral data determined for the protonated thymine radical anion and to other results, and some conclusions are drawn regarding the molecular sites of H-atom addition and anion protonation for thymine.

Absolute reaction rate constants for the important oxygenation reactions of thymine radical anion and thymine OH adduct were determined in the present work by direct observation of the decay of these species in appropriate oxygenated solutions of thymine at 10^{-2} M. These reactions also occurred in the period 10^{-8} to 10^{-6} sec following a 10^{-8} -sec radiation pulse.

Preliminary reports of this work have appeared elsewhere.¹³⁻¹⁵

Experimental Section

Electron pulses of 2 nsec or longer duration, and up to 10 A current and 12 MeV energy were provided by an L-band electron linear accelerator (Linac). High analyzing light intensity, important for the attainment of low shot noise in fast-response systems,¹⁶ was obtained by use of EG & G FX31 A/U and FX108 A/U flash lamps. A short response time for signal detection was obtained by coupling an Amperex XP1141 photomultiplier tube (2-nsec rise time) directly to a Tektronix 585 oscilloscope with a 3-nsec rise time preamplifier, giving a system rise time of *ca.* 5×10^{-9} sec.

The flash lamps are xenon filled and cylindrical (2-cm diameter \times 2-cm long) with a uv-transmitting window at one end, and they have an unrestricted 7-mm arc. They operate on a trigger-initiated capacitor discharge and produce a light flash with a half-height width of 6 to 8 μ sec. Figure 1 shows the pulse sequence used to synchronize the flash lamp and electron pulse. The lamp firing was adjusted so that the middle microsecond of the flash was used to monitor light absorption signals. Reproducibility of light

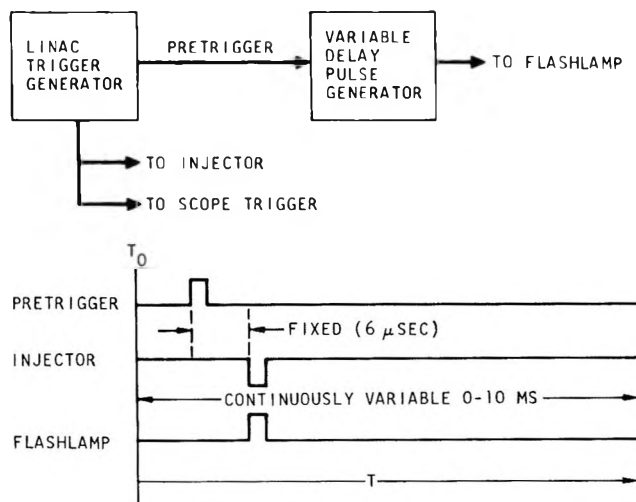


Figure 1. Diagram of pulse sequence and flash lamp timing.

intensity over this region for two successive flashes was usually within $\pm 5\%$.

The Amperex XP1141 PM tube produces an output current which is linear up to 1 A. With a low gain of 10^4 , the tube therefore generates a cathode current which is linear up to 100 μ A. Thus, it has the high-current handling capability necessary to monitor high-intensity light. The spectral response range of the PM tube is 3000 to 6500 \AA (Type S11). The PM photocathode sensitivity and impinging light intensity were sufficient to produce PM output currents exceeding 0.2 A over the spectral region 3250 to 6000 \AA (bandwidth 100 \AA); in the spectral region 4250 to 4750 \AA , filters (neutral density 1 or less) were required to maintain linear output. Thus, anode current output was adequate for direct coupling of the PM tube to the oscilloscope throughout the spectral region investigated.

The optical system employed front-surface aluminum-coated mirrors for reflection and focusing of the analyzing light beam. A multiple-reflection optical assembly employing the White design¹⁷ was adjusted for four passes of the light beam through cylindrical sample cells 2 cm long. The analyzing light was projected out of the irradiation room into an adjacent data-taking room in which the monochromator (Bausch and Lomb), PM tube, and oscilloscope were located.

(10) H. Loman and J. O. H. Blok, *Radiat. Res.*, **36**, 1 (1968).

(11) R. A. Holroyd and J. W. Glass, *Int. J. Radiat. Biol.*, **14**, 445 (1968).

(12) A. D. Lenherr and M. G. Ormerod, *Nature (London)*, **225**, 546 (1970).

(13) L. Theard and F. C. Peterson, Gulf General Atomic Report GA-8872, submitted to U. S. Atomic Energy Commission, Sept 1968.

(14) L. M. Theard, F. C. Peterson, and L. S. Myers, Jr., *Advan. Chem. Ser.*, No. 81, 603 (1968).

(15) L. S. Myers, Jr., and L. M. Theard, *J. Amer. Chem. Soc.*, **92**, 2868 (1970).

(16) J. W. Hunt and J. K. Thomas, *Radiat. Res.*, **32**, 149 (1967).

(17) J. U. White, *J. Opt. Soc. Amer.*, **32**, 285 (1942).

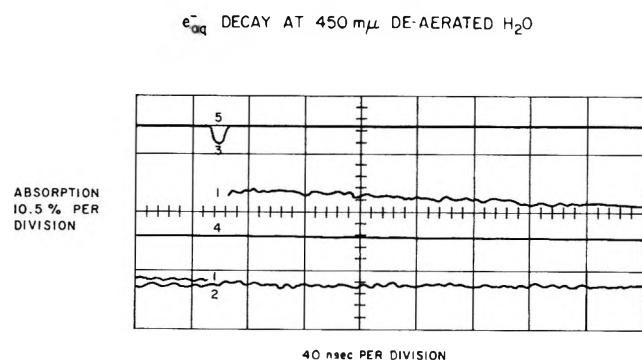


Figure 2. Oscilloscope traces demonstrating method of data taking and rise time of apparatus for light-absorption-signal detection. Absorption is for e_{aq}^- at 450 nm in argon-saturated water. Traces represent: 1, absorption signal; 2, absorption base line; 3, Cerenkov light signal from electron pulse; 4, analyzing light flash, no radiation pulse; 5, no analyzing light flash, no radiation pulse.

Intensity of each electron pulse was monitored by an electrometer which measures the integrated charge deposited in an aluminum block by the electron beam after it traverses the sample cell. The readings were checked for linearity and were calibrated for absolute dosimetry from optical densities measured for e_{aq}^- at 5780 Å in argon-saturated water, assuming

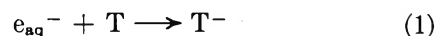
$$\epsilon_{e_{aq}^-}^{5780\text{\AA}} = 10,600^{18}$$

Samples were irradiated from the side, perpendicular to the direction of the analyzing light through the sample. Fresh samples were used for each absorption measurement. A modification of the method used by the Manchester group¹⁹ was employed for the saturation of sample reservoirs with various gases and for remote changing of samples for irradiation. Aqueous solutions were prepared from high-purity commercially available compounds and triply distilled water.

Figure 2 demonstrates the speed of the apparatus and the types of oscilloscope traces photographed. The data of Figure 2 were obtained by irradiating argon-saturated water with a 10-nsec electron pulse and monitoring changes in absorption of e_{aq}^- at 4500 Å. Five traces are shown as follows: (1) absorption signal—response to radiation pulse with analyzing light on; (2) absorption base line—no radiation pulse, with analyzing light on, vertical sensitivity same as (1); (3) Cerenkov light signal—response to radiation pulse with no analyzing light, vertical sensitivity same as (1); (4) analyzing light intensity—response to light flash, no radiation pulse; (5) reference trace—response to scope trigger, no analyzing light, no radiation pulse. Trace 2 shows the degree of flatness (variation of intensity) of the light flash over the period of signal detection. Trace 3 shows the pulse shape and the contribution of Cerenkov light to trace 1. Traces 4 and 5 give the magnitude of the 100% absorption signal.

Discussion of Results

Protonation of Thymine Radical Anion. Figure 3 shows oscilloscope traces at λ 325 nm for 20-nsec pulse irradiation of argon-saturated solutions of thymine ($0.9 \times 10^{-2} M$) and ethanol ($0.9 M$) at pH 6.0, 4.0, and 3.5. The calculated half-life for the formation of thymine radical anion, T^- , from the reaction



assuming $k_1 = 1.7 \times 10^{10} M^{-1} \text{sec}^{-1}$, is 4.5 nsec for these solutions.²⁰ Reaction of e_{aq}^- with ethanol ($k \leq 10^5 M^{-1} \text{sec}^{-1}$)¹ is three orders of magnitude slower. Therefore, the exclusive fate of e_{aq}^- is reaction 1. Reaction of OH with ethanol ($k = 1.1 \times 10^9 M^{-1} \text{sec}^{-1}$)² occurs about 15 times faster than with thymine ($k \sim 7 \times 10^9 M^{-1} \text{sec}^{-1}$)³ at the concentrations used, and reaction of H with thymine ($k = 6.8 \times 10^8 M^{-1} \text{sec}^{-1}$ from the present work) is 2.4 times faster than with ethanol ($k = 1.6 \times 10^7 M^{-1} \text{sec}^{-1}$).²¹ Taking $G(\text{OH}) = 2.65$ and $G(\text{H}) = 0.5$, the G value for products of OH and of H reactions with thymine is 0.2 in each case.

Slight decay of the T^- signal in Figure 3A can be seen. In another study (to be detailed elsewhere) employing a 0.5- μsec response pulse radiolysis system, decay of T^- at 335 $m\mu$, in a solution of $5 \times 10^{-4} M$ thymine and $0.1 M$ ethanol, was found to be unaffected by increasing the thymine concentration to $2 \times 10^{-3} M$ or by increasing the ethanol concentration to $0.3 M$. However, a decrease of pH from 5.5 to 4.5 resulted in a decrease in decay time of the initial signal to a value ($< 0.5 \mu\text{sec}$) too low to resolve accurately with the apparatus used for that study. Figure 3B shows the effect of a decrease of pH from 6.0 to 4.0 as determined with the present fast-response apparatus. A portion of the T^- signal decays within 600 nsec, leaving a signal which decays much slower. Figure 3C shows a faster decay of the initial signal resultant from further decreasing the pH to 3.5. Figure 4 shows that the decay of the initial signal at pH 4.0 is exponential and that the decay time is invariant over a fourfold range of dose. An optical density (OD) equivalent to that observed at $t = 800$ nsec was subtracted from total OD to obtain the data plotted on the vertical coordinate of Figure 4.

The data of Figures 3 and 4 suggest that the initial absorption in Figures 3A, B, and C is attributable to T^- (produced from reaction 1) which decays at pH 4.0 and 3.5 *via*



(18) J. Rabani, W. A. Mulac, and M. S. Matheson, *J. Phys. Chem.*, **69**, 53 (1965).

(19) R. L. Willson, private communication.

(20) E. J. Hart, S. Gordon, and J. K. Thomas, *J. Phys. Chem.*, **68**, 1271 (1964).

(21) A. Appleby, G. Scholes, and M. Simic, *J. Amer. Chem. Soc.*, **85**, 3891 (1963).

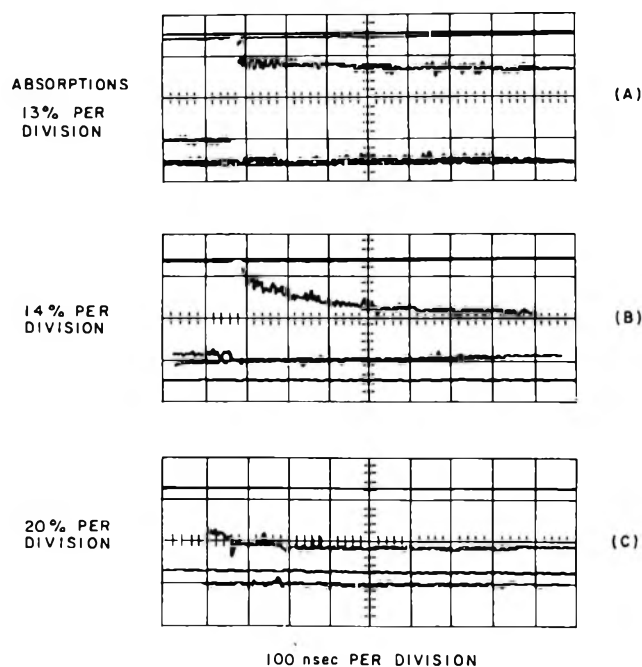


Figure 3. Oscilloscope traces of T^- absorption in deaerated $0.9 \times 10^{-2} M$ solutions of thymine containing $0.9 M$ ethanol at pH 6.0, A; pH 4.0, B; pH 3.5, C.

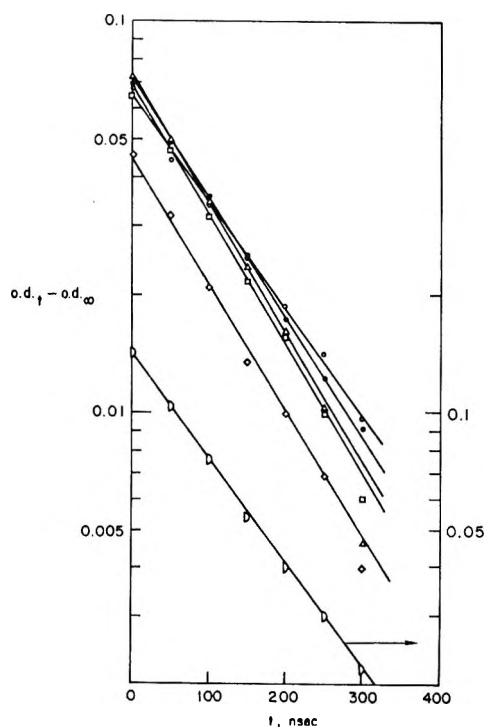


Figure 4. First-order test of data for decay of T^- via $T^- + H_3O_{aq}^+ \rightarrow TH + H_2O$ in deaerated $0.9 \times 10^{-2} M$ thymine solutions containing $0.9 M$ ethanol, pH 4.0, λ 325 nm, dose: \diamond , 1780 rads; \square , \circ , \bullet , \triangle , ca. 3200 rads; D, 7500 rads.

and that absorption which remains at 800 nsec at pH 4.0 and 3.5 (and presumably grows in at shorter times) is attributable to TH (an H-atom adduct of thymine). From the slopes of the decay curves of

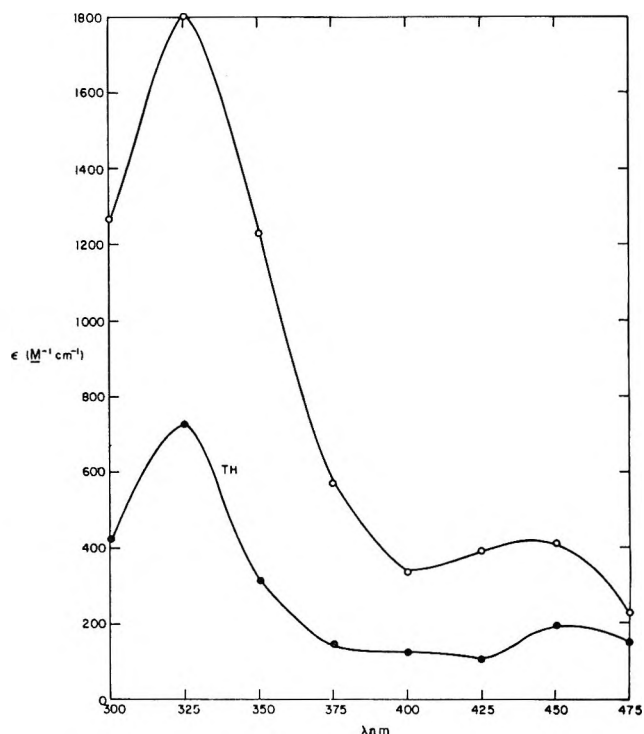


Figure 5. Absorption spectra of T^- , taken at end of 20-nsec pulse, and TH, taken 800 nsec after the pulse, for deaerated $0.9 \times 10^{-2} M$ thymine solution containing $0.9 M$ ethanol, pH 4.0.

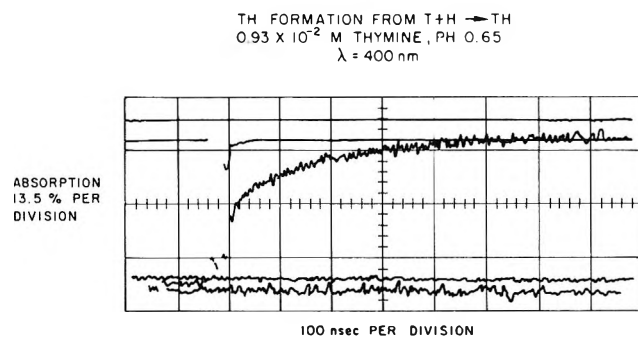
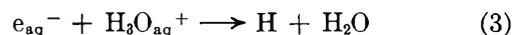


Figure 6. Oscilloscope trace of TH' formation from $H + T \rightarrow TH'$ for deaerated $0.9 \times 10^{-2} M$ thymine solution, pH 0.65, λ 400 nm, dose 5450 rads.

Figure 4 for doses near 3500 rads and pH 4.0, $k_2 = (6.4 \pm 0.3) \times 10^{10} M^{-1} \text{sec}^{-1}$. Results for two runs at pH 3.5 agree well with this value.

Figure 5 shows absorption spectra of T^- (taken at the end of 20-nsec electron pulses) and of TH (taken 800 nsec after the pulse) at pH 4.0. The spectra for these two species are similar in shape and location of the absorption maxima, but the intensity of the absorption of T^- is about twice that of TH.

Reaction of H Atoms with Thymine. Figure 6 shows oscilloscope traces at λ 400 $m\mu$ for an argon-saturated solution of thymine at $0.9 \times 10^{-2} M$ and pH 0.65. In this case the reaction



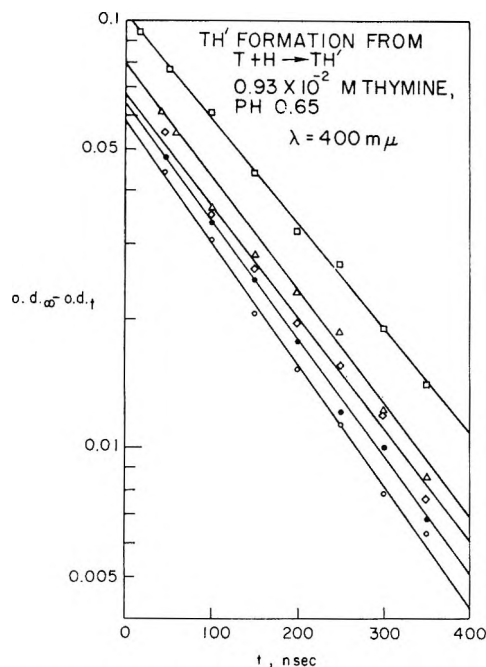
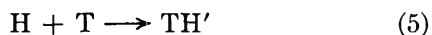


Figure 7. First-order test of data for formation of TH' via $H + T \rightarrow TH'$ in deaerated $10^{-2} M$ solutions of thymine, λ 400 nm, pH 0.65, dose: \circ , \bullet , \diamond , Δ , ca. 2200 rads; \square , 5450 rads.

occurs in less than 10^{-9} sec since $k_3 = 2 \times 10^{10} M^{-1} \text{sec}^{-1}$.²² Reaction of OH with thymine



occurs with a half-life of 10^{-8} sec, assuming $k_4 \sim 7 \times 10^9 M^{-1} \text{sec}^{-1}$.³ Figure 6 is interpretable in terms of an initial absorption by TOH produced at the end of the pulse followed by a slower grow-in of additional absorption by the H-atom adduct produced by the reaction



The product is represented by TH' to distinguish it from TH, the product of reaction 2. (Part of the thymine is protonated at pH 0.65 to give the cation HT^+ . Addition of H may give the radical cation, (HTH^+) , as well as TH'. We refer to both species as TH' in the following.) A decrease of thymine concentration to $0.3 \times 10^{-2} M$ resulted in a decrease of the rate of buildup of the slower signal, as required by reaction 5; the signal was still rising at the end of the usable scan period (*i.e.*, 800 nsec). Figure 7 shows that formation of TH' is exponential in agreement with the pseudo-first-order dependence on thymine concentration required by reaction 5. From the slopes of the curves of Figure 7, $k_5 = (6.8 \pm 0.2) \times 10^8 M^{-1} \text{sec}^{-1}$. This value is in good agreement with the value $8 \times 10^8 M^{-1} \text{sec}^{-1}$ determined by a steady-state competition method.¹⁰

Figure 8 shows spectra for the initial absorbing species, TOH, and the subsequently formed absorbing

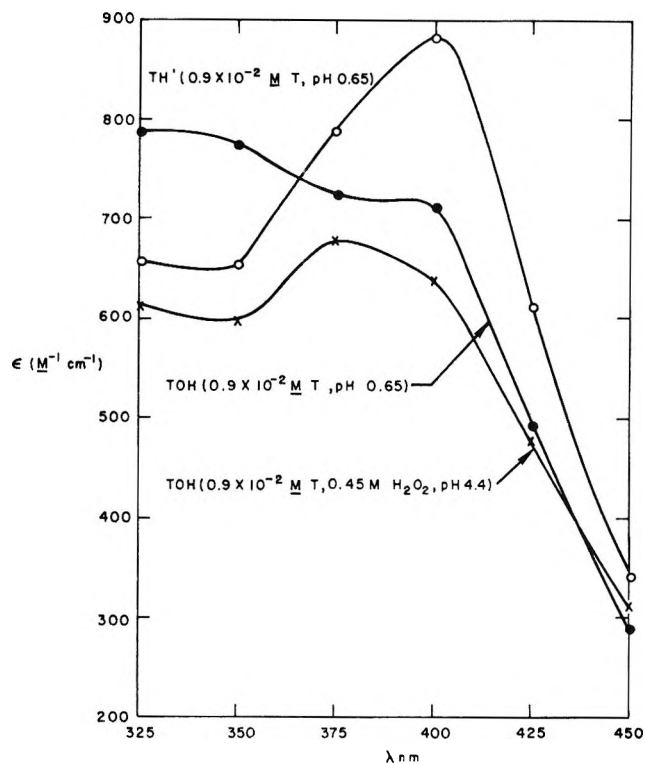


Figure 8. Absorption spectra of TH' and TOH for $0.93 \times 10^{-2} M$ thymine, pH 0.65, and TOH for $0.9 \times 10^{-2} M$ thymine containing $0.45 M H_2O_2$, pH 4.4.

species, TH', taken from data similar to those of Figure 6. The TH' absorption is obtained by subtracting the initial absorption (due to TOH) from the absorption 800 nsec after the pulse. A third spectrum shown in Figure 8 is that of TOH obtained for an argon-saturated solution of $0.9 \times 10^{-2} M$ thymine and $0.45 M H_2O_2$ in which e_{aq}^- is converted into OH *via* the reaction



with a half-life of 10^{-10} sec, since $k_6 \sim 1.2 \times 10^{10} M^{-1} \text{sec}^{-1}$.⁶ Subsequently, OH reacts with thymine. The fraction of OH which reacts with H_2O_2 can be estimated as 0.08 or 0.2 based on values of 1.2×10^7 or $4.5 \times 10^7 M^{-1} \text{sec}^{-1}$ reported^{23, 24} for the rate constant of this reaction. No correction is made in Figure 8 for this loss of OH, so actual extinction coefficients for TOH in the solution containing H_2O_2 are somewhat higher than indicated by the vertical scale.

Structure of TH' and TH. The spectra of TH' and TH are different (*cf.* Figures 5 and 8) suggesting that they are hydrogen atom adducts of thymine which differ not only by the reactions leading to their formation, but also by the location of the adduct hydrogen atom in the radical. This difference is explicable on

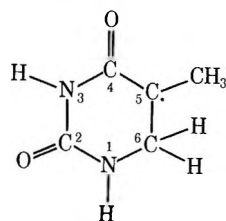
(22) J. P. Keene, *Radiat. Res.*, **22**, 1 (1964).

(23) H. Fricke and J. K. Thomas, *Radiat. Res., Suppl.*, **4**, 68 (1964).

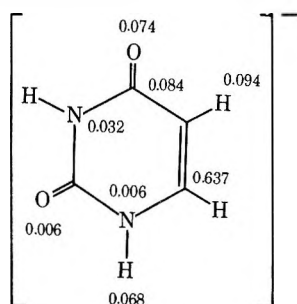
(24) H. A. Schwarz, *J. Phys. Chem.*, **66**, 255 (1962).

the basis that the site of protonation of T^- differs from the site of addition of H to thymine.

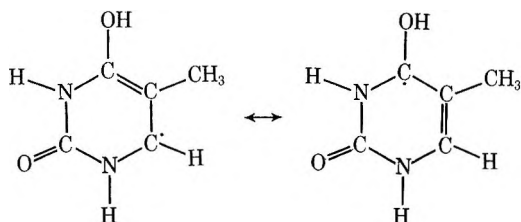
The spectrum of TH' is similar to the spectra of TOH reported here for pH 4.4, and, except at short wavelengths, for pH 0.65, and to the previously reported spectrum of TOH in N_2O saturated solutions of thymine at pH 9.³ In addition, it is almost identical with the spectra of radicals formed by reaction of H and OH at pH 6.8 and 1.0 with the saturated analog of thymine, dihydrothymine.¹⁵ This suggests that these radicals have similar structures. Other studies have shown that OH adds to the 5,6 double bond of thymine, that H and OH abstract hydrogen from the C-5 or C-6 position of dihydrothymine, and that H in the gas phase adds with a high specificity to the C-6 position of small thymine crystals.^{10,25-27} It thus seems likely that TH' is formed by addition of H to the 5,6 double bond and that the product is the 5,6-dihydrothymin-5-yl radical.



In the first step of the reaction sequence leading to formation of TH , the electron adds to the lowest vacant molecular orbital and is distributed over the entire molecule. Pullman²⁸ has suggested that the unpaired spin density for uracil radical anion (and similarly for thymine radical anion) is distributed as follows

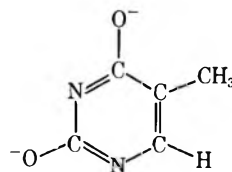


More than 60% of the unpaired spin is on C-6. The various resonance forms of this structure place the negative charge on C-5 or either of the oxygens. The present data do not permit a determination of which of these sites is protonated, but they are consistent with the conclusion of Hayon⁸ that an oxygen is protonated to give structures such as

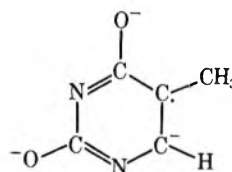


or a structure with the proton on the other oxygen.

Holroyd and Glass,¹¹ in contrast, concluded that thymine, thymidine, and thymidine-5'-phosphate anion radicals, formed in strongly alkaline glasses by bleaching of trapped electrons generated photolytically, undergo proton transfer from surrounding water molecules to the C-6 position of the thymine ring. This result is not necessarily in disagreement with the present conclusions because of the high pH. In strong alkali the parent thymine molecule is ionized and has a charge of -2

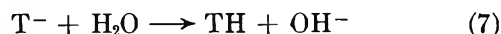


Addition of another electron can give the carbanion



and H^+ then may add to the 6 carbon atom. Addition of H^+ to the $-O^-$ is not likely to occur because at high pH, the resultant OH-group product is unstable.

Reaction of Thymine Radical Anion with Water. Figure 3A permits an estimate of an upper limit for k_7 , the rate constant for the reaction



The half-life for disappearance of T^- at pH 6.0 is of the order of 10^{-6} sec, according to Figure 3A. Therefore, $k_7 \leq 1.3 \times 10^4 M^{-1} \text{sec}^{-1}$ assuming that the half-life of reaction 7 cannot be less than 10^{-8} sec. The magnitude of k_7 then may be comparable to the rate constants (10^2 – $10^4 M^{-1} \text{sec}^{-1}$) for solvent protonation of several aromatic radical anions in aliphatic alcohols determined by Dorfman, *et al.*²⁹

The low magnitude of k_7 suggests that in biological systems anion radicals, formed by addition of hydrated electrons to nucleic acid pyrimidine moieties, may react before they are protonated by water, in which case the probable types and rates of reaction for the

(25) (a) D. E. Holmes, L. S. Myers, Jr., and R. B. Ingalls, *Nature (London)*, **209**, 1017 (1966); (b) H. C. Heller and T. Cole, *Proc. Nat. Acad. Sci. (U. S.)*, **54**, 1486 (1965); (c) J. Herak and W. Gordy, *ibid.*, **54**, 1287 (1955).

(26) G. Scholes, J. F. Ward, and J. J. Weiss, *J. Mol. Biol.*, **2**, 379 (1960); and M. N. Khattack and J. H. Green, *Int. J. Radiat. Biol.*, **11**, 131, 137, 577 (1966). These authors refer to earlier papers.

(27) M. G. Ormerod and B. B. Singh, *ibid.*, **10**, 533 (1966).

(28) B. Pullman in "Molecular Biophysics," B. Pullman and M. Weissbluth, Ed., Academic Press, New York, N. Y., 1965, pp 170–173. Note that the structures shown in Figures 12 and 13 have been interchanged.

(29) L. M. Dorfman, N. E. Shank, and S. Arai, *Advan. Chem. Ser.*, **No. 82**, 58 (1968).

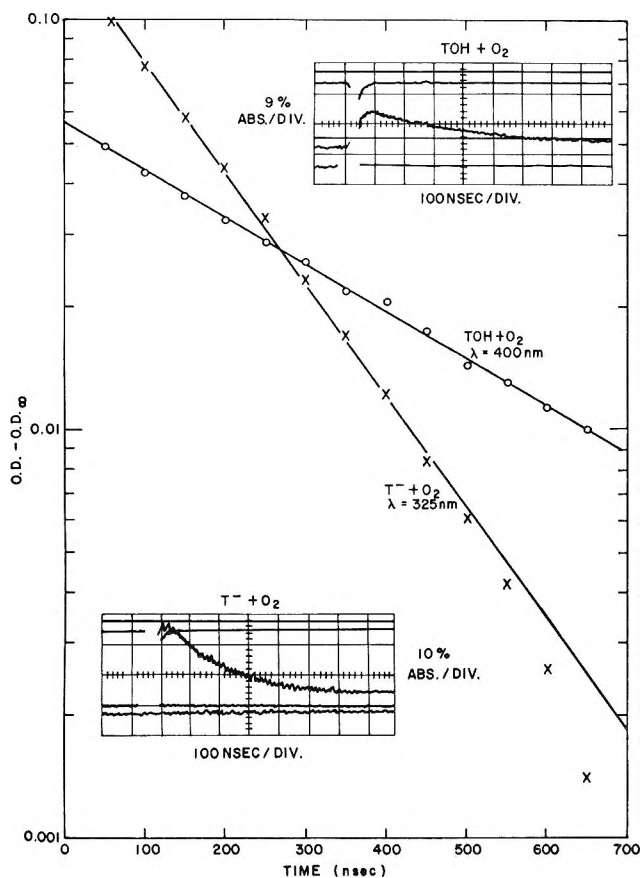
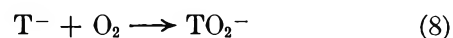


Figure 9. Oscilloscope traces and first-order test of data for decay of T^- , — \times —, at λ 325 nm, and TOH, — \circ —, at λ 400 nm in oxygen saturated solutions of $10^{-2} M$ thymine containing 1 M ethanol (T^-) and 0.5 M H_2O_2 (TOH).

anion might differ importantly from those expected if protonation were much faster.

Reaction of T^- and TOH with Oxygen. Figure 9 shows that the half-life of T^- in oxygen-saturated

$10^{-2} M$ thymine solution containing 1 M ethanol is ca. 120 nsec. The reaction



is first order according to Figure 9 and the data give $k_8 = 4.3 \times 10^9 M^{-1} \text{sec}^{-1}$, assuming an oxygen concentration of $1.4 \times 10^{-3} M$. Thus, reaction 8 is favored over reaction 7 at oxygen concentrations comparable to those important for biological systems.

Figure 9 shows also that for oxygen-saturated $10^{-2} M$ thymine solutions containing 0.5 M H_2O_2 decay of TOH is exponential and therefore is presumed attributable to the reaction



The half-life of TOH was found to be ca. 260 nsec which gives $k_9 = 1.9 \times 10^9 M^{-1} \text{sec}^{-1}$. This value, slightly lower than the values reported earlier,¹⁴ agrees well with values of 2.5×10^9 and $1.9 \times 10^9 M^{-1} \text{sec}^{-1}$ reported by other workers.^{30,31} Interpretation of the results of the oxygen-saturated systems in terms of reactions 8 and 9 is supported by the observation in the present work that decay of T^- and TOH is progressively slower in aerated and deaerated systems as compared to oxygen-saturated systems (cf. Figure 3A and Figure 9 for T^- decay).

Acknowledgments. We gratefully acknowledge support of this work by the Division of Biology and Medicine of the U. S. Atomic Energy Commission through contracts with Gulf Radiation Technology—A Division of Gulf Energy and Environmental Systems Inc., and the University of California, Los Angeles.

(30) P. T. Emmerson and R. L. Willson, *J. Phys. Chem.*, **72**, 3669 (1968).

(31) R. L. Willson, *Int. J. Radiat. Biol.*, **17**, 349 (1970).

On Physisorption of Water on Zinc Oxide Surface¹

by Mahiko Nagao

Department of Chemistry, Faculty of Science, Okayama University, Tsushima, Okayama, Japan (Received February 19, 1971)

Publication costs borne completely by The Journal of Physical Chemistry

To clarify the water adsorption anomaly on ZnO, that is, the appearance of a jump in the water adsorption isotherm, the physisorption of water has been investigated thermodynamically. On three kinds of ZnO samples, the specific surface area, the water content, and the water adsorption isotherm have been measured. For the purpose of exact thermodynamic treatment of the water physisorption data the following precaution was taken to ensure that the oxide surface was fully covered with only a monolayer of surface hydroxyl groups: the sample was degassed at room temperature after completion of the first water adsorption isotherm. This fully hydroxylated surface was then used for the measurements of water adsorption, from which the isosteric heat of adsorption and subsequently the differential entropy of adsorbed water were calculated. The results indicate that on the hydroxylated surface of ZnO there exist two groups of sites available for water physisorption, of heterogeneous and homotactic character. Moreover, it has become clear that when the pretreatment temperature of the sample rises, the number of homotactic sites available for water physisorption decreases and at the same time the number of heterogeneous sites increases. The present investigation concludes that lateral interaction of water molecules physisorbed on the homotactic hydroxylated surface of ZnO may lead to two-dimensional condensation at relatively high vapor pressure, resulting in the appearance of a jump in the isotherm.

Introduction

It is known that, even in the atmosphere, most metal oxides chemisorb water molecules to form surface hydroxyl groups on which further water molecules are adsorbed physically through hydrogen bonding. Moreover, these physisorbed water molecules can be desorbed by treating the sample *in vacuo* at room temperature, whereas the chemisorbed water (*i.e.*, surface hydroxyl groups) can be removed gradually by evacuating the sample at higher temperatures. The temperature at which the removal of the chemisorbed water begins, however, depends on the nature of the oxide: *e.g.*, 200° in the case of ZnO and about 100° in the case of TiO₂.²

The shape of the water adsorption isotherm on ZnO has been found to be quite different from those on other metal oxides: in the case of ZnO a jump appears in the adsorption isotherm in the relative pressure range of 0.2–0.3, while the isotherms of the other metal oxides usually represent the normal multilayer adsorption type.² The appearance of such a jump in the adsorption isotherm has been observed in systems containing a nonpolar adsorbate.^{3–11} The present system is the first example in which a jump has been observed in a system containing a polar adsorbent and a polar adsorbate. Egorov, *et al.*,¹² measured the adsorption isotherm on the same system as the present one, but they found no jump.

To elucidate the appearance of the jump in the adsorption isotherm on the system ZnO–H₂O, we have measured the differential heat of immersion on the same system.¹³ Among the thermodynamic quantities calculated therefrom, only the differential entropy

of adsorption shows a slight change corresponding to the jump in the adsorption isotherm. This result may be due to the following reasons. First, the heat effect is originally small near the jump, since it appears in the physisorption region at the relative pressure of 0.2–0.3, and second, the heat of immersion method is lacking in high accuracy because of sampling and other errors.

The purpose of the present study is to calculate the thermodynamic quantities for water adsorption on ZnO based on the measurement of the adsorption isotherms and to get a better understanding of the origin of the jump in the adsorption isotherm. On the basis of the adsorption isotherms measured at different temperatures on the monolayer of surface

(1) A part of this investigation was presented at the 21st Symposium on the Colloid and Interfacial Chemistry, Kyoto, Nov 1968.

(2) T. Morimoto, M. Nagao, and F. Tokuda, *Bull. Chem. Soc. Jap.*, **41**, 1533 (1968).

(3) (a) G. Jura and D. Griddle, *J. Phys. Chem.*, **55**, 163 (1951); (b) M. H. Polley, W. D. Schaeffer, and W. R. Smith, *ibid.*, **57**, 469 (1953).

(4) S. Ross and H. Clark, *J. Amer. Chem. Soc.*, **76**, 4291 (1954).

(5) S. Ross and H. Clark, *ibid.*, **76**, 4297 (1954).

(6) J. H. Singleton and G. D. Halsey, *J. Phys. Chem.*, **58**, 1011 (1954).

(7) B. B. Fisher and W. G. McMillan, *ibid.*, **62**, 549, 555, 563 (1958).

(8) S. Ross, J. P. Olivier, and J. J. Hinchin, *Advan. Chem. Ser.*, **No. 33**, 317 (1961).

(9) J. P. Olivier and S. Ross, *Proc. Roy. Soc., Ser. A*, **265**, 447, 455 (1962).

(10) W. R. Smith and D. G. Ford, *J. Phys. Chem.*, **69**, 3587 (1965).

(11) B. W. Davis and C. Pierce, *ibid.*, **70**, 1051 (1966).

(12) M. M. Egorov, N. N. Dobrovolskii, V. F. Kiselev, G. Furman, and S. V. Khrustaleva, *Zh. Fiz. Khim.*, **39**, 3070 (1965).

(13) M. Nagao and T. Morimoto, *J. Phys. Chem.*, **73**, 3809 (1969).

hydroxyl groups on ZnO, the relation between the amounts of physisorbed and chemisorbed water, the isosteric heat of adsorption, and the differential entropy of adsorbed water can be obtained. The interaction between surface hydroxyl groups on ZnO and water molecules is discussed.

Experimental Section

Materials. The original sample of ZnO used in this study was the same as that used in previous studies.^{2,13-15} It was obtained from the Sakai Kagaku Co. and had been made by burning zinc metal in air. Manufacturer's analysis showed that the purity of this sample was 99.8% and contained 0.002% Pb and 0.03% water-soluble substances as impurities. Three kinds of samples were prepared by treating this original sample under a reduced pressure of 10^{-5} Torr for 4 hr at different temperatures: 250, 450, and 800°, respectively. Water used as the adsorbate was purified by repeated distillation in a vacuum system.

Surface Area Measurement. The specific surface area of the samples was determined by applying the BET method¹⁶ to the nitrogen adsorption data obtained at -196° ; the cross-sectional area of a nitrogen molecule was assumed to be 16.2 \AA^2 .

Measurement of Water Vapor Adsorption Isotherm. To investigate the thermodynamics of physisorbed water on ZnO, the physisorption isotherms of water should be measured on the hydroxylated surface of ZnO. In so doing, it is important, first of all, to prepare a reproducible hydroxylated surface on the ZnO. In the present study, therefore, the adsorption measurements were carried out by the following procedure. First, the adsorption isotherm of water was measured on the sample after treatment at an elevated temperature (250, 450, or 800°) under a reduced pressure of 10^{-5} Torr. After completion of the first adsorption isotherm, the sample was degassed again at 30°, which should leave a monolayer of surface hydroxyl groups on the ZnO.² On the surface thus obtained the second adsorption isotherm of water was measured at a given temperature (e.g., 25°). Subsequently, after degassing at 30°, adsorption measurement at different temperatures (10 and 18°) were repeated on the same sample. When the water adsorption isotherms were measured at the same temperature after degassing at 30°, they were found to agree well with one another, which confirmed the hydroxylated surfaces to be reproducible.

The measurement of the water adsorption isotherm was carried out volumetrically by using an all-glass apparatus, and the equilibrium pressure was read by an oil manometer. Adsorption equilibrium could be attained within 30 min at lower relative pressures, whereas it took about 2 hr at higher relative pressures. The adsorption isotherm obtained as a pre-

liminary test showed no hysteresis, which proved the sample to be nonporous.

Water Content Measurement. The surface water content of ZnO, including chemisorbed and physisorbed water, was determined volumetrically by the successive ignition loss method¹⁷ as a function of the pretreatment temperature by using the same apparatus as that for the adsorption measurement.

Results and Discussion

The Relation between the Amounts of Physisorbed and Chemisorbed Water on ZnO. The water adsorption isotherms obtained on the ZnO surfaces pretreated at different temperatures are given in Figures 1-3. Each figure includes the first adsorption isotherm at 25° on the pretreated surface and the second adsorption isotherms at 10, 18, and 25° on the hydroxylated surface. All the adsorption isotherms obtained reveal a discontinuity in the relative pressure range of 0.2-0.3, similar to the results reported previously.^{2,13,15} The first and second adsorption isotherms at 25° are almost in parallel over the entire range of pressures studied, with the former lying above the latter, due to the occurrence of chemisorption in addition to physisorption in the first adsorption process.

The specific surface area, the amounts of physisorbed and chemisorbed water, and the water content of the ZnO samples are listed in Table I. The amount of physisorbed water listed was obtained directly from the second isotherm at 25°. V_m is the monolayer capacity of water calculated by applying the BET theory¹⁶ to the initial part of the first adsorption isotherm, and it includes the amounts of physisorbed and chemisorbed water. V_{p_1} and V_{p_2} are the amounts of physisorbed water which are obtained from the second adsorption isotherm according to the analysis method reported in the preceding paper.¹⁵ Here, two kinds of sites are assumed to exist on the hydroxylated surface of ZnO and to act differently for the physisorption of water molecules: water adsorption occurs on the first sites (V_{p_1}) up to the beginning of the jump in the adsorption isotherm and on the second sites (V_{p_2}) during the jump. Accordingly, the sum of V_{p_1} and V_{p_2} is the total amount of physisorbed water (V_p) in the first layer as discussed in the previous paper.

Since V_m contains the amounts of physisorbed and chemisorbed water, we can obtain the amount of chemisorbed water V_c in the first adsorption process by subtracting V_{p_1} from V_m .¹⁵ V_h is the surface water content

(14) T. Morimoto, M. Nagao, and M. Hirata, *Kolloid-Z. Z. Polym.*, **225**, 29 (1968).

(15) T. Morimoto and M. Nagao, *Bull. Chem. Soc. Jap.*, **43**, 3746 (1970).

(16) S. Brunauer, P. H. Emmett, and E. Teller, *J. Amer. Chem. Soc.*, **60**, 309 (1938).

(17) T. Morimoto, K. Shiomi, and H. Tanaka, *Bull. Chem. Soc. Jap.*, **37**, 392 (1964).

Table I: The Relation between the Amounts of Physisorbed and Chemisorbed Water on ZnO

Treat. temp., °C	Surface area, m ² /g	V _m , ml (STP)/m ²	Physisorbed amount, —H ₂ O molecules/100 Å ² —			Chemisorbed amount, —OH groups/100 Å ² —			$\frac{V_p}{V_c + V_h}$, H ₂ O/OH
			V _{p1}	V _{p2}	V _p	V _c	V _h	V _c + V _h	
250	5.29	0.137	3.28	3.92	7.20	0.91	6.60	7.51	0.96
450	4.79	0.247	3.47	4.52	7.99	6.27	1.10	7.37	1.08
800	2.16	0.212	2.31	3.10	5.41	6.78	0.05	6.83	0.79

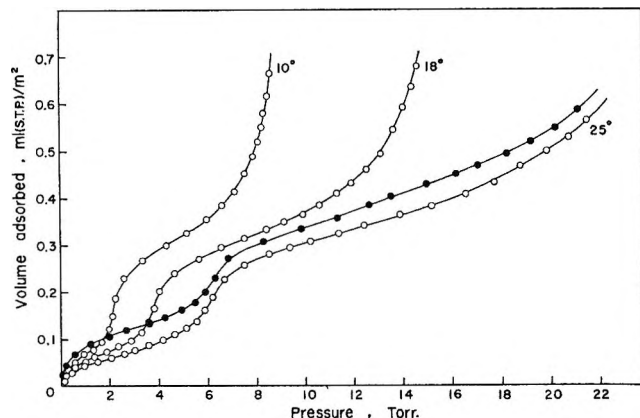


Figure 1. Adsorption isotherm of water on ZnO pretreated at 250°: ●, first adsorption at 25°; ○, second adsorption at 10, 18, and 25°.

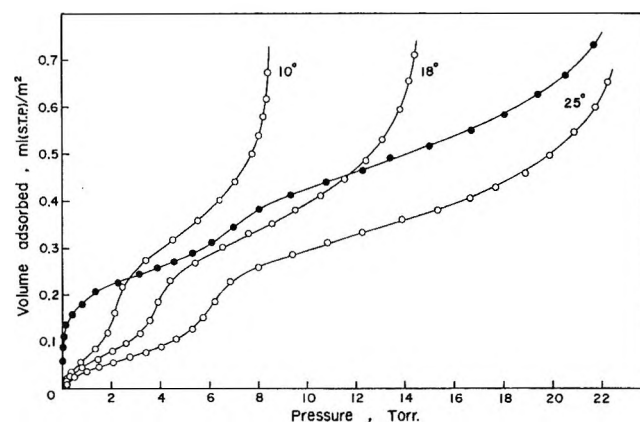


Figure 2. Adsorption isotherm of water on ZnO pretreated at 450°: ●, first adsorption at 25°; ○, second adsorption at 10, 18, and 25°.

remaining on the surface of ZnO treated at a given temperature. Of the three ZnO samples, the V_c of the 250°-treated sample is the smallest, while V_h for this sample is the largest. Since the value V_h for samples pretreated at higher temperatures than 250° as listed in Table I should be only chemisorbed water, the sum of V_c and V_h is considered to be the total amount of chemisorbed water on ZnO after the adsorption process. This sum is almost equal in the cases of 250°- and 450°-treated samples, as is seen in Table I. This fact suggests that partially dehydroxylated surfaces can be easily rehydroxylated on exposure to water vapor. On the contrary, with the

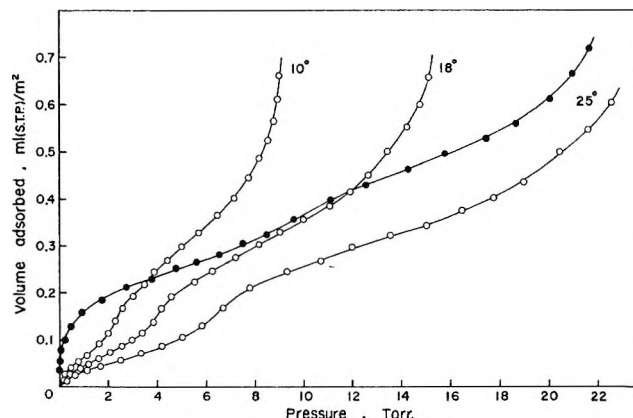


Figure 3. Adsorption isotherm of water on ZnO pretreated at 800°: ●, first adsorption at 25°; ○, second adsorption at 10, 18, and 25°.

800°-treated sample the total amount of chemisorbed water is slightly smaller than with the other samples, which is indicative of insufficient rehydroxylation after exposure to water vapor, in accordance with the results obtained by the heat of immersion measurement.¹⁴

The ratio of the total amount of physisorbed water to that of chemisorbed water is almost equal to 1:1 (H₂O:OH) except in the case of the 800°-treated sample, as has been found on ZnO samples which were different in origin.¹⁶ It is interesting that this ratio is 1:2 (H₂O:OH) on metal oxides such as TiO₂ (rutile) and α -Fe₂O₃ (hematite),¹⁸ on which the water adsorption isotherms represent the normal multilayer adsorption type, whereas it is 1:1 on ZnO which gives a discontinuity in the water adsorption isotherm.

Isosteric Heat of Adsorption of Water. So far, the interaction between the surface of ZnO and water molecules has been investigated by measuring the heat of immersion of ZnO in water¹⁴ and by joining the data on the adsorption isotherm with those of the heat of immersion isotherm.¹³ However, the adsorption anomaly of water on ZnO has not been elucidated thermodynamically by these investigations. In other words, a distinct change in the interaction energy has not been observed in the region of the discontinuity of the adsorption isotherm.

Thermodynamic studies of adsorption can also be

(18) T. Morimoto, M. Nagao, and F. Tokuda, *J. Phys. Chem.*, **73**, 243 (1969).

made by mathematically treating the adsorption isotherms obtained at different temperatures.^{19,20} The physisorption and chemisorption of water usually occurs simultaneously on the surfaces of metal oxides. Therefore, unless the amount of chemisorbed water is actually determined, the effect of uncertain amounts of chemisorbed water will probably be implicit in the thermodynamic data, such as the heat of adsorption and the entropy of adsorption, when they are discussed as a function of the coverage of the adsorbate. The adsorption procedure adopted in this experiment makes it possible to deal with only the physisorption of water and therefore to estimate the exact thermodynamic quantities for the physisorption of water on ZnO surfaces.

Isosteric heat of adsorption, q_{st} , can be calculated by using the Clausius-Clapeyron equation

$$q_{st} = RT^2 \left(\frac{d \ln P}{dT} \right)_T \quad (1)$$

This gives the heat of adsorption at a constant amount of adsorption, which is larger by RT than the differential heat of adsorption. Figure 4 is a plot of the isosteric heat of adsorption against the coverage θ , as calculated from the adsorption data at three temperatures, 10, 18, and 25°, in Figures 1-3. The broken line in Figure 4 shows the heat of liquefaction of water at 25°, and θ is the coverage referred to the first layer capacity of physisorbed water (V_{p1}). The arrows indicate the beginning of the jump in the adsorption isotherm. As is seen from Figure 4, the heat of adsorption of water is about 15 kcal/mol in the initial stage of physisorption on the hydroxylated surface of ZnO, and the net heat of adsorption is consequently about 5 kcal/mol, which coincides with the energy of hydrogen bonding.²¹ The isosteric heat q_{st} decreases with increasing amount of adsorption in the V_{p1} region. At the end of this stage the q_{st} value reaches the heat of liquefaction of water. When the adsorption of water proceeds, the value q_{st} increases and attains a maximum in the V_{p2} region, corresponding to the discontinuity in the adsorption isotherm, and then decreases again to the value of the heat of liquefaction. In the second layer of physisorption the isosteric heat remains almost constant. In the adsorption of xenon, methane, and ethane on the (100) plane of NaCl, which shows a discontinuity in the adsorption isotherm at low temperatures, Ross and Clark⁴ have found that q_{st} attains a maximum or a plateau after 50% surface coverage. The behavior of the present system is apparently similar to these systems, but there is a large difference in the polarity of the adsorbents and the adsorbates used in the two cases.

Generally, it is known that lateral interaction between adsorbed molecules becomes effective in the vicinity of the completion of the first monolayer

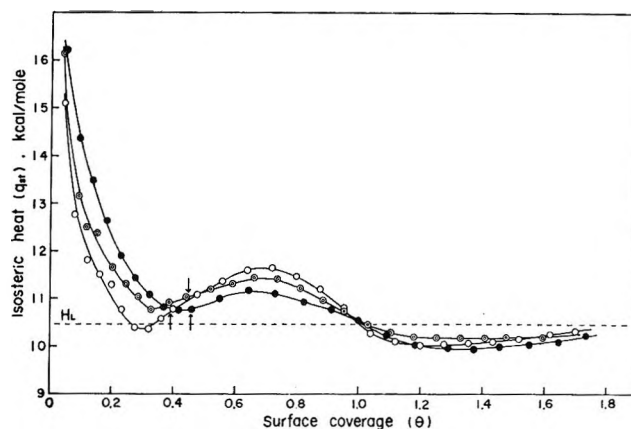


Figure 4. Isosteric heat of physisorption of water on ZnO pretreated at 250°, O; 450°, ⊙; 800°, ●.

coverage, resulting in the appearance of a maximum in the q_{st} - θ plot.^{22,23} It is also reasonable to expect that, if the surface is partially homogeneous, *i.e.*, "homotattic,"²⁴ and the portion of the homotattic surface increases, the contribution of the mutual attraction between the adsorbate molecules to the heat of adsorption will become enhanced. Accordingly, the initial decrease in the q_{st} value will end early, and at the same time the succeeding maximum will become larger.

As is seen in Figure 4, q_{st} decreases to a minimum in the V_{p1} region and passes through a large maximum in the V_{p2} region. Moreover, it should be noted that when the degassing temperature rises, the initial decreasing branch in the q_{st} curve decreases more slowly and extends to a larger coverage, and the height of the succeeding maximum region becomes lower. These facts, first of all, suggest that the hydroxylated surfaces of ZnO are homotattic for the physisorption of water. Moreover, the data indicate that the surface homogeneity of ZnO is reduced by heat treatment at the higher temperatures.

Beebe and Young²⁵ have investigated the differential heat of adsorption on the system spheron-argon by direct calorimetry and found that a maximum of the heat of adsorption appears just before completion of monolayer coverage and becomes more marked with the progress of graphitization of carbon black at higher temperatures. This result indicates that the contribution of the lateral interaction of the adsorbates

(19) T. L. Hill, *J. Chem. Phys.*, **17**, 520 (1949).

(20) T. L. Hill, P. H. Emmett, and L. G. Joyner, *J. Amer. Chem. Soc.*, **73**, 5102 (1951).

(21) L. Pauling, "The Nature of the Chemical Bond," 3rd ed, Cornell University Press, Ithaca, N. Y., 1960.

(22) C. Pierce and B. Ewing, *J. Phys. Chem.*, **68**, 2562 (1964); **71**, 3408 (1967).

(23) N. Glossman and M. L. Corrin, *J. Colloid Interface Sci.*, **23**, 237 (1967).

(24) C. Sanford and S. Ross, *J. Phys. Chem.*, **58**, 288 (1954).

(25) R. A. Beebe and D. M. Young, *ibid.*, **58**, 93 (1954).

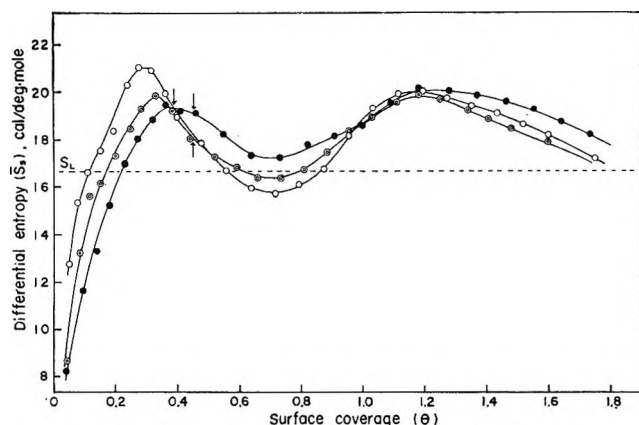


Figure 5. Differential entropy of physisorbed water on ZnO pretreated at 250°, ○; 450°, ⊙; 800°, ●.

increases with increasing degree of surface homogeneity. In the present ZnO–H₂O system the circumstances seem to be quite the same, but the temperature dependence is reversed: the higher the pretreatment temperature of ZnO, the less homotactic the surface of the sample becomes, as associated with the physisorption of water on the hydroxylated surface.

Differential Entropy of Adsorbed Water. To elucidate in more detail the state of adsorbed water on the ZnO sample the differential entropy was calculated according to the equation^{26,27}

$$\bar{S}_s = -\frac{q_{st}}{T} + R \ln \frac{P_0}{P} + S_g^\circ \quad (2)$$

Here, P_0 is the saturated vapor pressure, P the equilibrium pressure, and S_g° the standard entropy of water vapor (45.11 cal/deg mol at 25° and 1 atm). Figure 5 gives the plots of the calculated differential entropy of physisorbed water on the hydroxylated surface of ZnO against the coverage. The broken line indicates the standard entropy of liquid water at 25° and 1 atm ($S_L = 16.72$ cal/deg mol). As is seen from Figure 5, the differential entropy of adsorbed water on ZnO is generally larger than S_L , which indicates that the water molecules move more easily in the adsorbed state than in the liquid state. Only in the region of small coverage does the adsorbed water have less entropy than S_L . In this region, the entropy of adsorbed water decreases and the heat of adsorption increases with the rise in pretreatment temperature. These results imply that, for the three samples studied, water molecules are adsorbed most strongly on the heterogeneous surface of the 800°-treated sample, the surface homogeneity decreasing with the rise in pretreatment temperature. In addition to an entropy maximum near the completion of the monolayer coverage, another maximum appears at a coverage less than half that of the monolayer.

It should be noted that there appear two maxima in the differential entropy curve of adsorbed water on

ZnO, since in the cases of adsorption on usual metal oxides only one maximum appears near the completion of the monolayer coverage.^{26,28} Thus the curves of \bar{S}_s , as well as q_{st} , look as if the monolayer of water molecules on ZnO had been completed in the region of V_{p1} . Such a pseudomonolayer which appears only at a smaller coverage has been reported in the systems Fe₂O₃–heptane²⁹ and TiO₂ (anatase)–argon,²³ but not in a polar adsorbent–polar adsorbate system. The appearance of the pseudomonolayer in the systems cited here has been explained on the assumption that stronger adsorption sites exist in patches, and the maximum entropy appears just after completion of adsorption on these sites. Also, in the present case, the pseudomonolayer seems to appear after the completion of water adsorption in the heterogeneous and therefore stronger sites on ZnO. Here, the second entropy maximum appears at the commencement of the second layer of physisorption.

The following facts have been reported on the system ZnO–H₂O: (i) the water content of the surface decreases sharply at the degassing temperature of 200–400°,² while in the case of most metal oxides it decreases gradually with an increase of pretreatment temperature from room temperature; (ii) the heat of immersion values are almost constant for pretreatment at 100–200° and increase sharply at 200–400°;¹⁴ (iii) the monolayer volume of water remains almost constant for treatment at low temperatures and increases sharply at pretreatment temperatures of 200–400°. These results are probably caused by a single underlying fact: the desorption of chemisorbed water on ZnO is difficult on degassing at temperatures lower than 200° and occurs for the most part in the relatively narrow temperature range of 200–400°. This behavior of the chemisorbed water may reasonably result from a characteristic property of the surface of ZnO such as the homotacticity of the hydroxylated surface, as confirmed by the present investigation of the differential heat of adsorption and the entropy of adsorbed water. Furthermore, experimental facts indicate that the surface hydroxyl groups are strongly bonded to the solid surface of ZnO. The heat of surface hydration of ZnO calculated from the heat of immersion in water was found to be about 23 kcal/mol,¹⁴ which is larger than the values on Al₂O₃,¹⁷ SiO₂,³⁰ Fe₂O₃,³¹ and TiO₂.³² The site energy distribution curve, which was obtained by the differentiation of the differential heat

(26) R. M. Barrer, *J. Colloid Interface Sci.*, **21**, 415 (1966).

(27) J. E. Benson, K. Ushiba, and M. Boudart, *J. Catal.*, **9**, 91 (1967).

(28) G. J. Young, J. J. Chessick, F. H. Healey, and A. C. Zettle-moyer, *J. Phys. Chem.*, **58**, 313 (1954).

(29) M. L. Corrin, *ibid.*, **59**, 313 (1955).

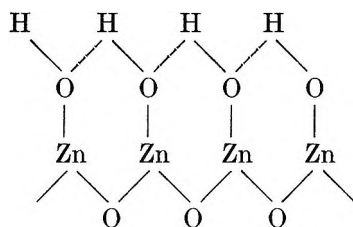
(30) G. J. Young and T. P. Bursh, *J. Colloid Sci.*, **15**, 361 (1960).

(31) T. Morimoto, N. Katayama, H. Naono, and M. Nagao, *Bull. Chem. Soc. Jap.*, **42**, 1490 (1969).

(32) T. Morimoto, M. Nagao, and T. Omori, *ibid.*, **42**, 943 (1969).

of adsorption derived from the heat of immersion isotherm, showed a large peak at about 23 kcal/mol associated with the chemisorption of water.¹³ The facts that the removal of the surface hydroxyl groups occurs at relatively higher temperatures and in a relatively narrower temperature range (200–400°) compared to the cases of other metal oxides and that the surface hydroxyl groups are bonded strongly on ZnO seem to suggest that the hydroxylated surface of ZnO is homotactic.

Homotactic Hydroxylated Surface of ZnO. As is seen from Table I, the number of hydroxyl groups on a fully hydroxylated surface of ZnO is about 7.5 OH/100 Å², which agrees well with that estimated crystallographically. Such close-packed surface hydroxyl groups bonded to the ZnO surface may easily lend themselves to the formation of mutual hydrogen bonding in the form



If the uniform oxide surface is produced at the moment of formation of ZnO, the subsequent chemisorption of water in the atmosphere will also give a uniform layer of surface hydroxyl groups bonded to each other through mutual hydrogen bonding, which can then act as a homotactic surface for the physisorption of water. The weakly physisorbed water molecules on such a hydroxylated surface may be plausibly mobile and bring about the two-dimensional condensation at higher relative pressure.

The Hill-de Boer equation for two-dimensional condensation is expressed in the form³³

$$W = \ln \frac{\theta}{1 - \theta} + \frac{\theta}{1 - \theta} - \ln P = \frac{2\alpha\theta}{RT\beta} - \ln K \quad (3)$$

Here, K is a constant, and α and β are the two-dimensional van der Waals constants, which are related to the three-dimensional van der Waals constants by the expression $2\alpha/\beta = a/b$. If we plot W against θ , we can get a linear relation, whose slope will give $2\alpha/RT\beta$. On the other hand, the apparent critical temperature will be given by the equation³⁴

$${}_aT_c = \frac{8\alpha}{27R\beta} \quad (4)$$

Thus, ${}_aT_c$ can be obtained from the slope of eq 3. Figure 6 shows the relation between W and θ in the present system. All the plots obtained at different temperatures on a single sample were the same, and the treatment temperature of the sample scarcely affected the results obtained.

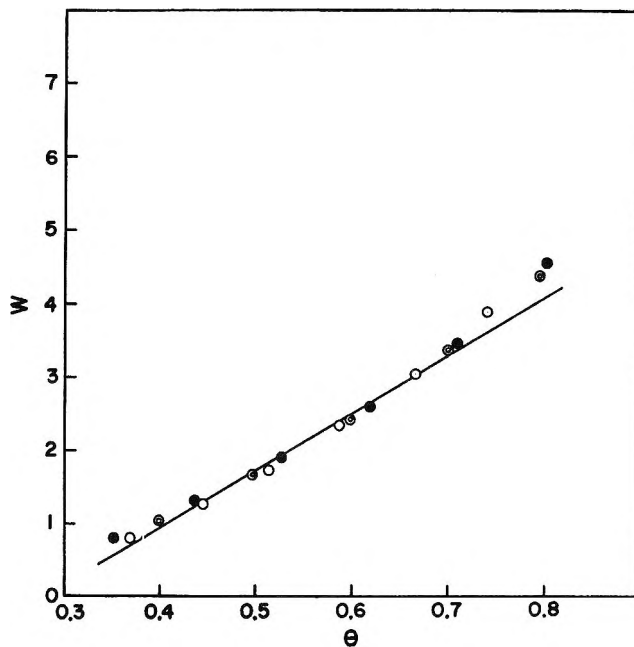


Figure 6. Relation between W and θ for the system ZnO-H₂O; pretreated at 250°, ○; 450°, ⊙; 800°, ●.

From the linear relationship in the range above 0.4 θ corresponding to the jump in the adsorption isotherm, we can find the two-dimensional critical temperature of water to be 318.1°K (44.9°). If we assume the two-dimensional critical temperature to be half of the three-dimensional one (647.1°K for water),^{34,35} then the two-dimensional critical temperature of water physisorbed on the hydroxylated surface of ZnO can be estimated to be 323.6°K (50.4°). In the present experiments the adsorption procedure has been carried out at the temperatures equal to and lower than 298.2°K (25°), and hence the two-dimensional condensation may reasonably occur.

In this way the characteristic fact that a jump appears in the adsorption isotherm of the system ZnO-H₂O has been explained in terms of the two-dimensional condensation of water which occurs on the energetically homotactic hydroxylated surface of ZnO. Such a surface will result from a crystallographically uniform surface of the original sample of ZnO. When the surface is treated at elevated temperatures, the surface homogeneity can be considered to decrease due to the enhanced mobility of the surface atoms, the adsorption of gas molecules, and the removal of the component atoms, resulting in a weakened two-dimensional condensation of water.

Acknowledgments. The author is greatly indebted to Professor Tetsuo Morimoto of Okayama University

(33) S. Ross and J. P. Olivier, "On Physical Adsorption," Interscience, New York, N. Y., 1964, p 140.

(34) T. L. Hill, *J. Chem. Phys.*, **14**, 441 (1946).

(35) H. M. Cassel, *J. Phys. Chem.*, **48**, 195 (1944).

for his helpful discussions and constant encouragement throughout this work. He also wishes to express his thanks to Professor Masaji Miura of Hiroshima

University for his kind advice and helpful suggestions and to Dr. Peggy Knecht for her assistance in the grammatical improvement of the article.

Metal-Ligand Bonding in Copper(II) Chelates—an Electron Paramagnetic Resonance Study

by I. Adato, A. H. I. Ben-Bassat,

*Department of Inorganic and Analytical Chemistry,
Hebrew University of Jerusalem, Israel*

and S. Sarel*

*Department of Pharmaceutical Chemistry, Hebrew University of Jerusalem, Israel
(Received December 29, 1970)*

Publication costs borne completely by The Journal of Physical Chemistry

Epr spectra of some cupric β -ketoenolates, α -dioximates, β -dioximates, and Schiff bases in chloroform solution were recorded at room temperature and at -160° (frozen state). The bonding parameters were calculated from spectral data. The bonding properties of the odd electron were derived as a function of the nature of the ligand donor atoms, the size of the chelate ring, and substituent effects. The relationship between covalency of π bonding and complex stability is discussed.

This work was aimed at studying the electron spin resonance spectra of several copper(II) complexes and to draw some conclusions concerning the bonding properties of the odd electron, depending on the nature of the donor atoms in the ligands, the size of the chelate ring, and effects of substituents on the chelate ring. The epr spectra of copper(II)-acetylacetonate type complexes have been treated by several authors.¹⁻⁶ In all of the above complexes, it was assumed that the Cu^{II} ion is surrounded by the four donor atoms in a planar configuration (D_{2h} symmetry) and that each donor atom has a $2s, 2p_x, 2p_y, 2p_z$ atomic orbital available for the formation of molecular orbitals with the atomic d orbitals of the central ion. From group theory, Gersmann and Swalen³ obtained the proper linear combinations of ligand orbitals with the copper d orbitals which form the antibonding wave functions of the planar cupric chelate compound. The expressions for the in-plane antibonding wave functions are

$$B_{1g} = \alpha d_{xy} - \frac{\alpha'}{2} [-\sigma_{xy}^{(1)} + \sigma_{xy}^{(2)} + \sigma_{xy}^{(3)} - \sigma_{xy}^{(4)}]$$

$$A_g = \beta d_{x^2-y^2} - \frac{1}{2}(1 - \beta^2)^{1/2} [-p_{xy}^{(1)} - p_{xy}^{(2)} + p_{xy}^{(3)} + p_{xy}^{(4)}]$$

The above wave functions are applicable also for

tetradentate Schiff base chelates of C_{2v} symmetry, where the corresponding symmetry designations are B_2 and A_1 , in the sense used by Swett and Dudek.⁵

The bonding parameters, α , β , and δ , are a measure of the covalency of the appropriate bonding. A value of 1 for the square of the parameter indicates a completely ionic character, while a value of 0.5 denotes essentially a purely covalent character. The odd electron is placed in the antibonding B_{1g} orbital in the ground state.

Overlap is included for the B_{1g} orbital, where α and α' are related

$$\alpha^2 + \alpha'^2 - 2\alpha\alpha'S = 1$$

For a ligand-to-metal distance of $R = 1.9 \text{ \AA}$, the overlap integral values (S) have been assigned as 0.076 in β -keto enolates, 0.093 in α -dioximates and β -dioximates, and the value 0.084 in Schiff base complexes.^{2,5}

(1) A. H. Maki and B. R. McGarvey, *J. Chem. Phys.*, **29**, 31, 35 (1958).

(2) D. Kivelson and R. Neiman, *ibid.*, **35**, 149 (1961).

(3) H. R. Gersmann and J. D. Swalen, *ibid.*, **36**, 3221 (1962).

(4) H. A. Kuska, M. T. Rogers, and R. E. Drullinger, *J. Phys. Chem.*, **71**, 109 (1967).

(5) V. S. Swett and E. P. Dudek, *ibid.*, **72**, 1244 (1968).

(6) S. Antosik, M. M. Brown, A. A. McConnell, and A. L. Porte, *J. Chem. Soc. A*, 545 (1969).

By applying the wave function for the B_{1g} state to the Hamiltonian of Abragam and Pryce,⁷ the magnetic parameters are shown to be³

$$g_{||} = 2.0023 - (8\lambda/\Delta E_{x^2-y^2})[\alpha^2\beta^2 - f(\beta)]$$

$$g_{\perp} = 2.0023 - (2\lambda/\Delta E_{xz})[\alpha^2\delta^2 - g(\delta)]$$

$$A_{||} = P[-\alpha^2(4/7 + \kappa) - 2\lambda\alpha^2(4\beta^2/\Delta E_{xy} + 3\delta^2/7\Delta E_{xz})]$$

$$A_{\perp} = P[\alpha^2(2/7 - \kappa) - 22\lambda\alpha^2\delta^2/14\Delta E_{xz}]$$

where

$$f(\beta) = \alpha\alpha'\beta^2S + \alpha\alpha'\beta(1 - \beta^2)^{1/2}T(n)/2$$

$$g(\delta) = \alpha\alpha'\delta^2S + \alpha\alpha'\delta(1 - \delta^2)^{1/2}T(n)/2$$

with the spin-orbit coupling constant for the Cu(II) ion $\lambda = -828 \text{ cm}^{-1}$, the free-ion dipole term $P = 0.036 \text{ cm}^{-1}$, and the Fermi contact term $\kappa = 0.43$ as defined earlier.³ The corresponding values of $T(n)$ are:^{2,5} $T(n)_{\text{nitrogen}} = 0.333$, $T(n)_{\text{oxygen}} = 0.22$, and $T(n) = 0.276$ for the Schiff base complexes.

Values of g_0 and $g_{||}$ were obtained from the spectra recorded at room temperature and at -160° , respectively. The g_{\perp} values were calculated from the equation $g_0 = 2g_{\perp}/3 + 1g_{||}/3$.

The values of α^2 were calculated from the copper hyperfine spectra, using the approximate formula²

$$\alpha^2 = -(A_{||}/P) + (g_{||} - 2) + 3(g_{\perp} - 2)/7 + 0.04$$

and the values of β were calculated from the expression of $g_{||}$ and the values of δ were calculated from the expression of g_{\perp} . Values of α' were also calculated from the nitrogen hyperfine splitting (W_L)³ exhibited by three complexes and then α^2 values were recalculated from the normalization condition of the B_{1g} state wave function and compared to those obtained from the approximate formula of Kivelson and Neiman.²

Adequate interpretation of the bonding parameters requires separation between the ground state term (σ^*, d_{xy}) and the excited state terms, ($\pi^*, d_{x^2-y^2}$) and (π^*, d_{xz}).

The relative positions of the molecular d orbitals in planar bis(ketoenolato)copper(II) complexes were determined by Cotton and Wise⁸ from polarization studies of single crystal spectra of $\text{Cu}(\text{DPM})_2$. It was concluded that the four d-d transitions occur within a range of a few thousand wave number and that d_{xz} , d_{yz} , $d_{x^2-y^2}$, and d_{z^2} orbitals lie close together, some $20,000 \text{ cm}^{-1}$ below the d_{xy} orbital. The possible d-d transitions within the planar cupric complex were arranged in the following order of increasing energy: $d_{xy} \leftarrow d_{z^2}$, d_{xz} , $d_{x^2-y^2}$, d_{yz} . In our estimations of the ligand field energies we counted on the above order of the d-d transitions. Due to the small difference between the coordinate systems of Gersmann³ and that of Cotton,⁸ the order in ligand field transitions is $\Delta E_{yz} < \Delta E_{x^2-y^2} < \Delta E_{xz}$.

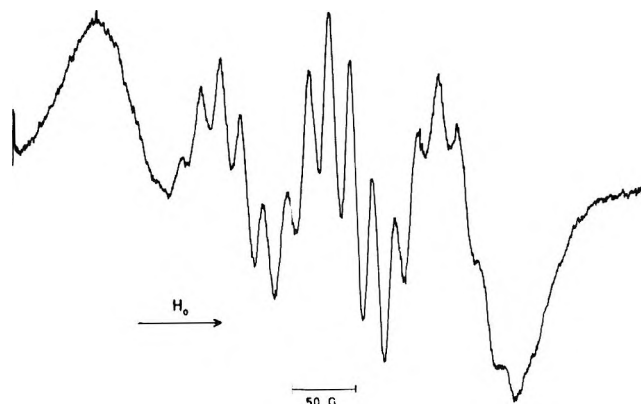


Figure 1. Epr spectrum of chloroformic solution of $\text{Cu}(\text{DMGL})_2$ at room temperature.

Results

The epr spectra recorded for β -ketoenolato complexes of copper(II) are characteristic of those of planar copper(II) compounds in their anisotropies in g and hyperfine coupling constants.

The epr spectra of bis(dimethylglyoximato)copper(II) " $\text{Cu}(\text{DMGL})$ " (Figure 1) and bis(diphenylglyoximato)copper(II) " $\text{Cu}(\text{DPGL})_2$ " in CHCl_3 solution recorded at room temperature consist of four almost equally spaced hyperfine lines characteristic to the Cu(II) nuclear hyperfine interaction. Onto each copper hyperfine line are superimposed the lines which are derived from the extrahyperfine interaction with the nitrogen nuclei of the donor ligand atoms. If we account for the distortions that might occur in the nitrogen spectrum and consider the relative intensities of the signals (the amplitude ratios) in the epr spectra of $\text{Cu}(\text{DMGL})_2$ and $\text{Cu}(\text{DPGL})_2$, we should find that four nitrogen atoms are bonded to the central Cu(II) ion. The spectrum of $\text{Cu}(\text{DMGL})_2$ at -160° is shown in Figure 2. The distinction between the components of the $g_{||}$ peak is very difficult, due to the overlap with the g_{\perp} peak. In low-temperature spectra the nitrogen hyperfine structure appears usually on the g_{\perp} component of the spectra. We used this component for the evaluation of g_{\perp} while $g_{||}$ was calculated from the approximate relationship $g_0 = 1/3(g_{||} + 2g_{\perp})$. The g values obtained this way approximate those obtained by Wiersema⁹ for $\text{Cu}(\text{DMGL})_2$ in alcoholic solution, and those by Schubel¹⁰ in pyridine solution. Due to uncertainty in evaluations of $A_{||}$ and A_{\perp} , we calculated the in-plane σ -bonding parameter using the splittings of the well-resolved nitrogen hyperfine lines of the spectra. The excellent agreement between the α^2

(7) A. Abragam and H. M. L. Pryce, *Proc. Roy. Soc., Ser. A*, **205**, 135 (1951).

(8) F. A. Cotton and J. J. Wise, *Inorg. Chem.*, **6**, 909, 915, 917 (1967).

(9) A. K. Wiersema and J. J. Windle, *J. Phys. Chem.*, **68**, 2316 (1964).

(10) W. Schubel and E. Lutze, *Z. Angew. Phys.*, **17**, 332 (1964).

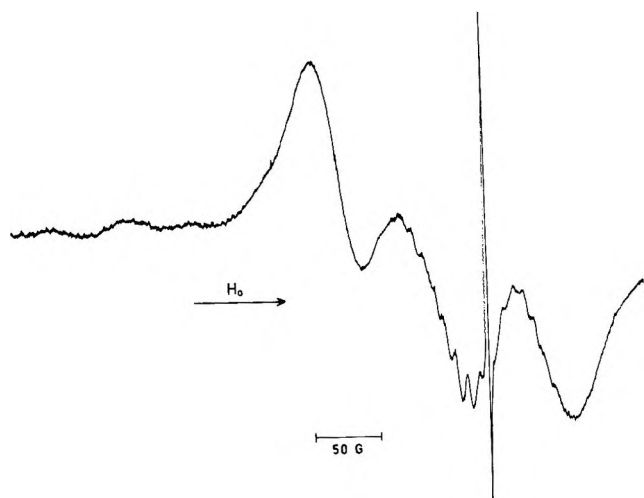


Figure 2. Epr spectrum of chloroformic solution of $\text{Cu}(\text{DMGL})_2$ at -160° .

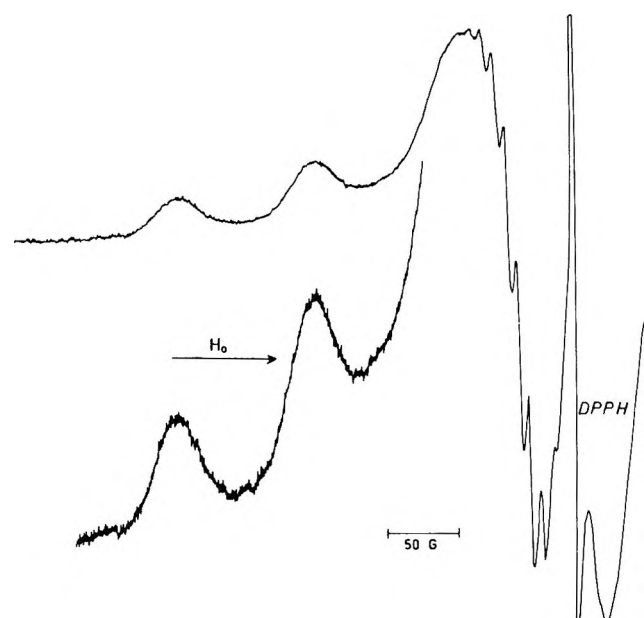


Figure 3. Epr spectrum of chloroformic solution of $\text{Cu}(\text{AADO})_2$ (at -160°).

value obtained from the epr spectra of $\text{Cu}(\text{DMGL})_2$ measured in this study and the α^2 value calculated by Ross¹¹ is noteworthy.

The CHCl_3 solution of bis(acetylacetonate)dioximato-copper(II) " $\text{Cu}(\text{AADO})$ " at -160° exhibits a characteristic epr spectrum of a planar $\text{Cu}(\text{II})$ complex compound, especially with nine well-resolved nitrogen hyperfine lines at the g_{\perp} component (Figure 3). The agreement between α^2 values obtained by the two different calculation methods (Kivelson's approximate formula and extrahyperfine structure splitting formula) is remarkable (Table II). In the spectrum of bis(benzoylacetone dioximato)copper(II) " $\text{Cu}(\text{BADO})_2$ " the resolution of the nitrogen hyperfine lines at the g_{\perp} component is indeed very poor. On the other hand, a



Figure 4. Epr spectrum of chloroformic solution of $\text{Cu}(\text{BADO})_2$ (at -160°).

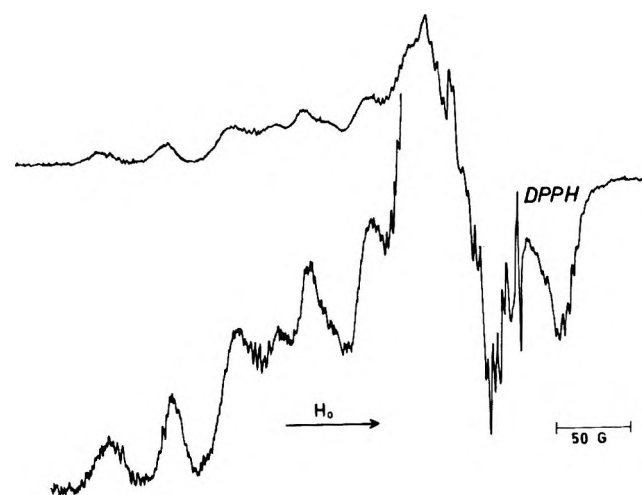


Figure 5. Epr spectrum of chloroformic solution of N,N' -bis(salicylaldehyde)ethylenediiminocopper(II) (at -160°).

large number of lines is observed especially at the low-temperature spectrum (Figure 4). Similar splitting in the epr spectrum of a frozen CHCl_3 solution of bis-(dibenzoylmethanato)copper(II) was noted by Kuska⁴ and attributed to the phenyl group protons.

The epr spectra of bis(N -pentylsalicylaldehyde)iminocopper(II) do not exhibit super hyperfine splittings and are characteristic of planar $\text{Cu}(\text{II})$ compounds.

The epr spectra of N,N' -bis(salicylaldehyde)ethylenediiminocopper(II) at -160° (see Figure 5) suggest that the $\text{Cu}(\text{II})$ is placed in two different environments in the complex molecule.

The magnetic and bonding parameters calculated from epr and electronic absorption data are given in Tables I and II.¹²⁻¹⁵

(11) B. Ross, *Acta. Chem. Scand.*, **21**, 1855 (1967).

(12) L. L. Funck and T. R. Ortolano, *Inorg. Chem.*, **7**, 567 (1968).

(13) D. P. Graddon and E. C. Watton, *J. Inorg. Nucl. Chem.*, **21**, 49 (1961).

Table I: Magnetic Parameters of Cu(II) Chelates in Chloroform

Compound	$g_{ }$	g_{\perp}	g_0	$A_{ } \times 10^4, \text{cm}^{-1}$	$A_{\perp} \times 10^4, \text{cm}^{-1}$	$A_0 \times 10^4, \text{cm}^{-1}$	Reference
β-Diketonates							
1. Bis(hexafluoroacetyl- acetonato)copper(II)	2.318 (2.306)	2.046 (2.051)	2.137 ...	174 (173)	24.6 (24.5)	74.4 ...	4 ^a
2. Bis(trifluoroacetylacetonato)- copper(II)	2.312 (2.308)	2.042 (2.040)	2.132 ...	165 (167)	25.2 (25.2)	71.8 ...	4 ^a
3. Bis(benzoylacetonato)- copper(II)	2.281 (2.281)	2.045 (2.046)	2.124 ...	178 (176)	26.5 (26.6)	77.0 ...	4 ^a
4. Bis(acetylacetonato)- copper(II)	2.283 (2.285) (2.266) (2.264)	2.047 (2.042) (2.053) (2.036)	2.126	173 (175) (160) (145.5)	28.1 (28.2) (19.0) (29.0)	76.4	4 ^a 1 ^b 3 ^c
β-Dioximates							
5. Bis(acetylacetonatodioximato)- copper(II)	2.171	2.088	2.116	189	20.0	76.3	
6. Bis(benzoylacetonatodioximato)- copper(II)	2.211	2.073	2.119	184	21.6	76.5	
α-Dioximates							
7. Bis(dimethylglyoximato)- copper(II)	2.167 (2.15)	2.054 (2.05)	2.092 ...	(144)	(14.6)	87.0 ...	9 ^d
8. Bis(diphenylglyoximato)- copper(II)	2.136	2.048	2.077			84.6	
Schiff bases							
9. Bis(<i>N</i> -pentylsalicylaldiminato)- copper(II)	2.225	2.067	2.120	170	30.5	77.0	
10. <i>N,N'</i> -Bis(salicylaldehyde)- ethylenediimino-copper(II)	2.209 (2.19)	2.046 ...	2.100 (2.11)	198 (208)	30.8 ...	86.5 ...	5 ^e

^a In CHCl₃. ^b Single crystal. ^c Toluene (60%)-CHCl₃ (40%). ^d Aqueous ethanol. ^e In 80% CHCl₃-20% toluene.

Table II: Ligand Field Energies and Bonding Parameters of Cupric Chelates

Compound	ΔF_{yz}	$\Delta E_{x^2-y^2}$	ΔE_{xz}	α^2	$\alpha^2(N)$	β^2	δ^2	Reference ^a
1.	14,000	15,800	18,000	0.861		0.836	0.777	12
2.				0.830				
3.	14,800		18,600	0.835			0.795	13
4.	15,600	16,800	18,000	0.824		0.913	0.866	8
	16,100	18,000	18,500	0.824		1.0	0.870	14
5.	16,600	18,000	27,000	0.774	0.777			
6.		14,814		0.793		0.65		
7.		18,000			0.714	0.843		15
8.					0.740			
9.				0.766				
10.		18,000		0.818		0.80		

^a The sources of the ligand field energies.

Discussion

Calvin and Wilson¹⁶ were the first to suggest the possibility that two force components might be responsible for containing the copper ion in the chelate: one is of the same nature for both copper and hydrogen, and the other, of quite different nature for copper than for hydrogen. The first component should manifest the ionic or coulombic effects, *i.e.*, the effects of charge and charge distribution of the ligand anion, and of the charge and radius of the cation. The second component, assumed to reflect the stabilization due to the enolate resonance system, plays a different and far

greater role in bonding the copper atom than in bonding hydrogen atom.

The in-plane σ -bonding coefficients α^2 gives the expected trend in covalency. From the epr spectrum of β -ketoenolates it can be seen that electron-withdrawing substituents in the acetylacetonate skeleton decrease the covalency of the σ bonding. The change in the

(14) C. Dijkgraaf, *Theoret. Chim. Acta*, **3**, 38 (1965).

(15) S. Yamada and R. Tsuchida, *Bull. Chem. Soc. Jap.*, **27**, 156 (1954).

(16) M. Calvin and K. W. Wilson, *J. Amer. Chem. Soc.*, **76**, 2003 (1954).

covalency may result from the first force component between the copper(II) and the ligand donors, *i.e.*, a change in the effective negative charge on the oxygen donor atom, caused by the inductive effects of the substituents. On the other hand, electron-withdrawing substituents on the β -ketoenolate skeleton cause an increase in the covalent character of the π bonding, especially of the out-of-plane π bonding.

Van Uitert, *et al.*,¹⁷ also pointed out that β -diketones of comparable pK_a values bearing one methyl and one aromatic substituent do not appear to chelate as strongly as those bearing two aromatic substituents. In view of the above epr data, Van Uitert's observation can be interpreted in terms of more covalent out-of-plane π bonding between the metal and the chelated ligand. The aromatic substituents induce a more effective condition toward formation of the enolate (benzenoid) resonance of the chelate ring. In fact, the polarizability of unsaturated molecules containing π bonds is greater than that of saturated molecules containing σ bonds only. On conjugation, the π electrons are delocalized and present in the extended π orbitals.

From Table II it can be seen that the greater covalent character in the in-plane σ bonding is exhibited by the α -dioximates. The copper(II) ion in the latter is surrounded by four nitrogen atoms which are part of two five-membered chelate rings. The increase in ring size in β -dioximate series results in a decrease in the covalent character of the σ bonding. This is due to the greater stability of the five- relative to the six-membered ring structure.

The observed greater covalent character of the in-plane σ bonding in the β -dioximates, as compared to similar bonding in β -ketoenolates, can be attributed to the difference in the electronic characteristics between the nitrogen and the oxygen atoms of the donor groups. The intermediate case, where two nitrogen and two oxygen donor atoms are similarly bonded to the central Cu(II) ion, is reflected in the bonding parameters of the Schiff base complexes. In these cases, one has to account for two different effects which operate in opposite directions on the stability of the complex: (a) the number of the chelate rings and (b) the decrease in benzenoid resonance of the salicylaldehyde derivatives. Calvin and Wilson¹⁶ have noted that the copper(II) chelates derived from β -diketones exhibit greater stability than the analogous chelates from salicylaldehyde of comparable ligand basicity. This was attributed to decrease in the resonance contribution from the active grouping in salicylaldehyde than in β -diketone. From application of polarographic techniques, Calvin and Bailes¹⁸ noticed that the increase in number of the rings in chelated Schiff bases is accompanied by an increase in the stability of the complex. It appears from epr data that the increase in the stability of the complex molecule is reflected by the de-

crease in the β^2 value, *i.e.*, implying an increase in the covalency of the π bonding. Swett and Dudek⁵ recorded the epr spectra of a series of bidentate and tetradentate Schiff bases and found that the covalency of the in-plane π bonding is greater in tetradentate Schiff bases, while the covalency of the σ bonding is in the opposite order. Table III gives the polarographic and epr data for bis(*N*-methylsalicylaldiminato)-copper(II) "A" and *N,N'*-bis(salicylaldehyde)ethylenediiminocopper(II) "B."

Table III

	$\epsilon^{1/2},^a$ V	α^{2b}	β^{2b}
A	+0.02	0.79	0.77
B	-0.75	0.80	0.64

^a Reference 18. ^b Reference 5.

The above data clearly indicate the importance of the π bonding on the stability of the complex molecules.

The large number of lines appearing in the epr spectra of bis(benzoylacetonedioximato)copper(II) (see Figure 4) suggest that additional hyperfine interactions occur with the phenyl protons. Kuska⁴ considered three possible mechanisms for these splittings. (1) In dilute solution the chelates constitute dimers where the phenyl group of the first complex molecule lies above the z axis of the second complex molecule. (2) The electron spin density σ -delocalized, as predicted by extended Hückel molecular orbital calculations of Wise.⁸ (3) The spin density is π -delocalized through a configuration interaction mechanism similar to that proposed by Kivelson¹⁹ and Fortman.²⁰

Kuska has found that proton splittings do not appear when one methyl group is substituted by a phenyl group in the β -ketoenolate skeleton [bis(benzoylacetono)copper(II)], and this phenomenon is difficult to explain in terms of σ delocalization. In contrast, bis(benzoylacetonedioximato)Cu(II) does exhibit proton splittings. We think that the higher covalency of the π bonding is the main cause for these interactions. Similar interactions in bis(salicylaldiminato)Cu(II) have been recorded.¹ The bonding parameters in the latter are very similar to those in bis(acetylacetonato)-Cu(II) which is devoid of proton splittings, except that the in-plane π bonding is more covalent in the case of the salicylaldehydime than it is for the acetylacetonate.¹ Substitution of the methyl groups by phenyl groups in β -ketoenolates and β -dioximates re-

(17) L. G. Van Uitert, W. Fernelius, and B. E. Douglas, *J. Amer. Chem. Soc.*, **75**, 2736 (1953).

(18) M. Calvin and R. H. Bailes, *ibid.*, **68**, 949 (1946).

(19) D. Kivelson and S. K. Lee, *J. Chem. Phys.*, **41**, 1896 (1964).

(20) J. J. Fortman and R. G. Hayes, *ibid.*, **43**, 15 (1965).

sults in a decrease in the covalent character of the σ bonding and in an increase in the covalent character of the π bonding. Hence, the change in the donor atoms from oxygen to nitrogen on going from bis(benzoylacetato)copper(II) to bis(benzoylacetone dioximato)copper(II) results in an intensification of the covalent character of both σ and π bonding; the interactions with the protons are therefore facilitated.

In conclusion, the effects of substitution, ring size, and the nature of the heteroatom on metal-ligand bonding parameters are as follows. (1) Substitution in the six-membered chelate ring by electron-withdrawing groups cause both (i) a decrease of the covalent character of the Cu(II)-ligand σ bonding and (ii) an increase of the out-of-plane π bonding. (2) Enlargement of ring-size of Cu(II) chelates from five (α -dioximates) to six (β -dioximates) entails a decrease of the σ bonding. (3) Replacement of the oxygen donor atoms around the Cu(II) ions in β -diketonates by nitrogen donor atoms (β -dioximates) causes an increase of the covalent character of the σ bonding. (4) The π bonding has an important role on the stability of the complex compounds. (The increase in stability of the complex molecule is reflected by the decrease in the β^2 value of the Schiff base complexes.) (5) Greater covalent character of the π bonding seems to facilitate the hyperfine interactions with the protons.

Experimental Section

All reagents used in this work are of "analytical pure" grade. Acetylacetone dioxime (AADO), mp 149°, was prepared according to the literature.²¹ Benzoylacetone dioxime (BADO), mp 86–87°, was prepared following the procedure of Muller and Auwers.²²

The copper(II) complexes of β -diketonates²³ and of α -dioximes¹⁵ used in this study were prepared by standard methods available in the literature.

The copper(II) complexes of β -dioximes were prepared by a modification of Donaruma's procedure:²⁴ a

mixture of 0.01 mol of cupric acetate and 0.02 mol of β -dioxime in 300 cm³ of toluene was refluxed for 3–4 hr; the toluene-acetic acid azeotropic mixture is distilled and the green oily residue dissolved in benzene and precipitated by addition of petroleum ether. The precipitate was recrystallized from CHCl₃, affording green crystals.

Anal. Calcd for Cu(AADO)₂, C₁₀H₁₈O₄N₄Cu: Cu, 19.7; N, 17.4. Found: Cu, 19.2, N, 17.5. Calcd for Cu(BADO)₂, C₂₀H₂₄O₄N₄Cu: Cu, 14.4; N, 12.5. Found: Cu, 14.0, N, 12.1.

Schiff base complexes, bis(*N*-pentylsalicylaldiminato)copper(II) and *N,N'*-bis(salicylaldehyde)-ethylenediiminocopper(II) were kindly supplied by Dr. Hana Shechter of our department.

The epr spectra of the cupric chelates in CHCl₃ solution were measured with a Varian Model V-4502 X-band spectrometer equipped with a 100-kc/sec field modulation unit and a Varian V-4257 variable temperature controller, allowing operation between +300 and -200°. Chloroform was found to be the best common, nondonor solvent for all the complexes included in this study. No use of other solvents was attempted, because the effect of changing the solvent could be larger than the others due to changes in the ring size and the substituents, etc.

The *g* values were compared with the free-radical standard, diphenyl picrylhydrazil (*g* = *g*_{DPPH} = 2.0036). *g*_{||} and *A*_{||} were obtained from frozen glass spectra at -160°, and the isotropic *g*₀ and *A*₀ values were obtained from solution spectra recorded at room temperature.

Optical absorption measurements were taken on a Cary Model 14 spectrometer.

(21) C. Harries and T. Haga, *Ber.*, **31**, 550 (1898); **32**, 1192 (1899).

(22) H. Muller and K. Auwers, *J. Prakt. Chem.*, **137**, 81 (1933).

(23) R. L. Belford, A. E. Martell, and M. Calvin, *J. Inorg. Nucl. Chem.*, **2**, 11 (1956).

(24) L. G. Donaruma, *Chem. Eng. Data*, **9**, 379 (1964).

Nuclear Magnetic Relaxation in a Homologous Series of Nematic Liquid Crystals

by C. R. Dybowski,¹ B. A. Smith,² and C. G. Wade*

Department of Chemistry, The University of Texas at Austin, Austin, Texas 78712 (Received July 15, 1971)

Publication costs assisted by the National Science Foundation

The spin-lattice relaxation times in the homologous series of 4,4'-bis(alkoxy)azoxybenzenes have been measured in the solid, liquid crystal, and liquid ranges of the substances at a frequency of 30 MHz. The measurements of the relaxation times indicate that the presence of the alkyl substituent is significant in determining the relaxation rate, a point not treated in present theoretical studies.

Introduction

The study of liquid crystal systems by pulsed nmr techniques has focused upon the structure and rotational motions in these systems.³⁻¹² It has been proposed that in addition to the usual Brownian motion contributions, thermal fluctuations of the orientational order (collective modes) of the nematic axis of the liquid crystal may be an important source of nuclear spin relaxation.^{3-8,13,14} The frequency spectrum of the thermal fluctuations exhibits an intense branch in the radiofrequency region¹³ which may allow the exchange of energy between the spin system and the lattice. Doane and Johnson⁵ have developed perhaps the most comprehensive theory of relaxation in the mesophases. This treatment, which relies upon the initial work of Pincus,³ includes Brownian motion and collective mode effects. Unfortunately, the theory is difficult to apply quantitatively because of a lack of data on the elastic constants of liquid crystals. The relative importance to T_1 of the collective modes compared to the Brownian motion effects has not been established experimentally. An effort has been made elsewhere¹⁵ to calculate the intramolecular Brownian motion contribution to phenyl proton relaxation. This model¹⁵ estimates the modulation of the dipole-dipole interaction of two phenyl protons in a linear nematogen which undergoes random motion with a time-independent, statistically preferred direction along the nematic axis. This model and the theory of Doane and Johnson represent the situation of the phenyl protons only. They do not treat intramolecular processes arising from motion in the alkyl groups.

In this paper we report results of measurements of relaxation times for several members of the homologous series of 4,4'-bis(alkoxy)azoxybenzenes which indicate that the length of the alkyl group is of significance. The compounds studied were 4,4'-bis(methoxy)azoxybenzene (PAA), 4,4'-bis(ethoxy)azoxybenzene (PAP), 4,4'-bis(propoxy)azoxybenzene (Pr-

AB), 4,4'-bis(butoxy)azoxybenzene (BAB), 4,4'-bis(pentoxy)azoxybenzene (PAB), and 4,4'-bis(hexoxy)azoxybenzene (HAB).

Proton relaxation studies are complicated because of a lack of knowledge of the relative importance of diffusion-controlled intermolecular contributions to T_1 .^{5b,c,16} This mechanism contributes equally to the relaxation of the phenyl and ester protons. $T_{1,inter}^{-1}$, calculated¹⁵ using the theory derived for isotropic fluids,¹⁷ yields a value of 0.32 sec⁻¹. This is in rea-

- (1) NDEA Fellow, 1969-71.
- (2) Robert A. Welch Fellow.
- (3) P. Pincus, *Solid State Commun.*, **7**, 415 (1969).
- (4) T. Lubensky, *Phys. Rev. A.*, **2**, 2497 (1970).
- (5) (a) J. Doane and D. Johnson, *Chem. Phys. Lett.*, **6**, 291 (1971); (b) J. J. Visintainer, J. W. Doane, and D. L. Fishel, *Mol. Cryst. Liquid Cryst.*, **13**, 69 (1971); (c) B. Cabane and W. G. Clark, *Phys. Rev. Lett.*, **25**, 91 (1970).
- (6) M. Weger and B. Cabane, *J. Phys. Radium, C*, **72** (1969).
- (7) R. Blinc, D. O'Reilly, E. Peterson, G. Lahajrjar, and I. Levstek, *Solid State Commun.*, **6**, 839 (1969).
- (8) (a) R. Blinc, D. Hogenboom, D. O'Reilly, and E. Peterson, *Phys. Rev. Lett.*, **23**, 969 (1969); (b) R. Blinc, "Spin-Lattice Relaxation, Unstable Lattice Modes and Critical Fluctuations," in "Magnetic Resonance," C. Coogan, N. Ham, S. Stuart, J. Pilbrow, and G. Wilson, Ed., Plenum Publishing Co., New York, N. Y., 1970.
- (9) J. Doane and J. Visintainer, *Phys. Rev. Lett.*, **23**, 1421 (1969).
- (10) R. Dong and C. Schwerdtfeger, *Solid State Commun.*, **8**, 707 (1970).
- (11) R. Dong, M. Marusic, and C. Schwerdtfeger, *ibid.*, **8**, 1577 (1970).
- (12) C. Tarr, M. Nickerson, and C. Smith, *Appl. Phys. Lett.*, **17**, 318 (1970).
- (13) Orsay Liquid Crystal Group, *J. Chem. Phys.*, **51**, 816 (1968).
- (14) A. F. Martins, *Mol. Cryst. Liquid Cryst.*, **14**, 85 (1971).
- (15) E. Samulski, C. Dybowski, and C. Wade, *Chem. Phys. Lett.*, **11**, 113 (1971).
- (16) C. Watkins and C. S. Johnson, Jr., *J. Phys. Chem.*, **75**, 2452 (1971).
- (17) (a) J. F. Harmon and B. H. Muller, *Phys. Rev.*, **182**, 400 (1969). This theory indicates that under certain conditions, the intermolecular contributions to T_1 may be frequency dependent. However, using the diffusion coefficient data for PAA of Yun,^{17b} we calculate a negligible frequency dependence for this contribution in PAA. (b) C. K. Yun and A. G. Fredrickson, *Mol. Cryst. Liquid Cryst.*, **12**, 73 (1970).

Table I: Transition Temperatures for the 4,4'-Bis(alkoxy)azoxybenzenes

Compound ^a		DTA, °C		
		Slope-intercept	Endothermal minimum	Literature value ^b (optical observations)
1. PAA	a.	118.1	121.6	118.2
	b.	135.0	136.0	135.3
2. PAP	a.	135.9	141.2	136.6
	b.	168.4	170.0	167.5
3. PrAB	a.	117.3	120.2	115.5
	b.	123.4	123.9	123.6
4. BAB	a.	103.7	105.8	102.0
	b.	136.5	137.0	136.7
5. PAB	a.	76.4	81.4	75.5
	b.	122.1	123.2	123.2
6. HAB	a.	79.0	82.3	81.3
	b.	127.7	128.2	129.1

^a The abbreviations are explained in the text of the article. ^b H. Arnold, *Z. Phys. Chem. (Leipzig)*, **226**, 146 (1964).

sonable agreement with the value of 0.28 sec^{-1} estimated by Dong, *et al.*,¹⁸ from the frequency dependence of T_1 in PAA. These estimated $T_{1,\text{inter}}$ values are larger than the T_1 values observed in the mesophases and are not sufficiently frequency dependent to account for all of the observed^{6,8,9} frequency dependence: $T_1 = f(\omega^n)$, $1/2 \leq n \leq 1$. Thus we assume the intermolecular effects are not dominant.

Experimental Section

The experimental apparatus and technique are discussed elsewhere.¹⁹ All the experiments were done at a frequency of 30 MHz, using either the saturation- τ -90 or the 180- τ -90 pulse sequence. The 90° pulse length was approximately $2 \mu\text{sec}$. An average of four signals was taken at each τ to improve the accuracy. The data were analyzed by computer using standard least-squares methods. Plots of $\ln(1 - M(\tau)/M(\infty))$ vs. τ were linear within the experimental error of $\pm 5\%$.

The compounds, obtained from Eastman Organic Chemicals, were purified by recrystallization from acetone and/or ethanol, degassed using conventional freeze-pump-thaw methods, and sealed under vacuum. To determine the transition temperatures, differential thermograms of each substance were taken using an R. L. Stone (Tracor) DTA-202. If a differential thermogram showed marked depression of either transition, the compound was recrystallized a second time. The final results of the determinations are given in Table I. All compounds have only a nematic liquid crystal phase.

Results and Discussion

The data are given in Figures 1 and 2. The data on PAA and PAP are in good agreement with results reported by other investigators^{6,8} while this study was in progress. The heptoxy homolog has nematic phase (95 to 124°) T_1 values⁹ which we estimate would have approximately the same numerical values as the hexoxy

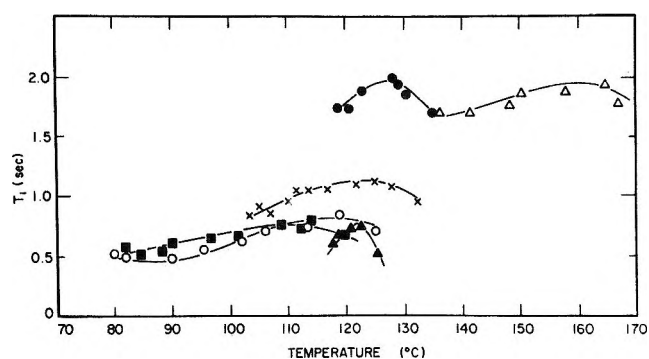


Figure 1. Spin-lattice relaxation time, T_1 , as a function of temperature in the nematic phases; ●, PAA; △, PAP; ▲, PrAB; ×, BAB; □, PAB; ○, HAB.

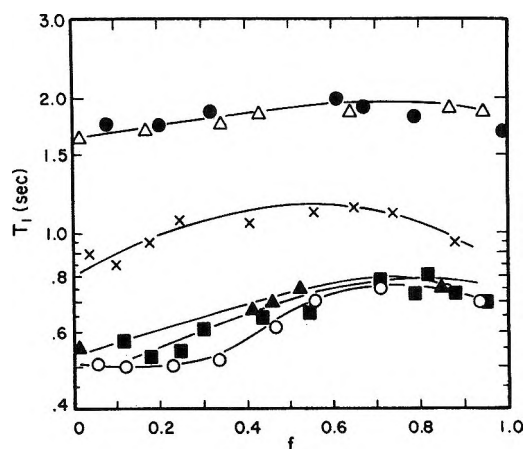


Figure 2. Relaxation time, T_1 , as a function of the fractional relaxation temperature, f , in the nematic phase. $f = 0 \rightarrow$ solid-nematic transition; $f = 1 \rightarrow$ nematic-isotropic transition: ●, PAA; △, PAP; ▲, PrAB; ×, BAB; □, PAB; ○, HAB.

values at a frequency of 30 MHz. Martins¹⁴ has measured the proton relaxation in PAA with deuterated

(18) R. Dong, M. Pintar, and W. Forbes, *Solid State Commun.*, **9**, 151 (1971).

(19) C. Dybowski and C. Wade, *J. Chem. Phys.*, **55**, 1576 (1971).

methyl groups (PAAD) at 56 and 24 MHz and finds relaxation times of 1.6 and 1.2 sec, respectively, which are *approximately* independent of temperature.

Figure 2 indicates that when considered as a fraction of the nematic range the temperature dependence of T_1 is similar in the homologs. This provides evidence that the mechanism is probably the same for all members in the series.

It is obvious from the data in Figure 1 that the alkyl groups are in some fashion significant factors in proton relaxation. Furthermore, as the alkyl chain lengthens a significant increase in the relaxation rate occurs when the number of carbons, n , in the alkyl chain reaches 3. The absence of data on the viscosities,²⁰ elastic constants, and order parameters for these compounds (with the exception of PAA and PAP) precludes a comparison with the theories. However, we infer that this increased relaxation rate is probably due to the increased dipolar interaction of the alkyl protons which may occur for $n \geq 3$ because of the geometry of the chain. It is well known²¹ that, as the alkyl chain is lengthened in these homologs, the changes in length, direction of the dipole moment, and dielectric anisotropies²² per added carbon depend on whether that carbon is added to a chain containing an even or odd number of carbons. For example, a molecular model shows that as the chain length is increased, the possible interaction between the terminal CH_3 and the phenyl protons undergoes a significant increase when n becomes 3.

It should be noted that the proton T_1 data of Martins¹⁴ are somewhat unusual in one respect. He finds that the phenyl proton relaxation time in PAAD is *shorter* than the relaxation time (phenyl plus methyls) in PAA. The liquid crystal range is the same for both compounds. The similarity of the temperature and frequency dependence of T_1 in PAA and PAAD implies that deuteration probably causes no drastic change in the type of relaxation process. To explain the observed relaxation data, the substitution of methyl

protons for deuterons must either increase the phenyl T_1 above that of PAAD or the methyls must have significantly longer T_1 's than the phenyls. The latter possibility might result in the observation of multiple T_1 values in PAA. Simulated data¹⁹ indicate that two relaxation times would be apparent in our data if they differed by a factor of 2 or more. We observed no such effects and none have been reported in PAA or PAP by other investigators.⁸ Ring and alkyl T_1 values have been measured for a number of perprotonated isotropic fluids using adiabatic fast passage methods under high-resolution conditions.²³ For fluids such as toluene, ethylbenzene, mesitylene, and methyl benzoate, the phenyl protons have relaxation times *longer* by at least 20 to 30% than the alkyl protons.²³ Unfortunately, there are no data on the partially deuterated analogs of these to permit an estimation of the changes in phenyl T_1 upon the substitution of deuterons for protons in an alkyl chain. Such data, even though for isotropic fluids, would contribute to an understanding of the relaxation processes in liquid crystals as would similar data on phenyl alkyl ethers.

Acknowledgments. This work was supported in part by the National Institutes of Health under PHS Grant HE-12528, the Robert A. Welch Foundation Grant F-370, the National Science Foundation Grant GY-8793, and the Research Corporation. We acknowledge Dr. E. T. Samulski for helpful discussions and suggestions. We thank Drs. D. E. Woessner and B. S. Snowden for computer programs and assistance. All computations were done at the University of Texas Computation Center.

(20) See, for example, R. Porter and J. Johnson, "The Rheology of Liquid Crystals," in "Rheology," Vol. IV, Academic Press, New York, N. Y., 1967.

(21) G. W. Gray, "Molecular Structure and the Properties of Liquid Crystals," Academic Press, New York, N. Y., 1962, p 215.

(22) W. Maier and G. Baumgartner, *Z. Naturforsch., A*, **7**, 172 (1952).

(23) J. G. Powles, *Ber. Bunsenges. Phys. Chem.*, **67**, 328 (1963).

Vibrational Spectra and Structure of Dimethylaminodichlorophosphine^{1,2}

by J. R. Durig* and J. M. Casper³

Department of Chemistry, University of South Carolina, Columbia, South Carolina 29208 (Received June 7, 1971)

Publication costs borne completely by The Journal of Physical Chemistry

The infrared spectra of dimethylaminodichlorophosphine and dimethylaminodichlorophosphine-*d*₆ have been recorded from 4000 to 33 cm⁻¹ in the gas and solid phases. The Raman spectra of the liquid and solid phases for both compounds were also recorded. The spectra were consistent with the presence of only one isomer over the range of phases and temperatures studied. Available experimental data were discussed in connection with the spectra, and it is concluded that the molecule exists in the gauche conformer with the PNC₂ portion of the molecule planar. A vibrational assignment is proposed for the molecule.

Introduction

An X-ray diffraction study⁴ of dimethylaminodifluorophosphine showed that the molecule existed in the gauche conformer in the solid phase. Furthermore it was reported that the PNC₂ part of the molecule is planar. The vibrational spectrum of the compound was reported⁵ to be consistent with the presence of only one isomer in the gas, liquid, and solid phases.

Imbery and Friebolin⁶ noted that the methyl protons of dimethylaminodichlorophosphine remain equivalent in the nmr spectrum from +80 to -80° and concluded that the compound is in the trans conformer. Recently the nmr spectrum was reinvestigated⁷ and when the temperature of the sample was lowered to -120°, the spectrum showed the protons to be inequivalent. The authors concluded that the molecule exists in the gauche conformer and postulated that it may have a planar nitrogen similar to dimethylaminodifluorophosphine. An electron diffraction study⁸ of dimethylaminodichlorophosphine has found the CNC angle to be 120° which indicates that nitrogen is planar. Some infrared and Raman work on (CH₃)₂NPCl₂ in the liquid phase has been reported.^{9,10} However, only fragmentary assignments have been made, and no structural conclusions were drawn from the data. Therefore, it was decided to study the infrared and Raman spectra of dimethylaminodichlorophosphine and the *d*₆ analog in order to determine the symmetry in all phases and assign the normal vibrations.

Experimental Section

Dimethylaminodichlorophosphine was prepared by the reaction of dimethylamine and phosphorus trichloride according to the procedure of Burg and Slota.¹¹ The compound was fractionally distilled and its purity checked by infrared and Raman spectroscopy.^{9,10} The only impurity found in any of the samples was phosphorus trichloride which could be monitored by the presence of a line at 257 cm⁻¹ in the Raman spectrum. Dimethylamino-*d*₆-dichlorophosphine was prepared by the above procedure with the substitution of dimethyl-

amine-*d*₆ in the above reaction. This sample was purified by trap-to-trap distillation.

The infrared spectra were recorded from 4000 to 250 cm⁻¹ with a Perkin-Elmer Model 621 spectrophotometer. The atmospheric water vapor was removed from the spectrophotometer housing by flushing with dry air. In the higher frequency region, the instrument was calibrated with standard gases.¹² The lower wave number region was calibrated by using atmospheric water vapor and the frequencies reported by Hall and Dowling.¹³ The spectra of the gaseous sample were recorded by using a 20-cm cell and a Beckman variable path length cell both equipped with KBr windows. The spectrum of the solid was obtained by condensing the sample on a silicon plate maintained at -190° with boiling nitrogen.

The Raman spectrophotometer used was a Cary Model 81 equipped with an He-Ne laser source. The spectrum of the liquid was taken with the sample sealed in a capillary tube. For elevated temperatures this tube was heated with a nichrome wire element sur-

(1) Presented at the Twenty-sixth Symposium on Molecular Spectra and Structure, Ohio State University, 1971, Paper Q7.

(2) Taken from the thesis of J. M. Casper submitted to the Department of Chemistry in partial fulfillment of the Ph.D. degree, June 1971.

(3) Predoctoral National Science Foundation Fellow.

(4) E. D. Morris, Jr., and C. E. Nordman, *Inorg. Chem.*, **8**, 1673 (1969).

(5) M. A. Fleming, R. J. Wyma, and R. C. Taylor, *Spectrochim. Acta*, **21**, 1189 (1965).

(6) D. Imbery and H. Friebolin, *Z. Naturforsch. B*, **23**, 759 (1968).

(7) A. H. Cowley, M. J. S. Dewar, W. R. Jackson, and W. B. Jennings, *J. Amer. Chem. Soc.*, **92**, 1085 (1970).

(8) L. V. Vilkor and L. S. Kharkin, *Dokl. Akad. Nauk SSSR*, **168**, 810 (1966); *Chem. Abstr.*, **65**, 8724a (1966).

(9) C. Christol and H. Christol, *J. Chim. Phys.*, **62**, 246 (1965).

(10) F. Herail and M. J. Leconte, *C. R. Acad. Sci., Ser. C.*, **262**, 22 (1966).

(11) A. B. Burg and P. J. Slota, Jr., *J. Amer. Chem. Soc.*, **80**, 1107 (1958).

(12) "IUPAC, Tables of Wavenumbers for the Calibration of Infrared Spectrometers," Butterworths, Washington, D. C., 1961.

(13) R. T. Hall and J. M. Dowling, *J. Chem. Phys.*, **47**, 2454 (1967).

Table I: Infrared and Raman Spectra of $(\text{CH}_3)_2\text{NPCl}_2$

Infrared				Raman				Assignment
Gas		Solid		Liquid		Solid		
Frequency, cm^{-1}	Rel. intensity	Frequency, cm^{-1}	Rel. intensity	Frequency, cm^{-1}	Rel. intensity	Polarization	Frequency, cm^{-1}	Rel. intensity
		3205	w					
2985	w							2804 + 216 = 3020
2940	m	2940	m					2804 + 191 = 2995
				2922	w			CH_3 stretch ^a
		2900	m	2903	w			CH_3 stretch
		2848	w	2850	m			CH_3 stretch
		2800	m	2804	m			CH_3 stretch
		2770	m					CH_3 stretch
		2476	m					1449 + 1028 = 2477
		2468	m					1440 + 1058 = 2468
		2450	w					1476 + 975 = 2451
		1601	w					1410 + 191 = 1601
		1484	m					CH_3 deformation
		1476	m	1475	vw			CH_3 deformation
		1459	m					CH_3 deformation
		1449	m					CH_3 deformation
		1440	m					1095 + 335 = 1430
		1438	m	1435	vw			CH_3 deformation
		1427	w					1028 + 394 = 1422
		1403	w	1410	vw			CH_3 deformation
1282	w	1298	m	1282	w			NC_2 antisymmetric stretch
		1272	w					1058 + 216 = 1274
		1173	m					CH_3 rock
1120	w							690 + 428 = 1120
		1095	w					CH_3 rock
		1058	m					CH_3 rock
		1028	m					CH_3 rock
988	s	984	s	975	vw		981	8
		894	m					NC_2 symmetric stretch
		731	vw					690 + 191 = 881
675	w	693	m	690	61	p	694	52
525	w							394 + 335 = 729
505	s	500	s	513	47	p	500	57
457	m	420	s	428	24	dp	417	60
396	m	400	m	394	32	p	391	44
341	m	335	m	335	100	p	340	100
		292	vw	304	w		293	20
		221	m	216	31	p	217	43
193	w	196	m	191	40	dp	197	41
		155	vw					PCl_2 wag
				124	22		142	m
		78	w					41
								PCl_2 deformation and twist
								P-N torsion
								Lattice mode

^a The spectral region from 2700 to 3000 cm^{-1} is very complex due to Fermi resonance of the fundamentals with the overtones of the methyl deformations.

rounded by asbestos. The spectra of the sample at temperatures below room temperature and spectra of the solid sample were obtained by using a cell which has been previously described.¹⁴

The far-infrared spectra were recorded from 33 to 500 cm^{-1} on a Beckman Model IR-11 spectrophotometer. The instrument was purged with dry air and calibrated with the frequencies reported for water vapor by Hall and Dowling.¹³ For the spectrum of the gas phase in this frequency region, a Beckman variable path length cell equipped with polyethylene windows was used. The cell used for recording the spectra of the solid at

-190° has been described earlier.¹⁵ The frequencies for all observed bands are expected to be accurate to $\pm 2 \text{ cm}^{-1}$. These frequencies with their relative intensities and proposed assignments are listed in Tables I and II for the light and deuterated compounds, respectively.

Results

A comparison of the Raman spectra of the liquid and

(14) D. J. Antion and J. R. Durig, *Appl. Spectrosc.*, **22**, 675 (1968).

(15) F. G. Baglin, S. F. Bush, and J. R. Durig, *J. Chem. Phys.*, **47**, 2104 (1967).

Table II: Infrared and Raman Spectra of $(CD_3)_2NPCl_2$

Infrared				Raman			Solid		Assignment
Gas		Solid		Liquid					
Frequency, cm^{-1}	Rel. intensity	Frequency, cm^{-1}	Rel. intensity	Frequency, cm^{-1}	Rel. intensity	Polarization	Frequency, cm^{-1}	Rel. intensity	
2220	vw			2224	m	dp	2220	s	CD_3 stretch ^a
2210	w	2205	w	2209	m	dp			CD_3 stretch
2125	w			2132	m				CD_3 stretch
2110	vw			2120	m		2122	m	CD_3 stretch
2072	m			2090	w	p	2084	w	CD_3 stretch
2065	m	2058	w	2067	s	p	2065	s	CD_3 stretch
		1222	m						$906 + 310 = 1216$
1201	s	1200	w	1205	vw				$832 + 363 = 1195$
		1190	vw						$827 + 363 = 1190$
1172	m	1163	m						$650 + 509 = 1159$
		1148	w						$832 + 310 = 1142$
				1110	4				CD_3 deformation
1055	m	1060	vw	1065	9		1069	18	NC_2 symmetric stretch
				1055	7				CD_3 deformation
1045	m	1047	m	1045	7		1041	14	CD_3 deformation
		1035	w						CD_3 deformation
		906	w						CD_3 rock
835	m	835	m	832	17	p	837	14	NC_2 symmetric stretch
828	m	827	m						CD_3 rock
795	w								CD_3 rock
640	m	643	m	649	72	p	650	55	P-N stretch
508	s	492	s	509	64	p	498	91	PCl_2 symmetric stretch
455	s	420	vs	427	43	dp	415	100	PCl_2 antisymmetric stretch
368	w	358	m	363	100	p	357	59	NC_2 rock
		308	m	310	71	p	310	44	NC_2 deformation
		265	w	287	w		274	29	NC_2 wag
		213	m	210	43	p	210	37	PCl_2 wag
		186	m	190	190	dp	188	19	PCl_2 deformation and twist
		140	w				142	15	Lattice mode
				110	25		119	27	P-N torsion
		102	vw						Lattice mode
		77	w				84	9	Lattice mode

^a The spectral region from 2000 to 2300 cm^{-1} is very complex due to Fermi resonance of the fundamentals with the overtones of the methyl deformations.

the solid showed that they were consistent with each other. The P-N stretching vibration, which is expected to be the most sensitive indicator of a conformational change, was found at 690 cm^{-1} in the liquid phase and 694 cm^{-1} in the solid for the light compound and at 649 and 650 cm^{-1} in the liquid and solid, respectively, of the d_6 compound. The spectra were then studied as a function of temperature over the range of +120 to -190°. There were no effects observed that could be attributed to isomeric changes. In the infrared spectra of the compounds in the gaseous state the P-N stretching vibration was observed at 675 and 640 cm^{-1} for the light and heavy compounds, respectively. Since no evidence of doubling of any of the skeletal vibrations was observed, and since previous studies¹⁶⁻¹⁹ have shown this to be a sensitive method of determining rotational isomerism, it must be concluded that the molecule exists in the same conformer in the liquid, solid, and gas phases in the temperature range studied.

The probable conformations for this conformer are the trans (C_s) and gauche (C_1) associated with a tetrahedral nitrogen, and the trans (C_s) and gauche (C_s) associated with a planar nitrogen. All vibrations of each of these symmetry species are infrared and Raman-allowed. For the C_1 species, all vibrations may be polarized in the Raman. For both trans (C_s) structures one predicts seven polarized Raman lines for the skeletal motions whereas for the gauche (C_s) one predicts eight polarized Raman lines for the skeletal motions. The Raman spectra of liquid dimethylaminodichlorophosphine and its deuterated analog each contain only six clearly polarized Raman lines that can be associated with skeletal fundamentals. Therefore, the data do

(16) J. R. Durig and J. W. Clark, *J. Chem. Phys.*, **48**, 3216 (1968).

(17) J. R. Durig and J. S. DiYorio, *Inorg. Chem.*, **8**, 2796 (1969).

(18) J. R. Durig and J. M. Casper, *J. Chem. Phys.*, **55**, 198 (1971).

(19) J. M. Casper, Ph.D. Thesis, University of South Carolina, June 1971.

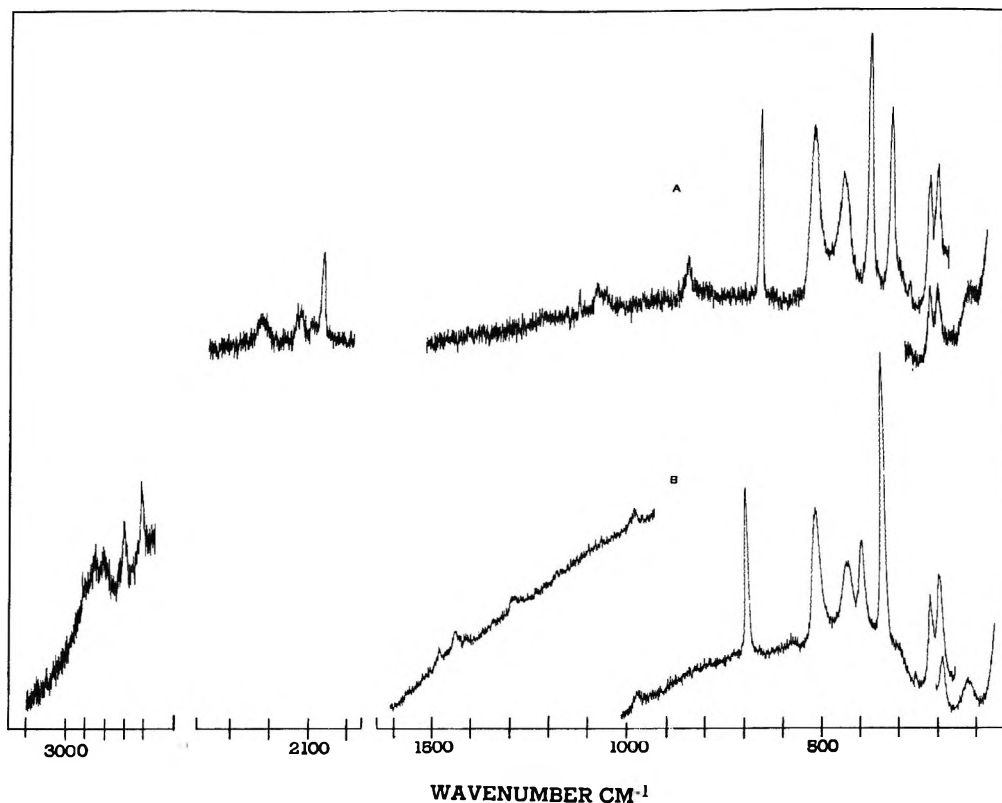


Figure 1. Raman spectra of dimethylaminodichlorophosphine- d_6 (A) and dimethylaminodichlorophosphine (B).

not directly lead to the conformation of the isomer present.

The structure of the conformer that is present may be obtained by comparison with the results of other methods of investigation. The nmr spectrum⁷ shows that below -120° the protons on the methyl groups are not equivalent. Therefore, the structure must be gauche. Above -120° the nmr results^{6,7} indicate that the methyl groups are rotationally averaged. Since a barrier to rotation about the P-N bond of 8.4 kcal/mol was calculated from the coalescence of the nmr peaks,⁷ all minima on the potential curve should be observable by vibrational spectroscopy. Therefore, since only one conformer was observed in the vibrational study of this molecule, the rotation observed by nmr must be a rotation between equivalent structures. For a gauche form the rotation involves passing through a trans structure without it representing a minimum on the potential curve. The trans isomer for the tetrahedral nitrogen structure is the sterically favored form whereas for the planar nitrogen it is sterically unfavorable. Since a second stable isomer was not observed for any of the phases, a planar nitrogen is indicated. This is in agreement with the electron diffraction results that report a CNC bond angle of 120° . Therefore, we concluded that, for the temperature range covered in this study, dimethylaminodichlorophosphine exists in the gauche conformer with the PNC₂ part of the molecule planar.

Vibrational Assignment

There are 30 fundamental vibrations for both dimethylaminodichlorophosphine and the d_6 analog. Of these, 18 are motions of the methyl group. For the gauche (C_s) structure, the skeletal motions are represented by $8a' + 4a''$. Both species are infrared and Raman-allowed and the a' motions may give rise to polarized Raman lines. A comparison of the Raman spectra of the light and heavy compounds (Figure 1) makes the assignment relatively straightforward.

The methyl motions, except the torsions, are found in the expected ranges. The suggested assignments are listed in Tables I and II for the CH₃ and CD₃ motions, respectively. There is considerable overlapping in some of the regions where these motions are observed and only a tentative assignment can be given. The isotopic shifts for all motions assigned to the methyl groups are in the range 1.28 to 1.38.

Harvey and Mayhood²⁰ assign the antisymmetric and symmetric NC₂ stretches in dimethylaminodichlorophosphine to infrared bands at 1175 and 1063 cm⁻¹, respectively. Herail¹⁰ assigned the antisymmetric stretch a frequency of 1062 cm⁻¹ and the symmetric stretch at 980 cm⁻¹. The Raman spectrum of the d_6 compound contains a polarized line at 832 cm⁻¹. The corresponding line in the light compound is at 975 cm⁻¹.

(20) R. B. Harvey and J. E. Mayhood, *Can. J. Chem.*, **33**, 1552 (1955).

This gives a shift of 1.17 which is in the range expected for an NC_2 symmetric stretch. If a similar shift is calculated for the 1175 or 1062- cm^{-1} assignments of the antisymmetric NC_2 stretching motion, the bands are predicted to appear in the spectrum of the deuterated compound where there are no observed bands at a reasonably close frequency. In addition these bands are only observed in the infrared spectrum of the solid and liquid phase which would be unexpected for NC_2 antisymmetric stretching vibrations. For $(\text{CH}_3)_2\text{NAsCl}_2$ ¹⁹ the antisymmetric NC_2 stretch is assigned to a band at 1258 cm^{-1} . There is a band at 1282 cm^{-1} in the Raman spectrum of dimethylaminodichlorophosphine that has counterparts in the infrared spectrum of the gas and solid. If this is assigned to the NC_2 antisymmetric motion, the isotopic shift would cause the band to be expected in the spectrum of the d_6 compound at about 1090 cm^{-1} . There are several lines in the Raman spectrum that would give reasonable shifts. The line at 1065 cm^{-1} in the spectrum of the d_6 compound is more intense than the neighboring lines and is observed in the infrared and Raman spectra of the solid as well as in the infrared spectrum of the gas phase. This line, therefore, must be attributed to the NC_2 antisymmetric stretch.

The P-N stretch of dimethylaminodichlorophosphine has been assigned at 694⁹ and 692 cm^{-1} .¹⁰ The intensity and polarization of the Raman line at 693 cm^{-1} in the light compound is in agreement with this assignment. The corresponding line in the d_6 compound is at 643 cm^{-1} .

The lines observed at 513 and 427 cm^{-1} have been assigned^{9,10} as the antisymmetric and symmetric PCl_2 stretching motions, respectively. The lack of isotopic shift confirms their assignment as PCl_2 stretching motions; however, the polarization data clearly indicate that the higher frequency line is the symmetric vibration.

Isotopic shifts show that the lines at 294, 335, and 304 cm^{-1} in the Raman spectrum are due to NC_2 bending motions. The two polarized lines can be assigned to the deformation and rocking motions; therefore, the weak band at 304 cm^{-1} in the Raman spectrum must be assigned to the NC_2 wag. Both the rock and the deformation are derived from the degenerate XY_3 bending and, therefore, must be arbitrarily assigned to the two observed polarized lines. The deformation has been assigned to the 335- cm^{-1} line and the rock has been assigned to the 394- cm^{-1} line.

The three PCl_2 bending motions and the P-N torsion are the only skeletal motions that remain to be assigned. The PCl_2 bends are expected to give rise to medium intensity Raman lines in the range of 150 to 250 cm^{-1} ; these lines should have an isotopic shift close to 1.0. The P-N torsion is expected around 100 cm^{-1} and should show an isotopic shift of about 1.2. The Raman spectrum of the liquid shows only three bands in this

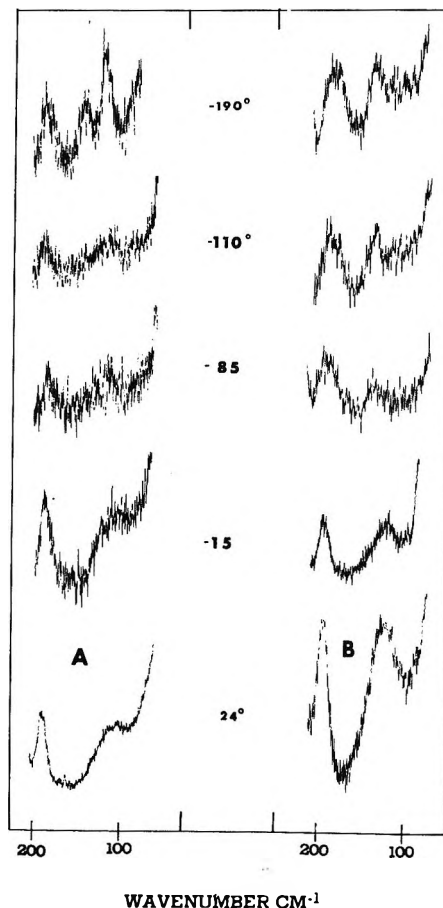


Figure 2. The effects of temperature on the Raman spectra of dimethylaminodichlorophosphine- d_6 (A) and dimethylaminodichlorophosphine (B).

frequency range that have not been assigned as fundamentals. A study of the spectra of the light and heavy compounds in this frequency range (Figure 1) shows that there are only two bands that have near 1.0 isotopic shifts. These lines at 216 and 191 cm^{-1} have to be assigned to the three PCl_2 bending modes. The lower frequency line is broad compared to the higher frequency one. The PCl_2 wag is derived from the ν_2 bend of PCl_3 and is expected to be at a higher frequency than the PCl_2 twist and deformation which are derived from the ν_3 degenerate bend of PCl_3 . Thus, it is reasonable to assign the polarized Raman line at 210 cm^{-1} to the PCl_2 wag and the broad band at 190 cm^{-1} to both the PCl_2 twist and the PCl_2 deformation. From a comparison of the spectra of the compounds in the solid state at -190° , it appears that there is a band at 142 cm^{-1} for both the heavy and the light molecule. Although the frequency is a little lower than expected, this could be assigned to the missing PCl_2 bend on the basis of the lack of an isomer shift. A temperature study (Figure 2) of this line indicates that it has a different origin in the light and heavy compounds. In the light compound, the 142- cm^{-1} line arises from the temperature shift of the line at 124 cm^{-1} in the spec-

trum of the liquid at room temperature. For the deuterated molecule, the 142-cm^{-1} line appears only in the solid phase. From a comparison of the spectra (Figure 2), it can be seen that the 142-cm^{-1} line in the spectrum of the light compound corresponds to the 119-cm^{-1} line in the spectrum of the d_6 analog. The isomer shift is 1.19 in the solid and 1.13 in the liquid. This line cannot be considered a difference tone because it is present at -190° , and it cannot be considered a lattice mode since it is present in the spectrum of the liquid. It must be a fundamental and only the P-N torsion and the two CH_3 torsions remain to be assigned. The frequency is too low for a methyl torsion and the isomer shift is reasonably close to the expected value for the P-N torsion. Therefore, this line is assigned as the P-N torsional frequency. The line that appears at 142 cm^{-1} in the spectrum of the deuterium compound has the behavioral characteristics of a lattice mode and is tentatively assigned as such, despite the unusually high frequency. The possibility of this line arising from the methyl torsion which shifts from 190 cm^{-1} with deuteration cannot be definitely ruled out.

The assignment of the fundamentals was discussed, for the most part, only in terms of the Raman spectra. This was done for the simplicity of the discussion. These assignments are consistent with the infrared spectra of the solid and gas (see Tables I and II). A summary of the assignments and an approximate description of the skeletal modes is presented in Table III.

Table III: Summary of the Skeletal Fundamental Vibrations

Approximate description	$(\text{CH}_3)_2\text{NPCl}_2^a$ frequency, cm^{-1}	$(\text{CD}_3)_2\text{NPCl}_2^a$ frequency, cm^{-1}	$\nu_{\text{H}}/\nu_{\text{D}}$
a'			
NC_2 antisymmetric stretch	1282	1065	1.20
NC_2 symmetric stretch	975	832	1.17
P-N stretch	690	649	1.06
PCl_2 symmetric stretch	513	509	1.00
NC_2 rock	394	363	1.09
NC_2 deformation	335	310	1.08
PCl_2 wag	216	210	1.03
PCl_2 deformation	191	190	1.00
a''			
PCl_2 antisymmetric stretch	428	427	1.00
NC_2 wag	304	287	1.06
PCl_2 twist	191	190	1.00
P-N torsion	124	110	1.13

^a The frequencies are from the Raman spectrum of the liquid.

In the assignment of the bands which are not attributed to fundamental vibrations, there were generally several possible combinations which would give a satisfactory fit. Only the closest fit is given in the tables, and these assignments must be considered provisional.

Discussion

From the observed spectra and the data previously reported for dimethylaminodichlorophosphine, it has been concluded that the molecule exists in only the gauche (C_s) conformer in the vapor, liquid, and solid phases. This is in agreement with the data reported for $(\text{CH}_3)_2\text{NPF}_2$. This compound was shown⁴ by X-ray diffraction to be in the gauche (C_s) conformation in the solid. A vibrational study⁵ of the compound has indicated that it exists in only one conformer in the solid, liquid, and gas phases. In an investigation¹⁹ of the vibrational spectrum of $(\text{CH}_3)_2\text{NAsCl}_2$, it was found that a different form of this molecule exists in the fluid states from that found in the solid phase. It was thought that this corresponding arsenic molecule has a tetrahedral nitrogen atom.

Cowley and Schweiger²¹ studied the scalar ^{15}N -H coupling in aminophosphines and aminoarsines and concluded that the present s character in the nitrogen orbitals indicated sp^2 hybridization for aminophosphines and sp^3 hybridization in aminoarsines. They suggested that the difference was due to the difference in $d\pi$ - $p\pi$ bonding ability of the arsenic 4d orbitals and the phosphorus 3d orbitals. The results of this study and our previous work on $(\text{CH}_3)_2\text{NAsCl}_2$ ¹⁹ are in agreement with this theory. However, more studies of aminoarsines and aminophosphines are needed to assess the relative importance of steric and electronic factors in the determination of the stable conformation.

The assignment of the 690-cm^{-1} line to the P-N stretching vibration is conclusive on the basis of the Raman intensity and the isotopic shift factor. Chittenden and Thomas²² have reported characteristic infrared absorption frequencies for phosphorus-nitrogen compounds. For series of 70 PNMe_2 compounds, they report characteristic infrared absorption bands in the regions of 1300, 1180, 1065, 975 cm^{-1} . It is quite evident from our isotopic shift data that the bands in these regions correspond to the antisymmetric NC_2 stretch, two methyl rocks, and the symmetric NC_2 stretch, respectively. Although they do not assign a P-N stretch for the PNMe_2 compounds they tentatively list such a vibration for PNHR aryl and alkyl molecules in the general frequency range of 873 to 1053 cm^{-1} .

For the majority of the compounds that they investigated the listed frequency for the P-N stretch was in the 900-cm^{-1} range. However, on the basis of our work it appears that a characteristic P-N frequency should be in the $650\text{-}750\text{-cm}^{-1}$ range. This range is consistent with the frequency postulated for this vibration by a number of previous workers,^{20,23} but in var-

(21) A. H. Cowley and J. R. Schweiger, *J. Chem. Soc. D*, 1492 (1970).

(22) R. A. Chittenden and L. C. Thomas, *Spectrochim. Acta*, 22, 1449 (1966).

(23) D. E. C. Corbridge, *J. Appl. Chem.*, 6, 456 (1956).

iance with the range suggested by Chittenden and Thomas²² and McIvor and Hubley.²⁴ Chittenden and Thomas²² rejected this range on the basis that many compounds containing P-N band have no infrared band in the region 660 to 775 cm^{-1} which they could assign to this normal vibration. It is quite probable that many of these compounds may have weak infrared bands arising from the P-N motion and that the Raman effect is much better suited for the determination of a characteristic frequency for the P-N bond. The analogy drawn between P-O-C and P-N-C bands is not expected to lead to a characteristic frequency for the P-N stretch since the coupling of the P-O and O-C motions^{25,26} is significantly different from the coupling found for the

P-N vibration in $(\text{CH}_3)_2\text{NPCl}_2$. Thus, the earlier frequency range suggested^{20,23,27,28} for the P-N single bond stretching vibration is correct.

Acknowledgment. The authors gratefully acknowledge the financial support given this work by the National Aeronautics and Space Administration through Grant NGR-41-002-033.

(24) R. A. McIvor and C. E. Hubley, *Can. J. Chem.*, **37**, 869 (1959).

(25) J. R. Durig and J. S. DiYorio, *J. Chem. Phys.*, **48**, 4154 (1968).

(26) J. R. Durig and J. W. Clark, *ibid.*, **50**, 107 (1969).

(27) B. Holmstedt and L. Larsson, *Acta Chem. Scand.*, **5**, 1179 (1951).

(28) L. Larsson, *ibid.*, **6**, 1470 (1952).

Equilibrium Constants for the Formation of Weak Complexes

by Robert L. Scott

Contribution No. 2212 from the Department of Chemistry, University of California, Los Angeles, California 90024
(Received March 25, 1970)

Publication cost assisted by the National Science Foundation

The determination of equilibrium constants for the formation of weak complexes is examined in the light of a quasi-chemical calculation for a lattice of donor, acceptor, and inert solvent molecules. It is apparent that the equilibrium constants determined from spectroscopic or other nonthermodynamic measurements (*e.g.*, using the Benesi-Hildebrand equation) are "sociation" constants which yield the number of "complexes" in excess of that calculated on the basis of random probabilities.

It is well known that the concentration of weak complexes in solution cannot be determined from thermodynamic measurements alone without the aid of a detailed (and unverifiable) molecular model. However, with the aid of spectroscopic or other nonthermodynamic measurements and with the additional assumptions of (a) Beer's law behavior for all species in the solution and (b) ideal solution behavior for all molecular species, concentrations and equilibrium constants can be deduced. For measurements of visible or ultraviolet absorption, the usual procedure is to use the Benesi-Hildebrand equation¹ or modifications thereof.²⁻⁵ Similar procedures have been used with nmr spectra in solution.^{6,7}

Some of the equilibrium constants so deduced are extremely small (*e.g.*, $K_c = 0.009 \text{ l. mol}^{-1}$ or $K_z = 0.07$ for benzene + carbon tetrachloride in *n*-hexane solution⁸), and one may reasonably question their physical significance. In particular, it has been pointed out⁹⁻¹¹ that in a plausible quasi-lattice model of the

solution, random contacts between donor and acceptor molecules lead to $K_z = z$, the number of nearest neighbors, or K_c 's of the order of 0.30 l. mol^{-1} , larger than many of those reported.

(1) H. A. Benesi and J. H. Hildebrand, *J. Amer. Chem. Soc.*, **71**, 2703 (1949).

(2) J. A. A. Ketelaar, C. van der Stolpe, A. Goudsmit, and W. Dzcubas, *Recl. Trav. Chim. Pays-Bas*, **71**, 1104 (1952).

(3) R. L. Scott, *ibid.*, **75**, 787 (1956).

(4) R. S. Drago and N. J. Rose, *J. Amer. Chem. Soc.*, **81**, 6138 (1959).

(5) G. Briegleb, "Elektronen-Donator-Acceptor Komplexe," Springer-Verlag, West Berlin, 1961.

(6) M. W. Hanna and A. L. Ashbaugh, *J. Phys. Chem.*, **68**, 811 (1964).

(7) R. Foster and C. A. Fyfe, *Trans. Faraday Soc.*, **61**, 1626 (1965); **62**, 1400 (1966).

(8) R. Anderson and J. M. Prausnitz, *J. Chem. Phys.*, **39**, 1225 (1963).

(9) R. L. Scott, Proceedings of the Third International Conference on Coordination Compounds, Amsterdam, 1955, p 345.

(10) J. E. Prue, *J. Chem. Soc.*, 7534 (1965).

(11) J. E. Prue, Chemical Society Symposium on the Physical Chemistry of Weak Complexes, Exeter, England, April 1967.

Of course, many complexes require a special orientation of donor and acceptor with respect to each other, a condition which only a small fraction of the random contacts would satisfy. This would seem to resolve the problem, except that Orgel and Mulliken¹² have shown that if there are several 1:1 complexes, each with equilibrium constant K_i and absorptivity ϵ_i , the "observed" K and ϵ are the appropriate averages $\Sigma_i K_i$ and $\Sigma_i K_i \epsilon_i / \Sigma_i K_i$. Thus the contact "complexes," even if they do not absorb light ($\epsilon = 0$) and contribute nothing to ϵ_{obsd} , would seem to contribute substantially to K .

A simple quasi-chemical calculation for a lattice of donor, acceptor, and inert solvent molecules (D, A, and S) can help to illuminate this problem. We assume a lattice of coordination number z , in which the site fractions of donor, acceptor, and solvent are x_D , x_A , x_S , respectively, and further that all pair interaction energies are the same except for a particular one of the z "faces" of D with a similar particular "face" of A, which differs from the others by an energy w and has an absorptivity ϵ . (This assumption is, of course, only for simplification; in any actual system, each interaction will have a somewhat different energy. However, even for "weak" complexes, it seems reasonable—physically and geometrically—to assume that one interaction is somewhat stronger than all the others.)

In a lattice of N sites, the number of random contact pairs DA will be Nx_Dx_Az , of which (in the random mixing approximation) only a fraction $1/z^2$ will have the "complex" orientation. If we introduce a factor η_c to allow for the energetic preference for complex formation, the number of "complexes" will be $Nx_Dx_A\eta_c/z$, in excess of the random value ($\eta_c = 1$).

Solution of the quasi-chemical equations for this model yields (see Appendix) an equation for η_c

$$x_Ax_D(\kappa^2 - 1)\eta_c^2 - [(x_A + x_D)(\kappa - 1) + z]\kappa z\eta_c + \kappa^2 z^2 = 0 \quad (1)$$

where $\kappa = e^{-w/kT}$, with w the usual interchange energy.

Where $x_D \gg x_A \approx 0$, an essential approximation in the Benesi-Hildebrand theory, eq 1 simplifies to

$$\eta_c \approx \frac{\kappa z}{(\kappa - 1)x_D + z}$$

The number of complexes is then

$$N_C = \frac{Nx_Ax_D\eta_c}{z} = \frac{N\kappa x_Ax_D}{(\kappa - 1)x_D + z} \quad (2)$$

and the absorption A per length l is

$$\frac{A}{l} = \frac{\epsilon N_C}{N} = \frac{\epsilon \kappa x_Ax_D}{(\kappa - 1)x_D + z} \quad (3)$$

In the Benesi-Hildebrand treatment when $x_A l/A$ is plotted *vs.* $1/x_D$ one interprets the intercept as $1/\epsilon$ and the slope as $1/K\epsilon$ where K is the mole fraction equilibrium constant. In the equivalent Scott modification

$x_Ax_D l/A$ is plotted against $1/x_D$ to yield an intercept $1/K\epsilon$ and a slope $1/\epsilon$. If we so transform eq 3

$$\frac{x_Ax_D l}{A} = \frac{z + (\kappa - 1)x_D}{\kappa \epsilon} \quad (4)$$

It is evident from eq 4 that the usual procedure yields

$$K_{\text{obsd}} = \frac{\kappa - 1}{z} = \frac{e^{-w/kT}}{z} - \frac{1}{z} = K - K_{\text{random}} \quad (5)$$

$$\epsilon_{\text{obsd}} = \frac{\kappa \epsilon}{\kappa - 1} = \frac{K \epsilon}{K - K_{\text{random}}} \quad (6)$$

Thus $K_{\text{obsd}}\epsilon_{\text{obsd}} = K\epsilon$, but $K_{\text{obsd}} < K$ while $\epsilon_{\text{obsd}} > \epsilon$.

Since $1/z$ is the entropy prefactor, it is evident that the "observed" constant is just the excess over the random. It is easy to generalize the treatment to include several 1:1 complexes, for which case the earlier Orgel-Mulliken formulation is replaced by

$$K_{\text{obsd}} = \frac{\Sigma_i (K_i - K_{i,\text{random}})}{\Sigma_i K_i \epsilon_i} \quad (7)$$

$$\epsilon_{\text{obsd}} = \frac{\Sigma_i K_i \epsilon_i}{\Sigma_i (K_i - K_{i,\text{random}})} \quad (8)$$

where, in the lattice of coordination number z , $\Sigma_i K_{i,\text{random}}$ is just z .

Consequently, it is evident that very small values of K_{obsd} can be physically significant if the uncertainties arising from experimental errors¹³ can be minimized.

Substantially these same equations were proposed earlier by Carter, Murrell, and Rosch,¹⁴ who analyzed the competition between solvent and donor molecules for the acceptor in the reaction



Their paper has not received the attention which it deserves because it seems to require a specific interaction ("solvation") between solvent and acceptor. Actually the solvent molecule occupies space (*e.g.*, a lattice site); it must be included in the bookkeeping because it is there.

Some years ago, Guggenheim¹⁵ suggested a distinction between a degree of "association" and a degree of "sociation," the latter being the *excess* over that based upon probabilities in a random mixture. The Benesi-Hildebrand K_{obsd} is clearly a "sociation" constant; only when one is sufficiently confident of the validity of a theoretical model for calculating K_{random} (or alternatively the "true" absorptivity of the complex) can one hope to evaluate the "association constant" K . For strong complexes ($K \gg K_{\text{random}}$) the relative am-

(12) L. E. Orgel and R. S. Mulliken, *J. Amer. Chem. Soc.*, **79**, 4839 (1957).

(13) W. B. Person, *ibid.*, **87**, 167 (1965).

(14) S. Carter, J. N. Murrell, and E. J. Rosch, *J. Chem. Soc.*, 2048 (1965).

(15) E. A. Guggenheim, *Trans. Faraday Soc.*, **56**, 1159 (1960).

biguity is small, but for weak complexes it can be great. It seems probable that experimental measurements never yield "association constants" but only "sociation" constants.

It is interesting to consider the evaluation of the heat of formation ΔH_f of the complex, *i.e.*, the parameter w in the quasi-chemical treatment. Two alternative methods are available.

(a) The intercept obtained when $x_A x_D l/A$ is plotted against x_D is $z/\kappa\epsilon$, or $1/K_{\text{obsd}} \epsilon_{\text{obsd}}$ in the Benesi-Hildebrand terminology. If one assumes¹⁶ that ϵ is independent of temperature, then when the logarithm of this intercept is plotted against $1/T$, the slope is w/k and can be interpreted, presumably correctly, as $\Delta H_f/R$.

(b) On the other hand, if K_{obsd} is regarded as a true equilibrium constant, a plot of $\ln K_{\text{obsd}}$ vs. $1/T$ yields a more complicated curve rather than a straight line, and the slope at a particular temperature is

$$\frac{\Delta H_{\text{obsd}}}{R} = \frac{-d \ln K_{\text{obsd}}}{d(1/T)} = \frac{-d \ln (e^{-w/kT} - 1)}{d(1/T)} = \left(\frac{w}{k}\right) \left[\frac{e^{-w/kT}}{e^{-w/kT} - 1} \right] \quad (9)$$

When $e^{-w/kT}$ is large by comparison with unity, this leads to w/k , but for weak complexes, this ΔH_{obsd} will be larger than the "true" ΔH_f . For example, for $\Delta H_f = -2RT$ (-5 kJ mol^{-1} at room temperature, the order of magnitude of ΔH_f for the benzene-iodine complex), $e^2/(e^2 - 1) = 1.16$, leading to a ΔH_{obsd} 16% high. For still weaker complexes, this procedure would yield even less reliable enthalpies of formation.

Comparisons with experimental data from the literature can be made (and were made by Carter, *et al.*¹⁴), but for this highly oversimplified model—a lattice of molecules of exactly equal size, all interactions but one equal—they are not likely to be very meaningful. The purpose of this paper is to clarify the problem with a simple model.¹⁷

Acknowledgments. I wish to thank Dr. J. Prue and Professor J. S. Rowlinson for helpful discussions of this problem. This work was supported in part by a grant from the National Science Foundation.

Appendix: The Quasi-Chemical Calculation

We assume a lattice of coordination number z and N sites, occupied by Nx_D donor molecules, Nx_A acceptor molecules, and Nx_S solvent molecules. All energies of interaction are equal except that between one unique "face" of D (designated as D') and one unique "face" of A (designated as A'); this D'A' interaction is the "complex" (designated as C) and differs from the others by an energy w and has an absorptivity ϵ . The $Nz/2$ nearest-neighbor pairs are of 15 types: SS, SD, SD', SA, SA', DD, DD', DA, DA', D'D', D'A, D'A' =

C, AA, AA', A'A', and we define for each of them a factor η which is the ratio of the actual number of such pairs to those in the random mixture (*e.g.*, the number of SS pairs $N_{\text{SS}} = (Nz/2)x_S^2\eta_{\text{SS}}$, $N_{\text{SD}} = (Nz/2)2x_Sx_D\eta_{\text{SD}} - (z-1)/z$, $N_{\text{DA}'} = (Nz/2)2x_Dx_A\eta_{\text{DA}'}(z-1)/z^2$, $N_{\text{D'A}'} = N_C = (Nz/2)2x_Ax_D\eta_C/z^2$, etc.) These 15 variables η are connected by 15 equations, five of which are simple conservation conditions

$$\begin{aligned} \text{S: } & x_S z \eta_{\text{SS}} + x_D [(z-1)\eta_{\text{SD}} + \eta_{\text{SD}'}] + x_A [(z-1)\eta_{\text{SA}} + \eta_{\text{SA}'}] = z \\ \text{D: } & x_S z \eta_{\text{SD}} + x_D [(z-1)\eta_{\text{DD}} + \eta_{\text{DD}'}] + x_A [(z-1)\eta_{\text{DA}} + \eta_{\text{DA}'}] = z \\ \text{D': } & x_S z \eta_{\text{SD}'} + x_D [(z-1)\eta_{\text{DD}'} + \eta_{\text{D'D}'}] + x_A [(z-1)\eta_{\text{D'A}} + \eta_C] = z \\ \text{A: } & x_S z \eta_{\text{SA}} + x_D [(z-1)\eta_{\text{DA}} + \eta_{\text{D'A}'}] + x_A [(z-1)\eta_{\text{AA}} + \eta_{\text{AA}'}] = z \\ \text{A': } & x_S z \eta_{\text{SA}'} + x_D [(z-1)\eta_{\text{DA}'} + \eta_C] + x_A [(x-1)\eta_{\text{AA}'} + \eta_{\text{A'A}'}] = z \end{aligned}$$

The other ten equations are the quasi-chemical ones; these can be written in several ways, but one such set is

$$\begin{aligned} \eta_{\text{SA}}^2 &= \eta_{\text{SS}}\eta_{\text{AA}} & \eta_{\text{DA}}^2 &= \eta_{\text{DD}}\eta_{\text{AA}} \\ \eta_{\text{SA}'}^2 &= \eta_{\text{SS}}\eta_{\text{A'A}'} & \eta_C^2 &= \eta_{\text{D'D'}}\eta_{\text{A'A}'}e^{-2w/kT} \\ \eta_{\text{SD}}^2 &= \eta_{\text{SS}}\eta_{\text{DD}} & \eta_{\text{DA}'} &= \eta_{\text{DD}}\eta_{\text{A'A}'} \\ \eta_{\text{SD}'}^2 &= \eta_{\text{SS}}\eta_{\text{D'D}'} & \eta_{\text{D'A}} &= \eta_{\text{D'D'}}\eta_{\text{AA}} \\ \eta_{\text{DD}'}^2 &= \eta_{\text{DD}}\eta_{\text{D'D}'} & \eta_{\text{AA}'} &= \eta_{\text{AA}}\eta_{\text{A'A}'} \end{aligned}$$

It is obvious by inspection that $\eta_{\text{SS}} = \eta_{\text{SA}} = \eta_{\text{DD}} = \eta_{\text{DA}} = \eta_{\text{AA}} = \eta$, $\eta_{\text{SD}'} = \eta_{\text{DD}'} = \eta_{\text{D'A}} = \eta_{\text{D'}}$, and $\eta_{\text{SA}'} = \eta_{\text{DA}'} = \eta_{\text{AA}'} = \eta_{\text{A'}}$. There remain six unknowns, η , $\eta_{\text{D'}}$, $\eta_{\text{A'}}$, $\eta_{\text{D'D'}}$, $\eta_{\text{A'A'}}$, and η_C , connected by six equations

$$\begin{aligned} [x_S z + (x_D + x_A)(z-1)]\eta + x_D \eta_{\text{D'}} + x_A \eta_{\text{A'}} &= z \\ [x_S z + (x_D + x_A)(z-1)]\eta_{\text{D'}} + x_D \eta_{\text{D'D'}} + x_A \eta_C &= z \\ [x_S z + (x_D + x_A)(z-1)]\eta_{\text{A'}} + x_D \eta_C + x_A \eta_{\text{A'A'}} &= z \\ \eta_{\text{D'}}^2 &= \eta_{\text{D'D'}}\eta \\ \eta_{\text{A'}}^2 &= \eta_{\text{A'A'}}\eta \\ \eta_C^2 &= \kappa^2 \eta_{\text{D'D'}}\eta_{\text{A'A'}} \end{aligned}$$

where $\kappa = e^{-w/kT}$.

Systematic elimination of the other η 's yields the equation for η_C given above as eq 1.

(16) T. M. Cromwell and R. L. Scott, *J. Amer. Chem. Soc.*, **20**, 4090 (1948).

(17) After this manuscript was substantially complete, I learned from Professor N. S. Bayliss that he had proposed a similar idea some years ago in a paper which has never been published.

Mechanism and Kinetics of Isotopic Exchange in Zeolites. I. Theory

by L. M. Brown, H. S. Sherry,* and F. J. Krambeck

Mobil Research and Development Corporation, Central Research Division, Princeton, New Jersey 08540
(Received May 17, 1971)

Publication costs assisted by Mobil Research and Development Corporation

A new model is presented for particle-controlled isotopic exchange of both bound (sited) and randomly distributed (mobile) cations contained in hydrated zeolites with ions in electrolyte solutions. Isotopic exchange in such systems can take place in one or more observable steps, depending on the number of crystallographically distinct cation sites and the relative rates of migration of the different types of cations. The observed kinetics are explained in terms of a mechanism that consists of coupled diffusional and exchange processes. Sited cations migrate by means of an intracrystalline exchange with mobile cations followed by diffusion. However, the model predicts cases of diffusion-controlled kinetics for the overall process when exchange is at least as fast as diffusion. The model is described mathematically by a linear combination of Fick's second equation for diffusion and first-order kinetics for exchange. An analytic solution of the rate equations for a two-step process is derived and discussed in relation to isotopic exchange and ion exchange in zeolites A and X.

I. Introduction

In limited cases the kinetics of particle-controlled isotopic exchange of cations in zeolites with ions in solution can be interpreted solely in terms of Fick's second equation. A more general model is needed, however, when the zeolite contains both bound (sited) cations and randomly distributed mobile (unsited and hydrated) cations. Isotopic exchange in such systems can take place in one or more observable steps.¹⁻⁵ Previous interpretations^{1-3,5} of the kinetics of two-step processes that have been observed experimentally were predicated on the assumption that the separate steps were independent diffusional processes. Although diffusion is rate controlling in the migration of mobile cations, it does not have to be the rate-controlling process in the migration of the bound cations; moreover, the elementary steps of the mechanism are not necessarily independent, as others have assumed.¹⁻³

Clues to the probable mechanism for specific cases of isotopic exchange can be inferred from the structure of the zeolite, which is known in many cases.⁶⁻⁸ If, for example, the lattice of the zeolite defines one network of large channels (which may be one-, two-, or three-dimensional) that contain only mobile cations or if it defines channels of this description and as well a noninterconnecting network of smaller cavities that also contain mobile cations, then diffusion could be rate controlling in all steps of the mechanism. In the latter case, cations in the zeolite would exchange with cations in the external solution in independent steps governed by Fick's second equation, and the rate of the overall process would be describable by a linear combination of two of these equations.

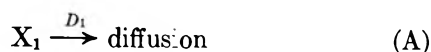
However, if mobile and bound cations are located in one network of large channels (as in zeolite A)⁸ or if channels of this description are joined to a network

of smaller cavities that contain bound cations (as in zeolite X),⁸ between which cations can migrate, diffusion would be rate controlling for the isotopic exchange of mobile cations with ions in solution but not necessarily for bound cations. For such systems, one must consider intracrystalline exchange between bound and mobile cations as the probable mechanism for the isotopic exchange of bound cations. If intracrystalline exchange is slow compared to diffusion, the former process, and not diffusion, will control the rate of isotopic exchange of bound cations. In this model exchange and diffusion are coupled and, therefore, are not independent of each other. The proposed model is developed in the text to show how it can explain isotopic exchange in zeolites A and X. It is assumed that diffusion is governed by Fick's second equation, and exchange of bound and mobile cations, by first-order rate expressions. An analytic solution of the rate equations for a two-step process is derived. Extension of the model to nonzeolitic ion exchangers and to ion-exchange processes is discussed.

II. Theoretical Development

A. Isotopic Exchange of Mobile Counterions. Isotopic exchange of mobile ions in a hydrated ion exchanger containing one network of channels is a simple diffusional process having the mechanism

- (1) E. Hoinkis and H. W. Levi, *Naturwissenschaften*, **53**, 500 (1966).
- (2) E. Hoinkis and H. W. Levi, *Z. Naturforsch. A*, **22**, 226 (1967).
- (3) E. Hoinkis and H. W. Levi, *ibid.*, **A**, **23**, 813 (1968).
- (4) E. Hoinkis and H. W. Levi, *ibid.*, **A**, **24**, 1672 (1969).
- (5) E. Hoinkis and H. W. Levi, "Ion Exchange in the Process Industries," Society of the Chemical Industry, London, 1970, p 339.
- (6) K. F. Fischer and W. M. Meier, *Fortschr. Mineral.*, **42**, 50 (1965).
- (7) W. H. Bauer, *Amer. Mineralogist*, **49**, 697 (1964).
- (8) L. Broussard and D. P. Shoemaker, *J. Amer. Chem. Soc.*, **82**, 1040 (1960).



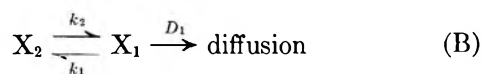
where X_1 represents mobile ions and D_1 their constant diffusivity. The process can be realized physically by labeling the ions in the solution or exchanger with a trace amount of its radioactive isotope; the driving force is then the concentration gradient of radioactive ions existing between the two phases. The variation of the concentration C_1 of radioactive ions along the radial coordinate r of a spherical particle is governed by Fick's second equation⁹

$$\partial C_1 / \partial t = D_1 (1/r^2) \partial / \partial r (r^2 \partial C_1 / \partial r) \quad (1)$$

The well-known solution of eq 1 is given in section III.

This model may also be used to interpret isotopic exchange data for exchangers that contain counterions in different networks of noninterconnecting channels. The overall exchange would then be described by a superposition of terms given by the solution of eq 1.

B. Isotopic Exchange of Mobile and Bound Counterions. When the exchanger contains bound and mobile counterions in one network of channels, as in zeolite A, the interpretation of isotopic exchange data cannot be made on the basis of a superposition of diffusional terms. The reason for this is that bound cations equilibrate with ions in solution by exchanging with mobile ions in the exchanger through cooperative desorption-sorption processes involving neighboring cation sites. Mobile ions migrate by diffusing through the large channels, and bound ions, by undergoing intracrystalline exchange with mobile ions and then diffusing through the large channels. These elementary steps are coupled and not independent as previously assumed.¹⁻³ In the most general case—when diffusion is fast compared to the intracrystalline exchange of bound and mobile cations—isotopic exchange will take place in two observable steps consistent with the mechanism



where X_1 and X_2 denote mobile and bound ions, k_1 and k_2 are the first-order rate constants for the postulated adsorption and desorption steps, and D_1 is the diffusivity of mobile cations.

The variations of the concentrations of labeled mobile ions C_1 and bound ions C_2 in the zeolite are expressed by the equations (in spherical coordinates)

$$\partial C_1 / \partial t = D_1 (1/r^2) \partial / \partial r (r^2 \partial C_1 / \partial r) + k_2 (C_2 - \alpha_{12} C_1) \quad (2)$$

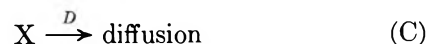
$$\partial C_2 / \partial t = k_2 (\alpha_{12} C_1 - C_2) \quad (3)$$

where r is the radial coordinate, $\alpha_{12} = C_2^* / C_1^* = k_1 / k_2$ is the equilibrium constant for the exchange of mobile

and bound ions, and C_1^* and C_2^* are equilibrium concentrations. The value of the equilibrium constant is fixed by the structure of the exchanger and is the ratio of the numbers of bound to mobile cations; this ratio is 2 for zeolite NaA, which contains eight bound and four mobile cations per unit cell (uc).⁸ The rate of the fast step is given by Fick's second equation (the first term on the right-hand side of eq 2); the contribution of the slower exchange to the fast step is given by a first-order rate expression (second term). The degree of overlapping of the two processes depends on the relative magnitudes of the diffusivity and the first-order rate constant. The rate of the slow step is clearly independent of the size of the exchanger particle, whereas the rate of the fast step depends on the radius of the particle. The solution of eq 2 and 3 is given in section III and derived in the Appendix.

Gaus and Hoinkis¹⁰ assumed that the slow step in the isotopic exchange of bound cesium ions in zeolite CsA was the desorption of bound cations and their sorption on mobile cation sites and that the desorbed cations then equilibrated with cations in solution by means of a rapid diffusional process. However, their model did not include the reverse replacement of desorbed bound cations by mobile cations, as required by microscopic reversibility.

Returning to zeolite A, we note that a special case arises if we assume that the rate of intracrystalline exchange is at least as fast as the rate of diffusion. In this case, bound and mobile ions will exchange so rapidly that labeled ions of both types will always be in equilibrium with each other, even though the entire system is not at equilibrium with respect to isotopic exchange. Mobile and bound ions will be kinetically indistinguishable, and isotopic exchange will take place in one observable step according to the apparent mechanism



where D is the apparent diffusivity of mobile ions, and X (X_1 plus X_2) represents bound and mobile cations. Clearly, the overall process is controlled by diffusion. The true mechanism—mechanism B—is disguised because the rate at which bound ions "leak" into the pool of mobile ions is fast compared to the rate of diffusion.

The overall rate of mechanism C is governed by Fick's second equation. However, the driving gradient for self-diffusion is $\partial C_1 / \partial r$, the gradient of labeled mobile ions in each volume element; it is related to the variation of the total concentration of labeled

(9) (a) F. Helfferich, "Ion Exchange," McGraw-Hill, New York, N. Y., 1962, pp 250-319; (b) "Ion Exchange," Vol. 1, J. A. Marinsky, Ed., Marcel Dekker, New York, N. Y., 1968, pp 65-100.

(10) H. Gaus and E. Hoinkis, *Z. Naturforsch. A*, **24**, 1511 (1969).

ions $\partial C/\partial t$ and the diffusivity of mobile ions D_1 by the relation

$$\partial C/\partial t = D_1(1/r^2)\partial/\partial r(r^2\partial C_1/\partial r) \quad (4a)$$

where $C = C_1 + C_2$. The concentration C_1 at any time can be related to the total concentration C by use of the equation $C_1 = C/(1 + \alpha_{12})$, which is obtained from the relation for C by using the equilibrium constant, now given by $\alpha_{12} = C_2/C_1$, to replace C_2 . Substituting the equation for C_1 in eq 4a, we obtain

$$\partial C/\partial t = D(1/r^2)\partial/\partial r(r^2\partial C/\partial r) \quad (4b)$$

where $D = D_1/(1 + \alpha_{12})$. It is noted that the effective diffusivity of the apparent pure diffusional process is smaller than the true diffusivity of mobile ions by the factor $1/(1 + \alpha_{12})$, which is the fraction of the cations that are unbound. The transition from a multistep process to a one-step process can be observed experimentally as the temperature of the system is increased. Because the elementary steps of mechanism B (see Table I) are coupled, there will be observed only one step at or above the transition temperature, the temperature at which the rates of the coupled steps become equal. This is unlike the behavior of a system of independent processes; in this case one step would be observed only at the transition temperature, and more than one step, at all other temperatures.

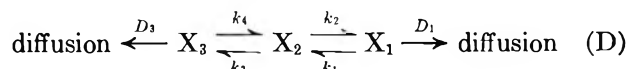
Table I: Mechanisms

Symbol	Mechanism
A	$X_1 \xrightarrow{D_1} \text{diffusion}$
B	$X_3 \xrightleftharpoons[k_1]{k_2} X_1 \xrightarrow{D_1} \text{diffusion}$
C	$X \xrightarrow{D} \text{diffusion}$
D	$\text{diffusion} \xleftarrow{D_3} X_3 \xrightleftharpoons[k_3]{k_4} X_2 \xrightleftharpoons[k_1]{k_2} X_1 \xrightarrow{D_1} \text{diffusion}$
E	$X_3 \xrightleftharpoons[k_3]{k_4} X_2 \xrightleftharpoons[k_1]{k_2} X_1 \xrightarrow{D_1} \text{diffusion}$
F	$X_3 \xrightleftharpoons[k_3]{k_4} X \xrightarrow{D} \text{diffusion}$

This model of isotopic exchange can be generalized to include any ion exchanger that behaves as a weakly dissociating salt, MR, where R is a fixed ionic group of unit charge and M is a counterion. In hydrated exchangers of this type the ratio of bound to mobile counterions, RM/M, is fixed by the dissociation constant K_D . If the dissociation of bound ions is slower than the diffusion of mobile ions, the kinetics of isotopic exchange will be describable by eq 2 and 3 in accordance with mechanism B; the derived diffusivity will be the true diffusivity of mobile ions. However, if dissociation is rapid compared to diffusion, the

kinetics will be given by eq 4b and the mechanism by (C); but the effective diffusivity will be $D = K_D D_1$, where $K_D = 1/(1 + \alpha_{12})$. This special case has already been treated in a study of self-exchange in a chelating ion-exchange resin.¹¹

The foregoing analysis can be extended readily to ion exchangers that contain bound counterion sites in two interconnecting networks of three-dimensional channels, one with large cages and one with small cages. We shall illustrate this with hydrated zeolite X. This zeolite contains 45 mobile cations and 24 bound cations per uc in a three-dimensional network of large channels or supercages.¹² The bound cations are located near the centers of rings of six (Al,Si)O₄ tetrahedra that form the entrances to a three-dimensional interconnecting network of small cages commonly called sodalite cages. There are also 16 bound (sited) cations per uc in the network of small cages.¹² Particle-controlled isotopic exchange in this zeolite can be described by the mechanism



where X_3 denotes cations in the network of small cages, D_3 is the constant diffusivity of these ions in the network of small cages, k_3 and k_4 are, respectively, the first-order specific rates of migration into the small cages of bound cations contained in the large cages and of migration into the large cages of bound cations contained in the small cages (it is assumed that the movement of cations between the small and large cages involves a single "jump"), and the other symbols have their previous meanings. The variations of the concentrations of labeled mobile and bound ions (C_1 , C_2 , and C_3) along the radial coordinate r for a spherical particle are given by

$$\frac{\partial C_1}{\partial t} = D_1(1/r^2)\frac{\partial}{\partial r}\left(r^2\frac{\partial C_1}{\partial r}\right) + k_2(C_2 - \alpha_{12}C_1) \quad (5)$$

$$\frac{\partial C_2}{\partial t} = k_2(\alpha_{12}C_1 - C_2) + k_4(C_3 - \alpha_{23}C_2) \quad (6)$$

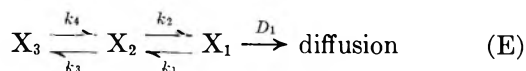
$$\frac{\partial C_3}{\partial t} = D_3(1/r^2)\frac{\partial}{\partial r}\left(r^2\frac{\partial C_3}{\partial r}\right) + k_4(\alpha_{23}C_2 - C_3) \quad (7)$$

where $\alpha_{23} = C_3^*/C_2^* = k_3/k_4$ is the equilibrium constant for exchange between bound cations in the networks of small and large cages. We now make the reasonable assumption that diffusion through the network of small cages is negligible. It is more probable that an ion in the network of small cages will migrate to the surface of the crystal by entering a large channel through a single ring of six tetrahedra and then diffusing rapidly through the network of large cages rather than by diffus-

(11) A. Schwarz, J. A. Marinsky, and K. S. Spiegler, *J. Phys. Chem.*, **68**, 918 (1964).

(12) D. H. Olson, *ibid.*, **74**, 2758 (1970).

ing through the network of sodalite cages along a path requiring its passage through a large number of such rings. Although this assumption would be unreasonable for a crystal consisting of one unit cell, because migration along either route would be important, it surely must be valid for an infinitely large crystal. The assumption that ions in the small cages enter the network of large cages and migrate to the surface of the crystal by diffusing through this network leads to the following mechanism and rate equations



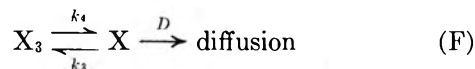
$$\partial C_1 / \partial t = D_1(1/r^2) \partial / \partial r (r^2 \partial C_1 / \partial r) + k_2(C_2 - \alpha_{12}C_1) \quad (8)$$

$$\partial C_2 / \partial t = k_2(\alpha_{12}C_1 - C_2) + k_4(C_3 - \alpha_{23}C_2) \quad (9)$$

$$\partial C_3 / \partial t = k_4(\alpha_{23}C_2 - C_3) \quad (10)$$

No attempt was made to solve eq 8-10 because experiment^{1,5,13} showed that self-diffusion in zeolite X conforms to a simpler two-step mechanism. Moreover, there seem to be no data in the literature on self-diffusional processes that take place in more than two observable steps.

The model does predict simpler kinetics when exchange is fast compared to the diffusion of mobile ions. Let us assume, in the first case, that bound ions (X_2) in the supercages exchange with mobile ions at least as fast as the latter diffuse, whereas bound ions in the small cages exchange much more slowly. Consequently cations in the supercages will always be in equilibrium with each other but not with bound ions in the small cages. This condition will hold even when the system as a whole is not in a state of equilibrium with respect to isotopic exchange. Isotopic exchange will then take place in two observable steps, according to the apparent mechanism



The mechanism consists of a fast step involving mobile and bound ions X (X_1 and X_2) contained in the supercages that diffuse with effective diffusivity D and a slow step for the exchange of bound ions X_3 contained in the small cages. The rate of the fast step is diffusion limited, because diffusion is the slower of the two elementary processes comprising this step (see mechanism E in Table I).

The variations of the total concentration of mobile and bound ions (C_X) in the supercages and of the concentration of bound ions (C_3) in the small cages are given by

$$\partial C_X / \partial t = D_1(1/r^2) \partial / \partial r (r^2 \partial C_1 / \partial r) + k_4(C_3 - \alpha_{23}C_2) \quad (11)$$

$$\partial C_3 / \partial t = k_4(\alpha_{23}C_2 - C_3) \quad (12)$$

Because labeled mobile and bound cations (X) in the supercage are always in equilibrium with each other, their concentrations at any time can be expressed separately in terms of C_X and the equilibrium constant $\alpha_{12} = C_2/C_1$ by means of the relations $C_1 = C_X/(1 + \alpha_{12})$ and $C_2 = C_X\alpha_{12}/(1 + \alpha_{12})$. These relations are now used to transform eq 11 and 12 to the forms

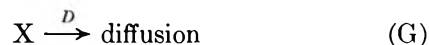
$$\partial C_X / \partial t = D(1/r^2) \partial / \partial r (r^2 \partial C_X / \partial r) + k_4(C_3 - \alpha C_X) \quad (13)$$

$$\partial C_3 / \partial t = k_4(\alpha C_X - C_3) \quad (14)$$

where $D = D_1/(1 + \alpha_{12})$ and $\alpha \equiv \alpha_{12}\alpha_{23}/(1 + \alpha_{12})$.

Mechanism F and the rate equations (13) and (14) are formally the same as mechanism B and eq 2 and 3; they differ only in the meanings of the effective diffusivity and the parameter α . The solutions of the rate equations for both mechanisms are the same and will be discussed in section III.

Mechanism E gives rise to still simpler kinetics when both exchange steps are at least as fast as the diffusion of mobile ions. In this case all bound and mobile ions will always be in equilibrium with each other, and diffusion will be rate controlling for the overall process. There will be one observed diffusional step consistent with the apparent mechanism



where X denotes mobile and bound ions X_1 , X_2 , and X_3 , and D is the apparent diffusivity of mobile ions. The mechanism is formally the same as mechanisms A and C.

The rate of this apparent diffusional process is given by Fick's second equation

$$\partial C / \partial t = D_1(1/r^2) \partial / \partial r (r^2 \partial C_1 / \partial r) \quad (15a)$$

where $C = C_1 + C_2 + C_3$ is the total concentration of labeled ions in the zeolite. The concentration of mobile ions, C_1 , now can be related to the equilibrium constants $\alpha_{12} = C_2/C_1$ and $\alpha_{13} = \alpha_{12}\alpha_{23} = C_3/C_1$ and to the total concentration C by means of the relation $C_1 = C/(1 + \alpha_{12} + \alpha_{13})$. On combining this relation for C_1 with 15a, we obtain

$$\partial C / \partial t = D(1/r^2) \partial / \partial r (r^2 \partial C / \partial r) \quad (15b)$$

where $D = D_1/(1 + \alpha_{12} + \alpha_{13})$ is the apparent diffusivity of mobile ions.

III. Solution of Rate Equations for Coupled Diffusion and Exchange

Isotopic exchange of mobile ions (mechanism A) is governed by eq 1, the linear form of Fick's second equation, in which the defined diffusivity is constant. If we specify that all labeled ions are located initially in the exchanger particles and that the concentration of

(13) L. M. Brown and H. S. Sherry, *J. Phys. Chem.*, **75**, 3855 (1971).

these ions in the solution phase is zero at all times, the solution⁹ of eq 1, when integrated over the radius R of spherical particles, becomes

$$U(t) = 1 - (6/\Pi^2) \sum_{n=1}^{\infty} (1/n^2) \exp(-n^2 Bt) \quad (16)$$

where $B = \Pi^2 D_1/R^2$ is a characteristic frequency, D_1 is the diffusivity of mobile ions, t denotes time, and n is an integer. $U(t)$ is the fractional attainment of equilibrium and is defined as

$$U(t) = [C(0) - C(t)]/[C(0) - C(\infty)]$$

where $C(0)$, $C(t)$, and $C(\infty)$ are total concentrations of labeled ions in the exchanger at initial time, at time t , and at equilibrium. Values of the dimensionless time parameter Bt and of $U(t)$ have been tabulated.¹⁴

An analytic solution has been obtained for the rate equations (eq 2 and 3 or 13 and 14) that govern the coupled diffusional and exchange processes described by mechanisms B and F. The form of the solution in terms of generalized constants α and k , derived for the same initial and boundary conditions assumed for eq 16, is

$$U(t) = 1 - \frac{6}{\Pi^2} \sum_{n=1}^{\infty} \frac{1}{n^2(u_n - v_n)} \times \left[u_n \left(1 + \frac{v_n}{k(1 + \alpha)} \right) \exp(v_n t) - v_n \left(1 + \frac{u_n}{k(1 + \alpha)} \right) \exp(u_n t) \right] \quad (17a)$$

$$u_n = -^{1/2}[(1 + \alpha)k + n^2 B_m] \times \left[1 - \left(1 - \frac{4kn^2 B_m}{[(1 + \alpha)k + n^2 B_m]^2} \right)^{1/2} \right] \quad (17b)$$

$$v_n = -^{1/2}[(1 + \alpha)k + n^2 B_m] \times \left[1 + \left(1 - \frac{4kn^2 B_m}{[(1 + \alpha)k + n^2 B_m]^2} \right)^{1/2} \right] \quad (17c)$$

where n is an integer and B_m is the characteristic frequency predicted by the model. The constants in eq (17a-c) are defined in Table II for each mechanism. The derivation of eq 17a is given in the Appendix.

Table II: Definitions of Constants Contained in Eq 17a-c

Constant	Mechanism B (zeolite A)	Mechanism F (zeolite X)
k	k_2	k_4
α	α_{12}	$\alpha_{12}\alpha_{23}/(1 + \alpha_{12})$
B_m	$\Pi^2 D_1/R^2$	$\Pi^2 D_1/R^2(1 + \alpha_{12})$

Values of $U(t)$ accurate to three decimal places can be calculated as a function of the dimensionless time parameter $B_m t$ by summing the infinite series in eq 17a over the first 100 terms for NaX and over the first 300

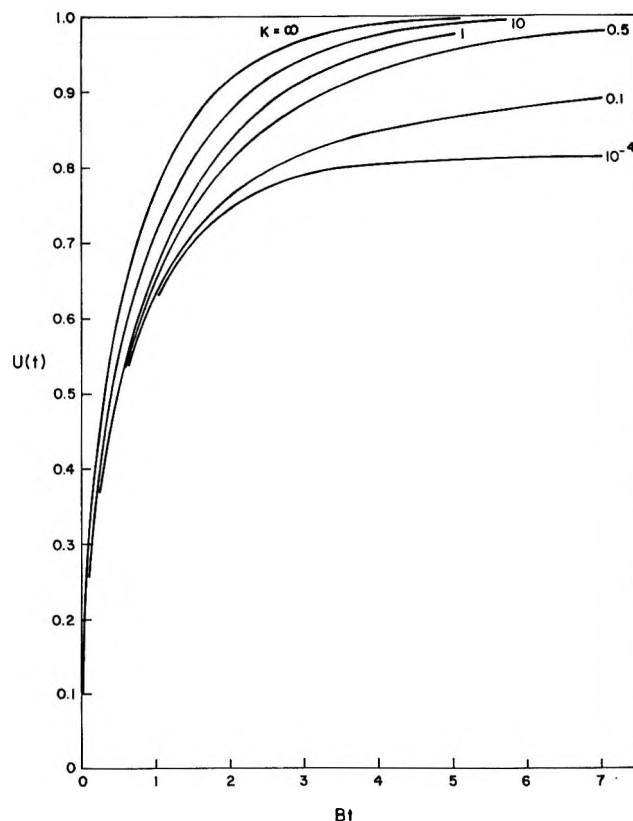


Figure 1. Fractional attainment of isotopic exchange equilibrium $U(t)$ in NaX ($\alpha = 0.232$) as a function of dimensionless time Bt predicted by eq 17a for various values of $K = k/B$.

terms for NaA. Profiles for self-diffusion in zeolites X and A, for various values of $K = k/B_m$, are shown in Figures 1 and 2. Values of α used to obtain these graphs were 0.232 for zeolite X and 2.0 for zeolite A.

Equation 17a assumes simpler forms when α or k attains limiting values. In these cases analysis of the experimental data is facilitated.

In the limit as $\alpha \rightarrow 0$, that is, when the bound ions are virtually trapped in dead-end cavities and the ions in the large channels migrate by a diffusional process, eq 17a reduces exactly to eq 16, the solution for a pure diffusional process, where $B = \Pi^2 D_1/R^2$.

When $k \rightarrow \infty$, self-diffusion of mobile and bound ions becomes an apparent one-step purely diffusional process, and eq 17a again reduces to eq 16. However, the characteristic frequency has new definitions: B_m is given by $\Pi^2 D_1/R^2(1 + \alpha_{12})$ for mechanism C and by $\Pi^2 D_1/R^2(1 + \alpha_{12} + \alpha_{13})$ for mechanism G. The behavior of systems of this and the previous limiting types are described by the curve designated $K = \infty$ in Figures 1 and 2.

In the limit as $k \rightarrow 0$, which could be the case either when bound ions are virtually trapped in dead-end

(14) F. Helfferich, "Ion Exchange," McGraw-Hill, New York, N. Y., 1962, p 584.

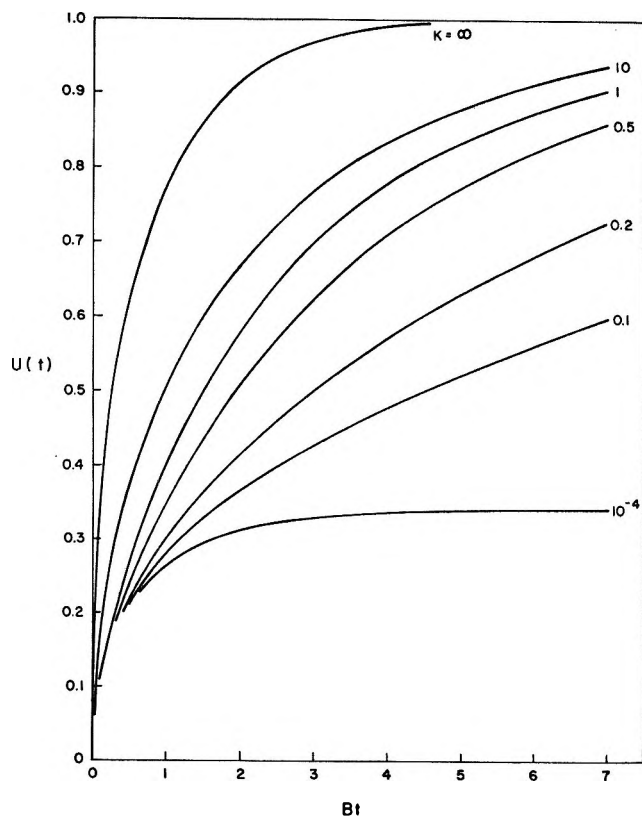


Figure 2. Fractional attainment of isotopic exchange equilibrium $U(t)$ in NaA ($\alpha = 2.0$) as a function of dimensionless time Bt predicted by eq 17a for various values of $K = k/B$.

cages or when the site binding energy is very high, eq 17a becomes

$$U(t) = \frac{1}{1 + \alpha} \left\{ 1 - \frac{6}{\Pi^2} \sum_{n=1}^{\infty} \frac{1}{n^2} \exp(-n^2 B_m t) \right\} \quad (18)$$

where α and B_m are defined in Table II for the appropriate mechanisms. Equilibrium in systems of this type is attained when $U(t) = 1/(1 + \alpha)$, which corresponds to completion of the fast diffusional process. Under these conditions, $U(t)$ would be approximately 0.81 for zeolite X (mechanism F), corresponding to the 69 out of a total of 85 cations per unit cell located in the supercages, and $1/3$ for zeolite A (mechanism B), corresponding to the 4 out of 12 cations per unit cell that are mobile. This behavior is described approximately by the curve designated $K = 10^{-4}$ in Figure 1 or 2. When the normalized quantity $(1 + \alpha)U(t)$ is plotted against $B_m t$, one obtains the curve designated $K = \infty$, which, as we have noted, describes a pure diffusional process.

The asymptotic solution of eq 17a is useful in analyses of experimental data. In the limit as $t \rightarrow \infty$, all but the first term of the infinite series in eq 17a may be neglected. One can show that, in view of the inequality $|V_n| > |u_n|$ (eq 17b and 17c), when $t \rightarrow \infty$, eq 17a becomes

$$U(t) \rightarrow 1 - \frac{6}{\Pi^2} \frac{v_1}{v_1 - u_1} \times \left\{ 1 + \frac{u_1}{k(1 + \alpha)} \right\} \exp(u_1 t) \quad (19)$$

Similarly, in the limit $t \rightarrow \infty$ for a purely diffusional process, eq 16 becomes

$$U(t) \rightarrow 1 + \frac{6}{\Pi^2} \exp(-Bt) \quad (20)$$

Now, the graph of Bt vs. time, for data corresponding to large values of t , will have a linear asymptote whose slope is $m = -u_1$. The expression for μ_1 , defined by eq 17b for $n = 1$, has the simpler limiting forms shown in Table III for the various mechanisms.

Table III: Asymptotic Values of u_1 (Eq 17b) for Limiting Values of α or k When $t \rightarrow \infty$

Limiting value of α	Limiting value of k	$m = -u_1$	Mechanism
0	...	$\Pi^2 D_1 / R^2$	B
0	...	$\Pi^2 D_1 / (1 + \alpha_{12})$	F
...	∞	$\Pi^2 D_1 / R^2 (1 + \alpha_{12})$	C
...	∞	$\Pi^2 D_1 / R^2 (1 + \alpha_{12} + \alpha_{13})$	G
...	0	k_2	B
...	0	k_4	F

IV. Analysis of Experimental Data

Evaluation of k and B is conveniently performed by obtaining a least-square fit of the series in eq 17a with the experimental data. Our curve-fitting technique makes use of the Newton-Raphson method¹⁵ in which first partial derivatives are estimated by the method of finite differences.

The magnitude of the constant α can be calculated if the distribution of counterions is known. If the structure of the exchanger is not known, α would have to be determined by means of a three-parameter, curve-fitting procedure, a less accurate approach.

Although α is related to the structure of the exchanger it cannot always be used to provide detailed structural data. It is recognized that α is defined as the ratio of the number of counterions per unit cell that are involved in the slow step to the number per unit cell involved in the fast step. In an exchanger like NaA (mechanism B), α is simply the ratio of bound to mobile ions. However, in exchangers like NaX (mechanism F), in which exchange in the large cages is fast compared to diffusion, α is the ratio of bound ions in the small cages to bound plus mobile ions in the supercages. Therefore, a knowledge of α alone will not give insight into the distribution

(15) H. Margenau and G. M. Murphy, "The Mathematical Methods of Physics and Chemistry," Van Nostrand, New York, N. Y., 1949, p 475.

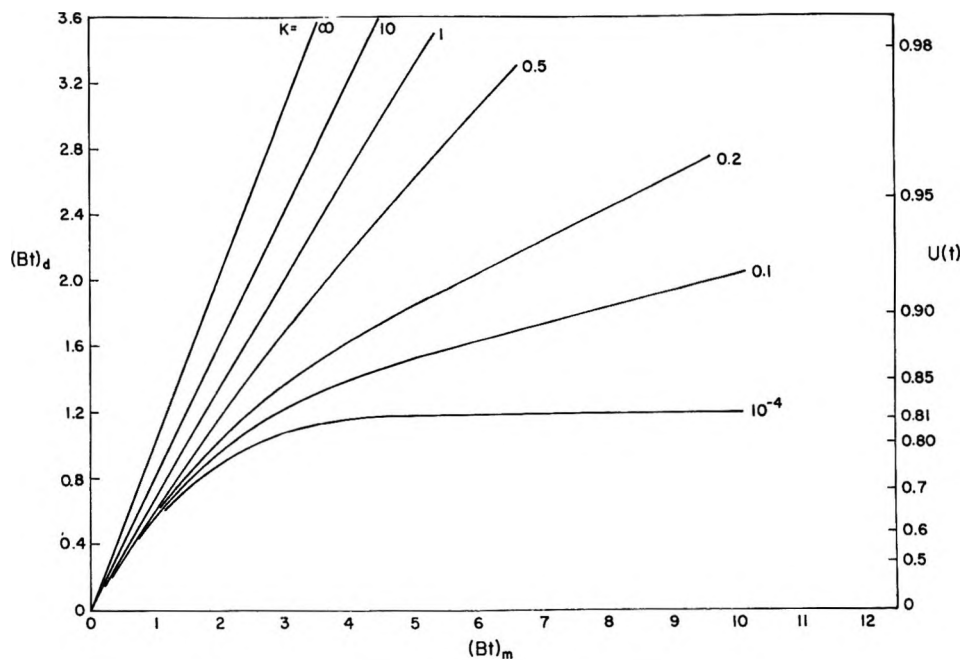


Figure 3. Comparison of dimensionless times $(Bt)_d$ and $(Bt)_m$ predicted by eq 2 and 17a, respectively, for isotopic exchange in NaX ($\alpha = 0.232$) for various values of $K = k/B$.

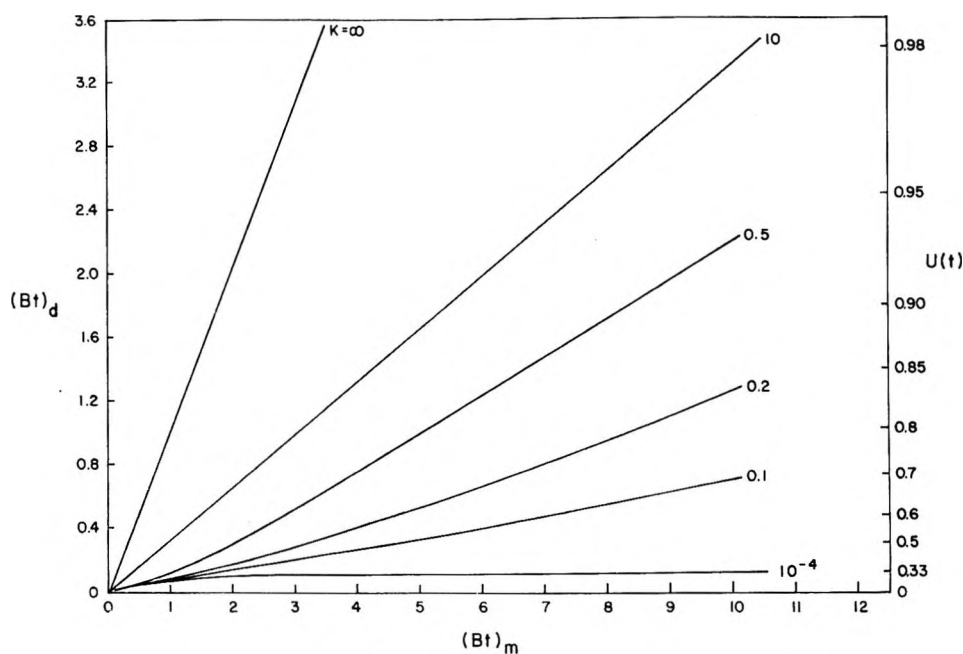


Figure 4. Comparison of dimensionless times $(Bt)_d$ and $(Bt)_m$ predicted by eq 2 and 17a, respectively, for isotopic exchange in NaA ($\alpha = 2.0$) for various values of $K = k/B$.

of bound and mobile ions involved in the fast step in this case.

Experimental data for isotopic exchange processes are often represented as graphs of Bt vs. t based on eq 16. The resultant curve for a purely diffusional process is linear, and its slope is equal to B . If, however, the mechanism consists of coupled diffusional and exchange steps that are observed separately, the curve will be linear in the initial and final (asymptotic solution)

phases of the process and nonlinear in the intermediate region. This behavior is illustrated in Figures 3 and 4. These are graphs of $(Bt)_d$ vs. $(Bt)_m$, the dimensionless time parameters predicted, respectively, by eq 16 and 17a, for various values of $K = k/B_m$ and corresponding values of $U(t)$. In Figures 3 and 4, $(Bt)_m$ can be viewed as the true time scale of a real system governed by eq 17a, and $(Bt)_d$ represents the time scale for the same system when it is assumed to obey eq 16.

When exchange is very slow compared to diffusion, that is, when $K \rightarrow 0$, the elementary steps become uncoupled, and one observes only the fast diffusional step, which approaches an equilibrium state defined by $U(\infty) = 1/(1 + \alpha)$ (see eq 18). However, when the normalized fractional attainment of equilibrium, $(1 + \alpha)U(t)$, is used to plot the data in the manner shown in Figures 3 and 4, the nonlinear graph that would be obtained for the nonnormalized data transforms to the linear curve designated $K \rightarrow \infty$, whose slope is $B_m = B_d$.

As K increases in magnitude, the initial linear region of the $(Bt)_d$ vs. $(Bt)_m$ graph extends progressively over a greater part of the reaction profile. In the limit as $K \rightarrow \infty$, the curve becomes linear throughout and attains a unit slope. The experimental $(Bt)_d$ vs. t curve is also linear, and its slope is B_m , because isotopic exchange is now indistinguishable from a purely diffusional process. This means that coupled exchange and diffusional processes degenerate phenomenologically to a limiting one-step process as the rate of exchange (temperature) increases. In contrast, if the mechanism consisted of independent (diffusional) processes, one step would be observed, in principle, at a single temperature, and more than one step would be observed at all other temperatures.

The slope of the initial linear region of the experimental curves having intermediate values of K does not lead to the correct value of B_m . The correction factor to be applied to this slope to obtain B_m is given by the slope of the curve having the correct value of K in a representation like that of Figure 3 or 4. Obviously this is not a feasible method of analysis, because K normally is not known.

The asymptotic solution (eq 19) may also be used to evaluate k and B_m . If the experimental data obtained for the later stages of the process are sufficiently accurate, the graph of $(Bt)_d$ vs. t will be linear in this region, and its slope m will be equal to $-u_1$. When α or k have limiting values, m reduces to the simpler relations described in Table III.

It is worth noting that the accuracy of the evaluation of k and B_m depends on the magnitude of α , that is, on the fraction of ions involved, say, in the slow step. If α is very small (NaX) or very large (NaA), D or k , respectively, dominates the greater part of the overall process. Hence the curve-fitting procedure will not be sensitive to one of the parameters, and the reliability of that parameter will depend heavily on experimental data in regions (small or large $U(t)$) where the accuracy is normally the lowest. This is reflected in the compression of the curves in Figure 3 as compared to those in Figure 4 having, for example, large values of K .

V. Discussion

The usefulness of the model described herein is not

limited to zeolites but can be generalized to include other crystalline exchangers¹⁶ of known structure that contain bound and mobile counterions. The model is also applicable to ion-exchange resins in which the counterions are partially dissociated from the fixed ionic groups, as is the case for the Na form of an oleophilic sulfonic acid resin in a nonaqueous solvent such as ethanol.¹⁷ It has been found¹⁷ that Na^+ isotopic exchange obeys the diffusion equation but that the rate of exchange is many orders of magnitude smaller than it would be for a swollen resin in aqueous solution. The rate of isotopic exchange is described by eq 4b. In this case the effective diffusivity is $D = K_D D_{\text{Na}}$, where D_{Na} is the true diffusivity of sodium ions in the exchanger and K_D is the dissociation constant for the fixed ionic groups.

Extension of the model to ion-exchange processes is obvious. The treatment differs from the one described for isotopic exchange only in the use of the nonlinear form of Fick's second equation in order to take into account the dependence of the interdiffusion coefficient⁹ on the concentrations and valences of the different types of exchanging ions. For example, the rate of ion-exchange of mobile and bound ions of type A in zeolite A with ions of type B in external solution would be described by expressions similar to eq 2 and 3, in accordance with mechanism B, with D_1 replaced by the (variable) interdiffusion coefficient D_{AB} . The magnitude of α_{12} can be determined from X-ray diffraction data on partially ion-exchanged crystals having the experimental equilibrium composition. Numerical solutions of the nonlinear rate equations should be derivable by the method of finite differences (see ref 18). When intracrystalline exchange of bound and mobile ions is at least as fast as the interdiffusion of ions between the solution and mobile ion sites, the model reduces to a form similar to 4b, and, as before, the interdiffusion coefficient D_{AB} is related to the true one by the factor $1/(1 + \alpha_{12})$. The nonlinear form of eq 4b has been solved previously.^{9,18,19}

The fact that the coupled processes (intracrystalline exchange and diffusion) of the mechanism have different functional dependencies on the radius of the exchanger particle provides a basis for testing the model. Clearly, the rate of the slow step will be independent of the particle size, whereas that of the fast step will vary inversely as the square of the radius. Moreover the temperature of transition from an apparent two-step to an apparent one-step mechanism will depend on particle size because of the dependence of the diffusional rate parameter on particle size.

(16) J. Harvie and G. H. Nancollas, *J. Inorg. Nucl. Chem.*, **30**, 273 (1968).

(17) H. P. Gregor, "Ion Exchange in the Process Industries," Society of the Chemical Industry, London, 1970, p 436.

(18) F. Helfferich and M. S. Plesset, *J. Chem. Phys.*, **28**, 418 (1958).

(19) F. Helfferich, *ibid.*, **38**, 1688 (1963).

Acknowledgments. We wish to thank Dr. L. H. Rieker for many helpful discussions. We are indebted to Mr. J. S. Hicks for designing the computer program used in the analysis of the model. We also wish to thank Mobil Research and Development Corp. for support of this work.

Appendix

The rate equations describing the self-diffusion of mobile and bound ions in two observable steps for spherical geometry have the general form

$$\partial x / \partial t = D(1/r^2) \partial / \partial r (r^2 \partial x / \partial r) + k(y - \alpha x) \quad (\text{A1})$$

$$\partial y / \partial t = k(\alpha x - y) \quad (\text{A2})$$

where x and y denote the concentrations in the exchanger of tracer mobile and bound ions that migrate in the diffusion- and exchange-controlled steps; the detailed significance of these and the other symbols in described for mechanisms B and F.

The analytic solution of these equations has been obtained for the boundary conditions

$$x = 0 \text{ at } r = R \quad (\text{A3})$$

$$\partial x / \partial r = 0 \text{ at } r = 0$$

and the initial conditions

$$y = \alpha / (1 + \alpha), x = 1 / (1 + \alpha), t = 0 \quad (\text{A4})$$

We now assume that the variables are separable so that x and y can be expressed as

$$x = h(t)f(r) \quad y = j(t)g(r) \quad (\text{A5})$$

Substituting eq A5 in eq A2 and rearranging terms, we find

$$\frac{j'(t)}{h(t)} + k \frac{j(t)}{h(t)} = k \alpha \frac{f(r)}{g(r)} \quad (\text{A6})$$

where $j'(t) = dj(t)/dt$. Because the left-hand side of (A6) is a function of t and the right-hand side is a function of r , both must be equal to a constant. Therefore, $f(r)$ is proportional to $g(r)$. Without loss of generality, we make the assumption $f(r) \equiv g(r)$ and let the term $h(t)/j(t)$ account for the proportionality constant.

Substituting eq A5 in eq A1, we obtain

$$\frac{h'(t)}{h(t)} - k \frac{j(t)}{h(t)} + \alpha k = \frac{1}{f(r)} \frac{D}{r^2} \frac{d}{dr} [r^2 f'(r)] \quad (\text{A7})$$

where $f'(r) = df(r)/dr$. Again, the left-hand side is a function of t , and the right-hand side is a function of r , and both must be equal to a constant, which we denote by $-\beta$. The two sides of eq A7 and eq A6 can be written as

$$\frac{1}{r^2} \frac{d}{dr} [r^2 f'(r)] + \frac{\beta}{D} f(r) = 0 \quad (\text{A8})$$

$$f'(r) = 0, f(R) = 0$$

$$h'(t) = -[\beta + \alpha k]h(t) + kj(t) \quad (\text{A9})$$

$$j'(t) = k\alpha h(t) = kj(t)$$

Equation A8 together with the boundary conditions given by eq A3 has solutions of the form

$$f(r) = \frac{\sin(n\pi r/R)}{n\pi r/R} \quad (\text{A10})$$

for integral values of n and values of β given by

$$\beta_n = n^2 \pi^2 D / R^2 \quad (\text{A11})$$

Solutions of eq A9 are given by

$$h_n(t) = a_n \left(\frac{k + m_1^{(n)}}{k\alpha} \right) e^{m_1^{(n)}t} + b_n \left(\frac{k + m_2^{(n)}}{k\alpha} \right) e^{m_2^{(n)}t} \quad (\text{A12})$$

$$j_n(t) = a_n e^{m_1^{(n)}t} + b_n e^{m_2^{(n)}t}$$

where $m_1^{(n)}$ and $m_2^{(n)}$ are roots of the equation

$$(m^{(n)})^2 + [(1 + \alpha)k + \beta_n]m^{(n)} + \beta_n k = 0 \quad (\text{A13})$$

and a_n and b_n are constants that depend on the initial conditions. Hence, simultaneous solutions of eq A12 gives

$$a_n = \frac{k\alpha h_n(0) - (k + m_2^{(n)})j_n(0)}{m_1^{(n)} - m_2^{(n)}} \quad (\text{A14})$$

$$b_n = \frac{(k + m_1^{(n)})j_n(0) - k\alpha h_n(0)}{m_1^{(n)} - m_2^{(n)}}$$

Because eq A1 and A2 are linear, the solutions can be superposed to give the expressions

$$x = \sum_{n=1}^{\infty} h_n(t) \sin(n\pi r/R) / (n\pi r/R) \quad (\text{A15})$$

$$y = \sum_{n=1}^{\infty} j_n(t) \sin(n\pi r/R) / (n\pi r/R)$$

On introducing the initial conditions given by eq A4, we obtain

$$\frac{1}{1 + \alpha} = \sum_{n=1}^{\infty} h_n(0) \sin(n\pi r/R) / (n\pi r/R) \quad (\text{A16})$$

$$\frac{\alpha}{1 + \alpha} = \sum_{n=1}^{\infty} j_n(0) \sin(n\pi r/R) / (n\pi r/R)$$

Equations A16 are solved for $h_n(0)$ and $j_n(0)$ by multiplying both sides of each equation by $r^2 \sin(m\pi r/R) / (m\pi r/R)$ and integrating over the interval $(0, R)$. The result is

$$\begin{aligned}
 h_m(0) &= \frac{2}{1+\alpha}(-1)^{m+1} \\
 j_m(0) &= \frac{2\alpha}{1+\alpha}(-1)^{m+1}
 \end{aligned}
 \tag{A17}$$

Equations A12–A15 and eq A17 form the solution of eq A1 and A2 in terms of $x(r, t)$ and $y(r, t)$. The average value of $x + y$ in the exchanger at any time, given by $U(t)$, can be calculated by applying the relationship

$$U(t) = 1 - \frac{3}{R^3} \int_0^R (x + y)r^2 dr \tag{A18}$$

Substituting eq A15 in eq A18 and integrating, we obtain

$$\begin{aligned}
 U(t) &= 1 - \frac{6}{\Pi^2} \sum_{n=1}^{\infty} \frac{1}{n^2(u_n - v_n)} \times \\
 &\quad \left\{ u_n \left[1 + \frac{v_n}{k(1+\alpha)} \right] e^{v_n t} - v_n \left[1 + \frac{u_n}{k(1+\alpha)} \right] e^{u_n t} \right\}
 \end{aligned}
 \tag{A19}$$

where

$$\begin{aligned}
 u_n &= -^{1/2}[(1+\alpha)k + \beta_n] \times \\
 &\quad \left[1 - \left(1 - \frac{4k\beta_n}{[(1+\alpha)k + \beta_n]^2} \right)^{1/2} \right] \\
 v_n &= -^{1/2}[(1+\alpha)k + \beta_n] \times \\
 &\quad \left[1 + \left(1 - \frac{4k\beta_n}{[(1+\alpha)k + \beta_n]^2} \right)^{1/2} \right] \\
 \beta_n &= n^2 \Pi^2 D / R^2
 \end{aligned}$$

Mechanism and Kinetics of Isotopic Exchange in Zeolites.

II. Experimental Data

by L. M. Brown and H. S. Sherry*

Mobil Research and Development Corporation, Central Research Division, Princeton, New Jersey 08540
(Received May 17, 1971)

Publication costs assisted by Mobil Research and Development Corporation

The kinetics of isotopic exchange of sodium ions in synthetic hydrated zeolites NaX and NaA were investigated by means of a radioactive-tracer technique. Exchange in these zeolites consisted of two observable steps involving structurally distinct cations. The experimental data were interpreted in terms of a new model containing two adjustable parameters representing the rate coefficients of the fast and slow isotopic exchange steps. The model assumes the rate-controlling processes are diffusion in the fast isotopic exchange of mobile ions and intracrystalline exchange (assumed to be first order) between bound and mobile ions in the slower isotopic exchange of bound ions. The behavior of NaX, in which bound and mobile ions in the large cages undergo isotopic exchange in a single apparent diffusional process, is explained by assuming that intracrystalline exchange is at least as fast as diffusion. A rigorous test of the model for zeolite X shows that the rate of the fast step varies inversely with the square of the mean equivalent radius of the crystals and that the rate of the slow step was independent of the size of the crystals, as required mechanistically. Best values of the diffusivities and specific rates of exchange were derived from least-squares fits of the data on the model by use of the known distributions of cations over the different kinds of sites.

Introduction

The rates of isotopic exchange of sodium ions in hydrated zeolites X and A have been measured by means of a radioactive-tracer technique. The primary objective of this study was to provide experimental data that could be used to ascertain the validity of the isotopic exchange model described previously.¹

Earlier attempts^{2,3} to investigate these systems were

limited by the immeasurably large rates in the small crystals available commercially. Measurable rates were achieved in the present study by the use of large single crystals of zeolites NaX and NaA, which were

(1) Part I: L. M. Brown, H. S. Sherry, and F. J. Krambeck, *J. Phys. Chem.*, **75**, 3846 (1971).

(2) E. Hoinkis and H. W. Levi, *Naturwissenschaften*, **53**, 500 (1966).

(3) E. Hoinkis and H. W. Levi, *Z. Naturforsch. A*, **22**, 226 (1967).

synthesized according to procedures developed by Charnell.⁴

Isotopic exchange in each of these zeolites involves more than one structurally distinct cation site. In NaX there are three cation sites, consisting of mobile and bound sites in a three-dimensional network of large cages, and bound sites in an interconnecting network of small cages.^{5,6} In NaA, there are two cation sites, consisting of mobile and bound sites in a single three-dimensional network of large cages.⁶ One would therefore expect exchange in zeolite X to take place in a maximum of three steps and exchange in zeolite A to take place in a maximum of two steps.

Experiment^{7,8} has shown that, with few exceptions, isotopic exchange of monovalent and divalent cations in these zeolites takes place in two observable steps. In all but one case these steps were thought to be independent diffusional processes. In the exchange of cesium ions in zeolite A,⁹ however, desorption of bound ions was considered to be rate controlling in the slow step.

Data obtained in this study have been interpreted in terms of a different model¹ which, we believe, is consistent with the crystal structure of the zeolites and accounts for all relevant modes of cationic migration. Briefly, the model states that the elementary isotopic exchange steps are not independent but are coupled processes. In zeolite A these processes consist of the diffusion of mobile ions in the fast step and of intracrystalline exchange between bound and mobile ions in the slow step. In zeolite X, where intracrystalline exchange between bound and mobile ions in the large cages is assumed to be fast compared to diffusion, the fast step is an apparent uniform diffusional process involving these two kinds of ions, and the slow step consists of the intracrystalline exchange between bound ions in the small and large cages. The model further assumes the equilibrium distribution of cations among the different kinds of sites, as determined from X-ray diffraction data,^{5,6} is maintained during the approach to isotopic exchange equilibrium.

Diffusivities and specific rates of intracrystalline exchange (assumed to be first order) were derived by means of a two-parameter fit of the data to the model for the known equilibrium distribution of cations. Data obtained for crystals of different radii show that the rate of the slow step in zeolite X is independent of particle size, consistent with the proposed model but inconsistent with the model that assumes diffusion to be rate controlling in the slow step.

Experimental Section

The crystals of zeolites X and A were synthesized in accordance with procedures perfected by Charnell.⁴ These procedures yielded well-formed octahedra of NaX as large as 100 μ in overall length and cubes of NaA as large as 60 μ in edge length. X-Ray crystal-

linities were obtained and found to be 150–160% of those for Linde 13X and Linde 4A crystals. Before they were used, the virgin crystals were washed once with a 0.1 *N* NaCl solution to ensure uniformity of the cation content and then washed carefully with distilled water until the pH of the slurry was in the range 10.5–11.0. The composition of each zeolite is shown in Table I.

Table I: Composition of Zeolites NaX and NaA

Zeolite (site)	Amt of Na, mequiv/g	—Amt, mmol/g—		—Atom ratios—	
		SiO ₂	Al ₂ O ₃	Si/Al	Na/Al
NaX (95 μ)	6.74	7.54	3.45	1.1	0.98
NaX (77 μ)	6.0	7.96	3.20	1.23	0.97
NaA (53 μ)	6.87	7.44	3.44	1.08	1.0

The crystals were classified into fractions having narrow size ranges by means of elutriation. The apparatus, adapted from that of Alyl and Latimer,¹⁰ is shown schematically in Figure 1. It is a closed, self-sustaining system in which ethyl alcohol is circulated continuously by means of a variable-speed tubing pump (A) through a series arrangement of five Pyrex tubes (B) having diameters in the range 2–3.5 in. The return of the alcohol to the first tube (B) was effected by pumping liquid from the top of Pyrex tube (C). This tube, immersed in a beaker containing alcohol, contains a column of glass beads (D) to trap crystals that enter it through the side arm. The pump speed was maintained constant within 1% by means of a solid-state controller; flow rates were monitored by means of a flowmeter (E). Mean sizes of the samples used in this research are given in Table II. Each result was obtained by measuring the dimensions of 300–500 crystals contained in calibrated photomicrographs of the type shown in Figure 2. The mean equivalent radii contained in Table II were used in analyses of the data.

The isotopic exchange system consisted of the zeolite crystals ($1/4$ to $1/3$ g) containing a trace amount of sodium-22 and a 0.1 *N* sodium chloride solution (600 ml). The reaction was performed in the apparatus shown schematically in Figure 3. The mixture was stirred (C) vigorously (5000 rpm) in a 1-l. resin flask

(4) J. Charnell, *J. Cryst. Growth*, in press.

(5) D. H. Olson, *J. Phys. Chem.*, **74**, 2758 (1970).

(6) L. Broussard and D. P. Shoemaker, *J. Amer. Chem. Soc.*, **82**, 1040 (1960).

(7) E. Hoinkis and H. W. Levi, *Z. Naturforsch. A*, **23**, 813 (1968).

(8) E. Hoinkis and H. W. Levi, "Ion Exchange in the Process Industries," Society of the Chemical Industry, London, 1970, p 339.

(9) H. Gaus and E. Hoinkis, *Z. Naturforsch. A*, **24**, 1511 (1969).

(10) H. F. Alyl and R. M. Latimer, *J. Inorg. Nucl. Chem.*, **29**, 2041 (1967).

Table II: Mean Sizes of Zeolitic Crystals

Zeolite	Mean length of octahedra or cubes, μ	Mean equiv spherical radius, cm
NaX	95 ± 10	2.7×10^{-3}
	77 ± 10	2.2×10^{-3}
NaA	53 ± 5	2.7×10^{-3}

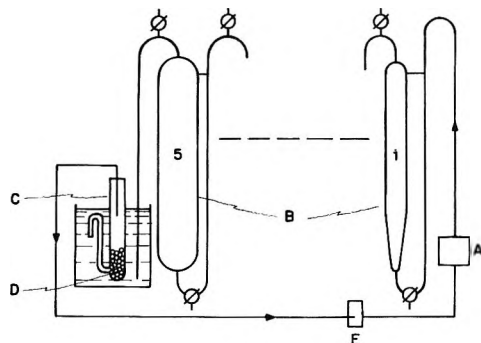


Figure 1. Elutriation apparatus (schematic): A, pump; B, elutriating tube; C, glass tube; D, glass beads; E, flowmeter.

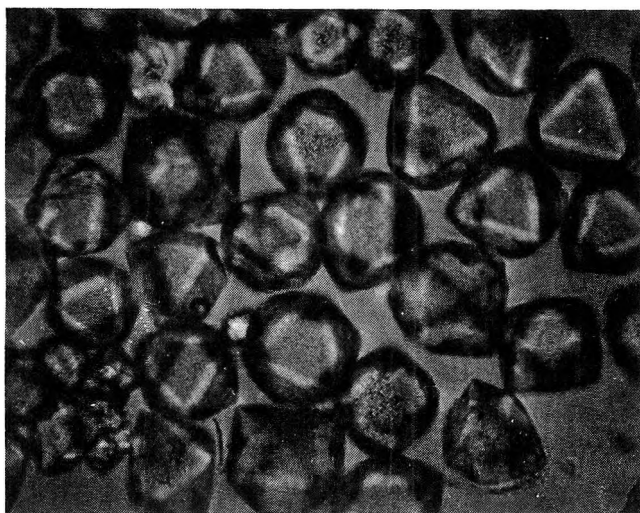


Figure 2. Photomicrograph of NaX crystals (77μ); magnification $520\times$.

(A) immersed in a constant-temperature bath and pumped (F) rapidly (2 l./min) through a filter (B). The filtered solution then passed through a Plexiglas cell (D) that was inserted in an opening in a Tl-doped NaI scintillation crystal (E) before returning to the resin flask. The U-shaped Plexiglas cell proved to be unsatisfactory, because bubbles tended to accumulate therein and consequently prevented the measurement of the true activity of the solution. This effect was eliminated by use of a steel tube, having a volume of 14 ml, that was mounted in another NaI crystal having a straight-through bore. Zeolite crystals were re-

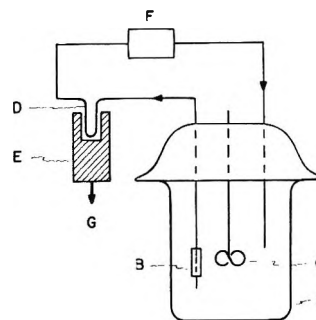


Figure 3. Experimental apparatus (schematic): A, 1-l. Pyrex vessel; B, filter holder; C, stirrer; D, plastic cell; E, NaI(Tl) crystal and electron multiplier tube; F, pump; G, electrical lead to analyzer-rate meter.

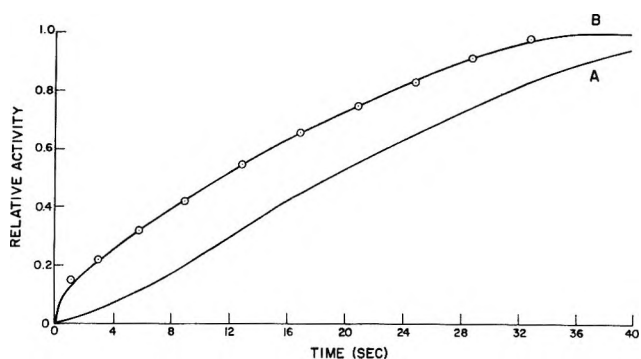


Figure 4. Relative activity of ^{22}Na vs. time in a test of the experimental method: open circles, relative activity of ^{22}Na added at known rate to reaction vessel; curve A, measured activity; curve B, activity corrected for time constant of rate meter.

tained in the flask by a Millipore Nylon filter contained in the holder (B); the average diameter of the filter pores was 14μ . The apparatus was modeled after that of Schwarz, *et al.*¹¹ The volume of the rubber tubing external to the solution was approximately 22 ml. For a flow rate of 2 l./min, the solution in the steel tube was replaced once every 0.2 sec.

The NaI crystal was sealed to a light-shielded electron multiplier tube, the output of which was fed sequentially into a preamplifier, pulse height analyzer, and linear rate meter. The output of the last was displayed on a 10-mV recorder. A correction was applied to the recorded signal to compensate for the distortion of the true signal by the time constant of the rate meter, set at 1.069 sec, by use of the finite-difference method of Vincent.¹² All such calculations were programmed for execution by an electronic computer. The sample standard deviation of the corrected relative activities from the least-squares smoothed curve through the data varied from ± 0.01 to ± 0.04 for data obtained at the lowest to highest temperature.

(11) A. Schwarz, J. A. Marinsky, and K. S. Spiegler, *J. Phys. Chem.*, **68**, 918 (1964).

(12) C. H. Vincent, *J. Sci. Instrum.*, **44**, 241 (1967).

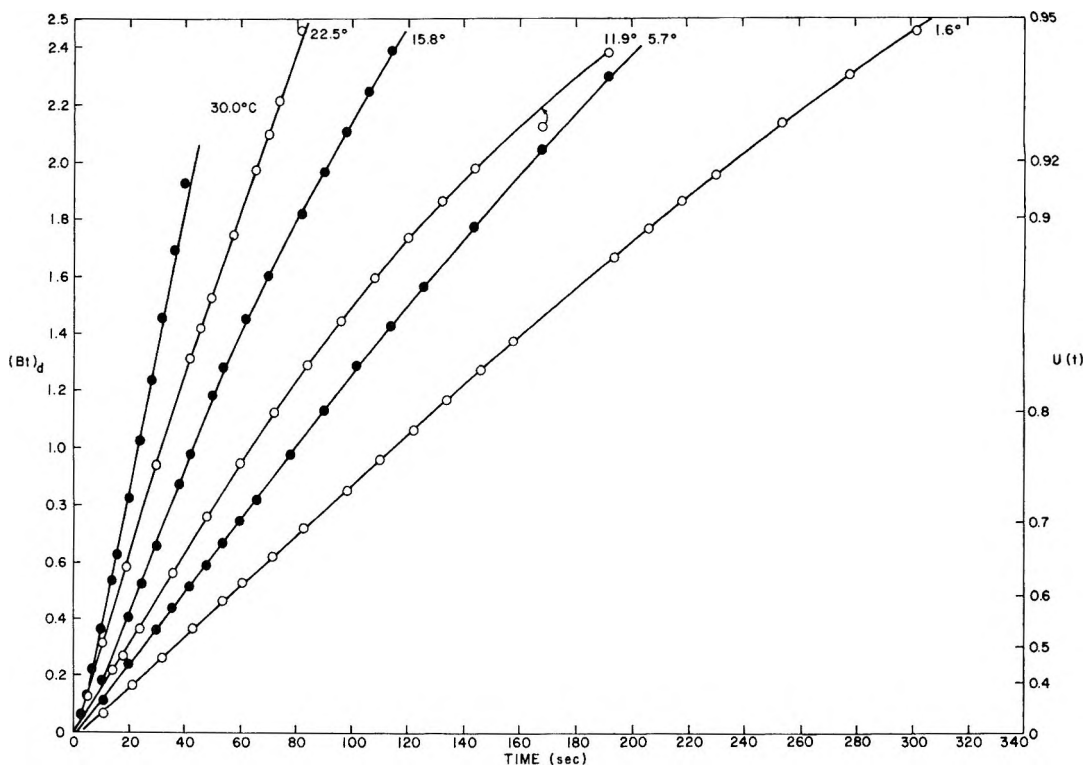


Figure 5. Dimensionless time parameter (diffusional model) $(Bt)_d$ vs. time for NaX (95μ).

The reliability of the overall experimental procedure was tested in a separate experiment. In this experiment 25 ml of a 0.1 *N* NaCl solution containing a known activity of ^{22}Na was added at a measured rate to 475 ml of an unlabeled NaCl solution contained in the resin flask. The experimental conditions were identical with those of a typical isotopic exchange experiment, except that the circulation rate was 1 l./min and the time constant was 7.11 sec. Figure 4 contains graphs of relative activity vs. time for the uncorrected (curve A) and corrected (curve B) data. The open circles superimposed on curve B indicate the known relative activities of the solution in the resin flask at various times. The agreement between the calculated and known relative activities indicates that after the first 2 or 3 sec it was possible to follow faithfully changes of activity in the solution for a process that goes to completion in about 40 sec. This is important, because the half-times for isotopic exchange in our crystals of NaX and NaA varied between 5 and 80 sec.

Results and Conclusions

Rates of isotopic exchange were measured in NaX at temperatures between 2 and 30° and in NaA between 3 and 40° for fractional attainments of equilibrium $U(t)$ at least as great as 0.9. Half-times for exchange varied between 5 and 40 sec for NaX and between 10 and 80 sec for NaA.

Isotopic exchange in both zeolites was a nonuniform process consisting of a fast initial step and an overlapping slow step. Each exchange was initially diffu-

sional but gradually departed from this behavior as the effect of the slow step increased. At the highest temperatures the two steps were no longer distinct, and the overall exchange degenerated to an apparent uniform diffusional process. This behavior is evident in the graphs showing the time variation of the dimensionless time parameter, $(Bt)_d$, defined for a pure diffusional process (eq 16, ref 1). These graphs are shown in Figures 5 and 6 for NaX (95- and $77\text{-}\mu$ crystals) and in Figure 7 for NaA ($53\text{-}\mu$ crystals). Values of $(Bt)_d$ corresponding to the experimental values of $U(t)$ were calculated, by use of an electronic computer, from approximate equations derived from the solution of Fick's second equation by Reichenberg.¹³ At the lower temperatures each curve is linear initially and becomes nonlinear at later times as the effect of the slow step increases. With increasing temperature the curves tend to become linear over the entire course of the exchange, reminiscent of a pure diffusional process, as the fast and slow steps tend to overlap.

In the case of NaX the curves are more nearly linear for the larger crystals than for the smaller ones. Clearly the rate of the fast (diffusional) step is lower in the larger crystals, and the concomitant greater overlapping in the larger crystals undoubtedly means that the rate of the slow step is independent of particle size and, hence, not diffusional.

The fact that isotopic exchange in NaX took place in two, and not three, observable steps indicates two of

(13) D. Reichenberg, *J. Amer. Chem. Soc.*, **75**, 589 (1953).

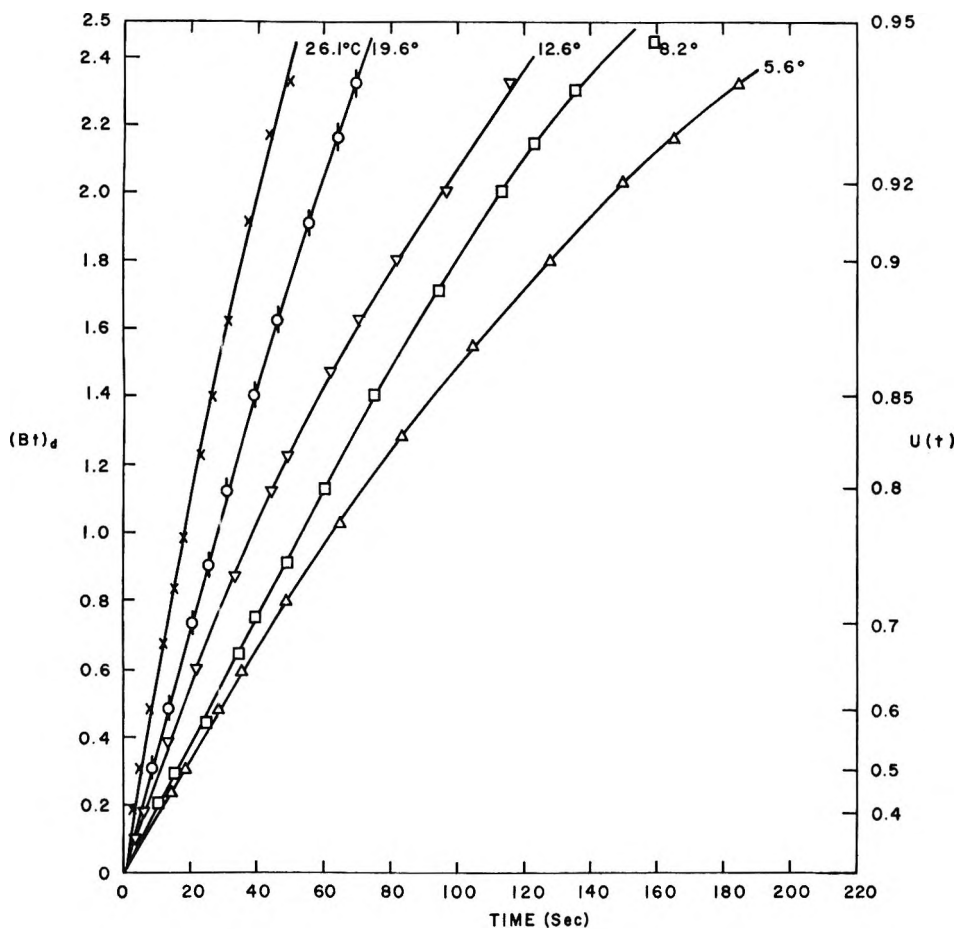


Figure 6. Dimensionless time parameter (diffusional model) $(Bt)_d$ vs. time for NaX (77μ).

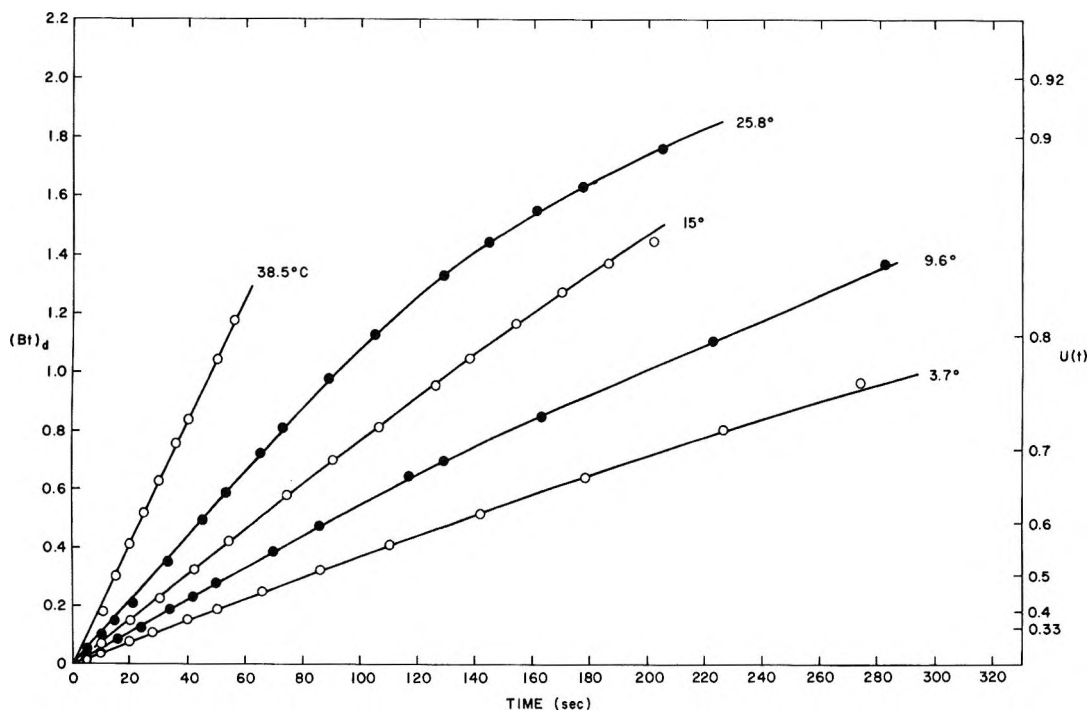


Figure 7. Dimensionless time parameter (diffusional model) $(Bt)_d$ vs. time for NaA (53μ).

the three kinds of cations^{5,6} migrate collectively in one of the steps. The initial linear region of the graphs

for NaX at the lowest temperatures in Figure 6 terminates at values of $U(t)$ close to 0.8. This fraction

corresponds almost exactly to the 69 out of 85 sodium ions per unit cell^{5,6} that are located in the supercages. It may therefore be concluded that the bound and mobile cations contained in the supercages give rise to the fast diffusional step in NaX. This result also means that at the lowest temperatures the fast step in the smaller crystals goes virtually to completion before the slow step produces a noticeable effect on the diffusional process. The behavior of SrX^{1,8} and of BaX⁸ was similar to this.

Correlations of the experimental data for zeolites X and A with the proposed model of exchange were made by obtaining least-squares fits of the data to equations 17a-c (mechanisms B and F) of ref 1. Best values of B_m (diffusivity parameter) and k (specific rate of exchange), defined in ref 1, were derived by means of a computer for values of α (equilibrium constant parameter) equal to 0.23 for NaX and 2.0 for NaA. Values of α were calculated in accordance with the definitions given in Table I of ref 1 and are based on the equilibrium distributions of cations derived from X-ray diffraction data.^{5,6} Typical results of the correlation are shown in Figure 8. The curves represent the experimental data, and the open circles denote values of $U(t)$ predicted by the model for the derived values of k and B_m . Rate parameters for all experiments are listed in Tables III and IV. In all cases the sample standard deviation of the calculated points from the experimental curve was approximately 0.02. The close correspondence of the experimental and predicted curves implies that the proposed model can explain the kinetics of isotopic exchange in NaX (mechanism F, ref 1) and in NaA (mechanism B, ref 1).

Table III: Rate Parameters for Isotopic Exchange in NaX

Temp. °C	$10^2 B_m$ sec ⁻¹	$10^2 k_4$ sec ⁻¹	$10^8 D_1$ cm ² /sec	k_4/B_m
95- μ Crystals				
1.6	1.07	5.8	1.5	5.5
5.7	1.57	8.0	2.2	5.1
9.0	1.76	12.8	2.5	7.3
11.9	1.93	10.2	2.7	5.3
15.8	2.64	11.2	3.8	4.2
22.5	4.06	14.9	5.8	3.7
30.0	5.3	14.3	7.6	2.7
77- μ Crystals				
5.6	2.04	16.1	1.9	7.9
8.2	2.35	12.7	2.2	5.4
19.6	4.27	10.6	4.1	2.5
26.1	7.3	17.0	7.0	2.4

In a more rigorous test of the model for NaX we were able to show directly that $B_1 (= \pi^2 D_1 / R^2 (1 + \alpha_{12}))$,¹ the rate parameter for the diffusional step, varied inversely with the square of the equivalent spherical

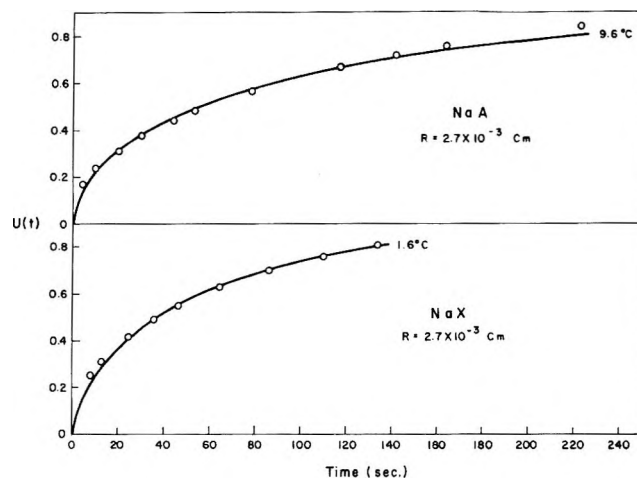


Figure 8. Fractional attainment of isotopic exchange equilibrium vs. time for NaA and NaX. Comparisons of experimental values (unbroken lines) and values derived from model (open circles).

Table IV: Rate Parameters for Isotopic Exchange in NaA (53- μ Crystals)

Temp. °C	$10^2 B_m$ sec ⁻¹	$10^2 k_4$ sec ⁻¹	$10^8 D_1$ cm ² /sec	k_4/B_m
3.4	5.9	4.3	4.2	0.07
3.7	4.3	5.4	3.1	0.12
9.6	6.1	8.1	4.3	0.13
15.0	7.7	12.5	5.5	0.16
25.8	10.2	18.3	7.3	0.18
38.5	15.3	40.3	10.8	0.26

radius and that k_4 , the rate parameter for the slow-exchange step, was independent of the radius. The former was indicated by the finding that D_1 , the diffusivity of mobile ions, was a constant, independent of radius. The results are presented in Figure 9 as Arrhenius-type plots of D_1 and k_4 . In both cases the data for crystals of different sizes are satisfactorily collinear. On this basis it is concluded that mechanism F of ref 1 is the probable model for isotopic exchange in NaX.

The effect of particle size on the rate parameters derived for NaA could not be determined, because isotopic exchange was too fast to be measured accurately with the smaller crystals separated from the large crystals during the classification process. Also, attempts to grow crystals larger than 53 μ on an edge were unsuccessful. Arrhenius-type plots for D_1 and k_2 for the 53- μ NaA crystals are shown in Figure 10.

The least-squares line through the points in Figures 9 and 10 are represented by the following expressions for NaX

$$D_1 = 10^{-0.10 \pm 0.21} \exp[-(9700 \pm 280)/RT] \text{ cm}^2/\text{sec}$$

$$D_1(25^\circ) = 6.7 \times 10^{-8} \text{ cm}^2/\text{sec}$$

$$k_4 = 10^{2.65 \pm 0.98} \exp[-(4750 \pm 1290)/RT] \text{ sec}^{-1}$$

$$k_4(25^\circ) = 0.15 \text{ sec}^{-1}$$

and for NaA

$$D_1 = 10^{-3.2 \pm 0.5} \exp[-(5360 \pm 710)/RT] \text{ cm}^2/\text{sec}$$

$$D_1(25^\circ) = 7.7 \times 10^{-8} \text{ cm}^2/\text{sec}$$

$$k_2 = 10^{5.7 \pm 0.6} \exp[-(10,140 \pm 800)/RT] \text{ cm}^2/\text{sec}$$

$$k_2(25^\circ) = 0.02 \text{ sec}^{-1}$$

An exploratory study of isotopic exchange in zeolite BaX was also conducted to provide additional insight into the mechanism of the slow step in zeolite X. Three samples of BaX were prepared by ion exchanging two batches of large crystals of NaX (30 and 60 μ) and one batch of Linde 13X crystal with a 300-fold excess of a 1 *N* BaCl₂ solutions at 50° for 14 days. In this time virtually all the sodium ions were replaced by barium ions, as shown in Table V. Isotopic exchange was carried out in each sample by agitating identical mixtures of BaX tagged with ¹³³Ba and a 0.1 *N* BaCl₂ solution in a water bath maintained at a temperature of 50°. The progress of the exchange was followed periodically by sampling the liquid phase and measuring its activity. Isotopic exchange consisted of a fast step, representing about 80% of the overall process, that went to completion in a matter of hours and a slow step that approached equilibrium in the course

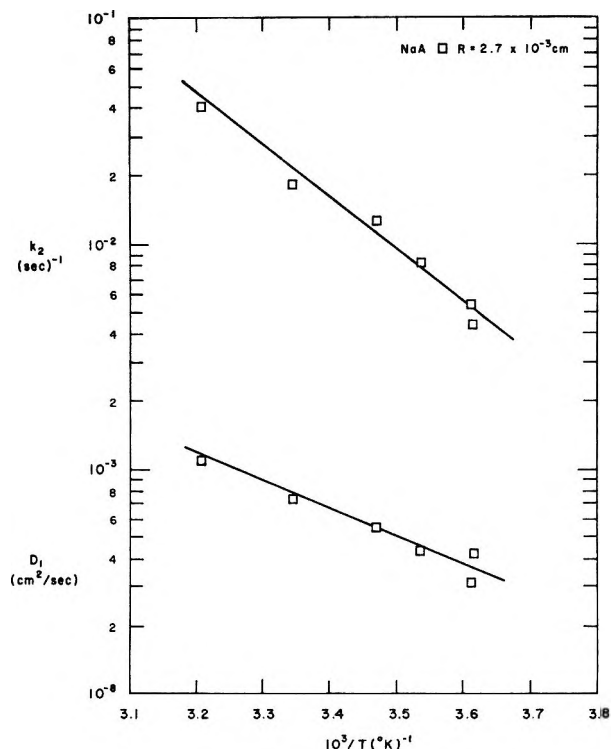


Figure 10. Semilogarithmic graphs of derived rate parameters vs. $1/T$ for NaA (53- μ crystals) showing diffusivity of mobile ions (lower graph) and specific rate of exchange (upper graph).

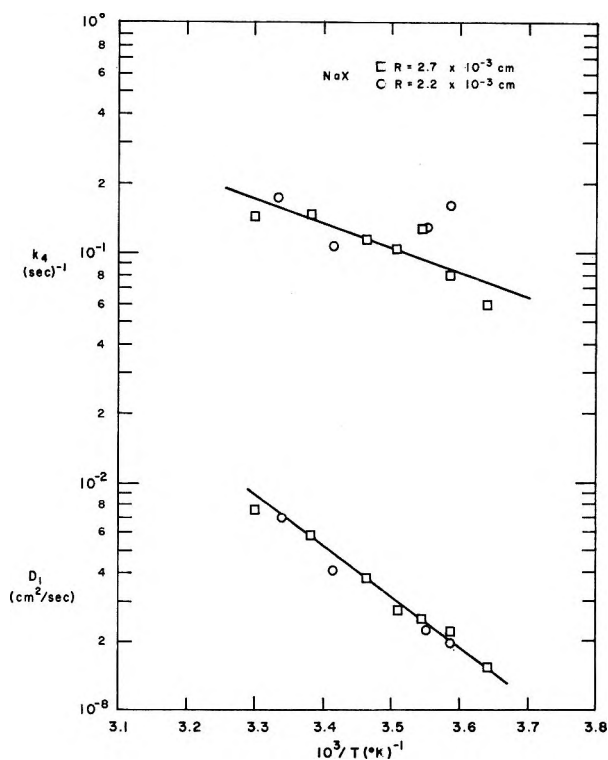


Figure 9. Semilogarithmic graphs of derived rate parameters vs. $1/T$ for NaX showing diffusivity of mobile ions (lower graph) and specific rate of exchange (upper graph): \square , 95- μ crystals; \circ , 77- μ crystals.

of several days; the overall degrees of exchange in the 30- and 60- μ crystals were 97 and 95% after 10 days, as shown in Table VI. Similar results were obtained by Hoinkis and Levi^{7,8} for isotopic exchange in BaX prepared from Linde 13X crystals; they reported half-times of 40 sec and 180 hr for the fast and slow steps at 40°, with the fast step accounting for approximately 80% of the cations. These results show that the rates of the slow step in crystals of different sizes were comparable and, consequently, were not controlled by diffusion. If diffusion had been rate controlling, then the half-times of the slow step in the large crystals, estimated from the data for Linde 13X^{7,8} (assumed to contain 1- μ crystals), would have been roughly 4.5 years for the 30- μ crystals and 18 years for the 60- μ crystals; and the overall degree of exchange in the large crystals after 10 days would have been approximately 80% and not 96%. In all probability the mechanism for isotopic exchange in BaX is the same as the one assumed herein for NaX, inasmuch as both zeolites contain the same kinds of cation sites.¹⁴

Consideration was given to the possibility that the rates of these fast processes were influenced significantly by diffusion through the film¹⁵ at the boundary of the crystals. However, the experimentally ob-

(14) D. H. Olson, unpublished work.

(15) F. Helfferich, "Ion Exchange," McGraw-Hill, New York, N. Y., 1962, pp 250-322.

Table V: Composition of Zeolite BaX Samples

Crystal size, μ	—Amt, mequiv/g—		—Amt, mmol/g—		—Atom ratios—	
	Ba	Na	SiO ₂	Al ₂ O ₃	2Ba/Al	Si/Al
60	5.0	0.13	6.21	2.49	1.0	1.25
30	4.73	0.12	6.27	2.49	0.95	1.26
a	4.89	0.22	6.09	2.47	0.99	1.23

^a Prepared from Linde 13X crystals.

Table VI: Progress of Isotopic Exchange in Zeolite BaX Crystals of Different Sizes at 50°

t, hr	U(t)		t, hr	U(t)	
	30- μ crystals	60- μ crystals		30- μ crystals	60- μ crystals
48	0.947	...	168	0.971	0.951
72	...	0.924	240	...	0.967
120	...	0.933			

served $1/R^2$ dependence of the rate of the fast step in NaX would seem to indicate this effect is negligible. Other evidence would also seem to support this conclusion. For example, the data for NaX did not obey the film-diffusion equation.¹⁵ Also, a value of 0.1 was calculated for the expression¹⁵ $7XD_1l/C_sD_fR$, which theoretically has a value that is much less than unity when diffusion in the solid phase is the rate-controlling step. The symbols in this expression (and their actual or assumed values for NaX) follow. X (6 mequiv/ml) is the concentration of fixed ionic groups, C_s (0.1 mequiv/ml) the concentration of the solution, D_1 (10^{-8} cm²/sec) the diffusivity of mobile ions, D_f (10^{-5} cm²/sec) the diffusivity in the film,¹⁵ l ($\sim 10^{-3}$) the film thickness for a well-stirred solution,¹⁵ and R (3×10^{-3} cm) the equivalent particle radius. The effect of solution concentration was also investigated, the rate decreasing by 16% when the concentration was changed from 0.1 to 0.05 N NaCl. This decrease of the rate is slightly outside the scatter of the data and may indicate a film effect in solutions more dilute than 0.1 N.

Discussion

The experimental results show that the model described previously¹ provides an adequate interpretation of the isotopic exchange of cations in zeolites NaX, BaX, and NaA. It is encouraging to find that a satisfactory fit of the data to the model was possible by use of two derived parameters and the known equilibrium distribution of cations among the different kinds of sites.

Our model may also be valid for isotopic exchange in zeolite SrX. Kinetically,^{2,8} exchange in SrX was found to consist of two observable steps as in BaX; and structurally,¹⁶ SrX (similar to BaX¹⁴) was found

to contain both bound ions (15 per unit cell) and mobile ions (16 per unit cell) in the supercages and bound ions (13 per unit cell) in the small cages.

As noted previously, the model could not be tested rigorously for zeolite NaA because of our inability to grow crystals of larger size than those used in this study. In view of the qualitative similarity of the cation sites in the large cages of NaX and NaA, it seems reasonable to assume that the mechanism of isotopic exchange of these cations in both zeolites would be similar.

The only other data on the self-diffusion of sodium ions in zeolite X are those derived by Stamires¹⁷ from electrical conductivity data. His value ($\sim 10^{-8}$ cm²/sec) for the field self-diffusion coefficient at 25° is in good agreement with our value (6.7×10^{-8} cm²/sec), although the reliability of his data has been questioned.¹⁸

In view of the similarity of the Si/Al ratios (1.25 for NaX and 1.0 for NaA), and therefore of the lattice charges, one would expect the activation energies for diffusion of mobile ions in these zeolites to be similar. It is not possible to show this experimentally, because the fast step in NaX is a composite of successive elementary processes—mobilization of bound ions by desorption from hexagonal rings containing three units of negative charge⁵ and of diffusion. Moreover, the experimental activation energy, $E_D(\text{NaX}) = 9.7$ kcal/g-ion, represents the height of the barrier to desorption, the larger of the barriers surmounted¹⁹ by the cations, and not the barrier to diffusion. It is therefore not surprising that this result is similar to the activation energy for the slow step in NaA ($E_s(\text{NaA}) = 10.1$ kcal/g-ion), because the latter also involves desorption from hexagonal rings that contain three units of negative charge. The activation energy of 5.4 kcal/g-ion for the fast step in NaA is the height of the barrier to diffusion of mobile ions. It is unlikely that the barrier to diffusion in NaX is much different from this number. The result for NaA may be compared with the figure 7 kcal/g-ion (approximately) that was reported²⁰ as the activation energy for the diffusion of alkali ions in chabazite, in which the cations are not sited but are bound by ion-dipole forces to water molecules that are attached to lattice oxygens.²¹

The activation energy of the slow step is 4.8 kcal/g-ion and is lower than that of the fast step. The slow step involves the movement of ions out of the small cages (hexagonal prisms and sodalite cages) and into

(16) D. H. Olson and H. S. Sherry, *J. Phys. Chem.*, **72**, 4095 (1968).

(17) D. N. Stamires, *J. Chem. Phys.*, **36**, 3174 (1962).

(18) B. Morris, *J. Phys. Chem. Solids*, **30**, 73 (1969).

(19) S. Glasstone, K. J. Laidler, and H. Eyring, "The Theory of Rate Processes," McGraw-Hill, New York, N. Y., 1941, p 99.

(20) R. M. Barrer, R. F. Bartholomew, and L. V. C. Rees, *J. Phys. Chem. Solids*, **24**, 51 (1963).

(21) J. V. Smith, F. Rinaldi, and L. S. D. Glasser, *Acta Crystallogr.*, **16**, 45 (1963).

the large cages. However, the detailed mechanism and rate-controlling step of this composite process are not known. The large uncertainties noted previously in this activation energy and in k_4 are the result of the combined effects of the insensitivity of the model to values of k_4/B_m as large as the experimental value of 5 (Table III) (see Figure 1, ref 1) and of experimental errors. Because of the former effect, experimental errors are magnified in the derivation of k_4/B_m from the data, and, unfortunately, the data that have the most important effect on the derived value of k_4 for

NaX are obtained in the last 20% of the exchange, the region in which the experimental error is the greatest

Acknowledgments. We are grateful to Drs. E. Dempsey and D. H. Olson for many helpful discussions and to Mr. E. B. Peterson and Mr. J. S. Hick for designing the computer programs required for the analyses of the data. Many thanks go to Mr. W. E. McCullough for his careful assistance in the conduct of the experimental work. We are indebted to Mobil Research and Development Corp. for its support of this work.

Interaction Virial Coefficients in Hydrocarbon-Fluorocarbon Mixtures¹

by E. M. Dantzler Siebert and C. M. Knobler*

Department of Chemistry, University of California, Los Angeles, California 90024 (Received May 24, 1971)

Publication costs borne completely by The Journal of Physical Chemistry

Measurements of the excess second virial coefficient, ϵ [$=B_{12} - \frac{1}{2}(B_{11} + B_{22})$], for binary mixtures of the normal hydrocarbons, methane through hexane, with the normal perfluorocarbons, perfluoromethane through perfluorohexane, at 25, 50, and 100° are presented. In general, the results can be fitted with a Kihara spherical-core potential with an interaction energy about 10% weaker than that calculated from the geometric mean. While no completely satisfactory way of correlating the departures from the geometric mean is found, a combination rule similar to that proposed by Hudson and McCoubrey is the most successful.

Introduction

This paper describes an investigation of the low-density equation of state of binary hydrocarbon-fluorocarbon mixtures. Two previous publications have dealt with similar studies of binary mixtures of normal alkanes^{2a} and binary mixtures of normal perfluoroalkanes.^{2b} A three-parameter corresponding-states approach was found to be effective in describing the behavior of the alkane and perfluoroalkane mixtures.

In I we showed that the corresponding-states treatment of the hydrocarbon mixtures could be couched in terms of the McGlashan-Potter equation,³ which fits the second virial coefficients of the pure *n*-alkanes, but the discussion in II for the fluorocarbon mixtures was based on the Kihara spherical-core potential. For both hydrocarbon and fluorocarbon mixtures the energy parameter describing the unlike interaction showed only small (1–2%) departures from the geometric-mean combination of the energy parameters of the pure components. There are good reasons to believe that the geometric mean should be a much poorer description of the unlike interaction in hydrocarbon-fluorocarbon mixtures.

In 1958, Scott⁴ concluded from a review of the available excess thermodynamic properties of hydrocarbon-fluorocarbon liquid mixtures that the large deviations between observed and predicted behavior in these systems resulted from a failure of the geometric mean. The data can be explained if it is assumed that the hydrocarbon-fluorocarbon interaction is abnormally weak. A more recent review of the data on liquid mixtures⁵ leads to the same conclusion. A few studies of gaseous hydrocarbon-fluorocarbon mixtures have been made,^{6–8}

(1) Contribution No. 2734 from the University of California, Los Angeles.

(2) (a) E. M. Dantzler, C. M. Knobler, and M. L. Windsor, *J. Phys. Chem.*, **72**, 676 (1968); hereafter referred to as I. (b) E. M. Dantzler and C. M. Knobler, *ibid.*, **73**, 1335 (1969); hereafter referred to as II.

(3) M. L. McGlashan and D. J. B. Potter, *Proc. Roy. Soc., Ser. A*, **267**, 478 (1962).

(4) R. L. Scott, *J. Phys. Chem.*, **62**, 136 (1958).

(5) J. S. Rowlinson, "Liquids and Liquid Mixtures," 2nd ed, Butterworths, London, 1969.

(6) D. R. Douslin, R. H. Harrison, and R. T. Moore, *J. Phys. Chem.*, **71**, 3477 (1967).

(7) T. B. Tripp and R. D. Dunlap, *ibid.*, **66**, 635 (1962).

(8) M. D. Garner and J. C. McCoubrey, *Trans. Faraday Soc.*, **55**, 1526 (1959).

Table I: Experimental Results

System	P_1 Torr	ΔP_1 Torr	ϵ , cm ³ /mol	$-B_{12}$, cm ³ /mol	Caled ϵ , cm ³ /mol	
					a	b
			25.0°			
CF ₄ -CH ₄	237.50	0.37	13 ± 1	52	-0.4	10
	769.95	0.39				
C ₄ F ₁₀ -C ₄ H ₁₀	749.70	2.54	158 ± 2	643	-94	174
	737.85	2.51				
			50.0°			
CF ₄ -CH ₄	672.60	0.16	13 ± 2	39	-0.4	9
	695.20	0.15				
CF ₄ -C ₂ H ₆	694.10	0.32	27 ± 1	87	-5	11
	709.05	0.35				
CF ₄ -C ₄ H ₁₀	637.65	1.77	166 ± 1	166	114	142
	682.00	2.01				
CF ₄ -C ₆ H ₁₄	297.85	1.26	537 ± 10	255	473	519
	205.65	0.58				
C ₂ F ₆ -CH ₄	687.25	0.61	51 ± 1	65	29	64
	715.60	0.66				
C ₂ F ₆ -C ₂ H ₆	720.05	0.42	33 ± 1	145	-26	31
	708.25	0.44				
C ₂ F ₆ -C ₄ H ₁₀	647.20	1.23	114 ± 1	282	19	110
	723.50	1.58				
C ₂ F ₆ -C ₆ H ₁₂	461.75	1.32	233 ± 2	353	126	244
	409.55	1.01				
C ₃ F ₈ -C ₃ H ₈	685.10	0.85	70 ± 1	311	-27	46
	675.55	0.82				
C ₄ F ₁₀ -CH ₄	684.70	3.19	260 ± 1	128	221	304
	683.25	3.19				
C ₄ F ₁₀ -C ₂ H ₆	679.45	2.16	178 ± 1	273	55	193
	737.15	2.56				
C ₄ F ₁₀ -C ₄ H ₁₀	616.80	1.29	130 ± 2	538	-74	152
	773.35	2.02				
C ₄ F ₁₀ -C ₆ H ₁₄	273.30	0.60	298 ± 6	830	10	382
	269.30	0.55				
C ₅ F ₁₂ -C ₆ H ₁₂	192.00	0.21	228 ± 10	853	-90	255
C ₆ F ₁₄ -C ₆ H ₁₄	255.85	0.53	315 ± 6	1297	-129	193
CF ₄ -C(CH ₃) ₄	637.00	1.81	168 ± 10	234	161	180
	631.70	1.79				
CF ₄ -SF ₆	798.05	0.30	19 ± 1	132	17	27
	827.75	0.34				
			100.0°			
CF ₄ -CH ₄	796.75	0.12	10 ± 1	22	-0.5	7
	821.80	0.16				
	746.20	0.12				
C ₂ F ₆ -C ₂ H ₆	775.90	0.38	28 ± 1	90	-24	21
	762.80	0.34				
C ₃ F ₈ -C ₃ H ₈	705.30	0.57	54 ± 1	212	-27	30
	735.75	0.66				
C ₄ F ₁₀ -C ₄ H ₁₀	772.35	1.20	90 ± 1	370	-68	102
	712.70	0.99				
C ₅ F ₁₂ -CH ₄	436.60	1.33	311 ± 3	95	283	358
C ₅ F ₁₂ -C ₆ H ₁₂	285.50	0.27	152 ± 6	588	-82	170
C ₆ F ₁₄ -CH ₄	258.80	0.72	484 ± 7	90	444	492
C ₆ F ₁₄ -C ₆ H ₁₄	394.55	0.73	211 ± 3	871	-114	109
CF ₄ -Ar	733.60	0.12	10 ± 1	14	10	11
	783.15	0.13				

^a Geometric mean. ^b Equation 4.

and they also suggest the inadequacy of the geometric-mean assumption. The observed interaction virial coefficients are smaller in magnitude than those predicted by the use of the geometric mean.

The conclusions about the failure of the geometric mean, which have been based on the thermodynamic properties of liquid mixtures, are not unequivocal. With present theories of liquid mixtures it is not possi-

ble to disentangle any failure in an assumption about the details of intermolecular forces from a failure in the theory itself. In fact, Scott's analysis of the mixture data was performed with the crude "regular solution" theory. Measurements on gaseous mixtures, on the other hand, are more directly relatable to intermolecular forces, but most of the pertinent data in the literature are not sufficiently precise to be useful. The present study is an attempt to provide sufficient information for a definitive test of the geometric-mean assumption for hydrocarbon-fluorocarbon mixtures.

Experimental Section

The sources and purities of the *n*-alkanes are listed in I; those of the *n*-perfluoroalkanes can be found in II. Argon (General Dynamics, 99–95%), sulfur hexafluoride (Matheson, 98.0%), and 2,2-dimethylpropane (Matheson, 99.0%) were used without further purification.

The apparatus has been previously described.⁹ The pressure change, ΔP , on mixing two gases at constant temperature and volume is determined. From this information it is possible to calculate ϵ , the excess second virial coefficient

$$\epsilon = B_{12} - \frac{1}{2}(B_{11} + B_{22}) \approx 2RT\Delta P/P^2 \quad (1)$$

Here B_{11} and B_{22} are the second virial coefficients of the pure components, B_{12} is the interaction second virial coefficient, P is the original filling pressure, T is the temperature, and R is the gas constant. The higher order terms are small and easily evaluated under the conditions of the experiment. Details of the data reduction can be found in ref 2a and 9.

Results

The experimentally determined excess second virial coefficients are listed in Table I along with the filling pressures and the pressure changes developed on mixing. The uncertainties in ϵ reflect the limitations of the differential pressure measurement. The absolute uncertainty in ΔP is ± 0.02 Torr. Where the low vapor pressure of one or both components limits the filling pressure, ΔP is small and as a result the error in ϵ is large. Also given in Table I are the values of B_{12} calculated from the observed ϵ 's and the virial coefficients for the pure components cited in I and II.

In Table II we compare our results with the few measurements of hydrocarbon-fluorocarbon mixtures which have been reported. Douslin, *et al.*,⁶ obtained virial coefficients for the methane-tetrafluoromethane system from gas density measurements over a temperature range of 0–350° and a pressure range of about 16–400 atm. At 50 and 100° the ϵ 's calculated from their values of B_{12} , B_{11} , and B_{22} agree with our data within experimental error. However, the disagreement at 25° of 4 cm³/mol is slightly greater than the overlap of stated experimental uncertainties.

Table II: Comparison between ϵ 's (in cm³/mol) of This Study and Those Derived from Previous Studies

System	Temp, °C	This work	Temp, °C	Other investigations
CF ₄ -CH ₄	25.0	13 ± 1	25.0	17.3 ^a
	50.0	13 ± 2	50.0	15.1
	100.0	10 ± 1	100.0	12.0
C ₄ F ₁₀ -C ₄ H ₁₀			10.0	206 ± 10 ^b
	25.0	158 ± 2		
			29.9	142 ± 12
C ₅ F ₁₂ -C ₅ H ₁₂	50.0	130 ± 2	50.0	90 ± 9
	100.0	90 ± 1		
			34.7	252 ^c
C ₅ F ₁₂ -C ₅ H ₁₂	50.0	228 ± 10	64.7	251
	100.0	152 ± 6		
			110.1	45

^a Reference 6. ^b Reference 7. ^c Reference 8.

Tripp and Dunlap⁷ obtained second virial coefficients of butane, perfluorobutane, and an equimolar mixture from compressibility measurements at 10.00, 29.88, and 50.05°. They calculated smoothed values by fitting their data to both the linear and quadratic virial expansions; the values listed are from the linear fit. Our data agree with those of Tripp and Dunlap at the lower temperatures, but their value at 50° is 40 cm³/mol less positive than ours.

The pentane-perfluoropentane mixture was studied by Garner and McCoubrey,⁸ who also used compressibility measurements to obtain values for the second virial coefficients of the pure components and some mixtures. They noted that their values of B lie consistently 10–30 cm³/mol lower than other literature values. Moreover, as seen in Table II, the ϵ 's derived from their data do not decrease smoothly with increasing temperature—another indication that the virial coefficients are unreliable.

Discussion

The Geometric Mean. In II we established that the Kihara spherical-core potential was adequate for the calculation of the second virial coefficients of perfluoroalkanes and their mixtures. This potential is given by

$$\phi(r) = \infty \quad r \leq 2a$$

$$\phi(r) = 4\epsilon[(\rho^\circ/\rho)^{12} - (\rho^\circ/\rho)^6] \quad r > 2a \quad (2)$$

where $\rho^\circ = \sigma - 2a$, $\rho = r - 2a$, r is the distance between molecular centers, $2a$ is the molecular hard-core diameter, σ is the low-velocity collision diameter, and $-\epsilon$ is the value of the minimum potential energy. The potential parameters that provided the best fit to the

(9) C. M. Knobler, *Rev. Sci. Instrum.*, **38**, 184 (1967).

Table III: Kihara Potential Parameters

	$\epsilon/k,$ $^{\circ}\text{K}$	$\sigma, \text{\AA}$	$a, \text{\AA}$		$\epsilon/k,$ $^{\circ}\text{K}$	$\sigma, \text{\AA}$	$a, \text{\AA}$
CH ₄	232.20	3.505	0.383	CF ₄	229	4.65	0.54
C ₂ H ₆	425.32	3.977	0.565	C ₂ F ₆	283	6.25	1.04
C ₃ H ₈	493.71	4.519	0.650	C ₃ F ₈	358	6.95	1.30
C ₄ H ₁₀	672.32	4.830	0.938	C ₄ F ₁₀	416	8.09	1.80
C ₅ H ₁₂	777.37	5.396	1.24	C ₅ F ₁₂	497	8.78	2.20
C ₆ H ₁₄	905.47 ^c	5.686 ^c	1.39 ^c	C ₆ F ₁₄	618	9.22	2.69
C ₇ H ₁₆	1023.30	5.996	1.60	C ₇ F ₁₆		9.73 ^c	3.19 ^c
C(CH ₃) ₄	625.88	5.395	1.01	SF ₆	353	5.12	0.732
C ₆ H ₆	975.37	4.938	1.14	CCl ₄	416	7.5	1.4
Ar	143.26	3.344	0.167				
Kr	206.68	3.587	0.208				

^a Reference 10. ^b Parameters are determined by the graphical procedure described in II. ^c Parameters are interpolated or extrapolated based on a regularity in the homologous series.

data for the pure perfluoroalkanes are given in Table III.

Tee, Gotoh, and Stewart¹⁰ have shown that the Kihara potential fits the second virial coefficients of the alkanes very well. Although in I we chose to analyze our measurements on hydrocarbons in terms of the McGlashan-Potter equation,³ the Kihara potential fits our data comparably well when the parameters derived by Tee, *et al.*, are used.

With the exception of the values for hexane, the potential parameters listed in Table III for the alkanes have been taken from ref 10. Tee, *et al.*, did not analyze virial coefficients for hexane; the parameters we list have been obtained by interpolation between their pentane and heptane values. The potential parameters in the homologous series show a fairly regular dependence on chain length and the hexane parameters so derived lead to calculated virial coefficients for hexane that are within 25 cm³/mol of the experimental values. This agreement is poorer than the 10–15 cm³/mol found in the case of the other *n*-alkanes, but when the parameters were varied to improve the fit, no better combination could be found. The McGlashan-Potter equation also shows poorer agreement with the hexane virial coefficients than it does for those of the other alkanes.

Only if the parameters ϵ_{12} and σ_{12} for the unlike interaction are specified can ϵ be calculated from the potential. (For the spherical core model the a_{12} parameter is simply the arithmetic mean of a_{11} and a_{22} .) In II we observed that with few exceptions the excess second virial coefficients for virtually all binary mixtures of the first six normal perfluoroalkanes could be calculated within experimental error by assuming the Lorentz-Berthelot combination rules, that is $\epsilon_{12} = (\epsilon_{11}\epsilon_{22})^{1/2}$ and $\sigma_{12} = (\sigma_{11} + \sigma_{22})/2$. The combining rules by which we calculated in I the pseudocritical temperatures and volumes for the analogous hydrocarbon mixtures are equivalent to these formulas for the molecular parameters, and

these combinations also lead to excellent agreement between experimental and calculated virial coefficients. When the Lorentz-Berthelot rules are applied to the hydrocarbon-fluorocarbon mixtures, the values of ϵ given in Table I are obtained. A comparison between experiment and calculation clearly indicates that the combining rules that were successful for hydrocarbons and fluorocarbons fail badly in the case of hydrocarbon-fluorocarbon mixtures.

Calculated excess second virial coefficients are rather insensitive to variations in σ_{12} , but they show a stronger dependence on ϵ_{12} . We therefore focus our attention on departures from the geometric-mean combination of energy parameters in an attempt to account for the discrepancies shown in Table I.

Departures from the Geometric Mean. The departures from the geometric mean can be expressed in terms of a factor k_{12} , which has been used extensively by Prausnitz and coworkers¹¹

$$\epsilon_{12} = (1 - k_{12})(\epsilon_{11}\epsilon_{22})^{1/2}$$

The factor k_{12} can be determined from virial coefficient data by adjusting ϵ_{12} in the Kihara potential to give the best fit to the experimental results. The values of $1 - k_{12}$ obtained from our hydrocarbon-fluorocarbon studies are listed in Table IV. In the case of CH₄-CF₄ the fit to the data is less sensitive to variations in ϵ_{12} than in the other systems. As a result the 2-cm³/mol uncertainty in ϵ leads to a 0.02 uncertainty in k_{12} for this system.

Roughly speaking, our data indicate that in hydrocarbon-fluorocarbon mixtures the interactions are about 10% weaker than those predicted by the geometric mean. Such behavior is consistent with that found for liquid mixtures of hydrocarbons and fluorocarbons. Scott⁴ used the solubility parameter theory to analyze

(10) L. S. Tee, S. Gotoh, and W. E. Stewart, *Ind. Eng. Chem., Fundam.*, **5**, 356 (1966).

(11) C. A. Eckert, H. Renon, and J. M. Prausnitz, *ibid.*, **6**, 58 (1967).

Table IV: Correction Factors ($1 - k_{12}$) to the Geometric Mean

System	Exptl	Eq 4 Hudson- McCoubrey	Eq 5 Hiza- Duncan
CF ₄ -CH ₄	0.94 ± 0.02	0.94	0.89
CF ₄ -C ₂ H ₆	0.89	0.94	0.82
CF ₄ -C ₄ H ₁₀	0.90	0.94	0.77
CF ₄ -C ₆ H ₁₄	0.92	0.93	0.75
C ₂ F ₆ -CH ₄	0.92	0.87	0.90
C ₂ F ₆ -C ₂ H ₆	0.88	0.88	0.82
C ₂ F ₆ -C ₄ H ₁₀	0.89	0.89	0.77
C ₂ F ₆ -C ₅ H ₁₂	0.90	0.88	0.76
C ₂ F ₆ -C ₆ H ₁₄	0.89	0.92	0.85
C ₄ F ₁₀ -CH ₄	0.92	0.83	0.94
C ₄ F ₁₀ -C ₂ H ₆	0.87	0.84	0.88
C ₄ F ₁₀ -C ₄ H ₁₀	0.88	0.86	0.83
C ₄ F ₁₀ -C ₆ H ₁₄	0.89	0.85	0.82
C ₆ F ₁₄ -C ₅ H ₁₂	0.88	0.87	0.84
C ₆ F ₁₄ -C ₆ H ₁₄	0.90	0.93	0.85

thermodynamic measurements on a number of fluorocarbon systems, and k_{12} values can be obtained from his results. The solubility parameter theory assumes a radial distribution function that, for liquid mixtures, is independent of composition. Moreover, it assumes that the potential energy of a pure liquid is equal to its energy of vaporization. These assumptions lead to an expression for the change in potential energy on mixing which can be written in terms of the cohesive energy densities (essentially the energy of vaporization per unit volume) of the pure components, C_{ii} , and an interaction energy parameter, C_{ij} . The departure of the interaction energy parameter from the geometric mean in liquid mixtures ($1 - \ell_{12}$) is given by¹²

$$\frac{C_{12}}{(C_{11}C_{22})^{1/2}} = \frac{\epsilon_{12}}{(\epsilon_{11}\epsilon_{22})^{1/2}} \frac{\bar{V}_{12}}{(\bar{V}_{11}\bar{V}_{22})^{1/2}} \quad (3)$$

where \bar{V} is the molar volume. From this equation, it can be seen that ℓ_{12} is equivalent to k_{12} only when the size parameters of the two components are equal; that is

$$1 - \ell_{12} = (1 - k_{12}) \frac{\bar{V}_{12}}{(\bar{V}_{11}\bar{V}_{22})^{1/2}}$$

Values of k_{12} obtained from the liquid data of Scott (using eq 3 and the molar critical volumes listed in I and II) are compared with k_{12} 's obtained from our gas-phase data in Figure 1. Although there is not a precise one-to-one correlation between our results and Scott's, there is a strong similarity between the two sets of values. Exact agreement would be fortuitous, however, because the solubility parameter theory used to treat the liquid data is relatively crude and is related to a two-parameter potential rather than the three-parameter formulation that we employ. It is most significant, however, that our results on a number of gaseous systems, free from the complications and approximations

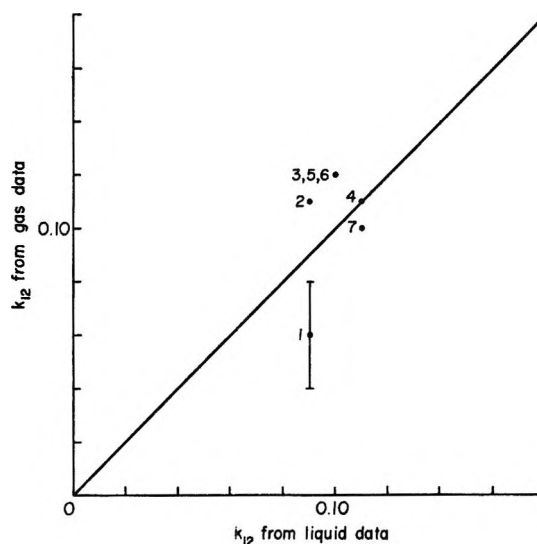


Figure 1. A comparison of k_{12} 's for gas and liquid mixtures studied in duplicate. The numbers indicate the following mixtures: 1, CF₄-CH₄; 2, CF₄-C₂H₆; 3, C₂F₆-C₂H₆; 4, C₃F₈-C₃H₈; 5, C₄F₁₀-C₄H₁₀; 6, C₆F₁₄-C₅H₁₂; 7, C₆F₁₄-C₆H₁₄.

of theories of liquid mixtures, show gross departures from the geometric mean for hydrocarbon-fluorocarbon mixtures. Our data, then, strongly support Scott's view that the anomalous behavior of hydrocarbon-fluorocarbon solutions is due to the inapplicability of the geometric mean.

Explanations for the Failure of the Geometric Mean. A number of explanations for the failure of the geometric mean have been discussed by Scott.⁴ Although no single cause can account for all the fluorocarbon systems that he considered, there are three factors that can be significant in weakening the unlike interaction: (1) noncentral forces, (2) large differences in ionization potentials between the components, and (3) large differences in size between the components.

It is clear from the virial coefficients of the pure components^{2b,3} that a central potential is not an adequate representation for hydrocarbon-fluorocarbon interactions. In the analysis of our data, however, we have taken account of noncentral interactions by the use of the Kihara potential, and this has not significantly diminished departures from the geometric mean.

Size and ionization potential differences can be treated in a semiempirical way by equating the r^{-6} attractive term in the potential to the London formula for the dispersion forces. A correction to the geometric mean derived in this way from the Lennard-Jones potential was proposed by Hudson and McCoubrey.¹³ If this approach is taken with the Kihara spherical-core potential, we obtain

(12) J. H. Hildebrand and R. L. Scott, "Regular Solutions," Prentice-Hall, Englewood Cliffs, N. J., 1962, p 97.

(13) G. H. Hudson and J. C. McCoubrey, *Trans. Faraday Soc.*, **56**, 761 (1960).

$$1 - k_{12} = \frac{2(I_1 I_2)^{1/2} (\rho^{\circ}_{11})^3 (\rho^{\circ}_{22})^3}{I_1 + I_2 (\rho^{\circ}_{12})^6} \quad (4)$$

where the subscripts denote the components and I is the first ionization potential. Values of the ionization potential and their sources are listed in Table V.

Table V: Ionization Potentials

Substance	I , eV	Ref	Substance	I , eV	Ref
CH ₄	13.16	d	C ₅ F ₁₂	15.8	c
C ₂ H ₆	11.65	a	C ₆ F ₁₄	15.4	c
C ₃ H ₈	11.08	a	C ₇ F ₁₆	~15.0	c
C ₄ H ₁₀	10.63	a	C(CH ₃) ₄	10.55	a
C ₆ H ₁₂	10.55	e	C ₆ H ₆	9.24	a
C ₆ H ₁₄	10.43	e	Ar	15.76	f
C ₇ H ₁₆	10.35	e	Kr	14.00	f
CF ₄	17.8	b	Xe	12.13	f
C ₂ F ₆	17.7	c	N ₂	15.51	f
C ₃ F ₈	16.4	c	SF ₆	19.3	g
C ₄ F ₁₀	16.3	c	CCl ₄	11.0	a

^a K. Watanabe, *J. Chem. Phys.*, **26**, 542 (1957). ^b L. Goldstein, *Ann. Phys.*, **9**, 723 (1938). ^c Calculated by method of T. M. Reed, *J. Phys. Chem.*, **59**, 425 (1955). ^d J. D. Morrison and A. J. C. Nicholson, *J. Chem. Phys.*, **20**, 1021 (1952). ^e R. E. Honig, *ibid.*, **16**, 105 (1948). ^f "Handbook of Chemistry and Physics," Chemical Rubber Publishing Co., Cleveland, Ohio, 1968. ^g Y. H. Dibeler and F. L. Mahler, *J. Res. Nat. Bur. Stand.*, **40**, 25 (1948).

Before making any comparisons between calculated and experimental values of k_{12} , we take a close look at eq 4. This equation differs substantially from the original Hudson-McCoubrey formulation because it is based on a three-parameter rather than a two-parameter potential. The constant ρ° is not simply related to σ , nor is $(\rho^{\circ})^3$ proportional to the critical volume; ρ° depends both on molecular size and shape. Thus the factor involving ρ° in eq 4 is a measure of differences in size and shape, not size alone.

The magnitude of the factor involving ionization potentials also needs to be considered. For the two substances in Table V that have the most disparate ionization potentials, CF₄ and C₆H₆, the first factor in eq 4 is 0.95. For all of the mixtures actually investigated, the ionization potential factor is equal to or greater than 0.98. In fact, the range of ionization potentials is very likely smaller than that shown in Table V. Of the fluorocarbons considered, it is only CF₄ for which the ionization potential has been measured,¹⁴ but this value is likely high by as much as 2 eV.¹⁵

The ionization potentials listed for the other fluorocarbons have been derived from the value for CF₄,¹⁶ and, as a result, these, too, are probably high. However, eq 4 puts the greatest emphasis on size/shape differences as the cause for departures from the geometric mean.

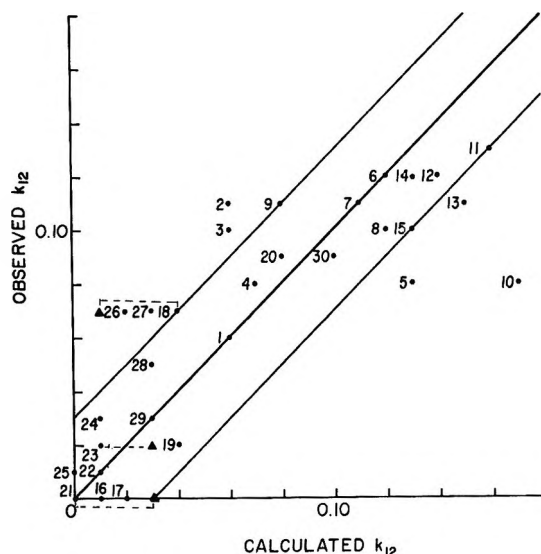


Figure 2. A comparison of observed k_{12} 's and those calculated by eq 4. The center line indicates perfect agreement and the outer lines indicate a 3% deviation of calculated values from observed k_{12} 's. The numbers indicate the specified mixtures; data are from this work unless otherwise referenced:

1, CF₄-CH₄; 2, CF₄-C₂H₆; 3, CF₄-C₄H₁₀; 4, CF₄-C₆H₁₄; 5, C₂F₆-CH₄; 6, C₂F₆-C₂H₆; 7, C₂F₆-C₄H₁₀; 8, C₂F₆-C₆H₁₂; 9, C₃F₈-C₃H₈; 10, C₄F₁₀-CH₄; 11, C₄F₁₀-C₂H₆; 12, C₄F₁₀-C₄H₁₀; 13, C₅F₁₂-C₆H₁₄; 14, C₆F₁₂-C₆H₁₂; 15, C₆F₁₄-C₆H₁₄; 16, Ar-CH₄ (M. A. Byrne, M. R. Jones, and L. A. K. Staveley, *Trans. Faraday Soc.*, **64** 1742 (1968)); 17, Ar-CF₄; 18, C₇F₁₆-C₇H₁₆; 19, C(CH₃)₄-CF₄; 20, SF₆-CH₄; 21, SF₆-CF₄, Ar-N₂; 22, CH₄-C₄H₁₀; 23, CH₄-C₆H₁₂; 24, N₂-Kr; 25, CH₄-C₆H₁₄; 26, C₂H₆-C₆H₁₄; 27, Ar-Kr; 28, CF₄-Kr; 29, C₇F₁₆-C₆H₆; 30, SF₆-C₃H₈. Triangular points connected by tielines for systems 18 (N₂-Xe), 21 (Ar-N₂), and 23 (N₂-Kr) indicate k_{12} 's calculated from parameters of ref 10.

Equation 4 has been used to calculate k_{12} 's for the 15 hydrocarbon-fluorocarbon systems studied, and the results are given in Table IV. There is fair agreement for the majority of systems, and it seems meaningful to test the validity of eq 4 for a variety of substances that differ in size/shape and/or ionization potential.

Figure 2 illustrates the agreement between observed and calculated values of $1 - k_{12}$ for a wide range of mixtures. First, we note that for the hydrocarbon and fluorocarbon mixtures studied in I and II the calculated k_{12} 's are at most 0.03. This is consistent with our observation that the geometric mean is a good representation of the interaction energy for these systems. We have included in the figure the four hydrocarbon mixtures for which size and ionization potential differences are largest (points number 22-25).

Systems containing globular molecules (e.g., SF₆-CH₄, C(CH₃)₄-CH₄, SF₆-CF₄) are of particular interest.

(14) L. Goldstein, *Ann. Phys.*, **9**, 723 (1938).

(15) R. W. Kiser and D. L. Holbrook, *J. Amer. Chem. Soc.*, **87**, 922 (1965).

(16) T. M. Reed, *J. Phys. Chem.*, **59**, 425 (1955).

Hamann, *et al.*,^{17,18} have concluded that the geometric mean fails in such systems when they are described in terms of either the Lennard-Jones 6-12 or 7-28 potentials. As shown in Figure 2 and in Table VI, as long as the values of ρ° are similar, the geometric mean is generally applicable, and where size/shape is significantly different the Hudson-McCoubrey type combination rule accounts reasonably well for the departures that are observed.

Table VI: Correction Factors ($1 - k_{12}$) to the Geometric Mean for Gaseous Systems Containing Pseudospherical Molecules

System	Ref	Exptl	Eq 4 Hudson- McCoubrey	Eq 5 Hiza- Duncan
Ar-CH ₄	<i>b</i>	1.00	0.99	0.94
	<i>d</i>	0.99		
Ar-CF ₄	<i>c</i>	1.00	0.975	0.97
C(CH ₃) ₄ -CH ₄	<i>a</i>	0.93 ± 0.01	0.96	0.94
C(CH ₃) ₄ -CF ₄	<i>c</i>	0.98 ± 0.02	0.96	0.94
SF ₆ -CF ₄	<i>c</i>	1.00	1.00	0.98
SF ₆ -CH ₄	<i>a</i>	0.91	0.92	0.84

^a Reference 18. ^b G. Thomaes and R. Van Steenwinkel, *Mol. Phys.*, **5**, 301 (1962). ^c This work. ^d M. A. Byrne, M. R. Jones, and L. A. K. Staveley, *Trans. Faraday Soc.*, **64**, 1742 (1968).

Even where the ionization potentials of the components are substantially different, *e.g.*, C₇F₁₆-CCl₄, C(CH₃)₄-CF₄, and C₇F₁₆-C₆H₆, the mixture behavior is closely approximated by the geometric mean as long as the sizes are about equal.

Finally, the importance of size differences is also evident in a comparison of the argon-methane and argon-perfluoromethane mixtures. The difference in ionization potentials between argon and methane is much greater than that between argon and perfluoromethane, yet the geometric mean works very well in both cases.

The correlation tends to be poor for some systems that include molecules such as nitrogen and carbon dioxide which have relatively large quadrupole moments. This is, in part, to be expected. When potential parameters are obtained for these substances from observed physical properties, the quadrupole-quadrupole contribution can be explicitly evaluated, or it can be grouped with the other angular-dependent terms. In principle, it is preferable to use potential parameters obtained by the former procedure to compute the interaction between quadrupolar and nonpolar molecules. For such systems there is, of course, no quadrupole-quadrupole interaction and the use of parameters that include quadrupole contributions can lead to apparent departures from the geometric mean.

To illustrate this we have computed two sets of k_{12} values for nitrogen with Ar, Kr, and Xe. One set is

based on the Kihara parameters for nitrogen obtained by Tee, *et al.*,¹⁰ who did not subtract the quadrupole contribution. Prausnitz and Myers,¹⁹ on the other hand, did subtract the quadrupole contribution, and their parameters have been used to compute the other set of values. In every case, the Prausnitz and Myer parameters lead to better agreement between observed and calculated k_{12} 's (see Figure 2).

Although these results suggest that it is possible to account for discrepancies between calculated and observed values of k_{12} , it is difficult to make quantitative calculations. There are few substances for which the quadrupole contribution can be evaluated with accuracy and for many systems the quadrupole-induced dipole interaction may well compensate for the loss of the quadrupole-quadrupole term.

There are several systems for which eq 4 is totally inadequate. It cannot account for the very large departures from the geometric mean reported for a number of mixtures containing helium or neon.²⁰ For example, in the case of helium-xenon, $k_{12} = 0.40$ and for helium-argon, $k_{12} = 0.22$, but the calculated values are only 0.11 and 0.04, respectively. Such radical departures from the geometric mean have also been obtained from analyses of transport data.²¹

Gordon²² has calculated values of C_6 , the coefficient of the r^{-6} term in the London forces, for all the rare gases and their mixtures. Where data exist, his results are in excellent agreement with coefficients obtained from studies of the *long-range* interaction from scattering and transport measurements. In none of the rare gas mixtures does C_6 depart radically from the geometric mean of the coefficients of the pure components. This suggests that one must look to the repulsive interaction or the detailed shape of the potential well to explain the large observed values of k_{12} for helium and neon mixtures.

Sikora²³ has derived a modified combining rule that is based in part on a model for the repulsive interaction. His formula does lead to large k_{12} values for helium and neon systems, but it gives poor results for mixtures containing another quantum gas, hydrogen. For the heavier rare gases and methane, Sikora's equation fits the data about as well as eq 4; but in its present form it cannot be applied to more complex molecules.

A totally empirical approach to correlating departures for the geometric mean has been proposed by

(17) S. D. Hamann, J. A. Lambert, and W. J. McManamey, *Aust. J. Chem.*, **7**, 1 (1954).

(18) S. D. Hamann, J. A. Lambert, and R. B. Thomas, *ibid.*, **8**, 149 (1955).

(19) J. M. Prausnitz and A. L. Myers, *AIChE J.*, **9**, 5 (1963).

(20) M. J. Hiza and A. G. Duncan, *ibid.*, **16**, 733 (1970).

(21) B. K. Annis, A. E. Humphreys, and E. A. Mason, *Phys. Fluids*, **11**, 2122 (1968).

(22) R. G. Gordon, *J. Chem. Phys.*, **48**, 3929 (1968).

(23) P. T. Sikora, *Proc. Phys. Soc. London (At. Mol. Phys.)*, **3**, 1475 (1970).

Hiza and Duncan.²⁰ They suggested the formula

$$k_{12} = 0.17(I_1 - I_2)^{1/2} \ln(I_1/I_2) \quad (5)$$

where component 1 has the higher ionization potential. This correlation is excellent for the binary systems containing hydrogen, helium, or neon with three different light hydrocarbons which they studied, and excellent agreement is obtained with other small and approximately spherical molecules. That this correlation is less adequate for mixtures containing larger, nonspherical molecules is indicated in the comparisons of Tables IV and VI where the Hiza-Duncan predictions consistently worsen as the chain lengths of the components increase.

It is obvious that eq 5 is very sensitive to the values of the ionization potentials, so a definitive test of its limitations is not possible with mixtures containing fluorocarbons. However, even if the ionization potential of CF_4 were 15.8 eV, eq 5 still shows less satisfactory agreement with values of k_{12} for these systems than eq 4.

Conclusion

The large departures from the geometric mean observed for fluorocarbon-hydrocarbon mixtures are shown to be the result of large departures from the geometric mean combination of the energy parameters. These departures are very likely due to large size differences between the components.

No completely acceptable solution has been found to the problem of obtaining interaction potential parameters from the properties of pure substances, but the modified Hudson-McCoubrey relation is generally better than the original form utilizing critical volumes. When no experimental values of k_{12} are available, the relation is useful as a first approximation—particularly to the properties of gas mixtures. However, it cannot be relied upon to give values sufficiently good to calculate accurately the properties of liquid mixtures.

Acknowledgment. We gratefully acknowledge that this work was supported in part by Allied Chemical Corporation.

Study of the Adsorption of Insoluble and Sparingly Soluble Vapors at the Gas-Liquid Interface of Water by Gas Chromatography

by Barry L. Karger,* Reynaldo C. Castells, Peter A. Sewell, and Arleigh Hartkopf

Department of Chemistry, Northeastern University, Boston, Massachusetts 02115 (Received February 4, 1971)

Publication costs assisted by the Office of Naval Research

This paper is a continuation of the study of the interfacial properties of water by gas chromatography. Adsorption characteristics at zero surface coverage of a large number of solutes at the gas-liquid interface of water are presented. In all cases of relatively nonpolar solutes, the differential heat of adsorption is found to be less negative than the heat of liquefaction, indicating the gas-liquid interface of water as a low energy surface. For *n*-propyl ether the heat of adsorption is 4 kcal/mol more negative than the heat of liquefaction, strongly suggesting hydrogen bond formation between the ethereal oxygen and the hydrogens from the water surface of the liquid. We have also studied the infinitely dilute solubility characteristics of several nonelectrolytes in the thin layers of water coated on wide pore diameter adsorbents. From layer thickness of ~ 15 up to 2000 Å, the solubility remains constant. Comparison with literature values, where available, strongly suggests that the water coating the adsorbent is quite similar to bulk water. Finally some preliminary adsorption and "sorption" isotherms, determined by gas chromatography, are presented.

Introduction

In a previous paper the use of gas chromatography as a tool for the measurement of the adsorption characteristics of insoluble vapors on water was illustrated.¹ In this method, water is coated on a porous solid and the carrier gas, helium, is presaturated with water at the column temperature, prior to its entrance into the

column. A steady-state condition is achieved with 2% reproducibility in retention volume. Thermodynamic functions of adsorption for various solutes can then be readily determined from a study of retention characteristics.

(1) B. L. Karger, P. A. Sewell, R. C. Castells, and A. Hartkopf, *J. Colloid Interface Sci.*, **35**, 328 (1971).

Our previous results indicated that water is a low energy surface in which for nonpolar vapors the differential heat of adsorption at zero surface coverage is less negative than the heat of liquefaction. This is in disagreement with the data of Ottewill² and Hauxwell and Ottewill,^{3,4} who extrapolated isotherms to zero coverage and found the heat of adsorption to be as much as 6 kcal/mol more negative than the heat of liquefaction. Our data also bring into serious question the picture of the adsorption process presented by Adamson.^{5,6} Here pockets of low entropy domains are postulated to form on the water surface when the adsorbate comes in contact with the water and the adsorbate then occupies these domains.

For aromatic hydrocarbons it was found that both adsorption and partition simultaneously occurred in the column. By proper isolation of the partition mechanism,¹ we were able to measure partition coefficients and heats of solution in water at essentially infinite dilution. Our results indicated that the solubility in a water layer of 50 Å (estimated) coated on porous glass was the same as for a 2000-Å layer. Because of the lack of good bulk water solubility data for the aromatic hydrocarbons at low partial pressures, a direct comparison was not possible; however, the partition coefficients were only 15% different from the values estimated making use of the vapor pressures and the saturation solubilities of the hydrocarbons in bulk water. This point is investigated further in this work.

In this paper we extend our gas chromatographic study to moderately polar solutes in order to examine further the conclusions of our previous paper. Both partition and adsorption can extensively contribute to the retention process. We show for the first time the probable existence of hydrogen bonding between the water surface and an electron-donating adsorbate. In addition to adsorption measurements at zero surface coverage, we present some initial adsorption isotherm measurements by gas chromatography. Finally, the infinitely dilute solution measurements in thin layers of water are found to agree with those obtained in bulk water, where adequate literature data are available.

Experimental Section

Apparatus. The apparatus used was the same as previously described,¹ except that for the isotherm determinations a heated injection port was used. The injection port temperature was maintained at about 70°. This temperature was arrived at experimentally, being the lowest temperature at which the liquid samples used in the isotherm determination could be injected without causing peak distortion due to slow volatilization.

Technique. (i) *Columns.* Chromosorb P (Johns-Manville), specific surface area $\sim 4 \text{ m}^2 \text{ g}^{-1}$, was used in most cases rather than the higher surface area Spherosil (Pechiney St. Gobain, France) $29 \text{ m}^2 \text{ g}^{-1}$, used in the

earlier study. This was to reduce the surface area/liquid volume ratio, which, as well as reducing the retention time for the less volatile solutes, also enhanced the contribution from solution to the retention mechanism.

The nature of the stationary phase and column packing preparation have been reported previously.¹

(ii) *Solutes.* The following additional solutes have been studied: chlorobenzene ($\text{C}_6\text{H}_5\text{Cl}$), fluorobenzene ($\text{C}_6\text{H}_5\text{F}$), 1,2-dichloroethane ($\text{CH}_2\text{ClCH}_2\text{Cl}$), *n*-propyl ether ($\text{C}_3\text{H}_7)_2\text{O}$, and methyl formate (MeFor). Samples were obtained from Fischer Scientific, N. J., and were used as received. Extended data were obtained for some of the solutes previously studied, namely *n*-heptane (*n*-C₇), *n*-octane (*n*-C₈), *n*-nonane (*n*-C₉), isooctane (2,2,4-TMC₈), benzene (C_6H_6), and toluene ($\text{C}_6\text{H}_5\text{CH}_3$).

Theory

The theory of the determination of the adsorption coefficient K_A and partition coefficient K_L , as well as the corresponding sorption heats for the two processes, has been discussed previously.¹

When partition and adsorption simultaneously occur, it is necessary to relate retention to a standard substance which undergoes only adsorption in the column in order to isolate one mechanism from the other. Since *n*-octane was eluted too rapidly from the water-Chromosorb P columns to use as the standard as previously, *n*-nonane was run as standard and the surface area value for the 20% water-coated Chromosorb P column was selected as the standard surface area and was estimated to be $1.0 \text{ m}^2/\text{g}$.⁷ The retention equation may then be written as

$$V_N^\circ = K_A \frac{(A_L)^{20}}{r} + K_L V_L^\circ \quad (1)$$

or

$$r V_N^\circ = K_A (A_L)^{20} + r K_L V_L^\circ \quad (2)$$

where $r = (A_L)^{20}/(A_L)^x$ and $(A_L)^{20}$ and $(A_L)^x$ are the liquid surface areas at 20 and $X\%$ liquid loading, respectively, and are obtained from the ratio of the retention volumes per gram of packing of *n*-C₉ on the 20 and $X\%$ columns. In eq 1 and 2, V_N° = net retention volume per gram of packing, V_L° = volume of water stationary phase per gram of packing, and K_A and K_L are the adsorption and partition coefficients, respectively.

(2) R. H. Ottewill, Ph.D. Thesis, University of London, 1951.

(3) F. Hauxwell and R. H. Ottewill, *J. Colloid Interface Sci.*, **28**, 514 (1968).

(4) F. Hauxwell and R. H. Ottewill, *ibid.*, **34**, 473 (1970).

(5) A. W. Adamson, L. M. Dormant, and M. Orem, *ibid.*, **25**, 206 (1967).

(6) M. W. Orem and A. W. Adamson, *ibid.*, **31**, 278 (1969).

(7) D. E. Martire, R. C. Pecsok, and J. H. Purnell, *Trans. Faraday Soc.*, **61**, 2496 (1965).

Isotherm Determination. The elution by characteristic point method (ECP) proposed by Cremer and Huber,⁸ Huber and Keulemans,⁹ and modified by Knozinger and Spannheimer¹⁰ was used to determine the sorption isotherm, *i.e.*, the plot of the amount sorbed (a) per gram of packing, or per cm² of surface area, *vs.* relative pressure (P/P^0) at constant temperature T . These quantities are given by

$$a = \frac{nS_p}{AW} \int_0^{P'} \lambda dp \quad (3)$$

$$P' = S_p P = \frac{jAF_m P}{nRT_m x} \quad (4)$$

where n is the number of moles of solute, T_m is the meter temperature and F_m is the carrier gas flow rate, j is the compressibility factor, x is the recorder chart speed, A is the peak area, W is the weight of sorbent/g of packing (or the surface area in cm²), S_p is the detector sensitivity (equal to h/P , where h = peak height), and λ is given by $x t_r$, where t_r is the retention time.

The integration was carried out graphically from the chromatogram by measuring the area from the inert peak to the peak maximum within the limits zero to P' . The area was determined using a planimeter. A discussion will be given in a later section on the corrections to these equations, *e.g.*, for diffusion and sorption.

Results and Discussion

Since a discrepancy exists between the gas chromatographic results and those obtained by extrapolation of static measurements, it was decided to examine in more detail several of the parameters in the gas chromatographic experiment which could result in an incorrect interpretation of the mechanism of retention. These parameters included (a) method of solid support preparation, (b) sample size, and (c) extension to very small percentages of H₂O on the solid support.

Solid Support Preparation. The influence of the underlying solid support on which the water is coated must be minimal for the thermodynamic functions to be those of gas-liquid adsorption and partition. Circumstantial evidence was given in the previous paper¹ that this influence was negligible in that adsorption coefficients and heats of adsorption were identical on the porous glass support-Spherosil and the diatomaceous earth support-Chromosorb P. In addition plots of rV_n° *vs.* rV_L° for aromatic hydrocarbons were found to fall on a single straight line for a given solute at a given temperature for both supports (after correction for the differences in bulk density).

A more direct test of this influence is to examine the effect of the washing procedure of a given support on the thermodynamic functions.¹¹ In the previous paper, we washed the support with concentrated acid for 4 hr, followed by doubly distilled H₂O rinsing until a neutral pH was reached. During the procedure, a

vacuum was applied for 10 min to remove occluded air. After washing, the support was dried at 120° for 24 hr.

A sample of acid-washed and dried Spherosil was saturated with concentrated ammonia, degassed for 15 min, and then allowed to stand for 1 hr. The sample was then decanted, rinsed several times with doubly distilled H₂O, and put in a rotary evaporator at 30° to pull off the ammonia gas. The complete removal of the ammonia was found when pH 7 was reached for the water rinses of this sample. The Spherosil was then dried in the usual way.

Two columns of this ammonia wash were constructed: 12 and 24% w/w H₂O on Spherosil. The test solutes were *n*-alkanes—pentane through octane, benzene, and toluene. The adsorption and partition coefficients and heats of adsorption and partition (where applicable) were within experimental error the same as those obtained with the acid washed Spherosil support. Thus, the type of washing procedure does not influence the thermodynamic parameters. This result strengthens the argument that the influence of the solid support is minimal.

Sample Size. If the thermodynamic parameters are to represent equilibrium adsorption at zero surface coverage and partition at infinite dilution, a necessary (but not sufficient) condition is that symmetrical peaks be obtained and that the capacity factor be independent of sample size. If a dependence on sample size resulted, this would indicate, among other effects, either poor injection or chromatographic operation in a region in which Henry's law does not hold.

The conditions for the study of the influence of sample size were as follows: column, 21% w/w H₂O on Chromosorb P, $T = 12.5^\circ$; solutes, *n*-C₉ and C₆H₅Cl. For *n*-C₉ a single mechanism of retention exists—interfacial adsorption—whereas for C₆H₅Cl both adsorption and partition simultaneously occur. In both cases, retention was found to be independent of sample size and the peaks remained Gaussian in shape over the range of 1–50- μ l vapor samples. Of course, at higher sample amounts asymmetrical peaks occur, and the isotherm becomes nonlinear (see later section on isotherm determinations).

Since less than 10- μ l vapor injections are routinely used, the adsorption and partition measurements are made in the Henry's law region. (A 10- μ l vapor sample is of the order of 10⁻⁷ g.)

Extension of Low Liquid Loadings. In the previous paper,¹ data were obtained over a range of liquid loadings from 40% H₂O to 9% water ($\sim 50 \text{ \AA}$ layer, assuming uniform coating of the support) on Spherosil.

(8) E. Cremer and H. Huber, *Angew. Chem.*, **73**, 461 (1961).

(9) J. F. K. Huber and A. I. M. Keulemans, "Gas Chromatography 1962," M. van Swaay, Ed., Butterworths, London, 1962.

(10) H. Knozinger and H. Spannheimer, *J. Chromatogr.*, **16**, 1 (1964).

(11) W. Drost-Hansen, private communication.

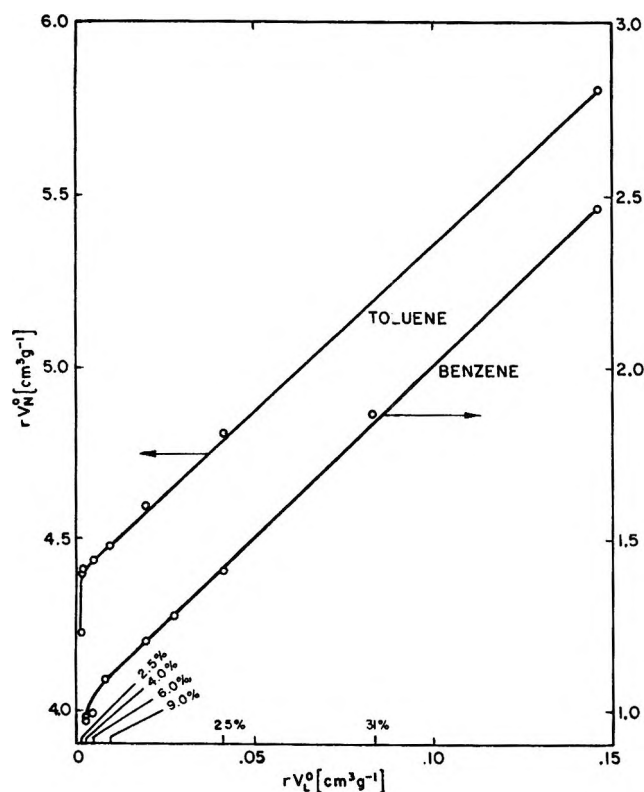


Figure 1. Corrected net retention volume per gram of packing vs. corrected stationary phase volume per gram of packing for toluene and benzene at $T = 12.5^\circ$. Support is Porasil D, and the various % w/w loadings of water are indicated on the plot. The standard solute is *n*-octane. See text for discussion of correction factor.

This has now been extended to lighter loadings. Figure 1 shows a plot of rV_N^0 vs. rV_L^0 for toluene and benzene down to a liquid loading of 2.5%. The lowest liquid loadings (2.2 and 2.6%) were obtained by saturating the column with water vapor at two different temperatures (6 and 16°). As seen from Figure 1, the plot starts becoming nonlinear at a liquid loading of 5% ($\sim 15 \text{ \AA}$ for a uniform layer); however, as seen from Table I the heats of sorption are reasonably constant down to a loading of 3.8%. The increase in ΔH below 3.8% may be the result of the coating procedure. Alternatively it may be due to either a change in the liquid structure at the lowest loadings or more likely to uncoated Spherosil contributing to the sorption process.

Table I: Heats of Sorption as a Function of Liquid Loading; Solid Support, Spherosil

Solute	% loading of H ₂ O			
	2.2	2.6	3.8	6.2
<i>n</i> -C ₇	10.2	10.3	7.6	7.5
<i>n</i> -C ₈	11.6	11.8	8.8	8.5
<i>i</i> -C ₈	10.9	11.0	8.0	7.8
C ₆ H ₅ H	9.3	9.3	7.7	7.6
C ₆ H ₅ CH ₃	10.8	10.9	8.9	8.7

It is not possible to ascertain the reason for the difference in ΔH for the low loaded columns without further experimentation.

It is surprising that K_L and ΔH (at infinite dilution) remain constant down to low loadings. One might anticipate that the structure of the water in the thin layers would be altered by the solid support.¹²⁻¹⁴ It is possible that solubility is not a good means for detecting subtle structural changes, since the parameter is essentially a gross macroscopic property. Also it may be that the water does not coat uniformly at the low loadings, so that domains of heavy loading occur.

These arguments, however, are unlikely to be correct in the system under study. First, the types of structural changes suggested by other authors ought to result in detectable changes in solubility at infinite dilution.¹² In addition, if puddling of the water occurred to any great extent, regions of either exposed support or liquid modified support would result. These regions would markedly affect the K_L values, as possibly can be seen for the very lightly loaded columns of Figure 1 and Table I. Finally, it must be kept in mind that the supports possess very wide pore diameters, e.g., Spherosil $\sim 770 \text{ \AA}$ and Chromosorb P $\sim 10^4 \text{ \AA}$. Nmr measurements of modified water are often performed on supports with pore sizes, for example, of 10 \AA ,¹⁵ a factor of roughly 100 smaller than in this paper. Of course, it is another question whether the water coating Spherosil or Chromosorb P is indeed bulk water. To examine this it is necessary to compare the solubility data obtained by the gas chromatographic experiment with static measurements at very low concentration. This will be discussed in a later section of this paper.

Polar Solutes. We have extended our study to solutes which are somewhat polar and thus are sparingly soluble in water. With such species mixed mechanisms of retention are expected.

Figures 2 and 3 are plots of the retention volume per gram of packing vs. % H₂O coated on Chromosorb P at 12.5° for the five polar solutes and *n*-C₉. For the *n*-alkane, we observe the expected trend of decreasing retention volume with increasing liquid loading. For (CH₂Cl)₂ and MeFor, the partition mechanism is clearly seen in the increase in V_N^0 with loading. For chlorobenzene and fluorobenzene, partition and adsorption exist to an extent that the retention volume is fairly independent of liquid loading. This behavior is unusual in gas chromatography. On the other hand, *n*-Pr₂O shows a marked decrease in V_N^0 with liquid loading, indicative of strong interfacial adsorption.

Table II presents the per cent adsorption and partition for the five polar solutes at two liquid loadings, 12

(12) W. Drost-Hansen, *Ind. Eng. Chem.*, **61**, (11), 10 (1969).

(13) J. C. Henniker, *Rev. Mod. Phys.*, **21**, 322 (1949).

(14) J. A. Schuffe and N. Yu, *J. Colloid Interface Sci.*, **26**, 395 (1988).

(15) H. A. Resing, *Advan. Mol. Relaxation Processes*, **1**, 109 (1968).

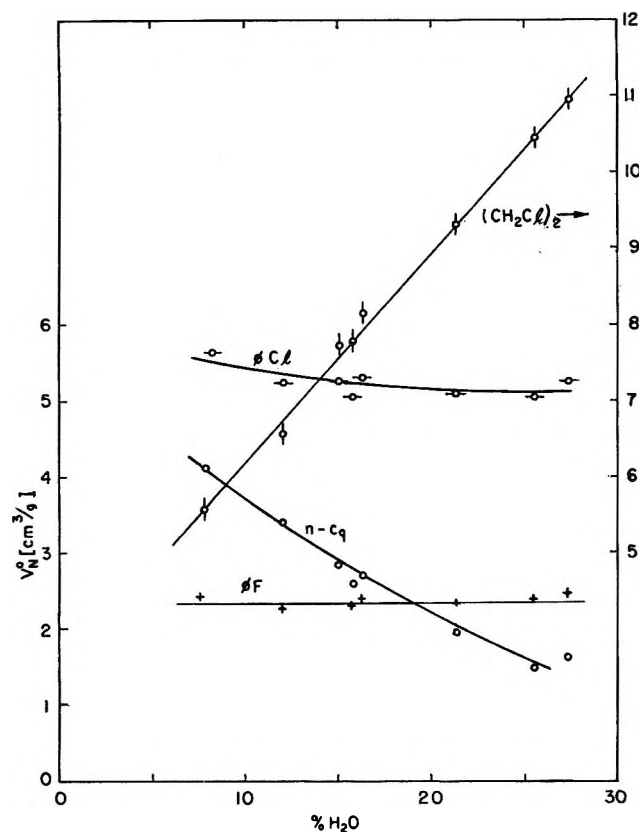


Figure 2. Net retention volume per gram of packing vs. % H₂O (w/w) on Chromosorb P; $T = 12.5^\circ$; $n\text{-C}_9 = n\text{-nonane}$; $\text{C}_6\text{H}_5\text{F} = \text{fluorobenzene}$; and $\text{C}_6\text{H}_5\text{Cl} = \text{chlorobenzene}$.

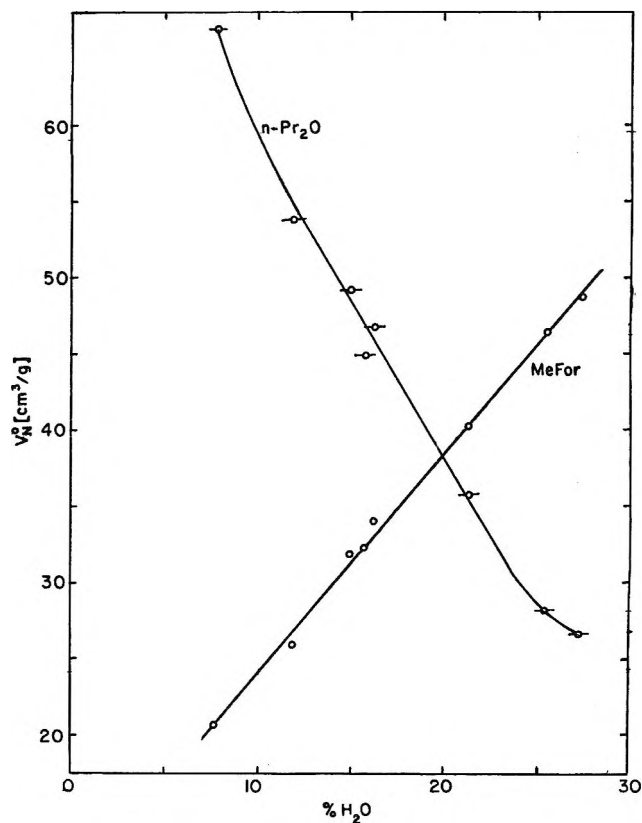


Figure 3. Net retention volume per gram of packing vs. % H₂O (w/w) on Chromosorb P; $T = 12.5^\circ$; $n\text{-Pr}_2\text{O} = n\text{-propyl ether}$; MeFor = methyl formate.

and 26%. The estimation is made from the equation

$$V_N^\circ = K_A A_L^\circ + K_L V_L^\circ \quad (5)$$

where A_L° is the interfacial surface area per gram of packing. K_A and K_L were determined by procedures described in the previous paper¹ and will be discussed again shortly. A_L° was estimated by assuming that the area of a 20% w/w H₂O on Chromosorb P column was 1 m²/g and using the r value for $n\text{-C}_9$. It can be seen that the extent of adsorption decreases in all cases for the more heavily loaded column. In addition, the order of per cent adsorption on each column for the five solutes agrees with the previous interpretation of Figures 2 and 3.

From an analytical point of view, mixed mechanisms of retention offer an attractive method for controlling

selectivity by liquid loading. For example, the relative retention value, α , for $n\text{-Pr}_2\text{O}/\text{MeFor}$ at 10% H₂O is 2.4, while at 25% H₂O it is 0.6. This represents a change in the free energy difference of distribution for the two solutes of 800 cal/mol. Rogozinski and Kaufman have also taken note of the value of mixed mechanisms for separation purposes.¹⁶

To isolate the two mechanisms of retention, eq 2 must be used. Figure 4 shows one such plot of rV_N° vs. rV_L° for $(\text{CH}_2\text{Cl})_2$ at five temperatures. The slope of each line is K_L , and from its temperature dependence the heat of solution may be obtained. Once K_L is known, K_A can be obtained from eq 5, with the estimation of A_L° as previously given. These results are discussed in the next several sections.

Adsorption Parameters. Table III presents the results for the thermodynamic functions of adsorption at zero surface coverage. For purposes of clarity, data on some compounds presented in the previous paper¹ are also included. For K_A (and thus ΔG_A°), the Kemball-Rideal standard state was chosen,¹⁷ and the liquid surface areas for the different columns were found as already noted. The error in reproducibility in the

Table II: Per Cent Interfacial Adsorption at Different Loadings of Water on Chromosorb P, $T = 12.5^\circ$

Solute	12% (w/w)	26% (w/w)
$\text{C}_6\text{H}_5\text{F}$	64	28
$\text{C}_6\text{H}_5\text{Cl}$	69	40
$(\text{CH}_2\text{Cl})_2$	34	11
$n\text{-Pr}_2\text{O}$	96	82
MeFor	22	7

(16) M. Rogozinski and I. Kaufman, *J. Gas Chromatogr.*, **4**, 413 (1966).

(17) C. Kemball and E. K. Rideal, *Proc. Roy. Soc., Sec. A*, **187**, 53 (1946).

Table III: Thermodynamic Functions of Adsorption of Vapors on Water at 12.5°

Solute	$K_A \times 10^{-4}$, cm	$-\Delta G_A^\circ$, kcal/mol	$-\Delta H_A^\circ$, kcal/mol	$-\Delta S_A^\circ$, cal/(mol deg)	$-\Delta H_L^\circ$, ^a kcal/mol
<i>n</i> -C ₅	0.09	2.8	5.7	9	6.4
<i>n</i> -C ₆	0.2	3.3	6.6	11	7.5
<i>n</i> -C ₇	0.4	3.7	7.5	13	8.7
<i>n</i> -C ₈	1.0	4.2	8.5	15	9.9
<i>n</i> -C ₉	2.3	4.7	9.5	17	11.1
<i>n</i> -C ₁₀	5.3	5.2	10.7	19	12.3
2-MeC ₇	0.9	4.2	8.3	15	9.5
2,4-DMeC ₆	0.7	4.0	8.0	14	9.0
2,2,4-TMC ₅	0.6	3.9	7.7	13	8.4
<i>c</i> -C ₇	0.5	3.8	7.5	13	9.2
<i>c</i> -C ₈	1.1	4.3	8.5	15	10.4
C ₆ H ₅ H	0.9	4.2	7.5	12	8.1
C ₆ H ₅ CH ₃	2.5	4.7	8.9	15	9.1
C ₆ H ₅ C ₂ H ₅	5.8	5.2	9.9	16	10.1
C ₆ H ₅ F	1.1	4.2	7.8	12	8.4
C ₆ H ₅ Cl	2.6	4.7	8.4	13	9.6
(CH ₂ Cl) ₂	1.7	4.5	7.8	12	8.5
<i>n</i> -Pr ₂ O	36.3	6.3	12.8	22	8.7
MeFor	4.7	5.1	7.8	9	6.2

^a Data obtained from J. D. Cop and G. Pilcher, "Thermochemistry of Organic and Organometallic Compounds," Academic Press, New York, N. Y., 1970.

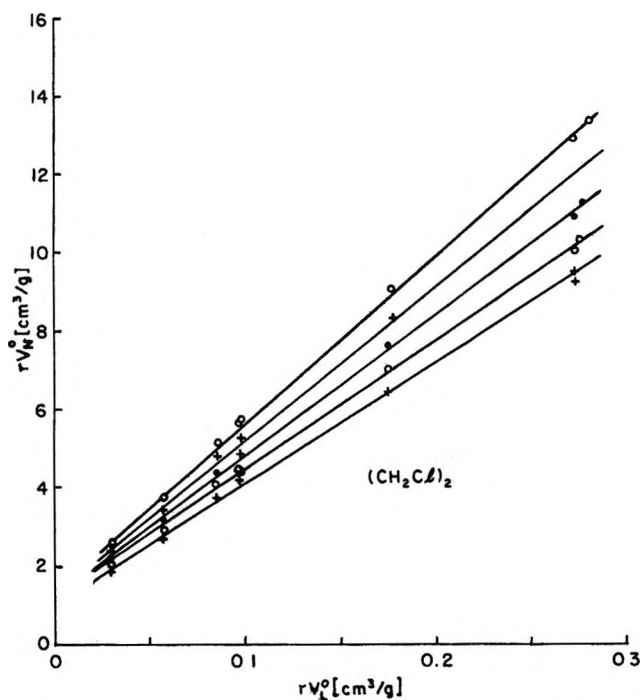


Figure 4. Corrected net retention volume per gram of packing vs. corrected stationary phase volume per gram of packing for dichloroethane; $T = 6, 7.5, 10, 12.5,$ and 16° ; support is Chromosorb P. The standard solute is *n*-nonane. See text for discussion of correction factor.

differential heat of adsorption, ΔH_A° , is 2% from column to column (*i.e.*, ± 0.2 kcal/mol). Also included in Table III are the heats of liquefaction for the various solutes.

The first point of the table is that for all solutes

except *n*-Pr₂O and MeFor, the heat of adsorption is less negative than the heat of liquefaction. This agrees with the results of our previous paper. ΔH_A° was found to be independent of liquid loading and solid support and was reproduced by three different workers. We now feel confident to state that at zero surface coverage, nonpolar vapors have a less negative heat of adsorption than ΔH_L° , contrary to the results of Ottewill² and Hauxwell and Ottewill.^{3,4} It is to be noted that ΔS_A° is also less negative (relative to ref 3, 4) in Table III, with a resultant ΔG_A° in fairly good agreement for the two studies. The type of measurement by Hauxwell and Ottewill was such that ΔG_A° was the most reliably determined function. We are not yet in a position to comment on the results of Orem and Adamson,⁵ who purported to find isosteric heats of adsorption more negative than ΔH_L° at low surface coverages for nonpolar vapors on the surface of ice down to -35° ; however, we are now in the process of determining the heats of adsorption of insoluble vapors on ice by gas chromatography.

It is clear that the liquid surface of water is a low energy surface for nonpolar vapors. It should be pointed out that the anti-Langmuir adsorption isotherm shape found by Hauxwell and Ottewill^{3,4} would also agree with this conclusion. It must therefore be concluded that the perturbation model of Adamson^{5,6} when an adsorbate comes in contact with the liquid water surface is unsupported by the results in Table III. Not only are the heats of adsorption too low, but the entropies of adsorption are also too low to account for trough formation.

n-Pr₂O and MeFor represent interesting exceptions

Table IV: Thermodynamic Functions of Partition of Vapors in Water at $T = 12.5^\circ$

Solute	K_L		$-\Delta H_S^\circ$, kcal/mol		$-\Delta G_S^\circ$, kcal/mol	$-\Delta S_S^\circ$, kcal/(mol deg)
	This work	Lit.	This work	Lit.		
C_6H_5H	9.6	7.8 ^a	8.4	7.8 ^a	1.3	25
$C_6H_5CH_3$	9.7	8.3 ^a	9.1	8.9 ^a	1.3	27
$C_6H_5C_2H_5$	9.6	7.9 ^a	12.1	10.0 ^a	1.3	38
C_6H_5F	6.8; (3.0 ^c)	3.2 ^c	8.1	...	1.1	25
C_6H_5Cl	13.5; (5.3 ^c)	5.1 ^c	9.2	...	1.5	27
$(CH_2Cl)_2$	36	36 ^b	8.2	7.8 ^b	2.0	22
MeFor	170	...	7.5	...	2.9	16
$n-Pr_2O$	20	...	17.6	...	1.7	56

^a The values of K_L were calculated from the solubility of the hydrocarbons in water (R. L. Bohon and W. F. Claussen, *J. Amer. Chem. Soc.*, **73**, 157 (1951), and the respective vapor pressures (R. R. Dreisbach, *Advan. Chem. Ser.*, **No. 15** (1955)). ^b Solubilities from A. Siedell, "Solubilities of Organic Compounds," Vol. II, 3rd ed, Van Nostrand, Princeton, N. J., 1941; vapor pressure from R. R. Dreisbach, *Advan. Chem. Ser.*, **No. 15** (1955); **No. 22** (1962). ^c References as b; comparison is made between the K_L calculated from the solubilities and vapor pressures at 30° and the K_L obtained by extrapolating the chromatographic data to 30° (i.e., value of K_L in parentheses is at 30°).

to the trends in Table III for the other solutes. For $n-Pr_2O$ the differential heat of adsorption at zero coverage is 4 kcal/mol more negative than the heat of liquefaction. In addition the entropy of adsorption is much more negative than expected from the simple loss of one translational degree of freedom.³ This points to a strong interaction between $n-Pr_2O$ and the water surface, and it is reasonable to assume that this interaction is hydrogen bonding between the lone-pair electrons on the ethereal oxygen and the hydrogens of the water molecule. This is the first evidence for the existence of hydrogen bonding in the adsorption on the liquid water surface. In addition, this result may indirectly support the theoretical predictions of Fletcher¹⁸ and some surface potential measurements^{19,20} that the hydrogens are directed toward the vapor phase on the water surface.

For MeFor, the more negative ΔH_A° , relative to ΔH_L° , may also be due to some hydrogen bonding between the electron-rich regions of the ester and the water surface. However, the relatively small entropy of adsorption and the fact that ΔH_A° is only 1.6 kcal/mol more negative than ΔH_L° may mean that this interaction is not great.

Returning to the other solutes in Table III, we first note that no specific interactions appear to occur between C_6H_5F or C_6H_5Cl and the water surface in view of the ΔH_A° values being less negative than the ΔH_L° values. The K_A and ΔH_A° values for these two adsorbates are in the order of increasing polarizability. ΔH_A° is also seen to become more negative and K_A larger with increased polarizability for the series $n-C_5-n-C_{10}$, $C_6H_5H-C_6H_5C_2H_5$, and $c-C_7-c-C_8$. For the n -alkane series ΔH_A° increases roughly at the rate of -1 kcal/mol and ΔS_A° at -2 eu for each additional methylene group. Also, ΔH_A° becomes less negative and K_A decreases in an isomeric series as branching increases (e.g., $n-C_3, 2-MeC_7$, $2,4-DMeC_6$, and $2,2,4-$

TMC_5). Finally, it is to be noted that the adsorption coefficients are essentially equal for the cycloalkanes ($c-C_7$ and $c-C_8$) and their straight chain analogs ($n-C_7$ and $n-C_8$), even though the ΔH_L° values are more negative for the cycloalkanes. This is in the expected direction for adsorption.²¹

Solution Parameters. Values for the partition coefficients K_L and heats of solution ΔH_S° obtained in the present work at 12.5° on Chromosorb P, together with values from the literature, are given in Table IV. Also included in this table are the free energies ΔG_S° and entropies ΔS_S° of solution. The enthalpies of solution of C_6H_5F , C_6H_5H , and C_6H_5Cl obtained in this work follow the trend in polarizability of these molecules, as do C_6H_5H , $C_6H_5CH_3$, and $C_6H_5C_2H_5$. The high negative enthalpy and entropy of solution of $n-Pr_2O$ are an indication of hydrogen bonding in this system. The very high solubility of MeFor is reflected in the relatively low entropy of solution, suggesting that in spite of the possibility of hydrogen bonding, there is a high degree of mobility of the molecule in the pseudo-liquid lattice of water.

In comparing K_L and ΔH_S° values from the literature with those in this work, it must be remembered that if the literature values are obtained from measurements at finite concentration, agreement will only be expected with the results obtained at infinite dilution, if Henry's law is applicable throughout the concentration region covered. In view of this, and the uncertainty in the accuracy of some of the literature values, agreement is seen to be reasonable. It seems fair to conclude that the water coating the wide pore diameter adsorbents

(18) N. H. Fletcher, *Phil. Mag.*, **18**, 1287 (1968).(19) B. Case and R. Parsons, *Trans. Faraday Soc.*, **63**, 1224 (1967).(20) M. Blank and R. H. Ottewill, *J. Phys. Chem.*, **68**, 2206 (1964).

(21) C. G. Scott, "Gas Chromatography 1962," M. van Swaay, Ed., Butterworths, London, 1962.

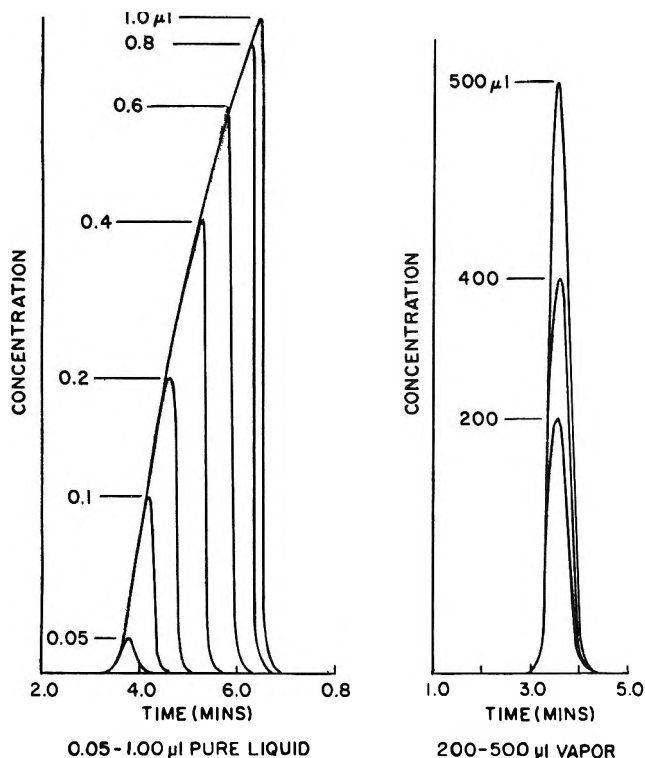


Figure 5. (A) Chromatograms of *n*-octane on 20% H₂O (w/w)-Porasil D as a function of liquid sample sizes; $T = 12.6^\circ$. (B) Chromatograms of *n*-octane on 20% H₂O (w/w)-Porasil D as a function of vapor sample sizes; $T = 12.6^\circ$, $F = 20$ ml/min.

is similar to bulk water in terms of solubility measurements, and that this bulk water character is maintained to very thin layers (see Figure 1). Unfortunately, there is a paucity of data on the thermodynamic properties of solution at infinite dilution for nonelectrolytes in water.

Isotherm Determination. The measurement of sorption isotherms by gas chromatography has become a standard procedure.²² There are several ways in which the isotherm can be measured including the ECP method outlined earlier and frontal analysis.²³ From the experimental point of view the ECP method is the simplest to use when the stationary phase is volatile. In this paper we will present some initial measurements of adsorption isotherms of insoluble vapors on water, as well as some sorption isotherms in which mixed mechanisms of retention occur. In a later paper, this subject will be examined in greater detail.

The simple ECP method has been criticized by Conder²³ and Conder and Purnell²⁴ in that the derived equations do not make allowance for the sorption effect (*i.e.*, the variation in gas velocity with concentration²⁵), for gas phase imperfection, for symmetrical band broadening in the column, or for a nonsharp input distribution.

The true flow velocity at concentration y , $F(y)$, taking into account the sorption effect, is given by

$$F(y) = \frac{F_0[1 + k']}{1 + k'[1 - y]} \quad (6)$$

where F_0 is the total volumetric flow rate when the sorption effect does not exist, measured at the column outlet pressure; y is the mole fraction of solute in the gas phase, and k' is the mass distribution coefficient of the solute. Because of the low adsorption coefficients found in this work, the correction for this effect on the retention of *n*-heptane and *n*-octane is less than 1% and has been neglected. The effect has also been neglected for methyl formate and *n*-propyl ether in which both adsorption and partition simultaneously occur. This is done because no attempt has been made to separate the two mechanisms. In later papers the two mechanisms will be studied individually.

The correction for nonideality in the gas phase has already been shown to be negligible in the present case. No correction has been made for a nonsharp input distribution; however, the elevated injection port temperature ensured that volatilization of the sample was rapid. To reduce band broadening, the carrier

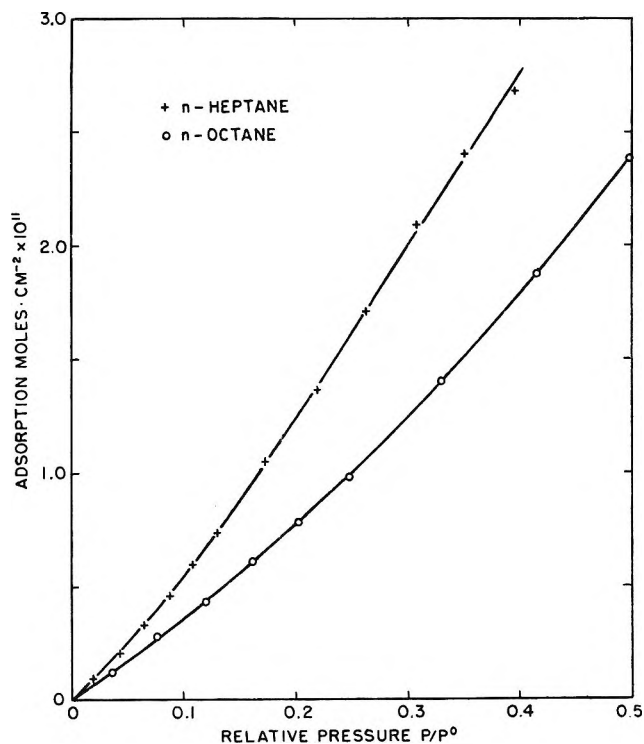


Figure 6. Adsorption isotherms for *n*-heptane and *n*-octane on 20% H₂O (w/w)-Porasil D; $T = 12.5^\circ$.

(22) A. V. Kiselev and Y. I. Yashin, "Gas-Adsorption Chromatography," J. E. S. Bradley, transl., Plenum Publishing Co., New York, N. Y., 1969.

(23) J. R. Conder, "Progress in Gas Chromatography," J. H. Purnell, Ed., Interscience, New York, N. Y., 1968.

(24) J. R. Conder and J. H. Purnell, *Trans. Faraday Soc.*, **65**, 824 (1969).

(25) D. L. Peterson and F. Helfferich, *J. Phys. Chem.*, **69**, 1283 (1965).

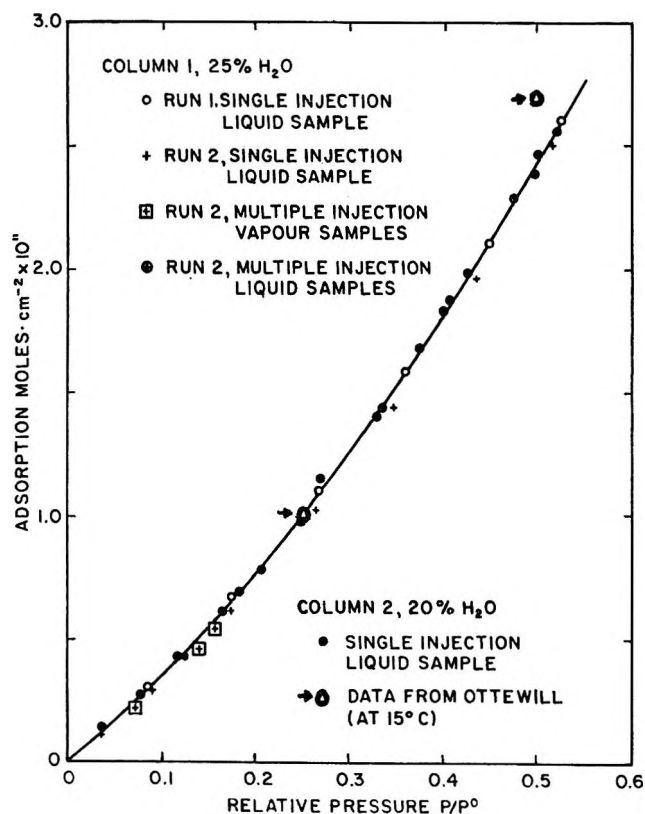


Figure 7. The effect of different methods of determination of the adsorption isotherm of *n*-octane on 20% H₂O (w/w) and 25% H₂O (w/w)-Porasil D columns, $T = 12.5^{\circ}$.

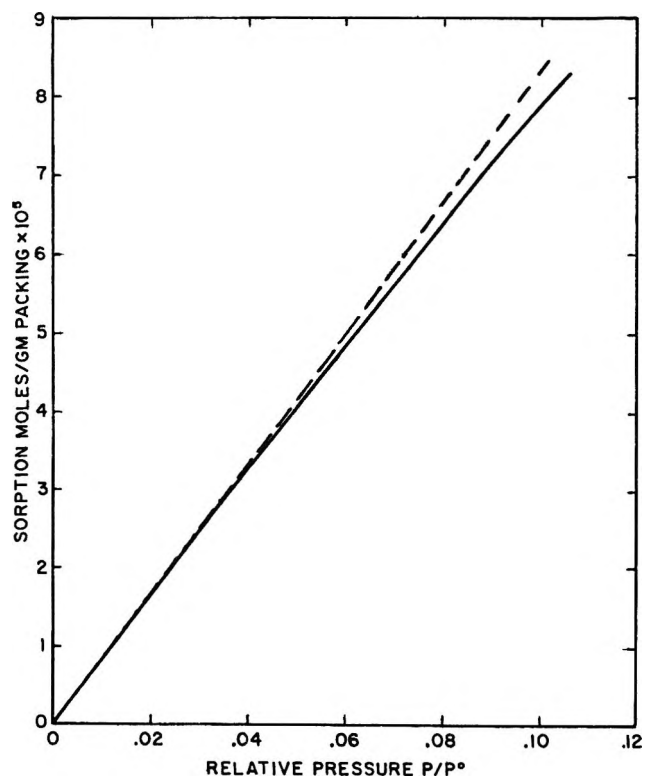


Figure 8. Sorption isotherm of methyl formate on 21% H₂O (w/w) on Chromosorb P; $T = 12.4^{\circ}$. Sorption is in terms of moles per gram of total packing where the total weight of packing in the column is 7.25 g. Dotted line is the extension of the linear portion of the isotherm.

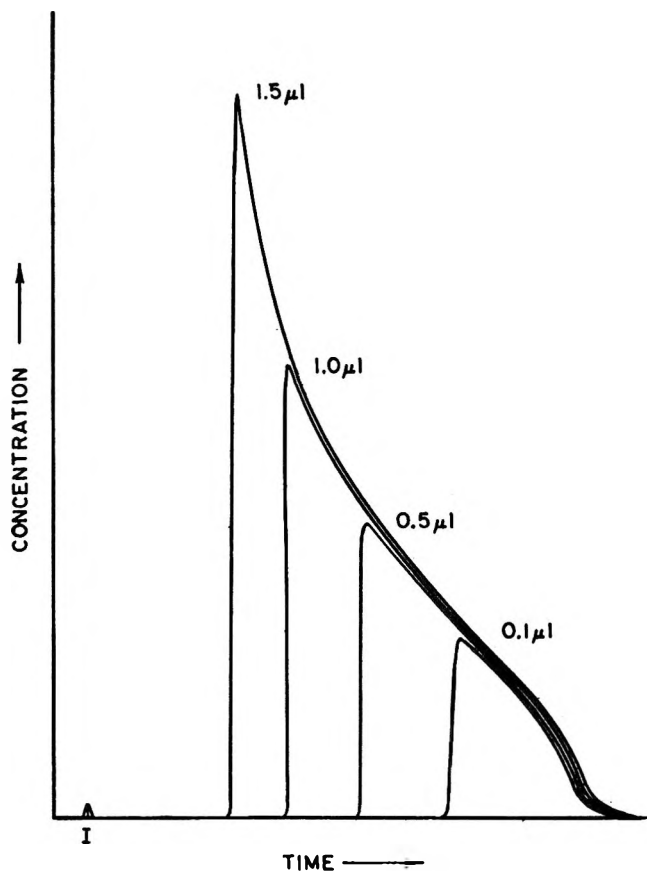


Figure 9. Chromatograms of *n*-propyl ether on 20% H₂O (w/w) on Chromosorb P as a function of sample size; $T = 12.6^{\circ}$.

gas flow was chosen to be in the region of the minimum plate height. The almost vertical sharp boundary obtained on the chromatograms indicates that band broadening was not a serious problem.

The total error introduced by using the ECP method is probably no greater than 5% and may even be considerably less (especially for the adsorption isotherms). In view of the uncertainty in the value for the area of the water surface, the mixed mechanism problem, and the preliminary nature of the study, it was felt that the error was acceptable.

Figure 5 shows chromatograms of *n*-C₃ as a function of liquid and vapor sample sizes on 20% w/w Porasil D (Spherosil). The excellent overlap of the leading edges lends weight to the validity of the ECP method in this case. Figure 6 shows the adsorption isotherms for *n*-C₇ and *n*-C₈ at 12.5° on the above column. The extent of adsorption is in terms of moles per square centimeter in which a 20% w/w Chromosorb P column is assumed to have an interfacial area of 1 m²/g. The isotherm shapes for both *n*-alkanes are "anti-Langmuir," *i.e.*, convex to the pressure axis, in agreement with the results of Hauxwell²⁶ and consistent with

(26) F. Hauxwell, Ph.D. Thesis, University of Bristol, 1969.

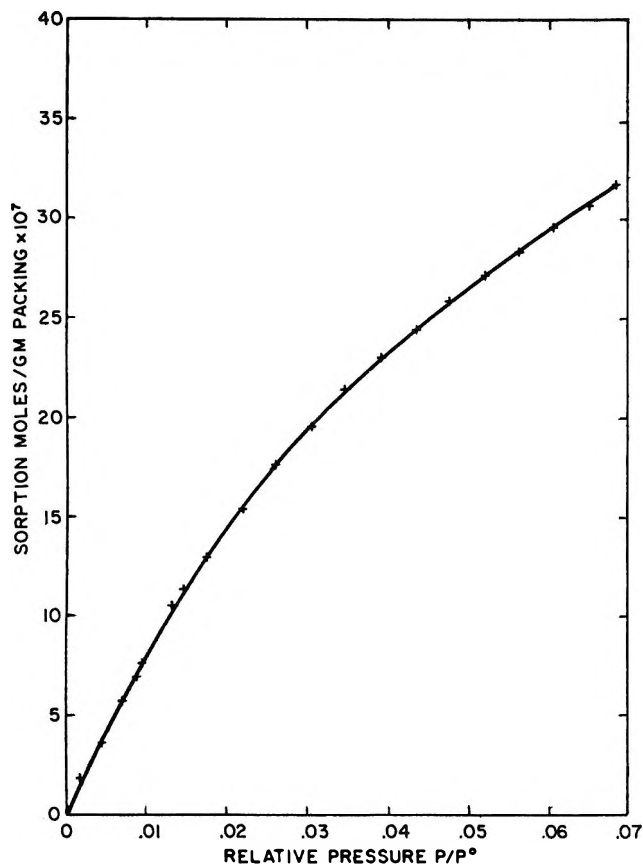


Figure 10. Sorption isotherm of *n*-propyl ether on 20% H₂O (w/w) on Chromosorb P; $T = 21.6^\circ$. Sorption is in terms of moles per gram of total packing where the total weight of packing in the column is 7.07 g.

prediction from the BET equation when the heat of adsorption is less than the heat of liquefaction.

Figure 7 gives an indication of the reproducibility of the data of *n*-C₈. Determinations were made on two different columns (column 1, 25%, and column 2, 20% loading). On the 25% column both liquid and vapor samples were used. In the figure, single injection refers to the isotherm built up from the diffuse edge by

taking points at different heights on the chromatogram; multiple injection refers to the isotherm built up by injecting samples of differing size and using each elution peak to give a point on the isotherm. As can be seen in the figure, there was little difference in the two methods. Consequently, because of the saving in experimental time the single injection method was used. Equilibrium on the column was always confirmed, however, by making two further injections of different sample size and checking the coincidence of the diffuse edges. Also shown in Figure 7 are several data points of *n*-C₈ taken from Hauxwell and Ottewill.⁴ The comparison of the two data cannot be more than qualitative because first, two different temperatures were used, and second, the surface area is an estimated value. However, the closeness of the fit is encouraging.

Figure 8 is a plot of the sorption isotherm of methyl formate on 21% w/w water on Chromosorb P. The term sorption is used since the isotherm is a composite for adsorption and partition. The deviation from linearity (dotted line) clearly indicates a "Langmuir" shape. Recall that the heat of adsorption is slightly greater than the heat of liquefaction in this case. Figure 9 shows the chromatographic band shape as a function of liquid sample size for *n*-propyl ether at $T = 12.6^\circ$. Note the complete reverse shape for this solute relative to *n*-C₈ in Figure 5. Figure 10 shows the sorption isotherm for this solute, with a pronounced "Langmuir" shape. Undoubtedly the shape of the isotherm is tied up with the strong interaction between *n*-propyl ether and water on the surface. Conder²³ has suggested a way in which the relative contribution from solution and adsorption can be determined. This will be included in a later publication along with the isosteric heats of adsorption.

Acknowledgment. The authors gratefully acknowledge the Office of Naval Research for support of this work under Contract N00014-68-A-0207-0002. The authors also appreciate the contributions of Dr. Amiya Chatterjee and Mr. Jerry King.

Proton Magnetic Resonance Study of Ion-Pairing Effects on Arsenic-75 Quadrupole Relaxation in Tetraalkylarsonium Ions

by David W. Larsen

Department of Chemistry, University of Missouri-St. Louis, St. Louis, Missouri 63121 (Received May 24, 1971)

Publication costs borne completely by The Journal of Physical Chemistry

An nmr study of solutions of $(\text{CH}_3)_4\text{As}^+\text{X}^-$ where X^- is Cl^- , I^- , and OH^- was made. The solutions were studied as a function of solvent, anion, concentration, and temperature. The nmr data were analyzed in terms of a rotational diffusion quadrupolar relaxation mechanism for ^{75}As . The results suggest that the "single kinetic entity" which constitutes the aqueous ion pair includes the counterions separated by 2.5–3.0 Å with at most a few H_2O molecules held between the counterions. The hydration layer surrounding the cations is not included a part of the "single kinetic entity."

Introduction

Recent nmr studies^{1–3} made in our laboratories on R_4N^+ salts in aqueous solution have allowed several conclusions to be drawn concerning geometric and motional parameters characterizing these ions in free and ion-paired environments. Of particular interest in the result that the ion pairs are of the "contact" type in dimethyl sulfoxide solution and are of the "solvent-separated" type in aqueous solution. However, the anticipated increase of the electric field gradient seen by ^{14}N when R_4N^+ forms an ion pair with a counterion is too small to be detected by our experimental technique. Thus little insight into the nature of the aqueous region surrounding the ion pairs was gained from the above studies.

However, R_4As^+ ions can act as probes for the small distortions of the electric field gradient caused by ion pairing in aqueous solution. The proton nmr spectrum^{4,5} of the $(\text{CH}_3)_4\text{As}^+$ ion shows that the AsH coupling is collapsed to a broad singlet in aqueous solution. This can be attributed to the fact that while the spin-coupling constant is much larger for $(\text{CH}_3)_4\text{As}^+$ than it is for $(\text{CH}_3)_4\text{N}^+$, the nuclear electric quadrupole moment is also much larger for ^{75}As than it is for ^{14}N ; the net result is the broad collapsed singlet. Studies were made by us of the nmr line shapes for the protons spin coupled to ^{75}As in the $(\text{CH}_3)_4\text{As}^+$ ion; the variable parameters were solvent, anion, concentration, and temperature. Analysis of the experimental results enabled some conclusions to be drawn concerning the nature of the ion-pair solvation. We presently report the results of these studies.

Experimental Section

Tetramethylarsonium Salts. The salts were prepared according to literature methods.⁵ Trimethylarsine was prepared by the reaction of a Grignard reagent

with arsenic trichloride at -78° under oxygen-free nitrogen. The trimethylarsine was distilled from the reaction mixture along with the solvent, *n*-butyl ether. The distillate was allowed to react with methyl iodide. The salt $(\text{CH}_3)_4\text{AsI}$ was recrystallized twice from ethanol. The hydroxide and chloride salts were prepared by treating an aqueous solution of the iodide salt with silver oxide, carefully filtering the precipitate, and then either evaporating the water to obtain the hydroxide or neutralizing the resulting basic solution with hydrochloric acid and evaporating to obtain the chloride.

Nmr Measurements. The spectra were recorded as previously indicated,^{2,3} using a Perkin-Elmer R-20 nmr spectrometer operating at 60 MHz.

Viscosity Measurements. Relative viscosities were determined using an Ostwald viscosimeter.⁶

Experimental Results

The nmr spectra of aqueous solutions of $(\text{CH}_3)_4\text{As}^+\text{X}^-$, where X^- is Cl^- , I^- , and OH^- , were recorded at two temperatures, 35 and 98° . The concentrations of salts studied covered the range 0.025 to 0.40 *M*. The spectra were broad singlets, approximately Lorentzian in shape, and the line widths at half-maximum, $\Delta\nu_{1/2}$, were measured from the recorded spectra. The theoretical expressions (*vide infra*) show that $(\Delta\nu_{1/2} - \Delta\nu_{1/2}^0)^{-1} \propto 1/T_{1\text{As}}$, where $\Delta\nu_{1/2}^0$ is the natural line width and $T_{1\text{As}}$ is the spin-lattice relaxation time for the ^{75}As nucleus. A plot of the

(1) D. W. Larsen, *J. Amer. Chem. Soc.*, **91**, 2920 (1969).

(2) D. W. Larsen, *J. Phys. Chem.*, **74**, 3380 (1970).

(3) D. W. Larsen, *ibid.*, **75**, 509 (1971).

(4) A. G. Massey, E. W. Randall, and D. Shaw, *Spectrochim. Acta*, **20**, 379 (1964).

(5) A. G. Massey, E. W. Randall, and D. Shaw, *ibid.*, **21**, 263 (1965).

(6) D. P. Shoemaker and C. W. Garland, "Experiments in Physical Chemistry," McGraw-Hill, New York, N. Y., 1967, pp 278–285.

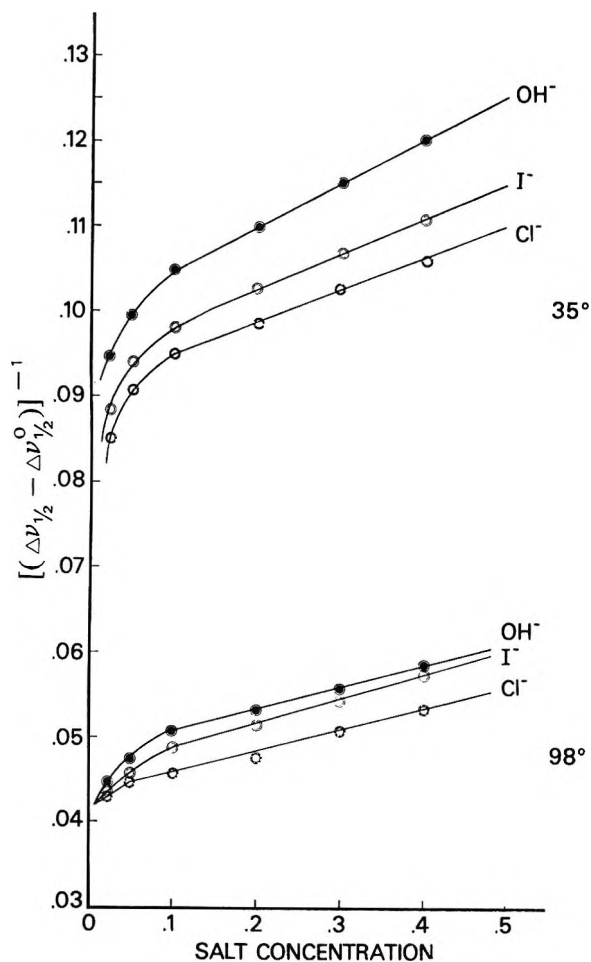


Figure 1. Plot of $[(\Delta\nu_{1/2} - \Delta\nu_{1/2}^0)^{-1}]^{-1}$ vs. salt concentration for $(\text{CH}_3)_4\text{AsX}$, where X is Cl, I, and OH, in aqueous solution at 35 and at 98°.

function $(\Delta\nu_{1/2} - \Delta\nu_{1/2}^0)^{-1}$ vs. salt concentration is presented in Figure 1.

It has been shown^{4,5} that the broad singlet observed for proton spectra of aqueous $(\text{CH}_3)_4\text{As}^+$ is due to incomplete washing out of the spin coupling to ^{75}As . The arsenic spin-lattice relaxation time, $T_{1\text{As}}$, is governed by the quadrupole relaxation mechanism⁷ according to

$$1/T_{1\text{As}} = \frac{1}{10}(QCC)^2\tau_q \quad (1)$$

where QCC is the quadrupole coupling constant, e^2Qq/\hbar ; Q is the nuclear electric quadrupole moment of ^{75}As ; q is the fluctuating electric field gradient; and τ_q is the correlation time for the relaxation mechanism. Allerhand and Thiele⁸ have shown that when the quadrupole multiplet collapses to a single line, an approximately Lorentzian line shape is obtained, with line width given by

$$(\Delta\nu_{1/2} - \Delta\nu_{1/2}^0) = 5\pi J_{\text{As}\alpha}^2 T_{1\text{As}} \quad (2)$$

where $\Delta\nu_{1/2}$ is the observed line width, $\Delta\nu_{1/2}^0$ is the natural line width, and $J_{\text{As}\alpha}$ is the spin-spin coupling constant between ^{75}As and the α protons.

We will interpret our experimental results in terms of a two-site case with rapid exchange between the sites. The sites correspond to free $(\text{CH}_3)_4\text{As}^+$ and ion-paired $(\text{CH}_3)_4\text{As}^+\text{X}^-$. The two sites are separated by a small chemical shift difference, and thus exchange broadening effects are absent.

Gore and Gutowsky⁹ have shown that for the two-site case, in the limit of $P_A \gg P_B$, where P_A and P_B are mole fractions in each site, eq 2 may be generalized for $I = 3/2$ to read

$$(\Delta\nu_{1/2} - \Delta\nu_{1/2}^0)^{-1} = (5\pi)^{-1} \left(\frac{p_A}{T_{1\text{As}}^A} + \frac{p_B}{T_{1\text{As}}^B} \right) J_{\text{As}\alpha}^{-2} \quad (3)$$

We have made computer simulations of line shapes in the collapsed multiplet region to which eq 3 applies using the complete expressions of Gore and Gutowsky. These simulations show that the difference between the simulated line widths and those predicted by eq 3 is less than a few per cent over the entire mole fraction range. Thus the restriction $p_A \gg p_B$ may be removed for our purposes since this error is not much larger than our estimated experimental error. In addition, we expect to obtain useful numbers from eq 3 only in the limit of $p_A \gg p_B$.

The values of $T_{1\text{As}}^A$ and $T_{1\text{As}}^B$ may be interpreted in terms of anisotropic rotational diffusion.¹⁰ In the present case, the principal axis of the field gradient is expected to lie along the internuclear axis in the ion pair, and the complex expression of Huntress¹⁰ reduces to

$$\frac{1}{T_{1\text{As}}^i} = \frac{(OCC)^2}{120} \frac{D_x^i + D_y^i + 4D_z^i}{D_x^i D_y^i + D_y^i D_z^i + D_z^i D_x^i} \quad (4)$$

where D_j^i is the rotational diffusion constant about the j th axis in the internal molecular coordinate system for the i th site. In this case, the internuclear axis lies in the Z direction.

If we let A and B refer to free $(\text{CH}_3)_4\text{As}^+$ and ion-paired $(\text{CH}_3)_4\text{As}^+\text{X}^-$, respectively, then eq 3 can be rewritten

$$(\Delta\nu_{1/2} - \Delta\nu_{1/2}^0)^{-1} = \left[\frac{p_F(QCC)^2_F F_D^F + p_P(QCC)^2_P F_D^P}{600\pi J_{\text{As}\alpha}^2} \right] \quad (5)$$

where F_D^i refers to the function of rotational diffusion constants given in eq 4 for the i th site (free site F or ion-paired site P). The rotational diffusion constant is given by¹⁰

$$D_j^i = \frac{(\tau_j)_j^i kT}{I_j^i} \quad (6)$$

(7) J. A. Pople, *Mol. Phys.*, **1**, 168 (1958).

(8) A. Allerhand and E. Thiele, *J. Chem. Phys.*, **45**, 902 (1966).

(9) E. S. Gore and H. S. Gutowsky, *J. Phys. Chem.*, **73**, 2515 (1969).

(10) W. T. Huntress, *Advan. Magnetic Resonance*, **4**, 1 (1970).

where $(\tau_j)^t$ is the "effective collision time" and I_j^t is the moment of inertia about the j th axis. To proceed from this point, an assumption concerning $(\tau_j)^t$ is necessary. We will assume that the macroscopic viscosity, η , is a measure of the "effective collision time" through the proportionality $(\tau_j)^t \propto \eta^{-1}$ for all j . Equation 5 then becomes

$$[(\Delta\nu_{1/2} - \Delta\nu_{1/2}^0)\eta/T]^{-1} \propto \frac{p_F(QCC)_F^2 F_I^F + p_P(QCC)_P^2 F_I^P}{J_{As\alpha}^2} \quad (7)$$

where

$$F_I^j = \frac{4I_X^t I_Y^t + I_Y^t I_Z^t + I_X^t I_Z^t}{I_X^t + I_Y^t + I_Z^t}$$

Equation 7 indicates that a plot of $[(\Delta\nu_{1/2} - \Delta\nu_{1/2}^0)\eta/T]^{-1}$ vs. salt concentration should have the shape characteristic of a system at equilibrium governed by mass action. The plot for the aqueous solutions in Figure 1 is shown in Figure 2, and it can be seen that the plots are consistent with essentially complete ion pairing above about 0.1 M for all salts studied.

Thus we have shown that above 0.1 M , the function $[(\Delta\nu_{1/2} - \Delta\nu_{1/2}^0)\eta/T]^{-1}$ becomes asymptotically a measure of $(QCC)_F^2 F_I^P / J_{As\alpha}^2$ for any ion pair of the type $(CH_3)_4As^+X^-$ in aqueous solution. The estimated asymptotic values are presented in Table I.

Table I: Experimental Asymptotic Values of $[(\Delta\nu_{1/2} - \Delta\nu_{1/2}^0)\eta/T]^{-1}$ for Aqueous Ion Pairs of the Type $(CH_3)_4As^+X^-$

Anion	$[(\Delta\nu_{1/2} - \Delta\nu_{1/2}^0)\eta/T]^{-1}$	
	At 35°	At 98°
Cl ⁻	38.6 ^a ± 2 ^b	63.5 ± 2
I ⁻	40.6 ± 2	68.5 ± 2
OH ⁻	44.0 ± 2	69.0 ± 2

^a Units, deg Hz⁻¹ cP⁻¹. ^b Estimated limit of error.

The validity of eq 7 and the significance of the values given in Table I rest upon the assumption $(\tau_j)^t \propto \eta^{-1}$. The relationship between viscosity and diffusion is a difficult problem;¹¹ *e.g.*, the "microviscosity" term in the hydrodynamic model has been shown¹² to differ from the macroscopic viscosity in some cases by an order of magnitude. However, the inverse shear viscosity should be a measure of the "effective collision time" even though the exact functionality is unknown. In the present case, the linear behavior with nonzero slopes in Figure 1 and the resulting zero slopes in Figure 2 support the validity of the assumption. In addition, another experimental test of eq 7 was made. Solutions of $(CH_3)_4As^+Cl^-$ and $(CH_3)_4As^+I^-$ in three nonaqueous solvents with different viscosities were studied. The experimental line widths

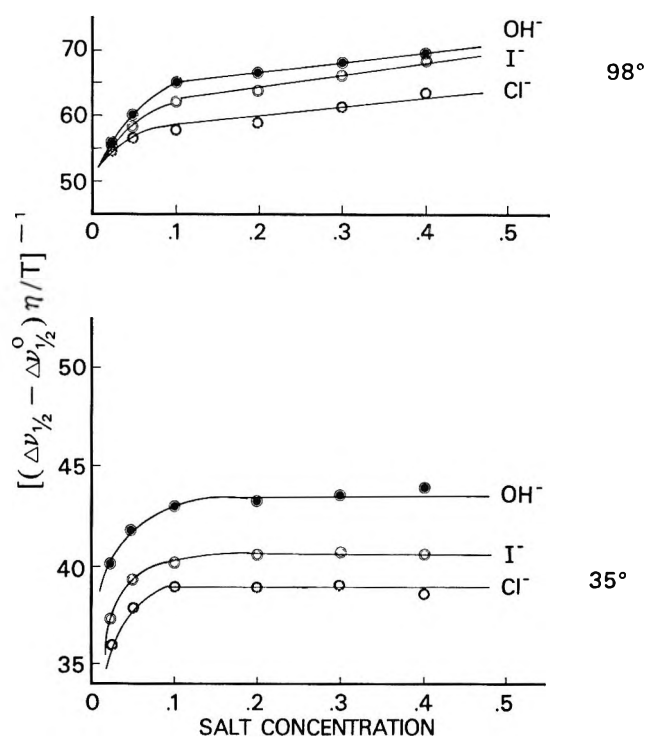


Figure 2. Plot of $[(\Delta\nu_{1/2} - \Delta\nu_{1/2}^0)\eta/T]^{-1}$ vs. salt concentration for $(CH_3)_4AsX$, where X is Cl, I, and OH, in aqueous solution at 35 and at 98°.

are presented in Table II. It is expected that the vastly predominant species present in each of these solvents are contact ion pairs. Thus these values of $[(\Delta\nu_{1/2} - \Delta\nu_{1/2}^0)\eta/T]^{-1}$ are measures of $(QCC)_F^2 \cdot F_I^P / J_{As\alpha}^2$, and this quantity should be solvent independent for any given salt, provided that the solvent contribution to $(QCC)_F$ is small. The functions are shown in Table II, and it can be seen that the functions are almost solvent independent within the estimated experimental error. The error in this experiment is quite large because of the limited solubility of the salts and the resulting weak nmr signals. Also, at higher temperatures, the lines were too broad to detect at these low concentrations, and consequently the temperature effects were not studied. The reported molecular reorientation times¹³ of the solvents in Table II and of water appear to be roughly proportional to the viscosity-moment of inertia product; this suggests that the effective collision times for solvent-solvent collisions should follow an inverse viscosity proportionality.¹⁰ We conclude that the inverse viscosity proportionality is also valid for the solvent-solute collisions.

Another feature of interest for the analysis of the

(11) P. A. Egelstaff, "An Introduction to the Liquid State," Academic Press, New York, N. Y., 1967, Chapter 12.

(12) W. B. Moniz and H. S. Gutowsky, *J. Chem. Phys.*, **38**, 1155 (1963).

(13) H. G. Hertz, *Progr. N.M.R. Spectrosc.*, **3**, 159 (1967), and references contained therein.

Table II: Experimental Line Width and Viscosity Data for $(\text{CH}_3)_4\text{As}^+\text{Cl}^-$ and $(\text{CH}_3)_4\text{As}^+\text{I}^-$ in Nonaqueous Solvents at 35°

Salt	Solvent	$(\Delta\nu_{1/2} - \Delta\nu_{1/2}^0)$, Hz	η , cP	$[(\Delta\nu_{1/2} - \Delta\nu_{1/2}^0)/\eta/T]^{-1}$
$(\text{CH}_3)_4\text{As}^+\text{Cl}^-$	CDCl_3	3.03	0.488	210 ± 30^b
	CD_3CN	2.95	0.345	300 ± 30
	$(\text{CD}_3)_2\text{CO}$	5.00	0.277	220 ± 10
$(\text{CH}_3)_4\text{As}^+\text{I}^-$	CDCl_3	1.64	0.488	390 ± 80
	CD_3CN	1.97	0.345	450 ± 70
	$(\text{CD}_3)_2\text{CO}$	2.53	0.277	440 ± 60

^a Units, deg Hz⁻¹ cP⁻¹. ^b Estimated limit of error.

experimental plots in Figure 2 is the contribution of the solvent dipoles to $(QCC)_P$. This question can be at least partially answered by extending the lower limit of salt concentration in the studies. Again the weak signals in this concentration range give rise to a large experimental error, but the measurements were extended to a lower limit of 0.01 *M* for $(\text{CH}_3)_4\text{As}^+\text{I}^-$. The pertinent plot is shown in Figure 3, and attempts to extrapolate the plot to zero concentration using equilibrium constant expressions and activity coefficient expressions indicate that this function is approximately zero at zero concentration, although the error is appreciable. It can be definitely concluded, however, that $(QCC)_F^2 F_I^F \ll (QCC)_P^2 F_I^P$. The significance of this point will be covered in the Discussion.

Discussion

Thus far we have presented evidence that the asymptotic values of $[(\Delta\nu_{1/2} - \Delta\nu_{1/2}^0)/\eta/T]^{-1}$ are

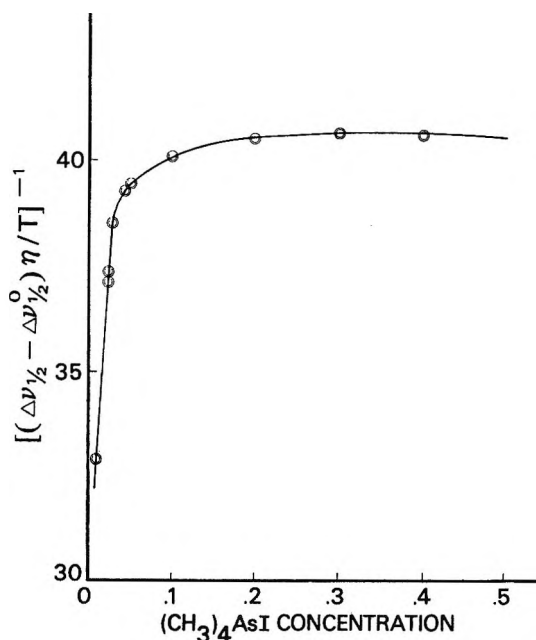


Figure 3. Plot of $[(\Delta\nu_{1/2} - \Delta\nu_{1/2}^0)/\eta/T]^{-1}$ vs. $(\text{CH}_3)_4\text{AsI}$ concentration in aqueous solution at 35°.

measures of $(QCC)_P^2 F_I^P$. We have also determined these values for the Cl^- , I^- , and OH^- salts of $(\text{CH}_3)_4\text{As}^+$ in aqueous solution and for the Cl^- and I^- salts in three nonaqueous solutions. Our ultimate purpose is to construct a rotational model for the aqueous ion pairs. The Cl^- and I^- ions were chosen for study because they are the extremes in size and mass for the halide ions (without the complication of hydrogen bonding). The OH^- ion was chosen for study because it is expected to strongly hydrogen bond to at least one water molecule, and this effect on the ion pair is of interest. Robinson and Stokes¹⁴ define "true" hydration numbers as the number of water molecules that move with the ions as a "single kinetic entity." It is our purpose to determine the stoichiometries and geometries of the single kinetic entities that constitute $(\text{CH}_3)_4\text{As}^+\text{X}^-$ ion pairs in aqueous solution. These quantities will be determined by comparing calculated relative values¹⁵ of $(QCC)_P^2 \cdot F_I^P$ with the asymptotic values shown in Tables I and II. A model for the electric field gradient must be assumed and geometric models must be used to calculate F_I^P . The credibility of this procedure rests in large part upon the features of the asymptotic values in Tables I and II: (a) the constancy of the values for any given salt in the nonaqueous solvents and the substantial anion dependence of the nonaqueous values, and (b) the order of magnitude smaller aqueous values and the small anion dependence of the aqueous values.

The value of $(QCC)_P$ can be considered to have potential contributions from three sources:³ (a) distortion of the As-C bonds from pure sp^3 hybridization due to ion pairing, (b) electric fields of the solvent dipoles, and (c) electric field of the anions. We will account for $(QCC)_P$ in terms of the last contribution alone, according to the following rationale. The concept of dielectric saturation near an ion¹⁴ indicates that a time average highly symmetric arrangement of solvent dipoles around an ion is to be expected. However, if a collision complex¹⁶ with a solvent molecule were formed for a short period of time, this would give rise to an electric field gradient modulated by rotational diffusion. We have shown above that: $(QCC)_P^2 F_I^P \gg (QCC)_F^2 F_I^F$. For a collision complex with solvent, $F_I^F \sim F_I^P$ (*vide infra*), and thus the inequality becomes $(QCC)_P \gg (QCC)_F$. We conclude from this that if solvent complexes are unimportant for "free" cations, they are also unimportant for "ion-paired" cations. The anion in the ion pair then

(14) R. A. Robinson and R. H. Stokes, "Electrolyte Solutions," Butterworths, London, 1955, Chapter 1.

(15) Relative values of this function must be considered for two reasons. First, the proportionality constant between τ_j and η^{-1} is unknown. Second, the value of $J_{A\alpha}$ is unknown; however, a lower limit can be established from the observed line width at 98°. This is $J_{A\alpha} > 7.6$ Hz.

(16) H. C. Torrey, *Phys. Rev.*, **130**, 2306 (1963).

Table III: Values of $r^{-6} F_{I^{\pm}}$ for Models of $(\text{CH}_3)_4\text{As}^+\text{Cl}^-$ and $(\text{CH}_3)_4\text{As}^+\text{I}^-$ Ion Pairs

$(\text{CH}_3)_4\text{As}^+$ salt	$d, \text{\AA}$	$r^{-6} F_{I^{\pm}}$			
		0 H ₂ O	1 H ₂ O	3 H ₂ O	9 H ₂ O
Cl ⁻	0	0.132 (1.00) ^a			
I ⁻		0.199 (1.51)			
Cl ⁻	1.5	0.041 (0.31)			
I ⁻		0.069 (0.52)			
Cl ⁻	2.0	0.029 (0.22)	0.032 (0.24)	0.035 (0.26)	
I ⁻		0.052 (0.39)	0.052 (0.39)	0.052 (0.39)	
Cl ⁻	2.5	0.022 (0.17)	0.023 (0.17)	0.027 (0.20)	0.082 (0.62)
I ⁻		0.039 (0.30)	0.039 (0.30)	0.043 (0.33)	0.087 (0.66)
Cl ⁻	3.0	0.017 (0.13)	0.018 (0.13)	0.020 (0.15)	0.062 (0.47)
I ⁻		0.030 (0.23)	0.031 (0.23)	0.033 (0.25)	0.067 (0.51)

^a Relative value normalized for Cl⁻ salt with $d = 0$.

either displaces some solvent in the case of a "contact" ion pair or slightly realigns the solvent between the counterions in the case of a "solvent-separated" ion pair. In the former case, the anion contribution should be predominant since the field gradient at a given distance from a specie of unit charge is much greater than that from the dipoles. In the latter case, the anion contribution is again predominant since the distortion of the highly symmetric dipole arrangement around the cation due to the anion should be small. If the anion is approximated as either a point charge or a charged sphere (neglecting polarizability distortion), the electric field gradient is proportional to r^{-3} , where r is the distance from the anion nucleus. Thus we will assume $(QCC)_P^2 \propto r^{-6}$ where r is the As-X internuclear separation.

The geometric model for the nonaqueous ion pairs; *i.e.*, the "single kinetic entity" will be assumed to be simply the two ions (with no solvent) and the As-X internuclear separation will be the sum of ionic radii.

Several geometric models will be used for the aqueous ion pairs. We will consider a nonsolvated model in which the As-X internuclear separation will be the sum of ionic radii + d (a variable distance). This variable distance d is expected¹ to be $\sim 2-3 \text{\AA}$. We will then consider solvation in the following ways: (a) one H₂O located midway along d between the two ions, (b) three H₂O molecules located on a plane midway along d between the two ions, giving approximated half-octahedral solvation for each ion, and (c) nine H₂O molecules, three between the ions and three on the outside of each counterion giving complete octahedral solvation for each ion.

The models will be first examined for the Cl⁻ and I⁻ salts of $(\text{CH}_3)_4\text{As}^+$. The ionic radii used were 3.0\AA for $(\text{CH}_3)_4^+$,^{17,18} 1.81\AA for Cl⁻,¹⁸ and 2.19\AA for Br⁻.¹⁸ Values of $r^{-6} F_{I^{\pm}}$, which represent relative values of $(QCC)_P^2 F_{I^{\pm}}$, are presented in Table III. The relative values in parentheses should correspond to the relative asymptotic values in Tables I and II.

The relative values in Table II can be considered as calibration points since they represent contact ion pairs. These average relative experimental values (Cl⁻:I⁻) are $1.00:1.60 \pm 0.4$, which agree very well with the relative values in Table III for $d = 0$ and no solvent. The relative values in Table I, normalized with respect to the nonaqueous Cl⁻ in Table II are for the Cl⁻: 0.14 ± 0.06 (35°) and 0.25 ± 0.10 (98°) and for the I⁻: 0.15 ± 0.06 (35°) and 0.26 ± 0.10 (98°). The limits of error correspond to the error in the normalization relative to nonaqueous $(\text{CH}_3)_4\text{As}^+\text{Cl}^-$. It can be seen that these values are consistent with both the nonsolvated model and the partially solvated models at values of d between 2.5 and 3.0\AA , but that the fully solvated octahedral model can be ruled out. Thus the "single kinetic entity" for the ion pair in aqueous solution is the counterions with at most a few H₂O molecules held between the counterions, but apparently no H₂O molecules are carried along on the exterior of the ion pair. The essentially identical values for the Cl⁻ and I⁻ salts suggest a slightly larger value of d ($\sim 0.5 \text{\AA}$) for the I⁻ salt than for the Cl⁻ salt. Also an increase temperature apparently increases d for both salts. These effects are outside the limits of the experimental error and could conceivably reflect differences in hydration sizes, although the relatively small magnitude of these effects suggests that they could be a consequence of the $\tau_J \propto \eta^{-1}$ assumption.

We now wish to examine the models for the OH⁻ salt. The ionic radius¹⁸ used for OH⁻ was 1.45\AA . A second set of calculations was also performed in which the anion species was assumed to be OH⁻·H₂O with an O-O internuclear distance¹⁸ of 2.45\AA . The calculated values of $r^{-6} F_{I^{\pm}}$ are shown in Table IV. The relative asymptotic values from Table I, normalized with respect to the nonaqueous $(\text{CH}_3)_4$

(17) Reference 14, pp 119-121.

(18) F. A. Cotton and G. Wilkinson, "Advanced Inorganic Chemistry," Interscience, New York, N. Y., 1966, pp 45, 105, 115.

Table IV: Values of $r^{-6}F_{1P}$ for Models of $(CH_3)_4As^+OH^-$ and $(CH_3)_4As^+OH^- \cdot H_2O$ Ion Pairs

$(CH_3)_4As^+$ salt	d , Å	$r^{-6}F_{1P}$			
		0 H ₂ O	1 H ₂ O	3 H ₂ O	9 H ₂ O
OH ⁻	1.5	0.032 (0.24) ^a			
OH ⁻ ·H ₂ O		0.070 (0.53)			
OH ⁻	2.0	0.022 (0.17)	0.027 (0.20)	0.033 (0.25)	
OH ⁻ ·H ₂ O		0.052 (0.39)	0.055 (0.41)	0.061 (0.46)	
OH ⁻	2.5	0.016 (0.12)	0.019 (0.15)	0.024 (0.18)	0.093 (0.71)
OH ⁻ ·H ₂ O		0.038 (0.29)	0.040 (0.30)	0.045 (0.34)	...
OH ⁻	3.0	0.012 (0.09)	0.014 (0.11)	0.018 (0.13)	0.070 (0.53)
OH ⁻ ·H ₂ O		0.029 (0.22)	0.030 (0.23)	0.034 (0.25)	...

^a Relative value normalized for Cl⁻ salt with $d = 0$.

As⁺Cl⁻ in Table II, are for $(CH_3)_4^+OH^-$; 0.16 ± 0.06 (35°) and 0.26 ± 0.10 (98°). It can be seen these values are consistent with the hydrogen-bonded OH⁻ model with d between 2.5 and 3.0 Å for both the unsolvated and partially solvated configurations. Again the fully solvated model can be ruled out. However, the nonhydrogen-bonded model also predicts satisfactory values with d between 1.5 and 2.0 Å for both the unsolvated and partially solvated configurations. Thus the extent of the hydrogen bonding for the OH⁻ ion with H₂O cannot be determined by this technique, although the nonhydrogen-bonded OH⁻ model requires a value of d approximately 1 Å less than for the Cl⁻ and I⁻ models, and this seems unlikely.

A statement of the major conclusions from the present work and the previous work^{2,3} on R₄N⁺X⁻ ion pairs is in order. If it is assumed that aqueous R₄N⁺X⁻ and R₄As⁺X⁻ ion pairs are essentially identical in geometric and dynamic behavior, then these ion pairs have the following characteristics: (a)

solvent-separated ion pairs, (b) rapid inertial¹⁰ reorientation of the cations within their hydrate cages, essentially unaffected by ion pairing, and (c) diffusional¹⁰ reorientation of ion pairs, including at most a few water molecules between the counterions.

Studies made by Hertz and coworkers¹³ indicate that solvent motion is rapid with respect to the translational motion of the ions, and this suggests that the diffusion approach for ion-pair motion is appropriate. The effects of ion pairing were neglected in the treatment of Hertz,¹³ but if the "single kinetic entities" are the bare ion pairs diffusing through the solvent, then the influence of ion pairing on ionic hydration spheres may be negligible. However, the present studies do not eliminate the possibility that the water molecules between the ion-paired counterions may differ from those in the remainder of the hydration spheres. In this latter case, the parameters determined by Hertz¹³ would be averages over the two different types of hydration.

Continuous γ and Pulse Radiolysis of Aqueous Benzene Solutions:

Some Reactions of the Hydroxycyclohexadienyl Radical

by Anastasia Mantaka, D. G. Marketos,

Nuclear Research Center "Democritos," Radiation Chemistry Laboratory, Aghia Paraskevi-Attikis, Athens, Greece

and Gabriel Stein*

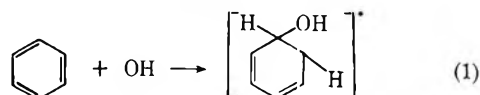
The Hebrew University of Jerusalem, Department of Physical Chemistry, Jerusalem, Israel (Received March 15, 1971)

Publication costs assisted by the Greek Atomic Energy Commission

The radiation chemistry of aqueous benzene solutions in the presence of N_2O was investigated using ^{60}Co γ -ray continuous irradiation (at varying benzene concentrations and at dose rates of 100 to 4000 rads min^{-1}) and 5 MeV, 200 mA, 0.3 or 1.5- μ sec electron pulses. The products are identical in both cases. They are, under these conditions, mainly due to the reactions of the hydroxycyclohexadienyl radical (BOH). Allowing for absorption due to the corresponding H atom adduct (BH), the spectrum of BOH was determined. $\epsilon_{313}^{BOH} = (4.7 \pm 0.6) \times 10^3 M^{-1} cm^{-1}$ at the maximum. The bimolecular rate constant k ($2BOH \rightarrow (BOH)_2$) has the value of $(7 \pm 0.9) \times 10^8 M^{-1} sec^{-1}$. The final product observed is mainly the dimer $(BOH)_2$ which decomposes to give (phenol + benzene + H_2O) and (biphenyl + $2H_2O$).

Introduction

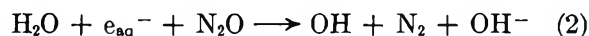
The reactivity of aromatic rings with free radicals may be studied by radiolytic techniques when the free radicals are produced by the action of ionizing radiations. In aqueous solutions the main species of free radicals thus produced are e_{aq}^- , H, and OH. Benzene as the simplest aromatic solute in water was often studied in this manner. Stein and Weiss¹ used this system for an early basic study of radiation chemistry and postulated the addition of OH radicals to benzene



producing the hydroxycyclohexadienyl radical (BOH) as the first stage in the sequence of reactions leading to final chemical products, phenol, biphenyl, and hydrogen in deaerated solutions. They assumed that BOH reacts to give the phenyl radical. Using continuous irradiation a number of detailed investigations²⁻⁸ were carried out including³ work on the reactions of BOH, which indicated that phenyl radicals are not the intermediates. Dorfman and coworkers,⁹⁻¹² using pulse radiolysis, obtained the absorption spectrum of BOH, the rate constant of its formation and that of some of its reactions, particularly in the presence of oxygen. The results were complicated by the simultaneous formation of the e_{aq}^- (B^-) and H atom (BH) adducts.¹³ The latter has recently been studied separately by Sauer and Ward.¹⁴ Kartasheva and Pikaev¹⁵ extended the information in aerated solutions.

In the present work we attempted to obtain more accurate information concerning the OH adduct under

conditions where interference by other radicals is greatly reduced. We used N_2O saturated solutions, where the reaction



leads to the elimination of reactions of the hydrated electron with benzene and the role of OH is enhanced.^{12,13} In the absence of O_2 , the only initial radical other than BOH is BH. Under our conditions BH forms only about 10% of the total radicals ($G_{OH} = 2.70$, $G_{e_{aq}^-} = 2.75$, $G_H = 0.55$) and with the use of the results of Sauer and Ward¹⁴ can be allowed for.

We could thus study the spectrum and reactions of

- (1) G. Stein and J. Weiss, *J. Chem. Soc.*, 3245, 3254 (1949).
- (2) M. Daniels, G. Scholes, and J. Weiss, *ibid.*, 832 (1956).
- (3) E. V. Barelko, L. I. Kartasheva, P. D. Novikov, and M. A. Proskurnin, "Proceedings of the First All Union Conference on Radiation Chemistry, Moscow, 1957," English translation, Vol. II, Consultants Bureau, Inc., New York, N. Y., 1959, p 81.
- (4) P. V. Phung and M. Burton, *Radiat. Res.*, 7, 199 (1957).
- (5) K. C. Kurien, P. V. Phung, and M. Burton, *ibid.*, 11, 283 (1959).
- (6) J. H. Baxendale and D. Smithies, *J. Chem. Soc.*, 779 (1959).
- (7) J. Goodman and J. Steigman, *J. Phys. Chem.*, 62, 1020 (1958).
- (8) I. Loeff and G. Stein, *Nature*, 184, 901 (1959); *J. Chem. Soc.*, 2623 (1963).
- (9) L. M. Dorfman, R. E. Bühler, and I. A. Taub, *J. Chem. Phys.*, 36, 549 (1962).
- (10) L. M. Dorfman, I. A. Taub, and R. E. Bühler, *ibid.*, 36, 3051 (1962).
- (11) L. M. Dorfman, I. A. Taub, and D. A. Harter, *ibid.*, 41, 2954 (1964).
- (12) P. Neta and L. M. Dorfman, *Advan. Chem. Ser.*, No. 81, 222 (1968).
- (13) B. Chutny, *Nature*, 213, 593 (1967).
- (14) M. C. Sauer, Jr., and B. Ward, *J. Phys. Chem.*, 71, 3971 (1967).
- (15) L. I. Kartasheva and A. K. Pikaev, *Int. J. Radiat. Phys. Chem.*, 1, 243 (1969).

BOH itself. The rate of its formation under such conditions has previously been obtained by Neta and Dorfman,¹² Tsuda¹⁶ and Christensen and Gustafsson¹⁷ have studied the irradiation of aqueous benzene solutions in the presence of N_2O .

Experimental Section

The benzene used was Fluka (for uv spectroscopy) or Riedel-de Haen (AR for chromatography). They gave identical results. The concentration in aqueous solutions was determined spectrophotometrically.¹⁸ Water was triply distilled. Absorption spectra were taken on a Cary 14 recording spectrophotometer; OD's at fixed wavelengths on a Hilger Uvispek instrument. pH's were measured on a Metrohm E 187 instrument.

Irradiations were carried out using: (a) ^{137}Cs γ source, at a dose rate of 190 rads min^{-1} (Jerusalem); (b) ^{60}Co γ source, at dose rates of 100 and 4150 rads min^{-1} (Athens); γ doses were determined using the 0.8 N H_2SO_4 Fricke dosimeter; (c) Varian Linac pulsed electron source at 5 ± 0.6 MeV (V-7715B, Jerusalem). Pulse durations used were between 0.3 and 1.5 μsec . Beam current was usually 200 mA. The dose absorbed in the sample was determined¹⁹ using a freshly prepared air-saturated 10 mM $FeSO_4$ solution in 0.8 N H_2SO_4 without adding NaCl, assuming $G = 15.6$ and measuring O.D._{304 nm} on the Hilger instrument after irradiation or on the oscilloscope trace *in situ*, using the same cell as for the benzene irradiations.

The dose per pulse of 200 mA for 1.5 μsec at 5 MeV was about 2635 rads/pulse or 1.05×10^{11} rads/min.

The irradiation cells for the γ experiments and for pulse experiments in which final products only were determined were Spectrosil (Thermal Syndicate Ltd.), rectangular, with 10-mm optical path, fitted with ground stoppers which, when inserted, eliminated gas space over the solution. A small glass ball in the cell facilitated stirring.

For experiments under pulse radiolysis, where time-dependent analysis of intermediates and products was desired, a multiple reflection arrangement gave three light passes through the solutions, with a total light path of 6 cm for the analyzing light, from a 150-W xenon light source. The analyzing light was split into two beams passing through Bausch and Lomb 250-mm monochromators, one monitoring at a fixed wavelength, the other being varied. The light from the monochromator was fed into RCA IP28 photomultipliers and the output of these observed on Tektronix Type 549 storage oscilloscope, with 1A1 Dual trace plug-in unit and/or Type 556 dual beam oscilloscope with 1A1 or W plug-in unit. At wavelengths below 290-nm stray light was checked and allowed for. An automatic syringe sample changer was used to provide fresh solution, as required, after one or a few pulses. N_2O (Matheson Co.) was further purified

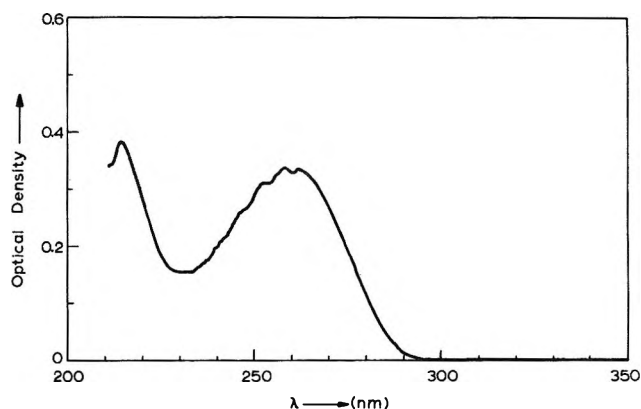


Figure 1. Difference absorption spectrum of irradiated aqueous N_2O saturated, neutral benzene solutions against a nonirradiated blank; $[C_6H_6] = 4.24 \times 10^{-3} M$; total dose = 40,000 rads.

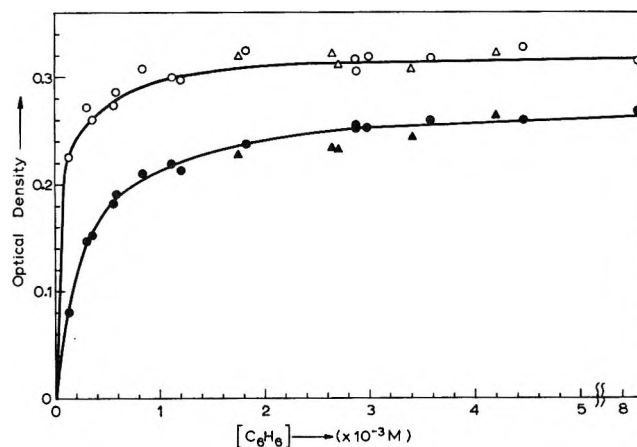


Figure 2. Effect of benzene concentration on the yields of products. N_2O -saturated, aqueous, neutral benzene solutions, irradiated to 30,000 rads: open signs, 213 nm; full signs, 260 nm; \circ , dose rate 4150 rads min^{-1} ; Δ , dose rate 100 rads min^{-1} .

by passing it through two bubblers of alkaline pyrogallol solutions, followed by one of triply distilled water (Jerusalem) while when N_2O was Aga-Chropi Co., Medical Grade (Athens), an additional bubbler containing 50% H_2SO_4 was inserted between pyrogallol and water.

Results

Nature of the Products. N_2O -saturated solutions at varying benzene concentrations were γ -irradiated without added buffer (pH ~ 6). Figure 1 shows the absorption spectrum of the irradiated solutions. The OD is a strictly linear function of dose at 260 and 213 nm up to doses of 40,000 rads, the highest dose used. The results under pulse irradiation are

(16) M. Tsuda, *Bull. Chem. Soc. Jap.*, **36**, 1582 (1963).

(17) H. B. Christensen and R. Gustafsson, *Nukleonik*, **12**, 49 (1969).

(18) D. G. Marketos, *Anal. Chem.*, **41**, 195 (1969).

(19) I. A. Taub and K. Eiben, *J. Chem. Phys.*, **49**, 2499 (1968).

similar and indicate that the final products are the same. Figure 2 shows the dependence of the yield on benzene concentration. The results at dose rates of 100 and 4150 rads min^{-1} , in the benzene concentration range 1.5 to $4 \times 10^{-3} M$, show no significant effect of dose rate.

Absorption Spectrum of BOH Radical. Figure 3 shows the absorption spectrum of the radical resulting from the addition of OH radical to benzene obtained from pulse experiments, by measuring the OD at different wavelengths on completion of a $1.5\text{-}\mu\text{sec}$ pulse, with the monitor set at a constant wavelength of 313 nm. Corrections were applied for scattered light and absorption by final products and also for the

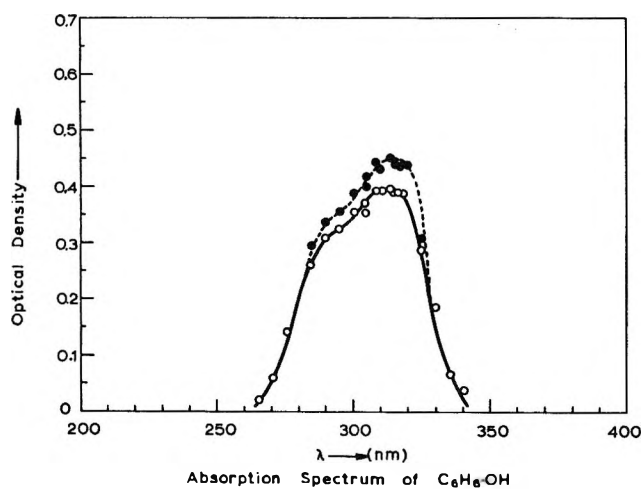


Figure 3. Transient absorption spectrum of the hydroxycyclohexadienyl radical (BOH) following a $1.5\text{-}\mu\text{sec}$ pulse of 2635 rads in N_2O -saturated, aqueous, neutral $2 \times 10^{-3} M$ benzene solutions: ●, actual spectrum; ○, corrected spectrum; $\lambda_{\text{max}}^{\text{BOH}}$ 313 nm; $\epsilon_{313}^{\text{BOH}} = (4.7 \pm 0.6) \times 10^3 M^{-1} \text{cm}^{-1}$.

contribution of BH to obtain the absorption curve. The absorption spectrum observed is the sum of contributions due to 5.45 BOH radicals and 0.55 BH radical for every 100 eV absorbed. From the work of Sauer and Ward¹⁴ at its maximum $\epsilon_{313}^{\text{BH}} = 5.4 \times 10^3 M^{-1} \text{cm}^{-1}$. At 313 nm, the maximum of BOH, $\epsilon_{313}^{\text{BH}}$ has nearly the same value. Allowing for this, from the absorption curve and results of dosimetry, we calculate $\epsilon_{313}^{\text{BOH}} = (4.7 \pm 0.6) \times 10^3 M^{-1} \text{cm}^{-1}$ at the peak. We also note the band at ~ 290 nm, which indicates the possibility of the absorption spectrum being composed of two components.

Rate Constants. From the pulse experiments at different total doses (0.3 and $1.5 \mu\text{sec}$ at 200 mA and 5 MeV) we derived the rate constant for the bimolecular disappearance of the cyclohexadienyl radicals in the radical-radical reaction, as $k = (7 \pm 0.9) \times 10^8 M^{-1} \text{sec}^{-1}$. Figure 4 shows that second-order kinetics are observed.

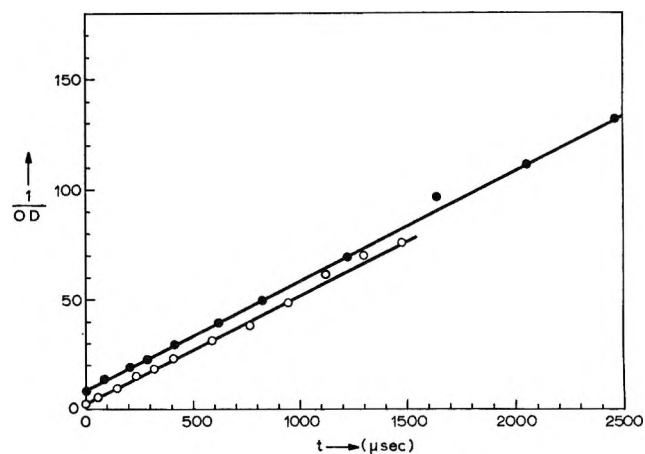


Figure 4. Second-order decay of the $\text{C}_6\text{H}_6.\text{OH}$ radical. N_2O -saturated, aqueous, neutral, $2 \times 10^{-3} M$ benzene solution: ○, 310-nm, pulse $1.5 \mu\text{sec}$, 200 mA, 5 ± 0.6 MeV; ●, 313-nm, pulse $0.3 \mu\text{sec}$, 200 mA, 5 ± 0.6 MeV.

Discussion

Since²⁰ $k_{\text{e}_{\text{aq}}^- + \text{N}_2\text{O}} = 8.7 \times 10^9 M^{-1} \text{sec}^{-1}$ and²¹ $k_{\text{e}_{\text{aq}}^- + \text{benzene}} = 1.2 \times 10^7 M^{-1} \text{sec}^{-1}$, direct addition of e_{aq}^- to benzene may be neglected.

Therefore, the radicals formed in our system will be BOH, about 90%, and BH, about 10%. The absorption spectrum after allowing for the contribution of BH, exhibits a main peak at 313 nm, as shown by Dorfman¹¹ and a subsidiary band at about 290 nm, which is also indicated in Dorfman's work.

As to the nature of the transition responsible for the peak at 313 nm, its similarity to the band of BH indicates that we may be dealing, in both cases, with a σ adduct on carbon. These maxima are unlike that of B^- which results from the slower attack^{13, 21} of e_{aq}^- on benzene.

From the data of Sauer and Ward¹⁴ it is difficult to judge the spectrum of BH below ~ 290 nm. However, Michael and Hart's results²¹ show the absence of a second band for BH. For BOH a second band with $\lambda_{\text{max}} \sim 290$ nm is now established.

The absorption spectrum immediately after irradiation (Figure 1) and that after admission of air and addition of alkali are similar and show that very little phenol ($\lambda_{\text{max}}^{\text{alk}} 287$ nm) is present. To ascertain the nature of the products we extracted the alkaline solution with *n*-hexane. Figure 5a shows that only benzene is extracted. The main product remains in the aqueous layer (Figure 5b) and shows λ_{max} 260 nm. On adding acid (Figure 6a) there is a large increase in absorbance and shift of λ_{max} to 247 nm. On adding alkali (Figure 6b) this peak is not shifted, and some additional absorption due to phenol at 287 nm emerges. From the alkali solution hexane now extracts biphenyl

(20) S. Gordon, E. J. Hart, M. S. Matheson, J. Rabani, and J. K. Thomas, *Trans. Faraday Soc.*, **36**, 193 (1963).

(21) B. D. Michael and E. J. Hart, *J. Phys. Chem.*, **74**, 2878 (1970).

(λ_{\max} 247 nm). The evidence is consistent with the sequence

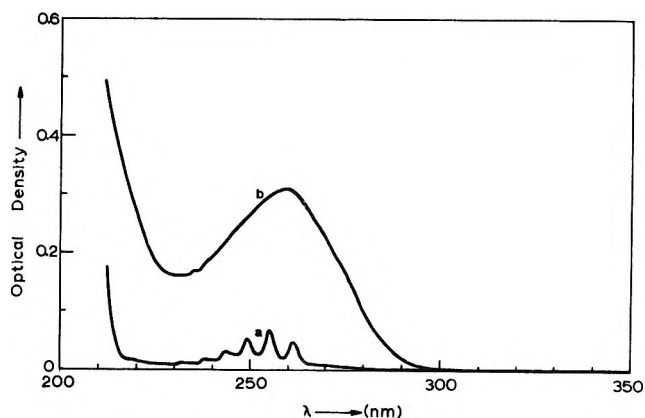
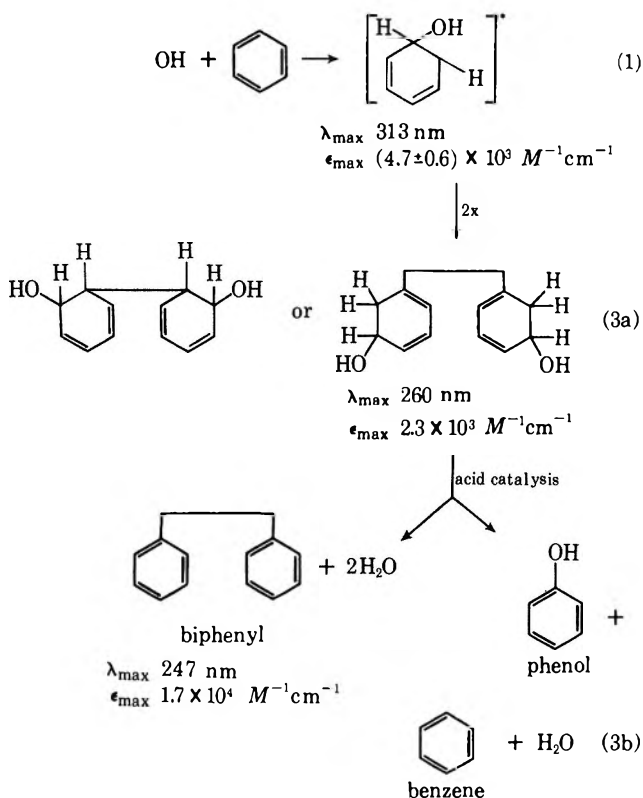


Figure 5. Absorption spectra of aqueous, N₂O-saturated, neutral, $4.24 \times 10^{-3} \text{ M}$ benzene solutions, irradiated to 40,000 rads, after admission of air, addition of alkali and extraction with *n*-hexane: curve a, hexane layer; curve b, alkali layer.

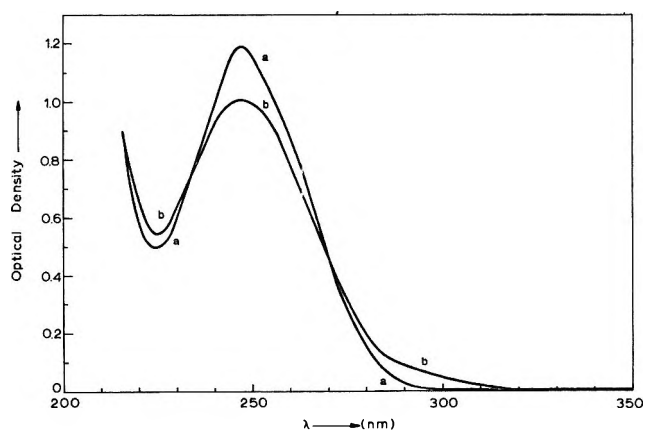


Figure 6. Absorption spectra, as in Figure 5, but: curve a, after addition of acid to the alkali layer; curve b, after addition of alkali to the acid layer.

The predominant initial product observed is thus the dimer,³ which yields biphenyl and phenol in a process which shows acid catalysis. Assuming $G = 3$ for this dimer, its $\epsilon_{\max} = 2300 \text{ M}^{-1} \text{ cm}^{-1}$ at 260 nm. Biphenyl is, of course, hardly soluble in water, but at the low concentrations ($\sim 10^{-5} \text{ M}$) produced at our total dosage it does not rapidly precipitate. We obtained its spectrum in H₂O (λ_{\max} 247 nm) but not its ϵ_{\max} with the required accuracy. We assume that, as is the case for benzene, $\epsilon_{\max}^{\text{biphenyl}}$ is nearly equal in hexane²² (ϵ_{247} 17,000) and water. Using these data we obtain $G(\text{phenol}) \sim 1.0$ and $G(\text{biphenyl}) \sim 2.1$ in N₂O-saturated aqueous benzene. The sum of their G values thus = 3.1 corresponding to $1/2 G_{(\text{OH}+\text{H})}$ in our system, in agreement with the sequence of reactions 1-3. Previous work¹ indicates that $\text{BH} + \text{BOH} \rightarrow (\text{HB}-\text{BOH})$ will yield the same products, though not necessarily in the same ratios.

Our results compare with $G(\text{phenol}) = 0.8$ and $G(\text{biphenyl}) = 3.0$ obtained by Christensen and Gustafsson.¹⁷ This would require more than the available radicals, if the reaction mechanism is accepted.

In the absence of N₂O, in deaerated solutions¹ $G(\text{phenol})$ was 0.45 and $G(\text{biphenyl}) = 1.35$, with $G(\text{H}_2) = 2.8$. The reaction $\text{BH} + \text{BH} \rightarrow (\text{BH})_2$ will assume greater importance, yielding biphenyl and H₂. The results in deaerated solutions and those in the present case of N₂O-saturated solutions establish the central role of the dimers in the mechanism of phenol and biphenyl formation in the absence of O₂.

Acknowledgment. G. S. acknowledges partial support from the U. S. Atomic Energy Commission, Biology Division. We thank Professor J. Rabani for his advice and Mr. D. Arapoglu and Y. Ogdan for their assistance.

(22) "U. V. Atlas of Organic Compounds," Vol. 1, D10/2, Verlag Chemie/Butterworths, London, 1966.

NOTES

A Further Examination of the Additivity Rule

by Jacob A. Marinsky¹*Department of Chemistry, State University of New York at Buffalo, Buffalo, New York 14214 (Received April 5, 1971)**Publication costs borne completely by The Journal of Physical Chemistry*

Isopiestic vapor pressure measurements of the ternary system, sodium polyacrylate (NaPAA)–NaCl–H₂O were reported in a recent paper by Okubo, Ise, and Matsui.² They employed a transform of the Gibbs–Duhem equation, previously derived by McKay and Perring,³ for the computation of the mean activity coefficient of polyelectrolyte and simple electrolyte in the experimental mixtures. To express the mean activity coefficient of the simple electrolyte in these mixtures the isopiestic ratio, R , was assumed to be a function of the following type

$$R = 1 - ax - bx^2 \quad (1)$$

In this equation

$$R = 2M_3/[2m_3 + (\alpha + 1)(m_2/z)] \quad (2)$$

and

 $x =$ polymer ionic fraction =

$$(\alpha + 1)(m_2/z)/[2m_3 + (\alpha + 1)(m_2/z)] \quad (3)$$

where $m_2 =$ concentration of polyelectrolyte in polyelectrolyte–NaCl solution in equivalents per 1000 g of water, $m_3 =$ molality of NaCl in polyelectrolyte–NaCl solution, $M_3 =$ molality of NaCl with same solvent vapor pressure as ternary solutions of total ionic concentration $2m_3 + (\alpha + 1)m_2/z$, $\alpha =$ net valency of macroion ($=\beta z$), and $z =$ stoichiometric valency of macroion.

To calculate R and x , the net valency of the polyelectrolyte, α , was defined as the fraction, β , of z ionizable groups that are ionized. The value of β was assigned from the results of transference experiments.⁴ Such an assignment is based on the conclusion that the fraction of counterions that are not free to move in solution ($1 - \beta$) is rigidly attached to the polyion and moves with it forming an integral part of a new "complex" macroion.

This association concept has been criticized.⁵ Indeed the appropriate interpretation of the electrochemical properties of polyelectrolytes has not been resolved. Incorporation of a β term obtained in this manner in an

otherwise thermodynamically rigorous treatment thus seems inappropriate. The quantities R and x have consequently been redefined by the elimination of β to facilitate the analysis that follows.

When this is done, in the region where R is essentially linear ($R = 1 - ax$) interaction between polyelectrolyte and salt is apparently absent. (The average deviation in the value of a was only very slightly improved by employment of the quadratic equation.) If this is indeed the case the colligative properties of the NaCl–NaPAA mixtures in these experimental situations should be additive, each component retaining its characteristic osmotic coefficient at the experimental water activity. Also, since in these isopiestic studies the chemical potential of the solvent in the various mixtures is equal

$$\phi_2 m_2 + 2\phi_3 m_3 = 2\phi_3 M_3 \quad (4)$$

By dividing both sides of eq 4 by $(m_2 + m_3)\phi_3$ and subtracting unity from each side of the resultant equation we obtain

$$\frac{\phi_2}{\phi_3} \left(\frac{m_2}{m_2 + 2m_3} \right) - \frac{m_2}{m_2 + 2m_3} = \frac{2M_3}{m_2 + 2m_3} - 1 \quad (5)$$

Eventually

$$1 + \left(\frac{\phi_2}{\phi_3} - 1 \right) \left(\frac{m_2}{m_2 + 2m_3} \right) = \frac{2M_3}{m_2 + 2m_3} \quad (6)$$

By substituting the definitions of R and x eq 6 takes the form

$$1 + \left(\frac{\phi_2}{\phi_3} - 1 \right) x = R \quad (7)$$

to lead to the identification of the a parameter of eq 1 with $(1 - \phi_2/\phi_3)$ when $b = 0$. The validity of this assignment is shown in Table I given below by the excellent agreement between a , computed from the isopiestic data, in eq 1 ($b = 0$) and $(1 - \phi_2/\phi_3)$, calculated by

(1) Visiting Professor, 1970–1971, Chemistry Department, McGill University, Montreal, Quebec, Canada.

(2) T. Okubo, N. Ise, and F. Matsui, *J. Amer. Chem. Soc.*, **89**, 3697 (1967).

(3) H. A. C. McKay and J. K. Perring, *Trans. Faraday Soc.*, **49**, 163 (1953).

(4) (a) T. Okubo, Y. Nishizaki, and N. Ise, *J. Phys. Chem.*, **69**, 3690 (1965); (b) F. T. Wall and J. J. Eitel, *J. Amer. Chem. Soc.*, **79**, 1556 (1957).

(5) A. Katchalsky, Z. Alexandrowicz, and O. Kedem, "Chemical Physics of Ionic Solutions," B. E. Conway and R. G. Barradas, Ed., Wiley, New York, N. Y., 1966, Chapter 15.

using osmotic coefficient values corresponding to the pure components at the solvent vapor pressure employed to obtain a given set of data.

Table I: Comparison of a Parameter Computation^a for NaPAA-NaCl-H₂O

Set	$-\frac{(R-1)}{x} = a^b$	$\left(1 - \frac{\phi_2}{\phi_3}\right) = a$
1	0.666	0.658
2	0.638	0.640
3	0.616	0.621

^a The same net result is obtained *with* use of a β term. This equivalence is due to the fact that β is assigned constancy in a simplifying approximation of the transference results. However, strict interpretation of transference data according to the complexation model would not yield a constant β , and this resemblance of both approaches is significant only in that it provides support for the analysis that is recommended. ^b The average deviation in the value of a was only very slightly improved by employment of the quadratic equation.

On the basis of this analysis it seems appropriate to suggest that the earlier empirical additivity rule⁵⁻⁷ that has been employed to correlate the colligative properties of dilute polyelectrolyte-salt mixtures be modified by using in eq 4 the practical osmotic coefficient values corresponding to the pure components at the solvent vapor pressure of the mixture rather than to their values at the experimental polyelectrolyte and salt concentrations of the mixtures as in the earlier application of this empirical relationship.

In the more concentrated NaPAA-NaCl-N₂O systems (sets 4 and 5) R is best described by the quadratic in x to indicate the failure of any simple additivity relationship. It is interesting to note, however, that in these systems

$$a + b = \left(1 - \frac{\phi_2}{\phi_3}\right) \quad (8)$$

This result, demonstrated in Table II presented below,

Table II: A Comparison between the Sums of a and b Evaluated with Eq 1 and 8

Set	a (eq 1)	b (eq 1)	$a + b$ (eq 1)	$a + b$ (eq 8)
4	0.492	-0.168	0.234	0.233
5	0.354	-0.305	0.049	0.052

may be of fundamental importance. It suggests that the a parameter defined by $(1 - \phi_2/\phi_3)$ may be better

expressed by the incorporation of an additional term whose characteristic property is such that it will be of negligible magnitude in those systems where the ratio ϕ_2/ϕ_3 is not crowding unity. The addition of the empirical term $1/3(\phi_2/\phi_3)^3$ satisfies this requirement

$$a = 1 - \frac{\phi_2}{\phi_3} + \frac{1}{3} \left(\frac{\phi_2}{\phi_3}\right)^3 \quad (9)$$

with the b parameter corresponding to

$$-\frac{1}{3} \left(\frac{\phi_2}{\phi_3}\right)^3 \quad (9a)$$

With eq 9a the value of b is indeed small when the ratio ϕ_2/ϕ_3 is small and increases rapidly in value when the ratio approaches a value of unity. A comparison of b computed with eq 1 and 9a is presented in Table III. The correlation is acceptable to support this kind of interpretation of the observed results.

Table III: Comparison of Computed b Parameters for NaPAA-NaCl-H₂O

b (eq 1)	b (eq 9a)
-0.002	-0.013
+0.014	-0.016
-0.026	-0.018
-0.168	-0.150
-0.305	-0.284

It is believed that an important deficiency of the empirical additivity rule previously proposed to describe the colligative properties of polyelectrolyte, simple salt mixtures⁵⁻⁷ has been identified. Modification of this relationship that is facilitated by the excellent data of Ise and coworkers has yielded a more quantitatively correct expression. The real utility limits of this modification of the additivity rule may have been defined as well. When the ratio ϕ_2/ϕ_3 exceeds 0.5 to 0.6, the simple expression (eq 4) cannot be employed and resort to the use of eq 9 and 9a in eq 1 may provide a more generally applicable relationship for anticipating the colligative properties of polyelectrolyte-salt mixtures over a much extended concentration range.

Acknowledgment. The author wishes to express his appreciation to the U. S. Atomic Energy Commission for financial support through Contract No. AT(30-1)-2269.

(6) Z. Alexandrowicz, *J. Polym. Sci.*, **43**, 337 (1960).

(7) Z. Alexandrowicz, *ibid.*, **56**, 97, 116 (1962).

No Evidence for the Dimerization of Nitromethane in Carbon Tetrachloride and Benzene Solutions

by Glen Farmer and Hyunyong Kim*

Department of Chemistry, University of Missouri, Columbia, Missouri 65201 (Received April 19, 1971)

Publication costs borne completely by The Journal of Physical Chemistry

de Maine, *et al.*,¹ reported the presence of nitromethane dimer in solutions of carbon tetrachloride, methanol, and *n*-heptane. Their conclusion was based on the optical density measurements of uv spectra at 2750 Å over a wide concentration range, 0.001 to 4 mol/l. for the case of CCl₄ solution. They have observed that Beer's law is not obeyed at the low concentrations, less than 0.15 mol/l. The experimental data were treated assuming the dimerization of nitromethane



and the absorption peaks of both monomer and dimer occur at the same wavelength. The value they have obtained for the equilibrium constant at 20° was 105 l. mol⁻¹ in CCl₄ solution and ΔH for the reaction was -0.34 kcal mol⁻¹. de Maine also reported the ir study of the above solution in support of the dimer presence.²

Musulin, *et al.*,³ reported later that the analytical expression used by de Maine, *et al.*, for the analysis of their uv spectrum is not a well-defined function, and it does not lead to convergent values. More recently, Jones and Musulin⁴ reported new values of equilibrium constants which predict even higher concentrations of dimers.

Such a large degree of dimerization in solution is somewhat surprising, in that the earlier infrared and Raman study⁵ of nitromethane in the vapor and liquid phase showed no evidence for the presence of a dimer. Contrary to de Maine's assertion¹ that nitromethane solution deviates from the colligative laws of chemistry, we were not able to find such a study of this solution reported in the literature.

We therefore have studied the freezing point depression of nitromethane in carbon tetrachloride and benzene solutions. Chemicals used were reagent grade, and nitromethane was freshly distilled just before the experiment. Cryoscopic molality m' is expressed as⁶

$$m' = A\Delta T + B\Delta T^2$$

The ΔT is the observed freezing point depression; A is the inverse of the molal freezing point constants K_f ; the K_f values of 5.12 and 12.56 deg m^{-1} are used

for benzene and carbon tetrachloride solutions; and the B constants used are 2.15×10^{-3} and 2.8×10^{-4} m deg⁻².

Table I lists the solution concentration in molality and the experimental cryoscopic molality. The uncertainty in the cryoscopic molality arose mostly from the uncertainties in ΔT , the observed temperature lowering. The quoted values are the standard deviations of several such measurements.

Table I: Freezing Point Depression of Nitromethane Solutions

Solvent	Sample molality	Cryoscopic molality
Benzene	0.132 ± 0.001	0.138 ± 0.005
	0.182	0.178
	0.259	0.254
	0.302	0.291
	0.339	0.331
Carbon tetrachloride	0.175	0.192
	0.295	0.307
	0.329	0.347

The cryoscopic data indicate that there is no large degree of dimerization as reported in ref 1. In benzene solution, the agreement between the sample molality and cryoscopic molality is within the experimental uncertainties, and in carbon tetrachloride solution there is a slight deviation toward dissociation rather than association.⁷

Acknowledgment. This work was a part of student experiments in undergraduate physical chemistry laboratory courses. We thank Dr. Scott Searles for calling our attention to ref 1.

(1) P. A. D. de Maine, M. M. de Maine, A. A. Briggs, and G. E. McAlonie, *J. Mol. Spectrosc.*, **4**, 398 (1960).

(2) P. A. D. de Maine, *ibid.*, **4**, 407 (1960).

(3) B. Musulin, W. M. Lee, and R. L. Foley, *ibid.*, **9**, 254 (1962).

(4) W. J. Jones and B. Musulin, 5th Midwest Regional Meeting of the American Chemical Society at Kansas City, Mo., Oct 29-31, 1969.

(5) T. P. Wilson, *J. Chem. Phys.*, **11**, 361 (1943).

(6) D. P. Shoemaker and C. W. Garland, "Experiments in Physical Chemistry," McGraw-Hill, New York, N. Y., 1962, pp 132-141.

(7) EDITOR'S NOTE. Professor Musulin informed us in correspondence that he is in agreement with the interpretation given of his work in ref 3. Further, with regard to the paper presented by Jones and Musulin orally (ref 4), Professor Musulin indicates that Farmer and Kim misunderstood the purpose of that report; the focus of that effort was a study of the use of nonlinear least-squares techniques for the treatment of association constants. The conclusions regarding nitromethane were quite tentative and by no means asserted that the dimer dominated.

Professor de Maine pointed out in correspondence that the iterative methods he used in ref 1 were wrong, as was subsequently pointed out by W. Lee (*J. Mol. Spectrosc.*) and also reported in Vol. II of Professor de Maine's book on "Digital Computer Programs for Physical Chemistry," where more correct methods were discussed.

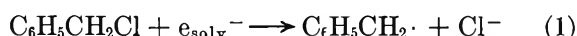
Conductometric Pulse Radiolysis Determination of Ionic Yields and Neutralization Kinetics in Liquid Ethanol

by J. Rabani,^{1a} M. Grätzel,* and
Shamim A. Chaudhri^{1b}

Hahn-Meitner-Institut für Kernforschung Berlin GmbH,
Sektor Strahlenchemie, 1 Berlin 39, Germany
(Received June 18, 1971)

Publication costs assisted by Hahn-Meitner-Institut

The method of conductometric pulse radiolysis has recently been applied for determining the radiation chemical yield of OH^- in water.² The same method has now been used to obtain the yields of e_{solv}^- and of other negative ions such as $\text{C}_2\text{H}_5\text{O}^-$ in the radiolysis of ethanol. Ethanol containing benzyl chloride as electron scavenger was irradiated by a 0.3- μsec pulse of 1.5-MeV electrons. The dose ranged from 40 to 200 rads per pulse. Since benzyl chloride is solvolyzed in ethanol at room temperature, the solutions were kept at -40° under helium and warmed up to 17° shortly before irradiation. The reaction



took place during the pulse. In pure ethanol, the half-life of e_{eth}^- was measured optically and found to be $\sim 5 \mu\text{sec}$. In the presence of $\text{C}_6\text{H}_5\text{CH}_2\text{Cl}$, no e_{eth}^- signal could be observed, showing that under our conditions practically all the e_{eth}^- reacted according to reaction 1. The conductivity increase on pulsing was caused by Cl^- and its positive counterion $\text{C}_2\text{H}_5\text{OH}_2^+$ as well as by all other ions, such as $\text{C}_2\text{H}_5\text{O}^-$, that were formed during the pulse and escaped spur recombination. After the pulse the conductivity signal decreased since neutralization processes took place. The signal finally reached a constant value which is due to the Cl^- ion and its positive counterion $\text{C}_2\text{H}_5\text{OH}_2^+$. From the known mobilities of these ions and the absorbed dose, the G value of e_{solv}^- and of heavier anions could be calculated. It should be noted that ethanol radicals do not interfere since they are unreactive toward benzyl chloride.³

Typical oscilloscope traces at different sweep rates are shown in Figure 1a. The final value of the conductivity increase which is reached after about 2 msec amounts to 46% of the initial value. (The initial conductivity was obtained by extrapolating the conductivity vs. time curve to $t = 0$.) The decay of the initial increase occurs in two steps. In the first step, 45% of the initial conductivity disappear in a first-order reaction the half-life of which is inversely proportional to the concentration of added HClO_4 . In the second step, 9% of the initial conductivity disappear in a first-order reaction, the half-life of which was independent of absorbed dose and

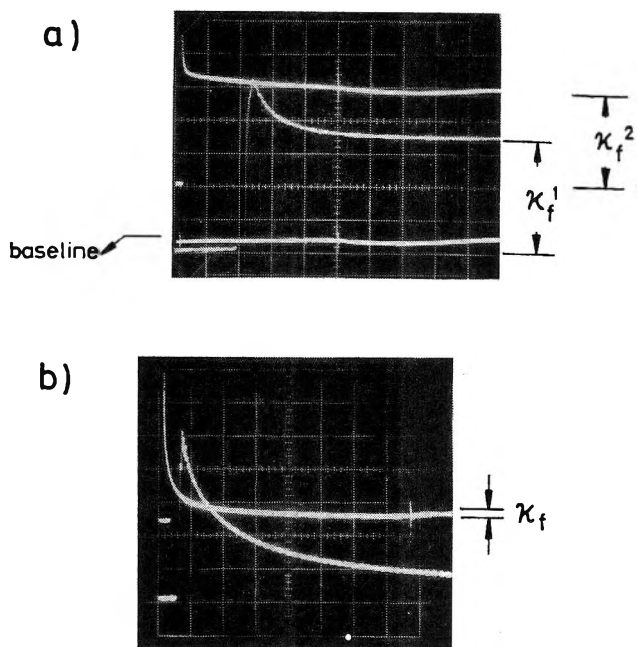
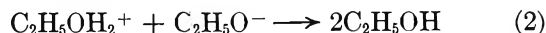


Figure 1. Conductance vs. time plots for (a) ethanol containing $[\text{C}_6\text{H}_5\text{CH}_2\text{Cl}] = 1.86 \times 10^{-3} M$ and $[\text{HClO}_4] = 9.6 \times 10^{-7} M$, sweep rate 500 $\mu\text{sec}/\text{large division}$, lower trace: sweep rate 20 $\mu\text{sec}/\text{large division}$, the base line is also shown at 500 $\mu\text{sec}/\text{large division}$; (b) pure ethanol, sweep rate 500 $\mu\text{sec}/\text{division}$, lower trace: sweep rate 50 $\mu\text{sec}/\text{division}$. The ordinate is 1 mV/division. A termination of 1 k Ω was used. The cell constant was 0.56 cm^{-1} , and the cell was operated at 100 V (field strength 300 V/cm).

of HClO_4 concentration. The concentration of benzyl chloride had no influence on the results in the investigated range from 1 to $3 \times 10^{-3} M$. $G(\text{e}_{\text{solv}}^-)$ was obtained as 1.8 ± 0.2 from the final value of the conductivity and the absorbed dose. This value is in good agreement with other determinations.^{4,5}

The first step in the conductivity decrease is attributed to the neutralization of ethoxy anions that were formed during the pulse



The rate constant obtained from logarithmic plots of traces such as shown in Figure 1 was determined to be $(5.1 \pm 0.4) \times 10^{10} M^{-1} \text{sec}^{-1}$. This value is in good agreement with the value reported by Fowles.⁶

The second step of the conductivity decrease could not be attributed to any elementary process. Since the rate constant is independent of the H^+ concentra-

(1) (a) Department of Physical Chemistry, Hebrew University, Jerusalem, Israel. (b) Postdoctoral Fellow from the Pakistan Atomic Energy Commission, Karachi, with a grant from the Alexander von Humboldt-Stiftung, Bad Godesberg, Germany.

(2) J. Rabani, M. Grätzel, S. A. Chaudhri, G. Beck, and A. Henglein, *J. Phys. Chem.*, **75**, 1759 (1971).

(3) G. A. Salmon, private communication.

(4) J. W. Fletcher, P. J. Richards, and W. A. Seddon, *Can. J. Chem.*, **48**, 1645 (1970).

(5) S. M. S. Akhtar and G. R. Freeman, *J. Phys. Chem.*, in press.

(6) P. Fowles, *Trans. Faraday Soc.*, **67**, 428 (1971).

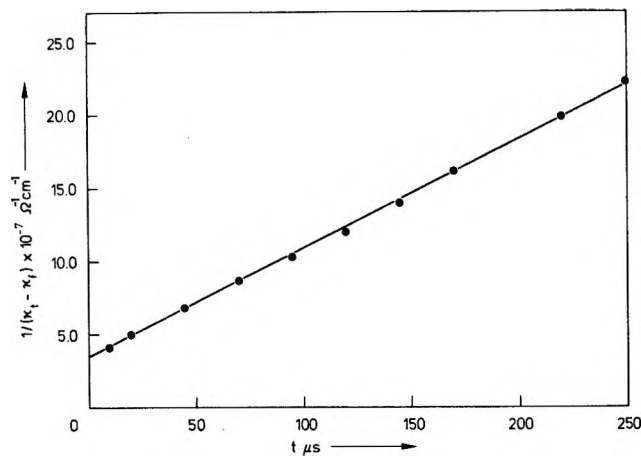


Figure 2. Plot of $1/(\kappa_t - \kappa_f)$ vs. time from the trace in Figure 1b.

tion, it is concluded that the neutralization of an anion is not the rate-determining step of this conductivity decrease. It is assumed that an unknown anion X^- of weak base character is formed by the pulse which subsequently reacts with ethanol to form an anion which is rapidly neutralized. The overall rate constant for this process was found to be $(1.4 \pm 0.2) \times 10^3 \text{ sec}^{-1}$.

If the conductivity increase immediately after the pulse is designated by κ_0 , the conductivity after the disappearance of $C_2H_5O^-$ (first step) by κ_f^1 , and after disappearance of X^- (second step) by κ_f^2 , the following equations can be written

$$\frac{\kappa_f^1 - \kappa_f^2}{\kappa_f^2} = \frac{[\Lambda(C_2H_5OH_2^+) + \Lambda(X^-)]G(X^-)}{[\Lambda(C_2H_5OH_2^+) + \Lambda(Cl^-)]G(e_{\text{solv}}^-)} \quad (3)$$

$$\frac{\kappa_0 - \kappa_f^1}{\kappa_f^2} = \frac{[\Lambda(C_2H_5OH_2^+) + \Lambda(C_2H_5O^-)]G(C_2H_5O^-)}{[\Lambda(C_2H_5OH_2^+) + \Lambda(Cl^-)]G(e_{\text{solv}}^-)} \quad (4)$$

The first factors in eq 3 and 4 which contain the molar conductances of the species involved can practically be set equal to unity since $\Lambda(C_2H_5OH_2^+)$ in ethanol is large as compared to the anion conductances which do not differ much among themselves ($\Lambda(C_2H_5OH_2^+) = 63.4$, $\Lambda(Cl^-) = 24.3$, and $\Lambda(C_2H_5O^-) = 24.5 \Omega^{-1} \text{ cm}^2 \text{ equiv}^{-1}$ at 25° .⁷ From the measured values of κ_0 , κ_f^1 , and κ_f^2 the yields of $C_2H_5O^-$ and of X^- were obtained as

$$G(C_2H_5O^-) = 1.8 \pm 0.07$$

$$G(X^-) = 0.34 \pm 0.04$$

The total yield of ions that escape spur recombination is therefore

$$G(\text{ion}) = 3.9 \pm 0.12$$

Experiments have also been carried out with pure ethanol. The electron disappears here *via* the reaction



A rate constant of $7 \times 10^3 \text{ M}^{-1} \text{ sec}^{-1}$ has previously

been reported.⁴ Figure 1b shows two traces of the conductivity at different sweep rates. Figure 2 shows a plot of $1/(\kappa_t - \kappa_f)$ vs. t . The straight line obtained indicates a second-order disappearance of the conductivity. A small residual conductivity is observed after the termination of the neutralization process (see Figure 2b). This is probably due to a small fraction of e_{eth}^- which reacted with impurities in the absence of an efficient scavenger.

In the presence of added $HClO_4$ the decrease in conductivity was of first order, the half-life being inversely proportional to the $HClO_4$ concentration. A rate constant of neutralization of $(5.4 \pm 0.2) \times 10^{10} \text{ M}^{-1} \text{ sec}^{-1}$ was obtained from these experiments which is in reasonable agreement with the value of k_2 mentioned above. For solutions containing $HClO_4$, κ_0 could be obtained by extrapolating $\log \kappa$ vs. t to $t = 0$. An average value for the total ion yield of 3.4 ± 0.1 was obtained in this way. The higher ionic yield observed in the benzyl chloride solutions may arise from small spur scavenging effects.

Acknowledgment. The authors are indebted to Dr. K.-D. Asmus and Professor Henglein for valuable discussions.

(7) Landolt-Börnstein, "Zahlenwerte und Funktionen," II/7, Springer-Verlag, Berlin, 1960, p 659.

Laser Photolysis of Perylene Solutions

by Chmouel R. Goldschmidt and Michael Ottolenghi*

Department of Physical Chemistry, The Hebrew University, Jerusalem, Israel (Received June 21, 1971)

Publication costs borne completely by The Journal of Physical Chemistry

The application of pulsed lasers as fast excitation sources in flash photochemical studies led to the detection of excited singlet-singlet transitions in aromatic molecules.¹ In the present work the above methods are applied to the perylene molecule with the purpose of recording the spectra of the lowest excited singlet state of the molecule, as well as that of the corresponding excimer. The excited singlet absorption data are subsequently used for monitoring the resonance transfer of energy from excited anthracene to perylene, yielding a new technique for the measurement of energy-transfer rates.

(1) (a) J. R. Novak and M. W. Windsor, *Proc. Roy. Soc., Ser. A*, **308**, 95 (1968); (b) R. Bonneau, J. Jousot-Dubien, and R. Bensasson, *Chem. Phys. Lett.*, **3**, 353 (1969); (c) G. Porter and M. R. Topp, *Nature (London)*, **220**, 1228 (1968); (d) A. Muller, *Z. Naturforsch. A*, **23**, 946 (1968); (e) D. S. Klinger and A. C. Albrecht, *J. Chem. Phys.*, **53**, 4059 (1970); (f) J. K. Thomas, *ibid.*, **51**, 770 (1969); (g) C. R. Goldschmidt and M. Ottolenghi, *Chem. Phys. Lett.*, **4**, 570 (1970); *J. Phys. Chem.*, **74**, 2041 (1970).

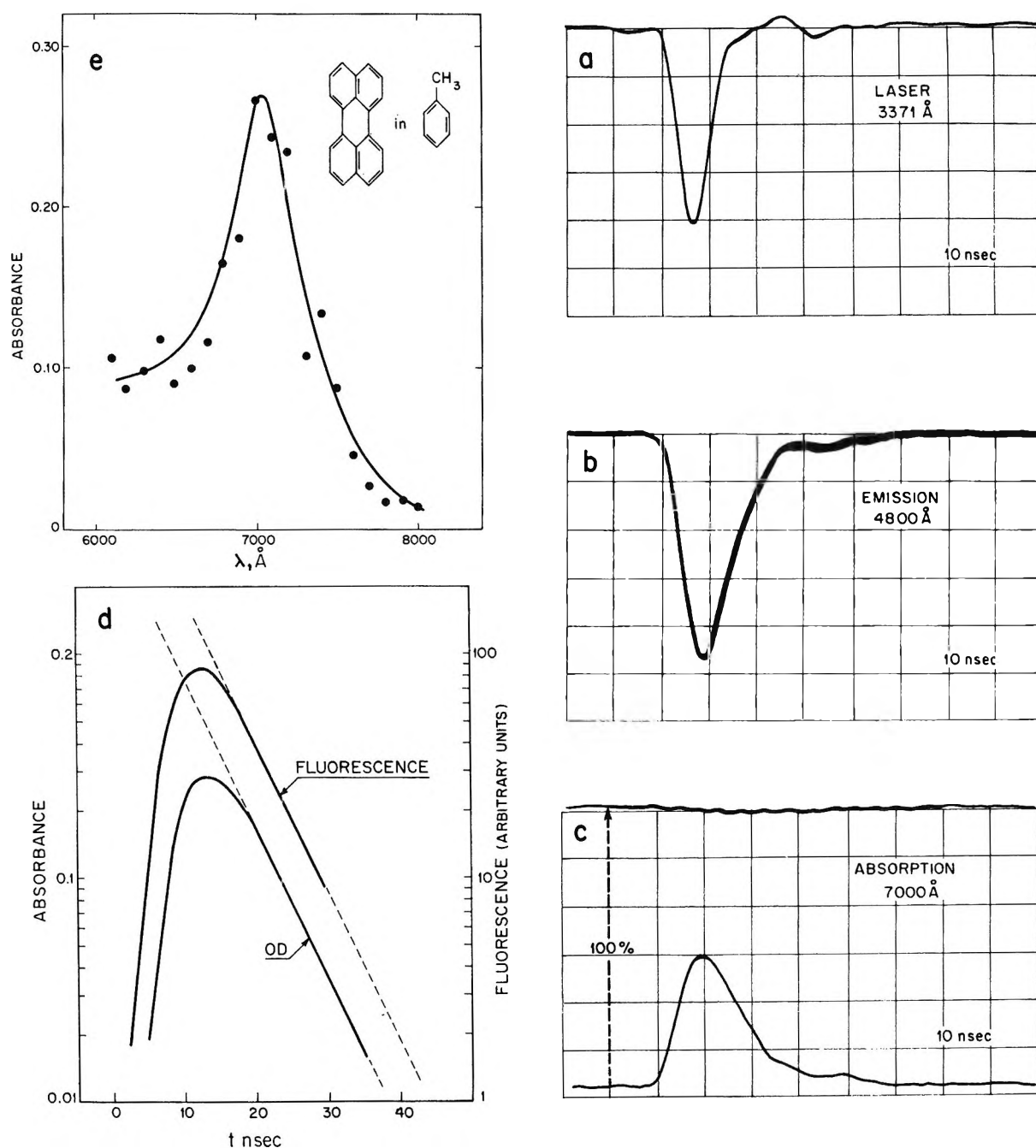


Figure 1. Excited singlet-singlet absorption in a dilute perylene solution.

Results and Discussion

(1) *Singlet-Singlet Spectra of Excited Perylene Monomer and Excimer.* Dilute ($8 \times 10^{-4} M$) solutions of perylene in toluene were excited by means of the 3371-Å, 10-nsec pulse of a (Avco-Everett) nitrogen laser using a pulsed photolysis apparatus which has been previously described.² Characteristic oscillograms showing the profile of the laser pulse, the perylene fluorescence at 4800 Å, and a transient absorption at 7000 Å are shown in Figure 1a-c. The matching of the absorbance profile with that of the fluorescence (Figure 1d) suggests the identification of the absorbing transient as the fluorescent state of perylene. In both

cases the same lifetime ($\tau = 6.5 \pm 0.5$ nsec) is obtained and is consistent with those previously reported for the fluorescence lifetime of perylene.³ The absorption spectrum of the excited perylene singlet state, derived from the corresponding absorbance profiles, is shown in Figure 1e.

A characteristic oscillogram at 7000 Å recorded in concentrated ($7 \times 10^{-3} M$) perylene solutions is shown in Figure 2a. The relatively long-lived fluores-

(2) C. R. Goldschmidt, M. Ottolenghi, and G. Stein, *Isr. J. Chem.*, **8**, 29 (1970).

(3) I. B. Berman, "Handbook of Fluorescence Spectra of Aromatic Molecules," Academic Press, New York, N. Y., 1965.

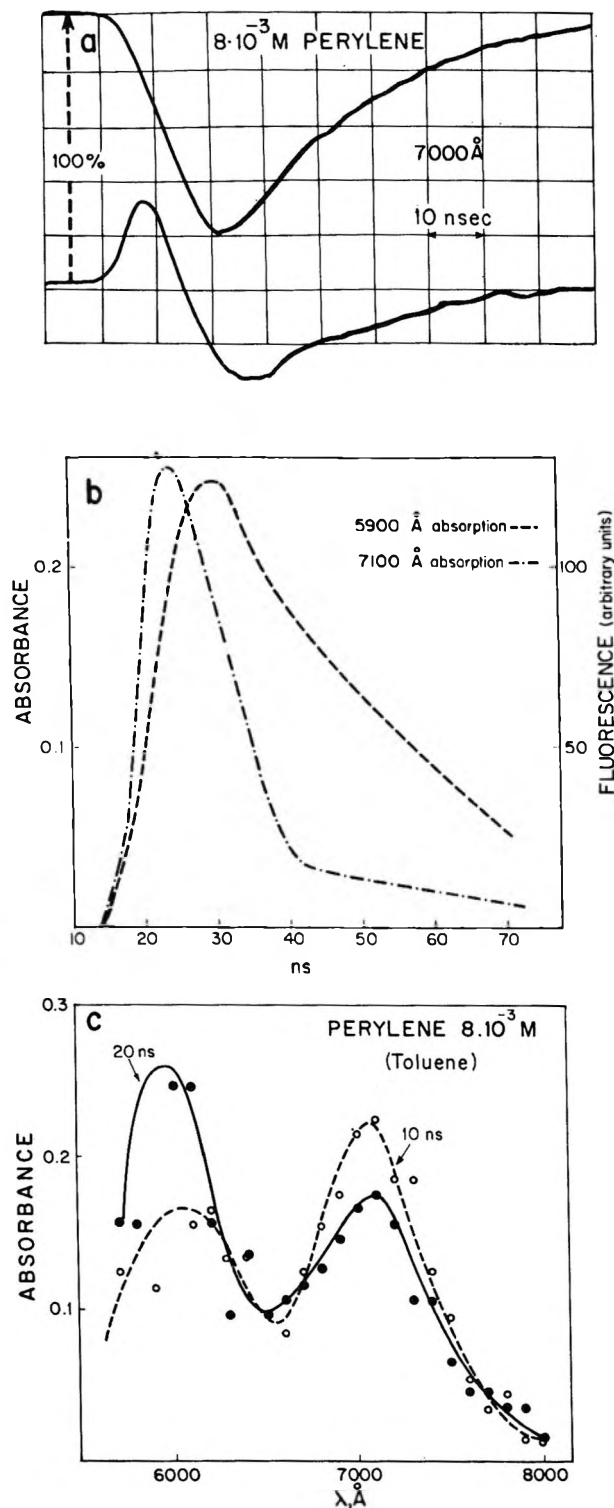


Figure 2. Laser photolysis in a concentrated perylene solution. (a) Characteristic oscillograms at 7000 Å. The upper trace was taken without the monitoring light beam. It represents the contribution of fluorescence to the lower trace, taken with the monitoring light on. (b) Transient absorbance profiles. (c) Transient spectra.

cence signal (τ 27 nsec), now present, is attributed to the excimer of perylene.⁴ Figure 2b shows the time-resolved absorbance patterns at 5900 and 7100 Å, after

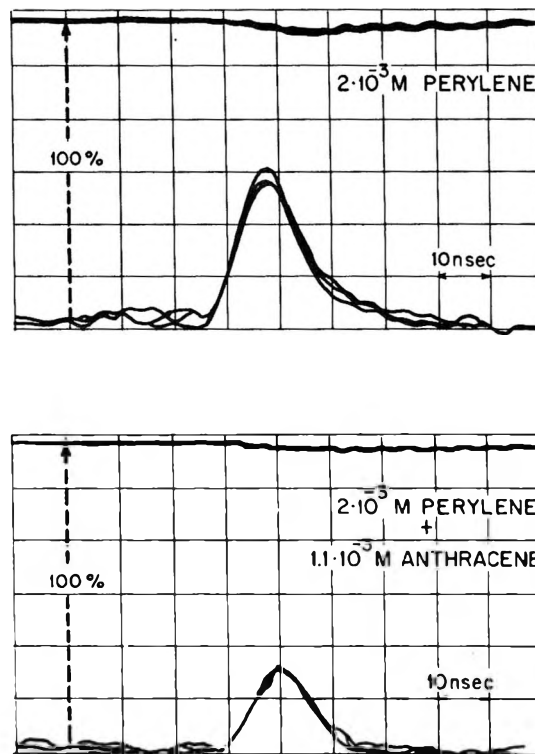
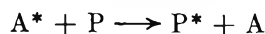


Figure 3. Oscilloscope traces showing the transient excited singlet-singlet absorption in a dilute perylene solution: top, by direct excitation of perylene; bottom, by energy transfer from excited anthracene (only 15% by direct excitation of perylene).

having been corrected for the corresponding contributions of fluorescence. It is evident that the decay of the absorbance at 7100 Å is associated with a matching growing in of the absorbance at 5900 Å and of the emission around 7000 Å. This identified the 5900-Å absorption as due to the perylene excimer. The detailed spectrum of the system 10 and 20 nsec after triggering the laser, showing the decay of the 7000-Å monomer band and the development of that of the excimer at 5900 Å, is shown in Figure 2c.

(2) *Energy Transfer from Excited Anthracene to Perylene.* Pulsed laser irradiation was also carried out in mixed anthracene-perylene solutions in toluene, under conditions in which most of the 3371-Å line was absorbed by anthracene. The efficient resonance energy transfer process taking place in the system was monitored by means of the absorption spectrum of the excited perylene system (see Figure 3). The assumption⁵ that a Stern-Volmer relation is satisfied by the competing processes (A, anthracene; P, perylene)



k_t (quenching *via* energy transfer)

(4) J. B. Birks and L. G. Christophorou, *Proc. Roy. Soc., Ser. A*, **277**, 571 (1964).

(5) W. R. Ware, *J. Amer. Chem. Soc.*, **83**, 4374 (1961).



$1/\tau_A$ (radiation and radiationless deactivation)

leads to the expression

$$\frac{[P^*]}{[P^*]_\infty} = \left[1 - \frac{1 - \beta}{1 + k_t[P]\tau_A} \right]$$

for the ratio between the amount of excited singlet perylene molecules $[P^*]$, formed at a concentration $[P]$, and the amount formed under total quenching conditions, *i.e.*, when $[P] = \infty$. β is the light fraction at 3371 Å absorbed directly by perylene [$\beta = D_p/(D_p + D_A)$]. $[P^*]_\infty$ has been estimated by direct excitation of perylene in anthracene-free solutions, where all 3371-Å light quanta are absorbed by perylene. The problem arises, of course, as to the way of determining the monomer concentrations $[P^*]$ and $[P^*]_\infty$, since the monomer formation is immediately followed by the fast excimerization process whose rate is proportional to $[P]$. This difficulty was avoided by carrying out the reference experiments in the absence of anthracene at the same perylene concentration present in the corresponding anthracene-perylene system where the energy transfer takes place. Since the degree of excimerization at any time depends only on $[P]$, the relative absorbance change in the two systems is assumed to be equal to the ratio $[P^*]/[P^*]_\infty$. (An alternative procedure to overcome the same problem could be that of carrying out the measurements around the isobestic point of the excited monomer-excimer spectrum (~ 6500 Å), where the absorbance remains practically unchanged during the excimerization process. Unfortunately, the intense fluorescence in this special range considerably reduces the accuracy of the absorbance data.) Experiments carried out at $[A] = 5.6 \times 10^3 M$ and $[P] = 2.0 \times 10^{-3} M$ yielded $[P^*]/[P^*]_\infty = 0.48 \pm 0.05$. Using $\tau_A = 4.9 \text{ nsec}^3$ and $\beta = 0.085$, this leads to the value $k_t = 0.9 \times 10^{11} \pm 0.3 M^{-1} \text{ sec}^{-1}$, which is very close to that obtained by Ware⁵ from fluorescent lifetimes measurements. The ratio $[P^*]/[P^*]_\infty$ was obtained from the ratios between the heights (or the areas) of the corresponding absorbance curves. This procedure neglects the small convolution broadening effect introduced by the ~ 2.5 -nsec decay time of A^* (at the above $[P]$ value) which is small relative to the combined effects of the laser pulse width (10 nsec) and the perylene fluorescence (6.5 nsec).

It should be finally pointed out that the above method, based on excited singlet absorption spectroscopy, is not associated with the serious problems of fluorescence absorption, present when attempting to estimate energy-transfer rates *via* steady-state emission spectroscopy.⁵ The new technique may also exhibit advantages over the methods involving fluorescence lifetime measurements,⁵ which monitor the quenching of the sensitizer but give no direct informa-

tion concerning the yields of the quenching products. It has been suggested that in some systems resonance energy transfer may not be the unique mode of interaction between excited donor and acceptor.⁶ In such cases excited singlet absorption spectroscopy may be applied for the discrimination between energy transfer and other quenching mechanisms. Work along these lines is now being carried out in this laboratory.

(6) C. R. Goldschmidt, Y. Tomkiewicz, and A. Weinreb, *Spectrochim. Acta, Part A*, 25, 1471 (1969).

Cationic Polymerization of Vinyl Monomers by Porous Glass

by John G. Koelling*

Research Laboratories, Corning Glass Works,
Corning, New York 14830

and Kenneth E. Kolb

Chemistry Department, Bradley University,
Peoria, Illinois 61606 (Received June 29, 1971)

Publication costs assisted by Corning Glass Works

While the adsorption or diffusion of organic compounds in high-surface-area porous glass has been extensively studied, there is only one reported case of polymerization initiated by glass. Little, *et al.*,¹ observed the slow polymerization of butenes over a period of days by porous glass. We have found that "dry" porous glass effects addition polymerization of certain vinyl monomers within minutes at room temperature. In this paper an investigation of the type monomer polymerized and the nature of the sites responsible for polymerization are reported.

Experimental Section

The porous glass used in these experiments was Corning's Code 7930 glass. The base glass, an alkali borosilicate glass, was subjected to a heat treatment at 590° for 3 hr and leached 4 hr in 1 N HNO₃ at 80° followed by thorough water rinsing. The plates were 21 mm in diameter and 0.15 mm thick. The resulting high-surface-area porous glass is 96% silica, about 3% boric oxide, and contains traces of aluminum oxide.² Activation of the glass was achieved by heating at 500° at 10⁻⁶ Torr to remove traces of water. Complete removal of trace water and organic contaminants was verified by infrared analysis. "Dry" porous glass exhibits a sharp major absorption at 3750 cm⁻¹ for

(1) L. H. Little, H. E. Klauser, and C. H. Amberg, *Can. J. Chem.*, 39, 42 (1961).

(2) I. D. Chapman and M. L. Hair, *Trans. Faraday Soc.*, 61, 1507 (1965).

SiOH and a very minor absorption at 3700 cm^{-1} for BOH.³

The silica powder, Cab-O-Sil (*ca.* $200\text{ m}^2/\text{g}$), used in this work was a product of the Cabot Corp. produced by flame hydrolysis of SiCl_4 . The high-surface (*ca.* $50\text{--}100\text{ m}^2/\text{g}$) alumina used was Alon-C produced by the Cabot Corp. The purified boric oxide was from J. T. Baker.

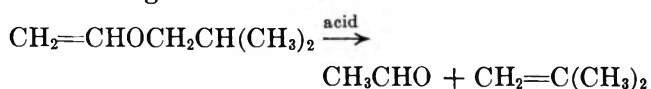
All the monomers used were distilled before use, and all except 3-phenylpropene gave single bands by gas-liquid partition chromatography. The 3-phenylpropene contained two isomers, the major one being 88% of the sample which is most probably the *trans* isomer.⁴

A high-vacuum (10^{-6} Torr) line using Kel-F 90 (3M Co.) and Apiezon K & N greases was used for adsorption and desorption of the monomers. The reaction cell which permitted infrared spectra to be taken under vacuum was essentially that described by Angell⁵ using Irtan-2 plates. Spectra were taken on Perkin-Elmer and 137G Infracord spectrophotometers.

Results and Discussions

Infrared examination of "dry" porous glass plates that have been briefly exposed to the vapors of certain vinyl monomers showed the presence of the corresponding polymers. Polymerization occurred within a matter of minutes for the following monomers in order of decreasing rate of polymerization: vinyl isobutyl ether > α -methylstyrene > styrene > 2-phenylpropene > *o*-chlorostyrene. Prolonged exposure of the "dry" glass to vapors of methyl methacrylate, vinyl acetate, and acrylonitrile resulted in no polymerization. These monomers were all readily removed by a few minutes of pumping at 10^{-6} Torr at temperatures below 100° , indicating that they were only physically adsorbed on the glass.

In all cases where polymerization occurred, the resulting infrared spectrum was that of the corresponding known polymer. The spectrum was free of both the vinyl CH stretching band at 3100 cm^{-1} and the vinyl C=C stretching band at 1600 cm^{-1} . The only case where unknown bands appeared was with vinyl isobutyl ether which, in addition to the infrared spectrum for polyisobutyl vinyl ether, gave a band at about 1625 cm^{-1} often characteristic of a carbonyl group. The appearance of a carbonyl function could be produced by splitting of vinyl isobutyl ether by an acidic site in the glass. Mooney and Qaseem⁶ have recently reported the splitting of various ethers at -80° by boron trifluoride to the corresponding alcohols and olefins. Thus, a vinyl ether could give acetaldehyde by the following reaction



Heating at 100° at 10^{-6} Torr quickly eliminated

the 1625-cm^{-1} band, indicating that it was not characteristic of the polymeric material which remained after heating. Overnight exposure of the glass plates to styrene resulted in a weight gain of coating of approximately 50% and gave samples of porous glass completely coated with polystyrene. The polymer was removed from the glass by refluxing in toluene. Films cast from the toluene gave infrared spectra identical with commercial polystyrene.

Variations in weight of polymer formed on the plates in a given time interval were small when the same plate was used repeatedly, with heat cleaning of the plate between experiments to remove the polymer. However, from plate to plate, the variations in rate were as much as twofold. Unfortunately, facilities were not available for determining surface areas of the plates so that a comparison of rate of polymerization could be made.

The polymerization of the various monomers by the glass could be stopped and restarted repeatedly. Polymerization of a monomer could be allowed to proceed for awhile, then interrupted by removing unreacted monomer by evacuation. Re-exposure of monomer vapor again allowed polymerization to proceed. This procedure could be repeated a half-dozen times with the intensity of the infrared being used to monitor continued growth. Thus the reaction seems to be an example of a living-polymer-type polymerization.

The monomers which were polymerized by porous glass are those known to be subject to free-radical or cationic initiation. Those monomers which did not polymerize are those known to be subject to free-radical or anionic initiation; thus, the initiation by the glass must be by cationic sites. The most probable sites would be either the acidic silanol groups, the B_2O_3 , or the Al_2O_3 . To ascertain which site was responsible for the polymerization, representative models of each site were examined. Exposure of styrene vapor to pressed disks of pure silica dried at 500° under vacuum gave no polymerization as determined by infrared spectroscopy. The styrene monomer was readily removed from the silica by pumping at 10^{-6} Torr for several minutes at room temperature showing that the styrene was only physically adsorbed. This indicates that the silanol group which is present both on the surface of silica and porous glass is not responsible for the polymerization.

A pressed disk of 100% Al_2O_3 did polymerize styrene. However, it also polymerized methyl methacrylate. Therefore, the trace of Al_2O_3 present in the glass is

(3) M. J. Low and N. Ramasubramanian, *Chem. Commun.*, 499 (1965).

(4) M. J. S. Dewar and R. C. Fahey, *J. Amer. Chem. Soc.*, **85**, 3645 (1963).

(5) C. L. Angell, *Instrument News*, **15** (No. 3), 12 (1964) (Perkin-Elmer Corp., Norwalk, Conn.).

(6) E. F. Mooney and M. A. Qaseem, *Chem. Commun.*, 230 (1967).

probably not the catalytic site, since methyl methacrylate was not polymerized by the glass. Since attempts to form pressed disks of anhydrous B_2O_3 were not successful, a physical mix of 5 wt % B_2O_3 and 95 wt % SiO_2 was pressed into disks at 12 tons/in.² pressure. As with porous glass, styrene was quickly polymerized while methyl methacrylate was only physically adsorbed. Although the environment of the boron in the B_2O_3 - SiO_2 mixture is not the same as it is in a glass, the evidence indicates that boron is probably the active cationic site responsible for polymerization.

To further elucidate the site responsible for polymerization, the glass was treated with excess ammonium fluoride.⁷ This reduced the number of silanol groups, but the inductive effect of the newly formed SiF should increase the acidity of the remaining silanols.⁸ A new infrared band appeared at 3420 cm^{-1} which was attributed to a NH stretch in a H-N---B-O-Si complex. Watanabe, *et al.*,⁹ reported an NH stretch of 3433 cm^{-1} in B-trichloroborazol. Since the boron in glass is attached to oxygen, which is more electron withdrawing than nitrogen or chlorine, the NH bond in the HN-BO combination should be lower in energy. Thus, the NH assignment for the 3420-cm^{-1} band appears reasonable. If this is the case, then the boron sites are blocked by NH, NH_2 , or NH_3 groups.

If polymerization is initiated by silanol groups, then the polymerization of styrene should be enhanced on fluorinated glass. When fluorinated glass was exposed to styrene vapors, there was no evidence of polymerization. Evidently the proposed complexing of the boron sites blocked the polymerization process. Thus the evidence indicates that the boron is the acidic site responsible for polymerization. The exact nature of the boron sites is not known at this time. The adsorption of water vapor on porous glass also blocked the polymerization of styrene. Since water is probably adsorbed on the boron sites as well as on silanol sites, the results are consistent with the hypothesis that boron sites are initiating the polymerization. Pyridine and alkylamines, which would be expected to also block the boron sites, both prevented polymerization.

Recently, Altug and Hair¹⁰ have examined the surface of porous glass by the pH titration method. Their work indicated that the surface contains two acidic sites. One with a pK_a value of about 7 was attributed to silanol, while the other stronger acid having a pK_a of 5.1 was said to be associated with boron. Thus for cationic initiations, the stronger acidic boron sites should be better initiators than the silanol sites. These results

indicate that the boron in porous glass is capable of polymerizing vinyl monomers with the boron sites most probably acting as a Lewis acid.

Photolysis of Gaseous 1,4-Dioxane at 1470 Å

by Robert R. Hentz* and C. F. Parrish¹

*Department of Chemistry and the Radiation Laboratory,²
University of Notre Dame, Notre Dame, Indiana 46556
(Received July 22, 1971)*

Publication costs assisted by the U. S. Atomic Energy Commission

The γ radiolysis of liquid 1,4-dioxane gives³ $G(H_2) = 1.3$.^{4,5} $G(H_2)$ is suppressed by cation, electron, and H-atom scavengers (D_2O , N_2O , $c\text{-C}_4F_8$, I_2 , and 1-hexene) to a limit of $G^*(H_2) \approx 1.0$ which has been attributed to molecular elimination from a directly excited state⁴ and, therefore, is designated as $G^*(H_2)$. A lifetime of less than $\sim 10^{-10}$ sec was estimated for such an excited state from the failure of 0.1 M benzene to affect $G^*(H_2)$. Excitation of liquid 1,4-dioxane with 12-MeV electrons⁶ or 1849-Å photons^{7,8} yields fluorescence with λ_{max} 2470 Å,^{6,7} a quantum yield of $\phi_f = 0.03$,⁷ and a lifetime of $\tau = 2.2$ nsec.⁸ From the absence of fluorescence ($\phi_f < 10^{-5}$) when 1,4-dioxane vapor (25 Torr) is excited at 1849 Å and from the behavior of τ , ϕ_f , and the absorption and emission spectra for liquid mixtures of 1,4-dioxane with inert solvents, Hirayama, *et al.*,⁷ have concluded that excited monomeric dioxane does not fluoresce and that the liquid fluorescence occurs from an excited dioxane aggregate formed subsequent to light absorption. Neither such an excited aggregate or its excited monomeric precursor is likely to be responsible for $G^*(H_2)$ for the following reasons: (1) $\tau = 2.2$ nsec,⁸ (2) traces of H_2O noticeably reduce ϕ_f and red-shift the fluorescence,⁷ (3) there is appreciable excitation transfer to 0.01 M anthracene,⁶ and (4) such excitation transfer is suppressed by N_2O .⁶ The possibility remains that $G^*(H_2)$ is a consequence of the rapid decomposition of a higher excited state which

(1) Chemistry Department, Indiana State University, Terre Haute, Ind.

(2) The Radiation Laboratory of the University of Notre Dame is operated under contract with the U. S. Atomic Energy Commission. This is AEC Document No. COO-38-789.

(3) The symbol G denotes a yield in molecules per 100 eV absorbed by the system; measured and primary quantum yields are denoted by Φ and ϕ , respectively.

(4) R. R. Hentz and W. V. Sherman, *J. Phys. Chem.*, **72**, 2635 (1968).

(5) J. H. Baxendale and M. A. J. Rodgers, *Trans. Faraday Soc.*, **63**, 2004 (1967).

(6) J. H. Baxendale, D. Beaumont, and M. A. J. Rodgers, *Chem. Phys. Lett.*, **4**, 3 (1969).

(7) F. Hirayama, C. W. Lawson, and S. Lipsky, *J. Phys. Chem.*, **74**, 2411 (1970).

(8) A. M. Halpern and W. R. Ware, *ibid.*, **74**, 2413 (1970).

(7) T. H. Elmer, I. D. Chapman, and M. E. Nordberg, *J. Phys. Chem.*, **67**, 2219 (1963).

(8) I. D. Chapman and M. L. Hair, *J. Catal.*, **2**, 145 (1963).

(9) H. Watanabe, M. Narisada, T. Nakagaus, and M. Kubo, *Spectrochim. Acta*, **16**, 78 (1960).

(10) I. Altug and M. L. Hair, *J. Phys. Chem.*, **71**, 4260 (1967).

does not have ionic precursors. Such considerations suggested study of the photochemistry of 1,4-dioxane. Photolysis of the vapor at 1470 Å was chosen for the initial study for elucidation of the decomposition modes of a higher excited state of *monomeric* dioxane and for comparison with our previous studies of the 1470-Å photolysis of cyclohexane vapor.⁹⁻¹¹

The 1,4-dioxane (Matheson Coleman and Bell spectroscopic reagent) was purified by the method of Hentz and Sherman.⁴ Prior to use, purified dioxane was transferred into a flask containing LiAlH₄. The flask was attached to a vacuum line and, after deaeration, the dioxane remained in contact with the LiAlH₄ for several days prior to transfer, on the vacuum line, into a flask with a sodium mirror. Samples for photolysis were taken from the thoroughly dried and deaerated dioxane in the latter flask.

The light sources, photolysis cells, and auxiliary equipment used were essentially the same as those used previously⁹ except that the cell used for determination of only the formaldehyde yields was modified with a side arm closed with a serum cap for introduction of the analytical reagents. Actinometry has been described.⁹ Intensities were in the range $(0.18-2.4) \times 10^{15}$ quanta sec⁻¹; there was no detectable effect of intensity on product yields. In all experiments the light was completely absorbed in the cell.

The transfer and measurement of a sample for photolysis¹¹ and the collection and measurement of gas products^{4,11} have been described. Gas products were analyzed by standard gas chromatographic techniques. Formaldehyde yields determined by gas chromatographic analysis of the gas products were not reproducible, and a material balance could not be obtained. At high conversions a volatile solid, which suggested paraformaldehyde or trioxane, was observed in the photolysis cell. Therefore, the chromotropic acid colorimetric method¹² was used for determination of formaldehyde in the postphotolysis mixture; both paraformaldehyde and trioxane are converted into formaldehyde under the conditions of analysis. Water (1 ml) was added through the serum cap and splashed over the entire surface of the cell immediately after a photolysis. After addition of 1 ml of the chromotropic acid reagent followed by 23 ml of concentrated sulfuric acid, the mixture was heated to 50° and allowed to stand 3 hr. Optical densities measured with a Beckman DU spectrophotometer at 580 nm were compared with a standard curve. The contribution of dioxane to the absorption was subtracted.

Quantum yields, with their average deviations, are presented in Table I. Quantum yields were independent of per cent conversion over the ranges studied at each pressure. Because the number of quanta absorbed was varied over approximately the same range at each pressure, $(6-90) \times 10^{16}$ quanta, the range of per cent conversion varied with pressure. Thus, each

Table I: Quantum Yields in the 1470-Å Photolysis of Gaseous 1,4-Dioxane

	P, Torr		
	2.7	12	155
	Temp, °C		
	25	25	95
$\Phi(\text{CH}_2\text{O})$...	1.6 ± 0.1	...
$\Phi(\text{C}_2\text{H}_4)$	0.89 ± 0.09	0.83 ± 0.04	0.80 ± 0.09
$\Phi(\text{H}_2)$	0.17 ± 0.02	0.20 ± 0.02	0.16 ± 0.02
$\Phi(\text{CO})$	0.07 ± 0.02	0.16 ± 0.01	0.07 ± 0.02

quantum yield in Table I is the average of four to eight values obtained at different per cent conversions which, based on $\Phi(-\text{C}_4\text{H}_8\text{O}_2) = 1.0$, were in the range 0.1-1.5 at 2.7 Torr, 0.03-0.45 at 12 Torr, and 0.002-0.03 at 155 Torr. Except for the anomalous CO yield at 12 Torr, there appears to be no significant effect of the changes in pressure and temperature on the quantum yields.

In the spectrum of gaseous 1,4-dioxane,¹³ 1470 Å corresponds to absorption in the third and fourth bands with a decadic extinction coefficient of $\epsilon = 205 \text{ cm}^{-1} \text{ atm}^{-1}$ at 25°. Because $\epsilon = 180 \text{ cm}^{-1} \text{ atm}^{-1}$ for C₂H₄¹⁴ and $\epsilon = 52 \text{ cm}^{-1} \text{ atm}^{-1}$ for CH₂O¹⁵ at 1470 Å, product photolysis should not have a significant effect on the quantum yields over the range of conversions studied. However, for conversions covering the range 0.002-1.5%, an effect on $\Phi(\text{C}_2\text{H}_4)$ and $\Phi(\text{H}_2)$ of a competition between C₂H₄ and dioxane for H should have been detectable; $k = 5.5 \times 10^8 \text{ M}^{-1} \text{ sec}^{-1}$ at 25° for H addition to C₂H₄¹⁶ and values of 10⁶ and 10⁷ M⁻¹ sec⁻¹ are reasonable estimates of k for abstraction from dioxane at 25 and 95°, respectively.¹⁷ Thus, $\phi(\text{H})$ appears to be insignificant.

The primary quantum yield for photodecomposition of CH₂O is essentially unity,¹⁸ and H is a major primary product. Consequently, present results indicate that there is no significant yield of electronically excited CH₂O in the 1470-Å photolysis of gaseous 1,4-dioxane. Moreover, the observed pressure independence of the quantum yields precludes a competition between collisional deactivation and decomposition of a vibrationally excited ground state of CH₂O. Thus, the

(9) R. R. Hentz and D. B. Peterson, *J. Phys. Chem.*, **74**, 1395 (1970).

(10) R. R. Hentz and R. J. Knight, *ibid.*, **72**, 4684 (1968).

(11) R. R. Hentz and S. J. Rząd, *ibid.*, **71**, 4096 (1967).

(12) A. P. Altshuller, D. L. Miller, and S. F. Sleva, *Anal. Chem.*, **33**, 621 (1961).

(13) G. J. Hernandez and A. B. F. Duncan, *J. Chem. Phys.*, **36**, 1504 (1962).

(14) M. C. Sauer, Jr., and L. M. Dorfman, *ibid.*, **35**, 497 (1961).

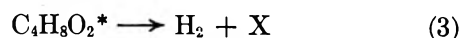
(15) S. Glicker and L. J. Stief, *ibid.*, **54**, 2852 (1971).

(16) T. Hikida, J. A. Eyre, and L. M. Dorfman, *ibid.*, **54**, 3422 (1971).

(17) H. A. Kazmi and D. J. LeRoy, *Can. J. Chem.*, **42**, 1145 (1964), report $k = 6.6 \times 10^{16} e^{-7.1/RT} \text{ M}^{-1} \text{ sec}^{-1}$ for abstraction from *n*-C₄H₁₀.

(18) J. G. Calvert and J. N. Pitts, Jr., "Photochemistry," Wiley, New York, N. Y., 1966, p 371.

results are most plausibly interpreted in terms of the decomposition modes 1-3 (in which X denotes unde-



tected products) with $\phi_1 = 0.75$, $\phi_2 = 0.10$, and $\phi_3 = 0.08$. Assuming a collision diameter of 6 Å for dioxane, the collision frequency is $3.7 \times 10^7 \text{ sec}^{-1}$ at 2.7 Torr and 25° and $1.9 \times 10^9 \text{ sec}^{-1}$ at 155 Torr and 95° . Absence of a significant effect of such a change in collision frequency on the quantum yields, as well as the absence of fluorescence ($\phi_f < 10^{-5}$)⁷ from dioxane vapor excited at 1849 Å, suggests that excitation at 1470 Å results in rapid decomposition (τ certainly less than 10^{-10} sec) with $\phi(-\text{C}_4\text{H}_8\text{O}_2^*) = 1.0$. Given the uncertainties in measured quantum yields and the possibility of small yields of undetected products, the sum $\phi_1 + \phi_2 + \phi_3 = 0.93$ is consistent with the conclusion that $\phi(-\text{C}_4\text{H}_8\text{O}_2^*) = 1.0$.

The 1470-Å photolysis of gaseous 1,4-dioxane is similar to oxetane photolysis¹⁹ in which decomposition into C_2H_4 and CH_2O accounts for 98% of the total decomposition. However, there is very little similarity to the 1470-Å photolysis of cyclohexane vapor¹¹ in which $\Phi(\text{H}_2) = 0.74$ and $\phi \leq 0.15$ for the analog of reaction 1. Decomposition of gaseous 1,4-dioxane at 10 Torr with the 6942-Å line of a ruby laser²⁰ gives relative yields of approximately 1, 2, and 3 for C_2H_4 , H_2 , and CO , respectively. Conversions in the laser photolysis, ~4%, were not appreciably greater than the highest conversion, 1.5%, studied in the 1470-Å photolysis. Consequently, the considerable difference between laser and 1470-Å product distributions must be ascribed to the enormous difference in absorbed intensities or to a difference in the excited states from which decomposition occurs. With the laser, as suggested by the authors,²⁰ excitation may be to a high vibrational level of the ground electronic state.

Product yields in the 1470-Å photolysis of gaseous 1,4-dioxane provide little support for the idea that an upper excited state is responsible for $G^*(\text{H}_2) = 1.0$ in the liquid radiolysis which also gives $G(\text{C}_2\text{H}_4) \approx 1.6$ and $G(\text{CO}) = 0.18$.⁴ It is possible that the relative yields of reactions 1-3 are appreciably altered in the liquid phase; Hirayama, *et al.*,⁷ have noted that there is a marked difference between the liquid and vapor absorption spectra which, they suggest, indicates a profound modification in the relative nuclear configurations of ground and excited states on condensation. It is clear, however, that elucidation of the origin of

$G^*(\text{H}_2)$ must await a thorough study of the photochemistry of 1,4-dioxane at both 1849 and 1470 Å and particularly in the liquid phase.

On the Nuclear Magnetic Resonance

Line Shape of Solid Heptane

by K. van Putte* and J. van den Enden

Unilever Research, Vlaardingen, The Netherlands
(Received May 26, 1971)

Publication costs assisted by Unilever Research

In order to study the methyl reorientation process in solid alkanes, Anderson and Slichter¹ investigated the proton spin-spin and spin-lattice relaxation behavior in these systems between 100 and 250°K. In this temperature range the proton spin-lattice relaxation is almost completely determined by the reorienting methyl groups.¹⁻³

At 150°K, the line shape of alkanes with less than 15 C atoms per molecule consists, according to Anderson and Slichter, of two peaks, differing by a factor of 7 in line width. These authors suggest that the narrow line corresponds with the reorienting methyl groups.

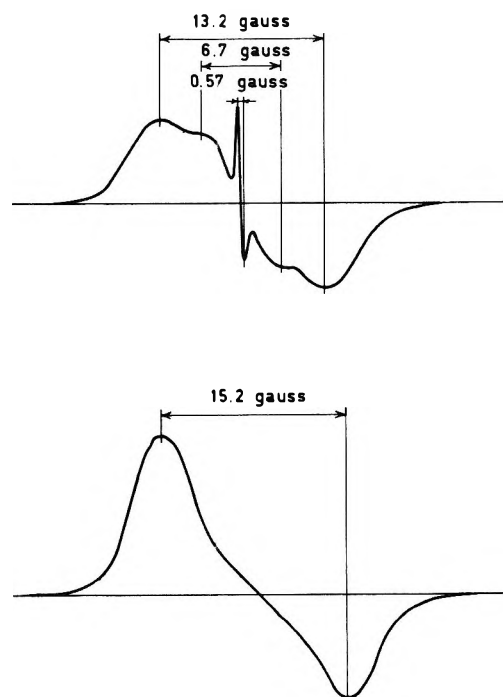


Figure 1. Derivative curve for heptane at 133°K (upper) and 93°K (lower).

- (1) J. E. Anderson and W. P. Slichter, *J. Phys. Chem.*, **69**, 3099 (1965).
- (2) K. van Putte, *J. Magn. Resonance*, **2**, 216 (1970).
- (3) K. van Putte, Thesis, Amsterdam, 1970.

(19) J. D. Margerum, J. N. Pitts, Jr., J. G. Rutgers, and S. Searles, *J. Amer. Chem. Soc.*, **81**, 1549 (1959).

(20) E. Watson, Jr., and C. F. Parrish, *J. Chem. Phys.*, **54**, 1427 (1971).

Studying the methyl reorientation process in further detail,³ we repeated the line shape measurement on heptane (purity >99%) at 133 and 93°K (Figure 1). The signal-to-noise ratio was improved by means of a spectrum accumulator.

Only one broad peak at 93°K, with a line width (δH) of 15.2 G, was observed, which suggests that the entire molecule can be considered rigid at this temperature. Contrary to the results of Anderson and Slichter, the line shape at 133°K consists of three rather than two peaks, the line width of the narrowest peak being 0.57 G. The intensity increases with increasing temperature. A repetition of the solidifying procedure, however, showed that the reproducibility of this peak is poor, which will be clear from a comparison of our results with those of Anderson and Slichter. The peak must be due to lattice defects, which give sufficient motional freedom to the surrounding molecules to narrow the line as observed.

The line widths of the two broader peaks are 13.2 and 6.7 G and differ by only a factor of 2. The peak with line width 6.7 G corresponds with the reorienting methyl groups. The narrowing factor agrees reasonably well with that found in solid methyl ketones.³

Acknowledgment. We thank Professor Dr. C. MacLean and Professor Dr. E. de Boer for many stimulating discussions.

Absolute Rate Constants for the Reaction of Atomic Oxygen with 1-Butene over the Temperature Range of 259–493°K

by Robert E. Huie,¹

*University of Maryland, College Park, Maryland, and
National Bureau of Standards, Washington, D. C.*

John T. Herron,

National Bureau of Standards, Washington, D. C.

and Douglas D. Davis*²

*University of Maryland, College Park, Maryland
(Received May 26, 1971)*

Publication costs assisted by The Petroleum Research Fund

Several studies have been made of the reaction of atomic oxygen in its ground electronic state with 1-butene.^{3–5} Typically, these investigations have involved the production of atomic oxygen in a mixture of two reactive species, with the relative rates of reaction determined by following the rate of production of characteristic reaction products. In only one study, using a discharge flow system, has an absolute rate measurement been made.⁶ Because there is disagreement

among the rate measurements with regard to the reaction's temperature dependence,⁷ we have applied the technique of flash photolysis–resonance fluorescence to this system in an effort to better define its kinetic rate parameters.

The apparatus and technique used in this study have been previously described^{8–10} and will be discussed here only briefly. In these experiments, a mixture of oxygen, 1-butene, and a large excess of argon is flash-photolyzed, producing between 10^{11} and 10^{12} oxygen atoms per cm^3 (3×10^{-3} to 3×10^{-2} mTorr). The oxygen atoms are excited by the absorption of oxygen resonance radiation from an oxygen resonance lamp and fluoresce in a time on the order of 10^{-8} to 10^{-9} sec. The fluorescence is monitored at right angles to the resonance and flash lamps using an electron magnetic multiplier detector, and the temporal history of the oxygen atoms is then followed by feeding the signal from the detector into a multichannel analyzer. Since single photon counting techniques are employed here, statistical fluctuations in the signal are reduced by taking many flashes (>50) to produce one kinetic curve. The gas mixture in these experiments is changed several times during the development of a kinetic curve to ensure that the total consumption of the 1-butene never exceeds 5%. The experiments are performed with an excess of 1-butene, so that first-order loss of atomic oxygen prevails. The pseudo-first-order rate constant for the loss of atomic oxygen, corrected for both diffusion of oxygen atoms from the reaction zone and reaction of O atoms with O_2 , can then be used to derive the second-order rate constant for the reaction. The diffusion and O plus O_2 reaction correction is typically 15% or less of the rate of reaction of O atoms with 1-butene.

The reaction has been studied over a pressure range of 20 to 200 Torr, using argon as a diluent gas, over a concentration range of 1-butene of 1.29 to 12.9 mTorr, and over an approximate initial oxygen atom concentration range of 2×10^{11} to 8×10^{11} atoms cm^{-3} (6×10^{-3} to 2.5×10^{-2} mTorr). The results given in Table I demonstrate that over these ranges the rate constant for this reaction is both independent of the total pressure and the concentration of either reactant.

(1) This research, carried out at the University of Maryland, is part of a thesis to be submitted to the Faculty of the University of Maryland in partial fulfillment of the requirement for the degree of Doctor of Philosophy.

(2) Acknowledgment is made by this author to the donors of The Petroleum Research Fund, administered by the American Chemical Society, for support of this research.

(3) R. J. Cvetanović, *J. Chem. Phys.*, **23**, 1063 (1960).

(4) I. M. W. Smith, *Trans. Faraday Soc.*, **64**, 378 (1968).

(5) D. Saunders and J. Heicklen, *J. Phys. Chem.*, **70**, 1950 (1966).

(6) L. Elias, *J. Chem. Phys.*, **38**, 989 (1960).

(7) R. J. Cvetanović, *Advan. Photochem.*, **1**, 115 (1963).

(8) W. Braun and M. Lenzi, *Discuss. Faraday Soc.*, **44**, 252 (1969).

(9) D. D. Davis, W. Braun, and A. M. Bass, *Int. J. Chem. Kinet.*, **2**, 101 (1970).

(10) D. D. Davis, R. E. Huie, J. T. Herron, M. J. Kurylo, and W. Braun, *J. Chem. Phys.*, in press.

Table I: Absolute Rate Constants for the Reaction $O(^3P) + 1\text{-butene} \rightarrow \text{products}^a$

$T, ^\circ\text{K}$	[1-C ₄ H ₈], mTorr	[O ₂], Torr	Total pressure, Torr, Ar	Flash energy, ^b J	k, cm^3 molecule ⁻¹ sec ⁻¹ \times 10^{12}
298	5.26	1	20	32	3.84
298	5.26	1	20	18	4.10
298	5.26	1	20	8	4.20
298	5.26	1	200	26	3.86
298	2.63	0.5	10	20	4.10
298	1.29	1	200	18	3.73
298	12.9	1	200	18	4.20
259	2.53	0.5	100	42	3.38
274	2.77	1	40	45	3.76
343	2.63	1	200	20	4.69
403	2.63	1	200	20	5.27
493	4.25	1	200	45	7.16

^a Products from this reaction would include α -butene oxide, n -butanal, carbon monoxide, and methyl ethyl ketone.⁷ ^b A flash energy of 45 J in this system corresponds to an incident light intensity at the reaction cell of $\sim 8 \times 10^{12}$ photons/cm².

A linear least-squares fit of the data to the Arrhenius expression yields

$k =$

$$(1.46 \pm 0.15) \times 10^{-11} \exp\left(\frac{-760 \pm 60 \text{ cal mol}^{-1}}{RT}\right)$$

$\text{cm}^3 \text{ molecule}^{-1} \text{ sec}^{-1}$

where $1 \text{ cal mol}^{-1} = 4.18 \text{ J mol}^{-1}$. The quoted error limits are the standard errors of the reported values based upon the least-squares treatment of all the data. Figure 1 shows the data in the Arrhenius form, along with the data of previous workers. The relative rate data of Saunders and Heicklen⁵ and Cvetanović³ were converted into absolute rate constants using the rate expression for the reaction of atomic oxygen with ethylene obtained in this laboratory¹⁰

$k(O + C_2H_4) =$

$$5.42 \times 10^{-12} \exp\left(\frac{-1130 \text{ cal mol}^{-1}}{RT}\right)$$

$\text{cm}^3 \text{ molecule}^{-1} \text{ sec}^{-1}$

The absolute values from Smith's data depend on the results of Klein and Herron¹¹ for the reaction of atomic oxygen with nitrogen dioxide.

The data points of the other workers all fall within about 25% of our computed Arrhenius line. With the exception of the activation energy derived from the relative rate data of Cvetanović ($E \sim -70 \text{ cal mol}^{-1}$), the

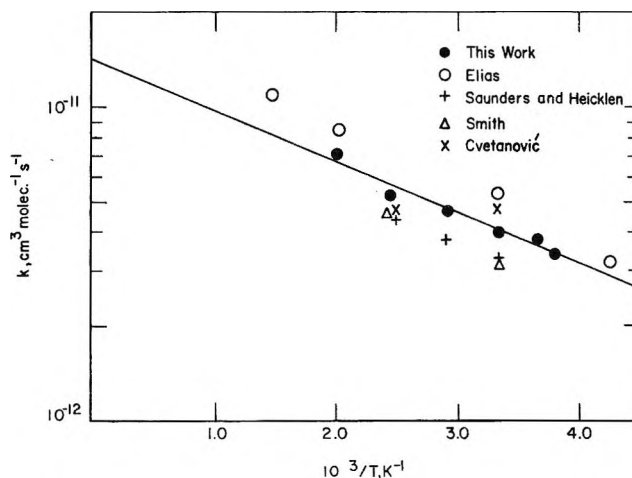


Figure 1. Arrhenius plot of the reaction of atomic oxygen with 1-butene.

activation energies predicted by these other data agree quite well with ours (within 15%). A comparison of our data for ethylene and 1-butene with the relative data of Cvetanović shows that for the ratio of 1-butene to ethylene at 298°K Cvetanović's results are 16% higher than ours (5.7 to 4.9). However, at 398°K we are 30% higher than Cvetanović (4.0 to 3.0). Thus, although the absolute discrepancy is not extremely large at either temperature, the combined deviations at the two temperatures result in a very significant difference in the calculated Arrhenius activation energy for 1-butene. The reason that the relative rate data of Cvetanović give such a large activation energy difference between ethylene and 1-butene is not, at present, obvious.

(11) F. S. Klein and J. T. Herron, *J. Chem. Phys.*, **41**, 1285 (1964).

COMMUNICATIONS TO THE EDITOR

A Case for Solvated Electrons

Publication costs assisted by Professor M. C. R. Symons

Sir: Tuttle and Graceffa¹ have drawn a comparison between solutions of alkali metals in amines (and ammonia) with those of sodium naphthalenide in ether-naphthalene mixtures. They seem to suggest that a common model may well be able to accommodate the similar esr results for these two systems and since, obviously, the "solvated electron" model is quite inapplicable to the naphthalenide system, they seem to favor the concept that the metal solutions are best described as comprising the alkali metal salts of the solvent (*i.e.*, Na^+NH_3^- , $\text{Na}^+\text{RNH}_2^-$ etc.).

If this analogy is accepted, it should be taken one step further. As was stressed,¹ Na^+N^- (N^- = naphthalenide) and N^- in dilute solution in inert solvents have esr spectra quite characteristic of the molecular system, the unpaired electron being in a highly localized π^* MO of the naphthalene. All attempts to reproduce this behavior for ammonia and amines in dilute solutions of inert solvents have failed. Even hexamethylphosphoramide, which is a very good solvent for metals, does not interact with sodium-ether systems despite the presence of relatively low-lying empty MO's for this compound² and despite the fact that "solvated electrons" are formed in such media.

Thus the analogy breaks down. True, nmr results indicate a large contact interaction with ^{14}N , but this could be spread out over several solvent molecules: there is nothing in the results to suggest that it is confined to one per electron.

The reason why most workers in this field accept that two distinct models are required for the systems under consideration is that only naphthalene has a low-lying MO into which the extra electron can move. Anions such as NH_3^- can be formed, in principle, by reaction between NH_2^- and hydrogen atoms. Indeed, when hydrogen atoms are trapped in polar media, it seems very likely that there is a real interaction with one or more "solvent" molecules³ which has the effect of hardly modifying their esr spectra, but introducing a characteristic optical absorption band.⁴ Perhaps the nearest example is that of HF^- , which is structurally comparable with NH_3^- . Such units are thought to be formed in $\text{CaF}_2\text{-H}$ systems, and again, the proton coupling is close to that for normal hydrogen atoms.⁵ Thus experimental evidence and calculations⁴ support the statement that the esr spectra of species such as NH_3^- are likely to be characterized by very large, positive, ^1H hyperfine coupling constants. In fact, however, the coupling detected by nmr is invariably

small and negative. This implies a spin polarization of (presumably) the N-H σ electrons by the unpaired electron, rather than a direct occupancy of a suitable antibonding orbital.

In the gas phase, anions such as NH_3^- would spontaneously lose an electron. If NH_3^- is formed in liquid or solid ammonia, in the absence of distortions, the electron would become delocalized over all the molecules as a conduction electron. This is certainly not the case in the systems concerned. If, however, the electron is momentarily confined to one ammonia molecule, and other solvent molecules re-orient to suit the negative charge, such delocalization would be prevented. Since, however, the electron is in an antibonding state, even greater stabilization (kinetic) would result if the central molecule were removed, leaving the electron in a cavity. There are plenty of analogies for this, perhaps the simplest being the conversion of an optically excited halide ion in an alkali halide crystal into an F center by removal of the central halogen atom.

There is a large volume of evidence in favor of the cavity-solvated electron model from the solid state.⁶ For example, glassy ethanol on irradiation gives trapped electrons, but crystalline ethanol does not. The former contain many cavities, the latter very few. At 4.2 K the former has a narrow esr singlet indicating weak coupling to solvent molecules, but on warming to 77 K it broadens markedly because of specific coupling to several (probably 4) OH protons. The link is now *via* the optical spectra. That at 4.2 K is probably comparable with electrons trapped in ether cavities: that at 77 K is characteristic of alcohols and links well with results for electrons in fluid alcohols.

The contrast between molecules with and without acceptor orbitals is again clear: alcohols, amines, ammonia, water, etc., do *not* give the corresponding negative ions, but methyl cyanide, benzene, etc., do. On the other hand, the former do give trapped and solvated electrons; the latter do not.

- (1) T. R. Tuttle and P. Graceffa, *J. Phys. Chem.*, **75**, 843 (1971).
- (2) R. Catterall, L. P. Stodulski, and M. C. R. Symons, *J. Chem. Soc., A*, 437 (1968).
- (3) P. W. Atkins, N. Keen, M. C. R. Symons, and H. W. Wardale, *ibid.*, 5594 (1963).
- (4) T. A. Claxton and M. C. R. Symons, *Chem. Commun.*, 379 (1970).
- (5) J. L. Hall and R. T. Schumacher, *Phys. Rev.*, **127**, 1892 (1962).
- (6) M. C. R. Symons, *Pure Appl. Chem.*, 309 (1970).

DEPARTMENT OF CHEMISTRY
THE UNIVERSITY
LEICESTER, LE1 7RH, ENGLAND

M. C. R. SYMONS

RECEIVED MAY 28, 1971

Solvated Electron in Any Case, but What Kind?

Publication costs assisted by the National Science Foundation

Sir: In a previous note¹ we have used an analogy between sodium solutions in a hydrocarbon-ether solvent on the one hand and in amine solvents on the other to support a solvent anion² model of the solvated electron as opposed to the widely accepted cavity model.³ Professor Symons has suggested this analogy breaks down if pushed far enough.⁴ While this is undoubtedly true, we have found attempts to extend the analogy both instructive and suggestive as to experiments which may help in determining the true structure of the solvated electron. For example, for both sodium dissolved in ammonia⁵ and sodium dissolved in hydrocarbon-ether⁶ mixtures the presence of solvent is essential for the stability of the ionic species produced.^{7,8} Thus, if one solvent is replaced by another there is no assurance in either case that the ionic species will remain stable. Failure to produce the ammonia anion, or the hexamethylphosphoramide anion in ether solution⁹ simply indicates that the ethers in question are inferior as solvating agents when compared to ammonia or hexamethylphosphoramide. Similarly, failure to produce the benzene anion in 2-methyltetrahydrofuran indicates that this ether is a poorer solvating agent than 1,2-dimethoxyethane in which the benzene anion is stable.¹⁰ In order to form a dilute liquid solution of ammonia anions we need a sufficiently good solvating agent which also has less attraction for the electron than the ammonia. Furthermore, this solvating agent should not react chemically with the alkali metal for obvious reasons. Such a combination of properties may be virtually impossible to find in a liquid solvent. However, an ionic crystal containing F centers may provide an adequate solvent to test for the formation of ammonia anions.

The volume expansion of the alkali metal-ammonia solutions provides another avenue through which the analogy may be explored with benefit. With the cavity model the volume expansion data are used to determine the size of the cavity and to test theoretical calculations.^{3,11}

With the solvent anion model theoretical calculations become more difficult, but because the electron is undoubtedly not strongly bound to an ammonia molecule its orbital is expected to be diffuse, and consequently the ammonia anion will be a large species. If this is a correct view then we may expect other anions such as aromatic hydrocarbon anions in which the electron is also not strongly bound¹² to the central molecule to be large species and solutions containing them to show volume expansion. This point may be tested through density measurements on solutions of alkali metal-hydrocarbon anion salts.

(11) W. N. Lipcomb, *J. Chem. Phys.*, **21**, 52 (1953); R. A. Stairs, *ibid.*, **27**, 1431 (1957).

(12) A. I. Shatenshtein and E. S. Petrov, *Russ. Chem. Rev.*, **36**, 100 (1967); G. Briegleb, *Angew. Chem. (Int. Ed.)*, **3**, 617 (1964).

DEPARTMENT OF CHEMISTRY
BRANDEIS UNIVERSITY
WALTHAM, MASSACHUSETTS 02154

T. R. TUTTLE, JR.*
PHILIP GRACEFFA

RECEIVED AUGUST 13, 1971

Solubilization of Benzene in Aqueous Cetyltrimethylammonium Bromide Measured by Differential Spectroscopy

Publication costs assisted by Shell Development Company

Sir: In a recent communication, Fendler and Patterson¹ reported that micelles influenced the rates of radiolytically generated radicals. Further, they found that the rate of hydrated electron attachment to benzene decrease in micellar (anionic) sodium dodecyl sulfate (NaDDS) and increased in micellar (cationic) cetyltrimethylammonium bromide (CTAB). They attributed the difference in rates to differences in solubilization sites of benzene in these micellar systems as recently reported by Eriksson and Gillberg² for CTAB and Rehfeld for NaDDS.³ On the basis of a proton magnetic resonance study ($\sim 35^\circ$) Eriksson and Gillberg proposed that benzene is adsorbed at the CTAB micelle-water interface² and differential ultraviolet (uv) spectroscopy investigations show that benzene is dissolved inside the hydrocarbon core of NaDDS micelles.³ However, Goerner⁴ concluded from a qualitative study of the uv spectra of benzene solubilized in aqueous solutions of various *N*-alkyl quaternary ammonium bromides that the site of solubilization is the hydrocarbon core of the micelle. Using the differential uv spectroscopy method

(1) T. R. Tuttle, Jr., and P. Graceffa, *J. Phys. Chem.*, **75**, 843 (1971).

(2) S. Golden, C. Guttman, and T. R. Tuttle, Jr., *J. Chem. Phys.*, **44**, 3791 (1966).

(3) J. Jortner, S. A. Rice, and E. G. Wilson, "Metal-Ammonia Solutions," G. Lepoutre and M. J. Sienko, Ed., W. A. Benjamin, New York, N. Y., 1963, p 222.

(4) See comment above by M. C. R. Symons.

(5) C. A. Kraus, *J. Amer. Chem. Soc.*, **29**, 1557 (1907).

(6) N. D. Scott, J. F. Walker, and V. L. Hansley, *ibid.*, **58**, 2442 (1936).

(7) C. A. Kraus and W. C. Bray, *ibid.*, **35**, 1315 (1913).

(8) D. E. Paul, D. Lipkin, and S. I. Weissman, *ibid.*, **78**, 116 (1956).

(9) R. Catterall, L. D. Stodulski, and M. C. R. Symons, *J. Chem. Soc. A*, 437 (1968).

(10) T. R. Tuttle, Jr., and S. I. Weissman, *J. Amer. Chem. Soc.*, **80**, 5342 (1958).

(1) J. H. Fendler and L. K. Patterson, *J. Phys. Chem.*, **74**, 4608 (1970).

(2) J. C. Eriksson and G. Gillberg, *Acta Chem. Scand.*, **20**, 2019 (1966).

(3) S. J. Rehfeld, *J. Phys. Chem.*, **74**, 117 (1970); also see S. J. Rehfeld, *J. Colloid Interface Sci.*, **34**, 518 (1970); M. Shinitzky, A. C. Dianoux, C. Gitler, and G. Weber, *Biochemistry*, **10**, 2106 (1971).

(4) J. W. Goerner, Ph.D. Thesis, Louisiana State University, 1966.

Table I: Position of the Second Maximum in the Progression of the Ultraviolet Vibrational Allowed Transition (2600-Å System), the Frequency Interval of the Progression ($\Delta\nu_1$), the Half-Widths ($\Delta\nu_{1/2}$), Molar Absorptivity (ϵ), the Integrated Intensities (I), and the Solute-Solvent Parameter (ϵ_S/ϵ_V) for Various Benzene Solutions (25°)^a

Benzene concn, mole fraction	$\lambda_{\max(2)}$ $\pm 1 \text{ \AA}$	$\Delta\nu_1$, $\pm 30 \text{ cm}^{-1}$	$\Delta\nu_{1/2}$, $\pm 30 \text{ cm}^{-1}$	$\epsilon_{\lambda \max(2)}$, $\pm 41. (\text{mol cm})^{-1}$	I , $(\text{mol}^{-1} \text{ cm}^{-1}) \text{ cm}^{-1}$	ϵ_S/ϵ_V
Solvent: Water (Saturated with Benzene)						
0.00043	2539	909	530	188	4.3	0.32
Solvent: Aqueous Solution of 0.1 M (CH ₃) ₄ NBr (Saturated with Benzene)						
0.00043	2539	909	530	190	4.3	0.32
Benzene Dissolved in Micellar Phase (Saturated with Benzene)						
0.70	2550	918	418	205	4.1×10^6	0.23
Solvent: <i>n</i> -Hexane						
1.0 (11.06)	2552	918	399	201	4.1	0.26
0.873 (9.12)	2551	915	413	204	4.1	0.24
0.525 (4.78)	2548	903	400	201	4.1	0.20

^a Spectral parameters for benzene dissolved in many other solvents are given in ref 3 and J. W. Eastman and S. J. Rehfeld, *J. Phys. Chem.*, **74**, 1438 (1970).

previously described,³ we have found that the solubilization site of benzene in micellar CTAB is in the hydrocarbon core just as was found in the case of micellar NaDDS.³ The CTAB and tetramethylammonium bromide used in these experiments were obtained from Eastman Organic Chemical Co. and before using were recrystallized three times from redistilled water.

The bands in the 2600-Å benzene system increase linearly³ above the cmc ($0.99 \times 10^{-3} M$) with CTAB concentration up to the limit of solubility of CTAB in water, $\sim 0.03 M$, at 25°. The amount of benzene solubilized plotted as a function of CTAB concentration fits the equation ($S = (0.99 \text{ mM}) + 2.55m$, where m is the CTAB concentration mmol/l. Table I gives the wavelength of the second maximum in the 2600-Å system, the absorption line widths, $\Delta\nu_{1/2}$, the band separation ν_1 , the molar absorptivity, ϵ at the second maximum, the integrated intensities, I , and the ϵ_S/ϵ_V the solvent-solute interaction parameter of these differential uv spectra. Note that the spectrum of benzene in aqueous 0.1 M tetramethylammonium bromide was the same as those observed for benzene dissolved in water.³ Only the spectrum of ~ 0.8 mole fraction of benzene in *n*-hexane closely resembles the spectrum of benzene in CTAB micelles. The benzene concentration in the CTAB micelle is found to be 0.7 mole fraction, 31% greater than found in micellar NaDDS. Using regular solution theory^{3,5} the activity coefficient (γ) of benzene in the CTAB micelle was calculated as 1.43; this value stands in strong contrast to the values of 2300 for benzene in water³ and 2.10 for benzene in NaDDS micelles.³ Extrapolation by conventional methods⁵ leads to an expected value of γ of ~ 1.1 for a solution of benzene in a normal paraffin liquid (nC_6 to nC_{12}) at a concentration in the vicinity of 0.7 mole fraction of benzene. Pye⁶

studied the temperature dependence of benzene solubility in aqueous micellar CTAB. His results show that the solubility of 0.72 mole fraction is nearly invariant between 20 and 40°. We found that an aqueous 0.1 M CTAB solution solubilized ~ 0.75 mole fraction of benzene at 35°. The differential spectrum of this solution was found to be the same as those observed at 25°. These data indicate that the solubilization site of benzene in micellar CTAB and NaDDS are the same; however, more benzene is dissolved in micellar CTAB probably due to a lower intramicellar pressure.³ In aqueous micellar CTAB solutions not saturated with benzene—at benzene concentrations less than 0.75 mole fraction based on the micellar phase—the sites of solubilization should be identical with those described above. As one adds benzene to the aqueous surfactant solution a reduction in the interfacial tension between the micellar phase and aqueous phase would occur, thus decreasing the intramicellar pressure. Solutions of benzene in water as well as in the micellar phase are nonideal. Therefore the ratio of benzene concentration, C (water)/ C (micelle) is likely to vary with the total concentration of benzene.

In view of our experimental results, the difference in rates of radiolytically generated radicals observed by Fendler and Patterson¹ is unlikely to be due to differences in solubilization sites.

(5) J. H. Hildebrand and R. L. Scott, "Regular Solutions," 1st ed, Prentice-Hall Inc., Englewood Cliffs, N. J., 1962, Chapter 7.

(6) E. L. Pye, Ph.D. Thesis, Louisiana State University, 1966.

SHELL DEVELOPMENT COMPANY
OAKLAND, CALIFORNIA 94623

SELWYN J. REHFELD

RECEIVED JUNE 1, 1971

Comment on "Solubilization of Benzene in Aqueous Cetyltrimethylammonium Bromide Measured by Differential Spectroscopy"¹

Publication costs assisted by Carnegie-Mellon University and the U. S. Atomic Energy Commission

Sir: The similarities between spectrometric absorption data of 0.7 mole fraction benzene in hexane and micellar hexadecyltrimethylammonium bromide (CTAB) have led Rehfeld² to propose that the solubilization site for benzene is the micellar hydrocarbon core. He has used this evidence to question our interpretation of hydrated electron reactivity differences toward benzene in water and various micellar systems.³ In the work cited we reported an enhanced reactivity in the presence of micellar CTAB relative to that in water. Our findings were rationalized in terms of a benzene solubilization at the micelle-water interface as reported by Eriksson and Gillberg⁴ over the concentration range of our work (0.04 to 0.25 mole fraction benzene in the micellar phase). The resulting electrostatic interactions between the π system of the benzene with the net positive charge at the CTAB micelle surface were interpreted as responsible for rendering benzene more susceptible to nucleophilic attack by the electron.

Eriksson and Gillberg observed that, at diminishing concentrations of benzene in 0.17 M CTAB, the nmr peak position of benzene approached the resonance line position of benzene in water. They state: "This observation indicates that at least at low solubilize contents benzene is solubilized by absorption at the micelle-water interface. . . further addition of solubilize gives rise to a rapid shift of the N-CH₃, -CH₂- and especially of the α -CH₂ hydrogen resonance lines toward higher fields. These shifts can be explained if one assumes that absorption at sites close to the α -CH₂ groups is the predominating solubilization mechanism and that this process involves a removal of those water molecules which presumably are present initially at these absorption sites. The proposed mechanism seems probable since the quite large shifts obtained for the α -CH₂-hydrogens (26 c/sec) are only expected to result from a combination of interfacial absorption of benzene and a change of the polarizing ability of the surrounding medium. At a benzene content approximately equal to 1.0 mole C₆H₆/mole CTAB [0.5 mole fraction] there is a marked change in slope of the shift curves for C₆H₆ and for the α -CH₂ and C-CH₃ groups that can be interpreted as being due to absorption saturation and a transition to solubilization through dissolving of benzene in the central parts of the micelle."

Their interpretation suggests that, under the conditions of the uv study, well over half the benzene would lie in the interior of the CTAB micelle. The present work of Rehfeld, confined to one CTAB-benzene con-

centration of 0.7 mole fraction, is not adequate to show a clear contradiction between his results and those of Eriksson and Gillberg and our interpretation.

A problem inherent to both nmr and absorption spectrophotometric analysis of dynamic substrate solubilization sites in micellar systems, however, is the lack of appropriate reference solvents since there is experimental evidence interpreted as indicating that the micellar interior contains water molecules.⁵ Thus one may question the validity of comparing the proton magnetic shifts of benzene extrapolated to zero solubilize concentration to that in pure water or to pure hexane. Likewise it may be argued that the similarity of the observed absorption spectrum of 0.48 mole fraction of benzene in methanol, a polar solvent, [$\lambda_{\max(2)} = 2548 \pm 1 \text{ \AA}$; $\Delta\nu_I = 918 \pm 30 \text{ cm}^{-1}$; $\Delta\nu_{1/2} = 440 \pm 30 \text{ cm}^{-1}$; $\epsilon_{\lambda_{\max(2)}} = 198 \pm 4 \text{ l. (mol cm)}^{-1}$; $I = 4.2 \text{ (mol}^{-1} \text{ cm}^{-1}) \text{ cm}^{-1}$; $\epsilon_S/\epsilon_V = 0.26$]⁶ to that of 0.52 mole fraction of benzene in apolar hexane² renders absorption spectrophotometry a somewhat tenuous method of contrasting the absorption spectra of 0.7 mole fraction of benzene in CTAB to that of 0.00043 mole fraction of benzene in water.² Additionally, at high benzene concentrations the shape and size of micelles are likely to undergo profound changes which may alter both nmr and uv spectra. However, our recent examination of the proton magnetic resonance frequencies (chemical shifts) of benzene and those of NaLS as a function of benzene concentration suggests, when compared to similar data for CTAB,⁴ that the *solubilization sites of benzene* in these surfactants *are different*⁷ as required by our interpretation of the observed reactivities of e_{aq}⁻ with benzene in the presence of these micellar surfactants.

(1) Supported in part by the U. S. Atomic Energy Commission.

(2) S. J. Rehfeld, *J. Phys. Chem.*, **75**, 3905 (1971).

(3) J. H. Fendler and L. K. Patterson, *ibid.*, **75**, 4608 (1970).

(4) J. C. Eriksson and G. Gillberg, *Acta Chem. Scand.*, **20**, 2019 (1966).

(5) W. L. Courchene, *J. Phys. Chem.*, **68**, 1870 (1964); N. Muller and R. H. Birkhahn, *ibid.*, **71**, 957 (1967).

(6) S. J. Rehfeld, *ibid.*, **74**, 117 (1970).

(7) The magnitude of upfield shifts for the C₆H₆ and that for the terminal CH₃ of the detergent are considerably greater (by a factor of ca. 2) for NaLS than that for CTAB for comparable substrate and surfactant concentrations (C. Day, E. J. Fendler, and J. H. Fendler, unpublished results).

DEPARTMENT OF CHEMISTRY
TEXAS A & M UNIVERSITY
COLLEGE STATION, TEXAS 77843

JANOS H. FENDLER

RADIATION RESEARCH LABORATORIES
CARNEGIE-MELLON UNIVERSITY
PITTSBURGH, PENNSYLVANIA 15213

LARRY K. PATTERSON*

RECEIVED JULY 23, 1971

Comment on a Recent Vibrational Analysis for the Molecules Gallium Oxide, Indium Oxide, and Thallium Oxide

Publication costs borne completely by The Journal of Physical Chemistry

Sir: In a recent paper by Carlson, *et al.*,¹ vibrational assignments are given for the molecular species Al_2O , Ga_2O , In_2O , and Tl_2O isolated in low-temperature matrices. We have been studying these systems with the aid of ^{18}O isotope enrichment and believe that some of the band assignments given are incorrect.

In particular, Carlson observes bands at 595.6, 416.5, and 822.6 cm^{-1} for gallium oxide isolated in an argon matrix, and he assigns these as the ν_1 , ν_2 , and ν_3 fundamentals of Ga_2O . In a nitrogen matrix, the same assignment is given to three corresponding bands at 590.4, 425.8, and 808.1 cm^{-1} . Our ^{16}O experiments on gallium oxide yield essentially the same absorption frequencies (*e.g.*, 590.9, 423.9, and 809.4 cm^{-1} in a nitrogen matrix), but although there is general agreement that the band at ~ 800 cm^{-1} should be assigned² as ν_3 Ga_2O , our experiments with ^{18}O enrichment definitely indicate an alternative assignment for the other two bands.

^{18}O atom enrichment on this system produces a doublet at high frequency corresponding to the ν_3 fundamentals of Ga_2^{16}O and Ga_2^{18}O , and from these peaks an estimate has previously been made² of the apex angle in Ga_2O . However, a quite different pattern is produced associated with the other two "fundamentals" at ~ 590 and ~ 420 cm^{-1} , and this is shown in Figure 1. Two triplets are observed, each with an approximate intensity ratio 1:2:1 for 50% ^{18}O enrichment. These triplets are characteristic of a molecule containing two equivalent atoms of oxygen and cannot be explained by Carlson's assignment. Furthermore, in our diffusion experiments, which are conveniently controlled using the "back pressure" regulator of our Cryotip,³ these bands at ~ 590 and ~ 420 cm^{-1} often *increased* in intensity at the expense of ν_3 . We believe that these bands are associated with a dimer species Ga_4O_2 . This molecule need not be present in the vapor phase, but it could be formed during deposition when the matrix is still soft.

Parallel studies on the indium oxide system lead us to believe that Carlson's identification of the corresponding ν_1 and ν_2 fundamentals of In_2O is similarly incorrect. Here, ^{18}O enrichment experiments again show a simple doublet² for ν_3 , but triplet structures for the bands assigned as ν_1 and ν_2 . In a nitrogen matrix these triplets occur at 550.3, 532.0, and 522.1 cm^{-1} , and 412.2, 402.8, and 393.0 cm^{-1} , and for 50% ^{18}O enrichment, an intensity pattern similar to that shown in Figure 1 is obtained.

The infrared spectrum of matrix-isolated thallium oxide has been studied by Brom, *et al.*⁴ Their diffusion studies indicate that the bands assigned by Carlson as the ν_1 and ν_2 fundamentals of Tl_2O are probably due to a polymeric species Tl_4O_2 .

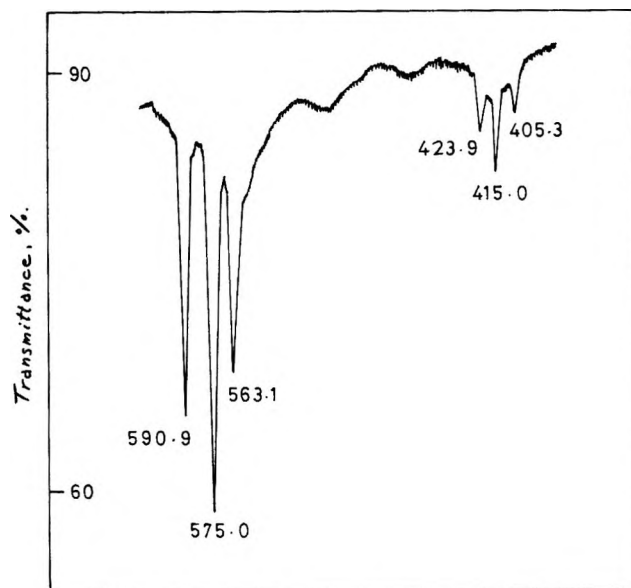


Figure 1. Infrared spectrum (400–600 cm^{-1}) of gallium oxide with $\sim 50\%$ ^{18}O atom enrichment isolated in a nitrogen matrix.

Although we have presented evidence which indicates that the ν_1 and ν_2 fundamentals of Ga_2O , In_2O , and possibly Tl_2O have been incorrectly identified, we cannot unfortunately provide alternative frequencies which may definitely be assigned as the ν_1 and ν_2 vibrations of these molecules. Our diffusion studies indicate that there are one or two possible candidates for ν_1 Ga_2O in the frequency region 400–500 cm^{-1} , but the absorptions are very weak, and we have not yet been able to obtain sufficient intensity in our ^{18}O enrichment experiments to make identification definite.⁵

(1) D. M. Makowiecki, D. A. Lynch, Jr., and K. D. Carlson, *J. Phys. Chem.*, **75**, 1963 (1971).

(2) A. J. Hinchcliffe and J. S. Ogden, *Chem. Commun.*, 1053 (1969).

(3) J. S. Anderson and J. S. Ogden, *J. Chem. Phys.*, **51**, 4189 (1969).

(4) J. M. Brom, Jr., T. Devore, and H. F. Franzen, *ibid.*, **54**, 2742 (1971).

(5) EDITOR'S NOTE. Professor Carlson has advised us in correspondence that similar isotopic studies have recently been carried out in his laboratory, with the appearance of the same triplet splitting and similar conclusions. In his laboratory, as in Dr. Ogden's, further studies are in progress which hopefully will permit definitive identification of the carriers and assignments of the vibrational modes.

INORGANIC CHEMISTRY LABORATORY
UNIVERSITY OF OXFORD
OXFORD, ENGLAND

A. J. HINCHCLIFFE
J. S. OGDEN*

RECEIVED SEPTEMBER 7, 1971

American Chemical Society

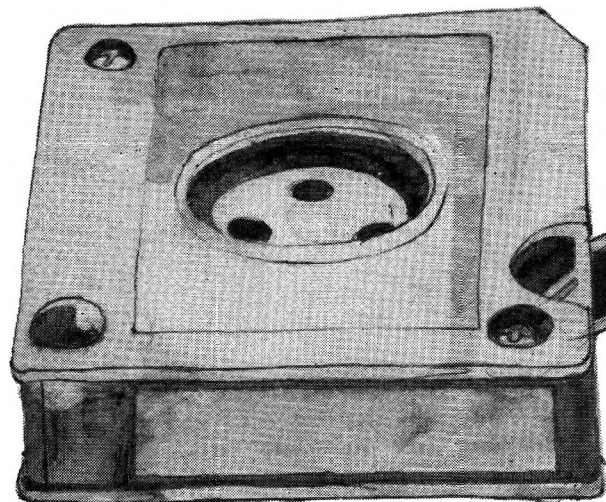
"Primary Publications on Microfilm"

Your Key to—

■ Dramatic savings in archival space and dollars . . . over 873,000 pages of chemical literature contained in a carousel measuring only 17" x 17" x 39".

■ Faster access to needed data. Slash costly search and retrieval time required of your scientists and librarians.

■ Unlimited distribution of copyrighted scientific data. "ACS Primary Publications on Microfilm" are available under a unique licensing agreement permitting you to make as many enlarged photocopies per page as desired . . . for distribution throughout your company.



American Chemical Society Primary Publications included in this microfilm program:

JOURNAL OF THE AMERICAN CHEMICAL SOCIETY (1879-1969)
INDUSTRIAL & ENGINEERING CHEMISTRY (1909-1969)
CHEMICAL & ENGINEERING NEWS (1923-1969)
ANALYTICAL CHEMISTRY (1929-1969)
JOURNAL OF PHYSICAL CHEMISTRY (1896-1969)
JOURNAL OF AGRICULTURAL AND FOOD CHEMISTRY (1953-1969)
JOURNAL OF ORGANIC CHEMISTRY (1936-1969)
JOURNAL OF CHEMICAL AND ENGINEERING DATA (1956-1969)
CHEMICAL REVIEWS (1924-1969)
JOURNAL OF CHEMICAL DOCUMENTATION (1961-1969)
INDUSTRIAL & ENGINEERING CHEMISTRY—FUNDAMENTALS (1962-1969)
INDUSTRIAL & ENGINEERING CHEMISTRY—PROCESS DESIGN AND DEVELOPMENT (1962-1969)
INDUSTRIAL & ENGINEERING CHEMISTRY—PRODUCT RESEARCH AND DEVELOPMENT (1962-1969)
BIOCHEMISTRY (1962-1969)
INORGANIC CHEMISTRY (1962-1969)
JOURNAL OF MEDICINAL CHEMISTRY (1959-1969)
CHEMISTRY (1962-1969)
ENVIRONMENTAL SCIENCE & TECHNOLOGY (1967-1969)
ACCOUNTS OF CHEMICAL RESEARCH (1968-1969)
MACROMOLECULES (1968-1969)

For information on "ACS Primary Publications on Microfilm", write or call:
Mr. George Virvan
Special Issues Sales
American Chemical Society
1155 16th Street, N.W.
Washington, D.C. 20036
(202-737-3337)

Keep pace with the new...

through these basic research journals of the American Chemical Society

The Journal of the American Chemical Society

The premier American chemistry journal publishing original research papers in every field. Biweekly.

*ACS members: U.S. \$22.00	Canada, PUAS \$26.50	Other nations \$27.50
Nonmembers: U.S. \$44.00	Canada, PUAS \$48.50	Other nations \$49.50

The Journal of Organic Chemistry

Embraces the field, from synthesis to structure to behavior. Biweekly publication.

*ACS members: U.S. \$20.00	Canada, PUAS \$24.50	Other nations \$25.50
Nonmembers: U.S. \$40.00	Canada, PUAS \$44.50	Other nations \$45.50

The Journal of Physical Chemistry

Maintains a balance between classical areas of chemistry and modern structural quantum oriented areas. Biweekly.

*ACS members: U.S. \$20.00	Canada, PUAS \$24.00	Other nations \$25.00
Nonmembers: U.S. \$40.00	Canada, PUAS \$44.00	Other nations \$45.00

Biochemistry

Covers enzymes, proteins, carbohydrates, lipids, nucleic acids and their metabolism, genetics, biosynthesis. Biweekly.

*ACS members: U.S. \$20.00	Canada, PUAS \$23.00	Other nations \$23.50
Nonmembers: U.S. \$40.00	Canada, PUAS \$43.00	Other nations \$43.50

The Journal of Agricultural and Food Chemistry

Places special emphasis on the chemical aspects of agricultural and food chemistry. Bimonthly.

*ACS members: U.S. \$10.00	Canada, PUAS \$13.00	Other nations \$13.50
Nonmembers: U.S. \$20.00	Canada, PUAS \$23.00	Other nations \$23.50

The Journal of Medicinal Chemistry

Emphasis is on synthesis, mode of action and pharmacology of medicinal agents. Monthly.

*ACS members: U.S. \$15.00	Canada, PUAS \$18.00	Other nations \$18.50
Nonmembers: U.S. \$30.00	Canada, PUAS \$33.00	Other nations \$33.50

The Journal of Chemical and Engineering Data

Quarterly journal presenting data on properties and behavior of both new and known chemical systems.

*ACS members: U.S. \$15.00	Canada, PUAS \$18.00	Other nations \$18.50
Nonmembers: U.S. \$30.00	Canada, PUAS \$33.00	Other nations \$33.50

Inorganic Chemistry

Publishes original research, both experimental and theoretical, in all phases of inorganic chemistry.

*ACS members: U.S. \$18.00	Canada, PUAS \$21.00	Other nations \$21.50
Nonmembers: U.S. \$36.00	Canada, PUAS \$39.00	Other nations \$39.50

Macromolecules

Presents original research on all fundamental aspects of polymer chemistry. Bimonthly publication.

*ACS members: U.S. \$12.00	Canada, PUAS \$15.00	Other nations \$15.50
Nonmembers: U.S. \$24.00	Canada, PUAS \$27.00	Other nations \$27.50

American Chemical Society / 1155 Sixteenth Street, N.W., Washington, D.C. 20036

Please enter a one year subscription for the following journals:

1 _____	2 _____	3 _____
4 _____	5 _____	6 _____
7 _____	8 _____	9 _____

name _____ position _____

address _____

city _____ state/country _____ zip _____

your company _____ nature of company's business _____

I am an ACS member I am not an ACS member Bill me for \$ _____

Payment enclosed (*payable to American Chemical Society*) in the amount of \$ _____. Payment must be made in U.S. currency, by international money order, UNESCO coupons, or U.S. bank draft; or order through your book dealer.

*NOTE: Subscriptions at ACS member rates are for personal use only.